



# RESEARCH

2007-11

## Pavement Design Using Unsaturated Soil Technology

Take the



steps...

*Research...Knowledge...Innovative Solutions!*

**Transportation Research**

## Technical Report Documentation Page

1. Report No. MN/RC-2007-11	2.	3. Recipients Accession No.	
4. Title and Subtitle Pavement Design Using Unsaturated Soil Technology		5. Report Date May 2007	
		6.	
7. Author(s)  Satish Gupta and Andry Ranaivoson  Tuncer Edil, Craig Benson, and Auckpath Sawangsuriya		8. Performing Organization Report No.	
		10. Project/Task/Work Unit No.	
9. Performing Organization Name and Address Department of Soil, Water, & Climate Borlaug Hall 1991 Upper Buford Circle St. Paul, MN 55108		11. Contract (C) or Grant (G) No.  (C) 81655 (wo) 103	
		13. Type of Report and Period Covered	
12. Sponsoring Organization Name and Address Minnesota Department of Transportation 395 John Ireland Boulevard Mail Stop 330 St. Paul, Minnesota 55155		14. Sponsoring Agency Code	
		15. Supplementary Notes <a href="http://www.lrrb.org/PDF/200711.pdf">http://www.lrrb.org/PDF/200711.pdf</a>	
16. Abstract (Limit: 200 words)  Pavements are constructed on compacted soils that are typically unsaturated. The negative pore-water pressure (soil suction) due to the ingress of water in between soil particles has a significant effect on pavement foundation stiffness and strength. The study characterized the effects of soil suction on shear strength and resilient modulus of four soils representing different regions of Minnesota. The deviator stress in shear strength measurements followed a power function relationship with soil suction. Resilient modulus also followed the power function relationship with suction but these relationships fell within a narrow range. We present models for incorporating suction effects in shear strength and resilient modulus measurements of highly compacted subgrade soils. We also briefly outline a framework for incorporating these models in the resistance factors of MnPAVE. Since soil water content and the resulting soil suction under the pavement varies with season, adjustments are needed to account for increased strength and stiffness of the material as a result of unsaturated soil conditions. These adjustments will not only reflect the more realistic field conditions but will result in more reliable performance predictions than the current pavement design method.			
17. Document Analysis/Descriptors resilient modulus, water retention, shear strength,		18. Availability Statement No restrictions. Document available from: National Technical Information Services, Springfield, Virginia 22161	
19. Security Class (this report) Unclassified		20. Security Class (this page) Unclassified	
21. No. of Pages 245		22. Price	

# **Pavement Design Using Unsaturated Soil Technology**

## **Final Report**

Prepared by:

Satish Gupta and Andry Ranaivoson  
Department of Soil, Water, & Climate  
University of Minnesota, St. Paul, MN

Tuncer Edil, Craig Benson, and Auckpath Sawangsuriya  
Department of Civil Engineering  
University of Wisconsin

**May 2007**

Published by:

Minnesota Department of Transportation  
Research Services Section  
395 John Ireland Boulevard, MS 330  
St. Paul, Minnesota 55155-1899

This report represents the results of research conducted by the authors and does not necessarily represent the views or policies of the Minnesota Department of Transportation and/or the Center for Transportation Studies. This report does not contain a standard or specified technique.

The authors and the Minnesota Department of Transportation and/or Center for Transportation Studies do not endorse products or manufacturers. Trade or manufacturers' names appear herein solely because they are considered essential to this report.

## **ACKNOWLEDGEMENT**

The authors gratefully acknowledge the help and support of John Siekemier and Ruth Roberson of the Minnesota Department of Transportation during the conduct of this study. They were very generous with their ideas as well as in providing linkages with others ongoing and past studies in this area. The original project was intended as a collaboration with Dr. Sai Vanapalli of the Lakehead University, Thunder Bay, Ontario, Canada but because of his health and his move to the University of Ottawa, Ottawa, Ontario, Canada, this collaboration did not come to fruition. The senior author thanks Dr. Vanapalli for his ideas during the preparation of the proposal for this project. Drs. Gupta and Ranaivison also thank Dr. Toby Ewing of Iowa State University, Ames, IA for his help in running pore network simulation model.

# TABLE OF CONTENTS

ACKNOWLEDGEMENT .....	i
LIST OF TABLES .....	iii
LIST OF FIGURES .....	iv
LIST OF FIGURES .....	iv
EXECUTIVE SUMMARY .....	vii
I INTRODUCTION.....	1
OBJECTIVES .....	1
SCOPE.....	1
II LITERATURE REVIEW .....	3
SHEAR STRENGTH OF UNSATURATED SOILS.....	3
Effective Stress Approach: .....	3
Independent State Variable Approach: .....	6
STIFFNESS OF UNSATURATED SOILS.....	13
As-Compacted State: .....	15
Post-Compacted State: .....	17
III MATERIALS AND METHODS .....	22
WATER RETENTION CHARACTERISTICS.....	22
SHEAR STRENGTH TESTING .....	23
Specimen Preparation: .....	23
Specimen Saturation and Desorption:.....	23
Triaxial Testing:.....	25
Deviator Stress at 1% and 5% Strain: .....	28
STIFFNESS TESTING .....	28
Specimen Suction Conditioning-Soil-Water Characteristic Curve: .....	28
Stiffness Testing-Resilient Modulus:.....	33
IV RESULTS AND DISCUSSION .....	37
PHYSICAL CHARACTERISTIC OF THE SOILS.....	37
SOIL WATER RETENTIONS .....	37
DEVIATOR STRESS AT 5% STRAIN .....	37
DEVIATOR STRESS AT 1% STRAIN.....	51
SHEAR STRENGTH MODEL FOR UNSATURATED SOILS.....	51
RESILIENT MODULUS OF UNSATURATED SOILS.....	56
DEVELOPMENT OF MATHEMATICAL MODEL .....	83
MODEL VALIDATION.....	85
V LINKING SHEAR STRENGTH MEASUREMENTS TO RESILIENT MODULUS .....	92
POWER FUNCTION MODEL FOR RESILIENT MODULUS OF UNSATURATED SOILS .....	92
TESTING FOR SUCTION EFFECTS ON RESILIENT MODULUS .....	94
RELATIONSHIP BETWEEN RESILIENT MODULUS AND SHEAR STRENGTH .....	94
VI FRAMEWORK FOR DEVELOPING MnPAVE FACTORS FOR SUCTION EFFECTS.....	101
VII EXPECTED BENEFITS AND FUTURE RESEARCH NEEDS .....	103
VIII REFERENCES .....	104

## LIST OF TABLES

Table 1: Relationships describing the effects of suction on shear strength. (Taken from Garven and Vanapalli, 2006).	10
Table 2: Properties of Test Soils	29
Table 3: Example of spreadsheet for specimen and $M_r$ test data	34
Table 4: Soil name, optimum moisture, and density.	38
Table 5: Soil name, texture, and liquidity and plasticity parameters	38
Table 6: Value of Van Genuchten's function value for MnRoad soil at two densities.	38
Table 7: Value of Van Genuchten's function value for Red Wing soil at two densities.	38
Table 8: Value of Van Genuchten's function value for Duluth TH23 soil at two densities.	38
Table 9: Value of Van Genuchten's function value for Red Lake Falls soil at two densities	38
Table 10: Best fit value of the power function coefficients describing the change in deviator stress ( $\sigma_1 - \sigma_3$ ) at 5% strain as a function of soil suction ( $\mu_w$ ) for soils that have been compacted at 103% of Proctor density.	46
Table 11: Best fit value of the power function coefficients describing the change in deviator stress ( $\sigma_1 - \sigma_3$ ) at 5% strain as a function of suction ( $\mu_w$ ) for soils that have been compacted at 98% of Proctor density	46
Table 12: Best fit value of the power function coefficients describing the change in deviator stress ( $\sigma_1 - \sigma_3$ ) at 1% strain as a function of suction ( $\mu_w$ ) for soils that have been compacted at 103% of Proctor density	55
Table 13: Table 13: Best fit value of the power function coefficients describing the change in deviator stress ( $\sigma_1 - \sigma_3$ ) at 1% strain as a function of suction ( $\mu_w$ ) for soils that have been compacted at 98% of Proctor density.	55
Table 14: Correlation coefficients ( $R^2$ ) of "a" and "b" against % clay, % silt, % sand and plastic limit (PL) for soils compacted at 98% and 103% of standard Proctor density.	55
Table 15: Specifications for Load and Specimen Response Measurement Instrumentation (NCHRP 1-28A, 2003).	57
Table 16: Calibration of $M_r$ Instruments.	58
Table 17: SWCC parameters of four test soils.	58
Table 18: Summary of Resilient Modulus and Bender Element Test Results	59
Table 19: Summary of the fitting parameters of the mathematical model.	86
Table 20: Best fit value of the power function coefficients describing the change in resilient modulus ( $M_r$ ) as a function of suction ( $\square_w$ ) for four soils. $M_r$ values correspond to values measured using external LVDT.	98
Table 21: Best fit value of the power function coefficients describing the change in resilient modulus ( $M_r$ ) as a function of suction ( $\square_w$ ) for four soils. $M_r$ values correspond to values measured using internal LVDT	98
Table 22: Correlation coefficients ( $R^2$ ) of $\square_1$ and $\square_1$ against % clay, % silt, % sand and plastic limit (PL) for $M_r$ values measured using external and internal LVDT	98
Table 23: Table 23: Slope of the power function describing deviator stress ( $\sigma_1 - \sigma_3$ ) vs. suction and slope of the power function describing resilient modulus ( $M_r$ ) vs. suction for four soils.	99

## LIST OF FIGURES

Figure 1: Variation of $\chi$ as a function of degree of saturation for two soils tested by Bishop and Blight (1963). (Figure taken from Yong and Warkentin, 1975).....	5
Figure 2: Relationship between effective stress parameter ( $\chi$ and suction ratio $[(u_a - u_w)/(u_a - u_w)_b]$ for 17 studies. (Figure taken from Khalili and Khabbaz, 1998).....	5
Figure 3: Extended plot of Mohr-Coulomb failure envelopes for unsaturated soil. (Figure taken from Fredlund and Rahardjo, 1993).....	7
Figure 4: Two dimensional projections of failure envelopes at various suctions. (Figure taken from Fredlund and Rahardjo, 1993).....	7
Figure 5: Split mold used to construct specimens. Mold diameter was 3.81 cm.....	24
Figure 6: Molded soil specimens with rubber sleeves on the pressure plate in a pressure chamber. The pressure chamber was used to bring specimens to a given soil suction. ....	24
Figure 7: Equilibrated soil specimen ready for shearing in a triaxial cell. ....	26
Figure 8: Sheared soil specimen. ....	26
Figure 9: Variation in deviator stress as a function of strain for three MnROAD specimens at 5 kPa suction and a confining stress 6.9 kPa.....	27
Figure 10: Variation in deviator stress as a function of strain for three MnRoad specimens at 0.5 kPa suction and a confining stress 6.9 kPa. ....	27
Figure 11: Testing program flowchart. ....	30
Figure 12: Schematic of a suction cell. ....	32
Figure 13: Matric suction as measured with thermal dissipation sensor. ....	36
Figure 14: Effect of compaction (100% and 105% of the Proctor Density) on water retention characteristics of the MnROAD soil.....	39
Figure 15: Effect of compaction (100% and 105% of the Proctor Density) on water retention characteristics of the Red Wing soil. ....	39
Figure 16: Figure 16. Effect of compaction (100% and 105% of the Proctor Density) on water retention characteristics of the Duluth TH23 soil. ....	40
Figure 17: Effect of compaction (100% and 105% of the Proctor Density) on water retention characteristics of the Red Lake Falls soil. ....	40
Figure 18: Variation in deviator stress ( $\sigma_1 - \sigma_3$ ) at 5% strain as a function of confining stress ( $\sigma_3$ ) and soil suction for MN Road specimens at 103% of Proctor density. ...	41
Figure 19: Variation in deviator stress ( $\sigma_1 - \sigma_3$ ) at 5% strain as a function of confining stress ( $\sigma_3$ ) and soil suction for Red Wing specimens at 103% of Proctor density....	41
Figure 20: Variation in deviator stress ( $\sigma_1 - \sigma_3$ ) at 5% strain as a function of confining stress ( $\sigma_3$ ) and soil suction for Duluth TH23 specimens at 103% of Proctor density. ....	42
Figure 21: Variation in deviator stress ( $\sigma_1 - \sigma_3$ ) at 5% strain as a function of confining stress ( $\sigma_3$ ) and soil suction for Red Lake Falls specimens at 103% of Proctor density. ....	42
Figure 22: Variation in deviator stress as a function of soil suction for four soils. Lines are the best fit lines using the power function. ....	44
Figure 23: Variation in the power function coefficient $\alpha$ as a function of soil clay content.....	44

Figure 24: Variation in the power function coefficient $\beta$ as a function of soil clay content.	45
Figure 25: Variation in deviator stress ( $\sigma_1 - \sigma_3$ ) at 5% strain as a function of confining stress ( $\sigma_3$ ) and soil suction for MN Road specimens at 98% of Proctor density.	47
Figure 26: Variation in deviator stress ( $\sigma_1 - \sigma_3$ ) at 5% strain as a function of confining stress ( $\sigma_3$ ) and soil suction for Red Wing specimens at 98% of Proctor density.	47
Figure 27: Variation in deviator stress ( $\sigma_1 - \sigma_3$ ) at 5% strain as a function of confining stress ( $\sigma_3$ ) and soil suction for Duluth TH23 specimens at 98% of Proctor density.	48
Figure 28: Variation in deviator stress ( $\sigma_1 - \sigma_3$ ) at 5% strain as a function of confining stress ( $\sigma_3$ ) and soil suction for Red Lake Falls specimens at 98% of Proctor density.	48
Figure 29: Variation in deviator stress as a function of soil suction for four soils. Lines are the best fit lines using the power function.	49
Figure 30: Variation in the power function coefficient $\alpha$ as a function of soil clay content.	49
Figure 31: Variation in the power function coefficient $\beta$ as a function of soil clay content.	50
Figure 32: Variation in deviator stress as a function of soil suction for four soils. Lines are the best fit lines using the power function.	52
Figure 33: Variation in deviator stress as a function of soil suction for four soils. Lines are the best fit lines using the power function.	52
Figure 34: Variation in the power function coefficient $\alpha$ (103% Standard Proctor density at 1% strain) as a function of soil clay content.	53
Figure 35: Variation in the power function coefficient $\beta$ (103% Standard Proctor density at 1% strain) as a function of soil clay content.	53
Figure 36: Variation in the power function coefficient $\alpha$ (98% Standard Proctor density at 1% strain) as a function of soil clay content.	54
Figure 37: Variation in the power function coefficient $\beta$ (98% Standard Proctor density at 1% strain) as a function of soil clay content.	54
Figure 38: Compaction characteristic of four test soils.	60
Figure 39: SWCCs of four test soils compacted near the optimum.	61
Figure 40: Resilient Modulus (based on external displacement measurements) vs Matric Suction.	62
Figure 41: Resilient Modulus (based on internal displacement measurements) vs Matric Suction.	63
Figure 42: Bender Element Shear Velocity vs Matric Suction.	64
Figure 43: Resilient Modulus (based on external displacement measurements) vs Water Content.	65
Figure 44: Resilient Modulus (based on internal displacement measurements) vs Water Content.	66
Figure 45: Bender Element Shear Velocity vs Water Content.	67
Figure 46: A linear semi-logarithmic relationship between $M_r$ and matric suction.	68
Figure 47: Resilient Modulus Based on Internal versus External Displacement Measurement.	70

Figure 48: Matric Suction Measured by Thermal Dissipation versus Induced Target Matric Suction.....	71
Figure 49: Low-Strain Modulus from Bender Element versus Resilient Modulus based on External Displacement Measurement. ....	72
Figure 50: Low-Strain Modulus from Bender Element versus Resilient Modulus based on Internal Displacement Measurement. ....	73
Figure 51: Mr-matric suction relationship for the ML specimens compacted with 98% and 103% relative compaction.....	75
Figure 52: Mr-matric suction relationship for the CL-1 specimens compacted with 98% and 103% relative compaction.....	76
Figure 53: Mr-matric suction relationship for the CL-2 specimens compacted with 98% and 103% relative compaction.....	77
Figure 54: Mr-matric suction relationship for the CH specimens compacted with 98% and 103% relative compaction.....	78
Figure 55: Mr-volumetric water content relationship for the ML specimens compacted with 98% and 103% relative compaction. ....	79
Figure 56: Mr-volumetric water content relationship for the CL-1 specimens compacted with 98% and 103% relative compaction. ....	80
Figure 57: Mr-volumetric water content relationship for the CL-2 specimens compacted with 98% and 103% relative compaction. ....	81
Figure 58: Mr-volumetric water content relationship for the CH specimens compacted with 98% and 103% relative compaction. ....	82
Figure 59: Relationship of parameter $k_1$ with liquid limit and plasticity index. ....	89
Figure 60: Relationship of parameter $k_{us}$ with liquid limit and plasticity index.....	90
Figure 61: Relationship of parameters $k_1$ and $k_{us}$ with group index. ....	91
Figure 62: Relationship between resilient modulus at (measured using external LVDT) as a function of soil suction. Resilient modulus values correspond to bulk stress of 83 kPa and octahedral stress of 19 kPa. Data taken from Edil et al. (2007).....	95
Figure 63: Relationship between resilient modulus at (measured using internal LVDT) as a function of soil suction. Resilient modulus values correspond to bulk stress of 83 kPa and octahedral stress of 19 kPa. Data taken from Edil et al. (2007).....	95
Figure 64: Relationship between $\alpha_1$ vs. clay content. $\alpha_1$ values are for Mr data measured with external LVDT.....	96
Figure 65: Relationship between $\alpha_1$ vs. clay content. $\alpha_1$ values are for Mr data measured with internal LVDT.....	96
Figure 66: Relationship between $\beta_1$ vs. clay content. $\beta_1$ values are for Mr data measured with external LVDT.....	97
Figure 67: Relationship between $\beta_1$ vs. clay content. $\beta_1$ values are for Mr data measured with internal LVDT.....	97
Figure 68: Figure 68: Relationship between slope of Mr -ext vs. suction ( $\beta_1$ ) and slope of deviator stress at 1% strain vs. suction ( $\beta$ ). ....	102
Figure 69: Relationship between the slope of Mr-int vs. suction ( $\beta_1$ ) and slope of deviator stress at 1% strain vs. suction ( $\beta$ ).....	102

## EXECUTIVE SUMMARY

Pavements are constructed on compacted soils that are typically unsaturated with degrees of saturation varying from 75 to 90%. The negative pore-water pressure (soil suction) due to the presence of water in between soil particles has a significant effect on the pavement foundation stiffness and strength. Several design and maintenance measures are also undertaken to maintain unsaturated conditions in the pavement foundation because they provide favorable engineering soils properties. However, the conventional procedures for pavement design are often based on empirical procedures and not on unsaturated soil mechanics principles. The goal of this project was to develop a pavement design method based on the principles of unsaturated soil mechanics that is consistent with MnPAVE design framework. Specific objectives were: (1) To develop methods for predicting unsaturated shear strength of soils based on saturated shear strength and water retention characteristics curve, (2) To determine the resilient modulus of fine grained sub grade soils taking into account the influence of matric suction, (3) To determine the relationships between the resilient modulus and shear strength measurements, and (4) To extend the results of the above studies and propose a framework towards predicting seasonal pore suction resistance factors for use in the mechanistic pavement design.

The study characterized the water retention characteristics curves, shear strength vs. suction, and resilient modulus vs. suction relationships of four soils that were packed to near optimum water contents and at 98% and 103% of the standard Proctor density. The four soils represented four different regions of Minnesota and covered a wide range of textural differences. The soils were: a silty soil from Red Wing, a silty clay loam soil from Red Lake Falls, a loam soil from Mn/ROAD facilities near Monticello, and a clay soil from TH 23 near Duluth. Clay content of these soils varied from 4.8 to 75.2%. Shear strength and resilient modulus measurements were made on each soil at several suctions and two densities. Shear strength measurements were made on three replicates of moisture/density condition where as resilient modulus measurements were made on mostly one specimen for each moisture/density condition.

Shear strength measurements and modeling were done by the Soil Physics group at the University of Minnesota where as resilient modulus characterization and modeling were done by the Geo Engineering group of the University of Wisconsin as a subcontract.

In general, there were small differences in the water retention characteristics of a given soil when packed at two different densities. With increase in density, there was a small decrease in the water content at lower suction and an increase in water content near the mid to higher suctions. This indicates that increasing compaction slightly reduced the proportion of larger pores but slightly increased the proportion of medium and smaller pores, as would be expected.

Since all samples did not demonstrate a clear shear failure and in many of the samples bulging occurred during compression, it was difficult to calculate the values of cohesion and friction angle using standard engineering practices for a given soil at various suctions. Because of this limitation, we decided to use deviator stress at 1 and 5% strain

as indicators of shear strength in characterizing the effects of initial compaction and suction. In general, the deviator stress showed a power function relationship to soil suction ( $\mu_w$ ) expressed as:

$$(\sigma_1 - \sigma_3) = \alpha \mu_w^\beta \quad (1)$$

There was a downward shift in the deviator stress vs. suction curves with an increase in the soil clay content and the shift was nearly same at all suctions. In other words, the slope ( $\beta$ ) was nearly similar and  $\alpha$  intercept varied with soil type. Relationship of the coefficient  $\alpha$  with clay content showed that its value exponentially decreased with an increase in the clay content but there was a slight increase or no change in the coefficient  $\beta$  with an increase in clay content. Since shear strength is related to deviator stress and the deviator stress can be described as a function of soil suction, we suggest the following relationship for describing suction effects on shear strength:

$$\tau_{us} = c' (\mu_a - \mu_w)^\beta + (\sigma_n - \mu_a) \tan \phi' \quad (2)$$

where  $\tau_{us}$  is the shear strength of an unsaturated soil,  $c'$  is the effective cohesion of the saturated soil,  $\phi'$  is the effective angle of frictional resistance of saturated soil, and  $(\mu_a - \mu_w)$  is the soil suction.

The resilient modulus (Mr) tests were conducted in accordance with a new Mr testing protocol, NCHRP 1-28A. Resilient modulus was calculated based on both external and internal displacement measurement and at a bulk stress of 83 kPa and octahedral shear stress of 19.3 kPa. The Mr data fitted the five parameter log-log model:

$$Mr = k_1 p_a \left( \frac{\sigma_b - 3k_6}{p_a} \right)^{k_2} \left( \frac{\tau_{oct}}{p_a} + k_7 \right)^{k_3} \quad (3)$$

$[k_1, k_2 \geq 0; \quad k_3, k_6 \leq 0; \quad k_7 \geq 1]$

where Mr is the resilient modulus,  $\sigma_b$  is the bulk stress ( $\theta = \sigma_1 + \sigma_2 + \sigma_3 = \sigma_1 + 2\sigma_3$ ),  $\tau_{oct}$  is the octahedral shear stress ( $= \frac{1}{3} \cdot \sqrt{(\sigma_1 - \sigma_2)^2 + (\sigma_1 - \sigma_3)^2 + (\sigma_2 - \sigma_3)^2} = \frac{\sqrt{2}}{3} \cdot (\sigma_1 - \sigma_3)$ ),  $\sigma_1, \sigma_2, \sigma_3$  ( $\sigma_2 = \sigma_3$ ) are the principal stresses,  $k_1, k_2, k_3, k_6$ , and  $k_7$  are the fitting constants, and  $p_a$  is the atmospheric pressure ( $\sim 100$  kPa). The effect of density on Mr appeared to be relatively minor once the specimens are compacted to within 5% of the maximum dry unit weight or 98 to 103% of the standard Proctor density. There was a strong relationship between the resilient modulus calculated based on internal displacement measurement and that based on external displacement measurement for all soils. However, the internal measurements always resulted in higher resilient modulus (1.7 times on average with a maximum of 3 times).

Regardless of the relative compaction (when within the range of 98 to 103% of standard Proctor density) and type of soil, a linear semi-logarithmic equation described the

relationship resilient modulus (based on internal displacement measurement and at a bulk stress of 83 kPa and octahedral shear stress of 19.3 kPa) and matric suction ( $u_a - u_w$ ):

$$M_r = -54105 + 57898 \log(u_a - u_w) \quad (4)$$

Two different models were suggested to incorporate the effects of soil suction on resilient modulus. Both these models are consistent with suggested models in the literature. The first model implicitly incorporates the effect of suction with the normalized water content,  $\Theta$ .

$$(M_r)_{us} = k_1 p_a \left( \frac{\sigma_b}{p_a} \right)^{k_2} \left( \frac{\tau_{oct}}{p_a} + 1 \right)^{k_3} + k_{us} p_a \Theta^\kappa (u_a - u_w) \quad (5)$$

$$[k_1, k_2 \geq 0; \quad k_3 \leq 0; \quad k_{us} \geq 0]$$

where  $k_1$ ,  $k_2$ ,  $k_3$ ,  $k_{us}$  and  $\kappa$  are fitting parameters optimized to obtain a best-fit between the measured and the predicted values. The fitting parameters  $k_6$  and  $k_7$  in Eq. (5) were respectively close to 0 and 1 according to the experimental results. In addition, the fitting parameter  $\kappa$  of 1.0 appears to be appropriate within the measured suction range (< 10 MPa) when it was used to fit all of the data.

Like in shear strength measurements,  $M_r$  data also showed that it follows the power function relationship with suction:

$$M_r = \alpha_1 (\mu_a - \mu_w)^{\beta_1} \quad (6)$$

where  $\alpha_1$  and  $\beta_1$  are regression constants. Although the relationships between  $M_r$  vs. soil suction for various soils fell within a narrow range, it appeared that there are some differences between soil types. In general,  $\alpha_1$  values decreased whereas  $\beta_1$  values increased with an increase in clay content and plastic limit. Considering the above relationship of  $M_r$  to suction, a second model that explicitly incorporates the effect of suction in  $M_r$  was also proposed

$$M_r = \left( k_1 p_a \left( \frac{\sigma_b - 3k_6}{p_a} \right)^{k_2} \left( \frac{\tau_{oct}}{p_a} + k_7 \right)^{k_3} \right) + \alpha_1 (\mu_a - \mu_w)^{\beta_1} \quad (7)$$

In the report we present several regression equations for estimating the values of  $\alpha_1$  and  $\beta_1$  from clay content or plastic limit. These values in turn may be used in Eq. (7) to estimate the  $M_r$  values.

In the final section of the report, we briefly outline a framework for incorporating the effects of suction in the resistance factors of MnPAVE using the data collected in this study. Since soil water content and the resulting soil suction under the pavement varies with season and is not saturated most of the time, adjustments are needed to account for

increased strength and stiffness of the material as a result of unsaturated soil conditions. These adjustments will not only reflect the more realistic field conditions but will result in more reliable performance predictions than the current pavement design method.

## CHAPTER I: INTRODUCTION

Pavements are constructed on compacted soils that are typically unsaturated with degrees of saturation varying from 75 to 90%. The negative pore-water pressure (soil suction) due to the presence of water in between soil particles has a significant effect on pavement stiffness and strength. Several design and maintenance measures are also undertaken to maintain unsaturated conditions in the pavement because they provide favorable engineering properties. However, the conventional procedures for pavement design are often based on empirical procedures and not on unsaturated soil mechanics principles. This is partially because pavement design procedure preceded the development of unsaturated soil mechanics. Fredlund and his associates ((Fredlund and Morgenstern, 1977; and Fredlund et al., 1978; Fredlund and Rahardjo, 1993; Fredlund, 1995; Vanapalli et al., 1996) have proposed a theoretical framework for interpreting the engineering behavior of unsaturated soils into pavement design. The goal of this project was to develop a pavement design method that is consistent with MnPAVE design framework and is based on the principles of unsaturated soil mechanics.

### Objectives

Specific objectives of the study were:

- To develop methods for predicting unsaturated shear strength of soils based on saturated shear strength and water retention characteristics curve.
- To determine the resilient modulus of fine grained sub grade soils taking into account the influence of matric suction.
- To determine the relationships between the resilient modulus and shear strength measurements.
- To extend the results of the above studies and propose a framework towards predicting the seasonal pore suction resistance factors.

### Scope

The study characterized the water retention characteristics curves, shear strength vs. suction, and resilient modulus vs. suction relationships of four soils that were packed at near optimum water contents and at 98% and 103% of the standard Proctor density. The four soils represented four different regions of Minnesota and covered a wide range of textural differences. The soils were: a silty soil from Red Wing, a silty clay loam soil from Red Lake Falls, a loam soil from MnROAD facilities near Monticello, and a clay soil from TH 23 near Duluth. Clay content of the soils varied from 4.8 to 75.2%. Shear strength and resilient modulus measurements were made on each soil at several suctions and two densities. Shear strength measurements were made on three replicates of

moisture/density condition where as resilient modulus measurements were made on mostly one specimen for moisture/density condition. The study also characterized the water retention characteristics of specimens taken from a box set-up used by the Civil Engineering department to simulate field compaction. Many of these data have already been transmitted to Mn/DOT. This report concentrates on the effect of soil suction on shear strength and resilient modulus measurements and modeling and how these findings can be incorporated into MnPAVE model.

Shear strength measurements and modeling was done by the Soil Physics group at the University of Minnesota where as resilient modulus characterization and modeling was done by the Geo Engineering group of the University of Wisconsin as a subcontract. Although the text from both groups is merged in various sections, authorships of the text is outlined at the start of each section.

## CHAPTER II: LITERATURE REVIEW

### Shear Strength of Unsaturated Soils

This section was written by Drs. Satish Gupta and Andry Ranaivoson, University of Minnesota.

Pavements are constructed on compacted soils that are typically unsaturated with degrees of saturation varying from 75 to 90%. The negative pore-water pressure (soil suction) due to presence of water in between soil particles has a significant effect on pavement strength. Several design and maintenance measures are also undertaken to maintain unsaturated conditions in the pavement because they provide favorable engineering soils properties. This literature review summarizes the development of theory and concepts that form the basis for soil suction effects on shear strength measurements.

Principally, theoretical development of unsaturated soil mechanics can be grouped into two tracks: (1) effective stress approach of Bishop (1959) and Bishop and Blight (1963), and (2) independent variable approach of Fredlund and Morgenstern (1977) and Fredlund et al. (1978). The following text details the highlight of these theoretical developments.

**Effective Stress Approach:** Shear strength of the soil refers to its resistance to slide on a failure plane (Das, 1979). Shear strength measurements are based on Mohr's theory of material rupture. The theory states that material failure occurs at a critical combination of shear ( $\tau$ ) and normal ( $\sigma_n$ ) stresses. Thus the shear strength at failure ( $\tau_f$ ) can be expressed with Mohr-Coulomb law as:

$$\tau_f = c' + \sigma_n \tan \phi' \quad (1)$$

where  $c'$  is cohesion of the soil and  $\phi'$  is the angle of internal friction. This function was later modified by Terzaghi (1936) to account for the presence of pore water pressure in saturated soils. He reasoned that total normal stress at a point is sum of the stress carried by soil solids and the stress due to pore water pressure ( $u$ ). He defined the stress carried by solids as effective stress ( $\sigma' = \sigma_n - u$ ). Thus, the Mohr Coulomb formulation for saturated soils can be written as:

$$\tau_f = c' + (\sigma_n - u) \tan \phi' \quad (2)$$

This equation was later modified by Bishop (1959) and Bishop et al. (1960) to account for the effects of soil suction in unsaturated soils. These authors reasoned that since the unsaturated soil is a three phase system (solid, pore water, and pore air) and water in voids is not continuous, the total stress will be the sum of intergranular stress, the pore air ( $u_a$ ) pressure, and the pore water pressure. They suggested that the effective stress ( $\sigma'$ ) in unsaturated soils can be expressed as:

$$\sigma' = (\sigma_n - u_a) + \chi(u_a - u_w) \quad (3)$$

where  $\chi$  is the fractional cross sectional area of the soil occupied by water. For dry soil,  $\chi$  will be zero and for saturated soil  $\chi$  will equal to 1. Thus, Mohr-Coulomb relationship for describing shear strength of unsaturated soils can be expressed as:

$$\tau_f = c' + [(\sigma_n - u_a) + \chi(u_a - u_w)] \tan \phi' \quad (4)$$

Bishop et al. (1960) pointed out that  $\chi$  value although primarily depends on the degree of saturation, it is also influenced by soil structure and stress pathway (wetting and drying) leading to a given degree of saturation. Figure 1 shows examples of the deviation of  $\chi$  value from the degree of saturation for two materials. Similar relationships have been presented in the literature and all point out to the difficulty of using Eq. (4) because of the difficulty of predicting the  $\chi$  value.

Since the presentation by Fredlund et al. (1978) that suction is an independent state variable, there has been limited use of the effective stress concept in predicting shear strength of soils. However, efforts have been made once a while to revive this concept. Two of the recent efforts are by Khalili and Khabbaz (1998) and Khalili et al. (2004). Khalili and Khabbaz (1998) used the shear strength data from 17 studies (including that of Fredlund and his associates) in the literature and showed that  $\chi$  value was uniquely related to the ratio of suction to air-entry value (Eq. 5).

$$\chi = \left[ \frac{(u_a - u_w)}{(u_a - u_w)_b} \right]^{-0.55} \quad (5)$$

where  $(u_a - u_w)_b$  refers to air entry value. The correlation coefficient for Eq. (5) was 0.94 (Fig. 2). Khalili et al. (2004) further reviewed additional studies from the literature and concluded that shear strength can be predicted using the effective stress concept. These authors proposed an incremental form of effective stress parameter to account for suction effects. The authors suggested that for suctions greater than air entry,  $\chi$  value varies as outlined in Eq. (5) but for suction less than air entry,  $\chi$  value was equal to 1.0. These authors tested their concept of incremental effective stress on shear strength data from Geiser (1999), Wheeler and Shivkumar (1995), Cui and Delage (1996), and Maatouk et al. (1995), and volume change data from Fleureau et al. (1993), Blight (1965), and Vicol (1990) and found good agreement between the measured and predicted values in all cases.

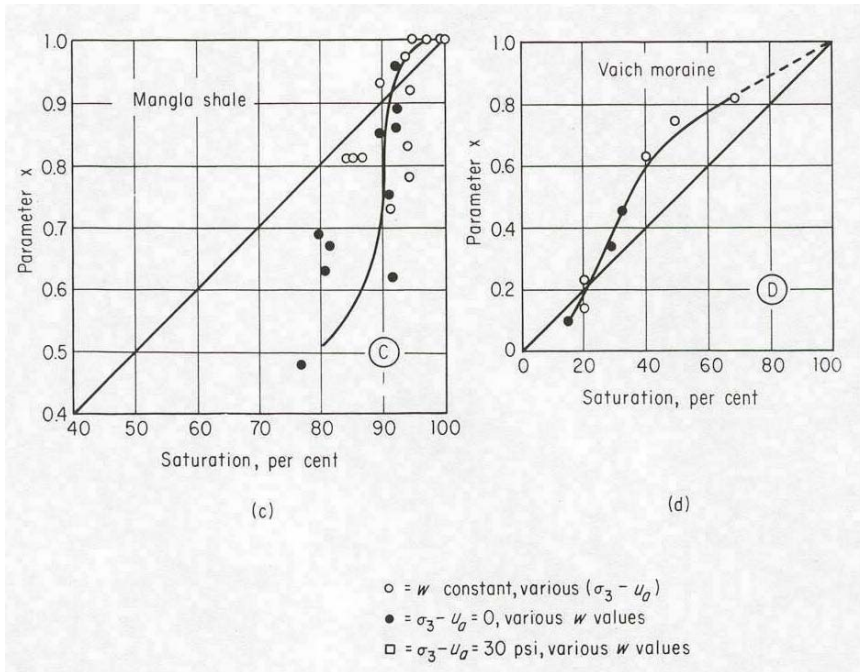


Figure 1: Variation of  $x$  as a function of degree of saturation for two soils tested by Bishop and Blight (1963). (Figure taken from Yong and Warkentin, 1975).

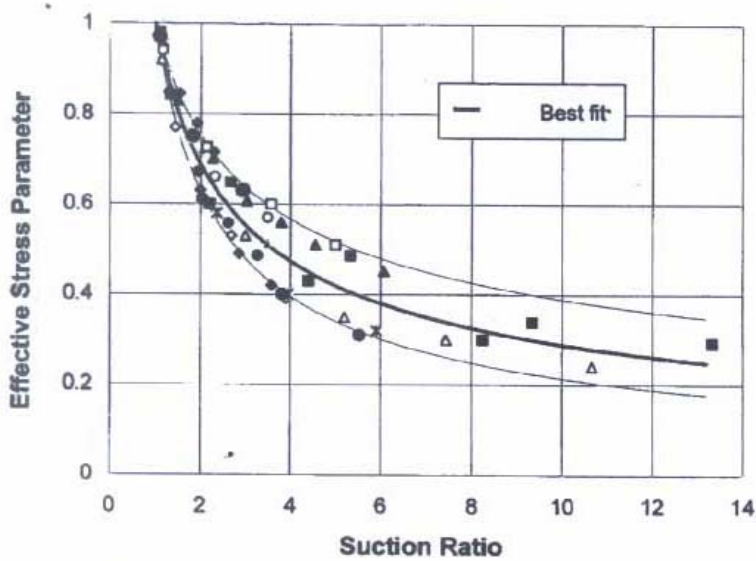


Figure 2: Relationship between effective stress parameter ( $x$ ) and suction ratio  $[(u_a - u_w)/(u_a - u_w)_b]$  for 17 studies. (Figure taken from Khalili and Khabbaz, 1998).

**Independent State Variable Approach:** The independent state variable approach was proposed by Fredlund and associates in a series of papers (Fredlund and Morgenstern, 1977; and Fredlund et al., 1978; Fredlund and Rahardjo, 1993; Fredlund, 1996). These investigators showed that stress state of an unsaturated soil can be described by any two of the three possible combinations of stress variables, namely: total normal stress ( $\sigma$ ), pore air pressure ( $u_a$ ), and pore water pressure ( $u_w$ ). Possible combinations are: ( $\sigma-u_a$ ) and ( $u_a-u_w$ ), ( $\sigma-u_w$ ) and ( $u_a-u_w$ ), and ( $\sigma-u_a$ ) and ( $\sigma-u_w$ ). These researchers showed that ( $\sigma-u_a$ ) and ( $u_a-u_w$ ) were the most advantageous combination because only one stress state variable was affected when pore water pressure changed. Using these combinations, these authors suggested the following relationship for describing shear strength of unsaturated soils.

$$\tau_f = c' + (\sigma_n - \mu_a) \tan \phi' + (\mu_a - \mu_w) \tan \phi^b \quad (6)$$

where  $\tan \phi^b$  is the slope of the shear strength vs. matric suction relationship. These authors also observed that although the Mohr-Coulomb failure plot for saturated soil is plotted in two dimensions, the corresponding plot for unsaturated soil must be a 3-dimensional diagram (Fig. 3). Fredlund and Rahardjo (1993) further showed that since the intercept of the failure envelope intersects the shear stress vs. matric suction plane (Fig. 3), the relationship between the shear stress vs. matric suction can be described as

$$c = c' + (\mu_a - \mu_w) \tan \phi^b \quad (7)$$

where  $c$  is the intercept of the Mohr-Coulomb failure envelope at specific matric suction and zero net normal stress (Fig. 4).

Over the years, many experimental efforts have been made to test the relationship between shear strength and soil suction (Eq. 6). One of the difficulties has been in keeping soil suction constant as the specimen is being sheared. In careful experiments, Drumright (1989) and Drumright and Nelson (1995) showed that Fredlund's relationship (Eq. 6) applies to unsaturated soils, however, the intersection of the failure surface with the plane containing suction was curved. These authors also showed that there was no appreciable difference in curved surface between the consolidated-drained (CD) and constant water content (CW) conditions. Based on this similarity, these authors concluded that there was a unique failure surface for a given suction stress history.

Several other studies have also shown variations to the proposed relationship of Fredlund et al. (Eq. 6) either in terms of constancy of friction angle ( $\phi$ ) at various suctions or to the linear effect of suction on cohesion ( $c$ ). Several of these studies have been presented at a series of international conferences on unsaturated soils (Alonso and Delage, 1995; Houston and Fredlund, 1997; Shackelford, et al., 2000; Miller et al., 2006).

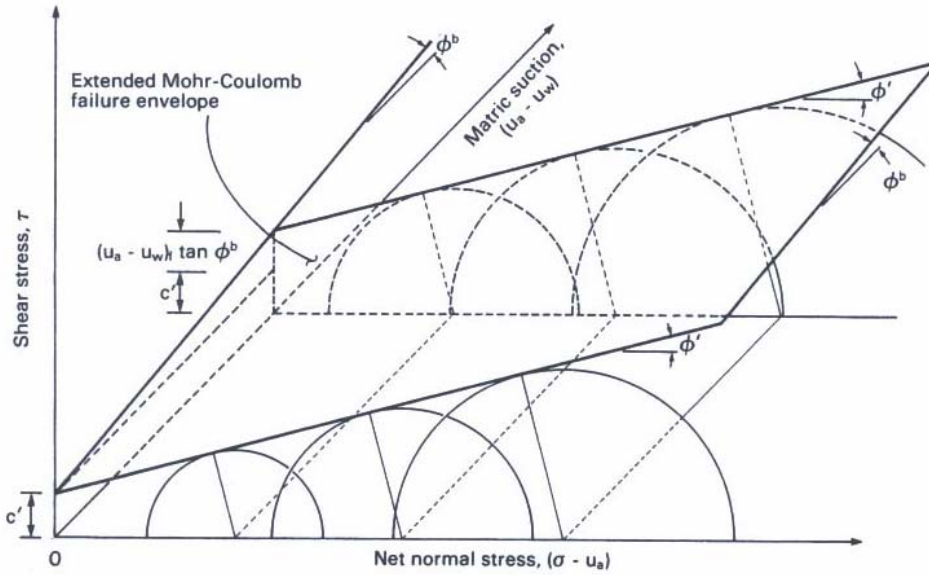


**Figure 3: Extended plot of Mohr-Coulomb failure envelopes for unsaturated soil. (Figure taken from Fredlund and Rahardjo, 1993).**

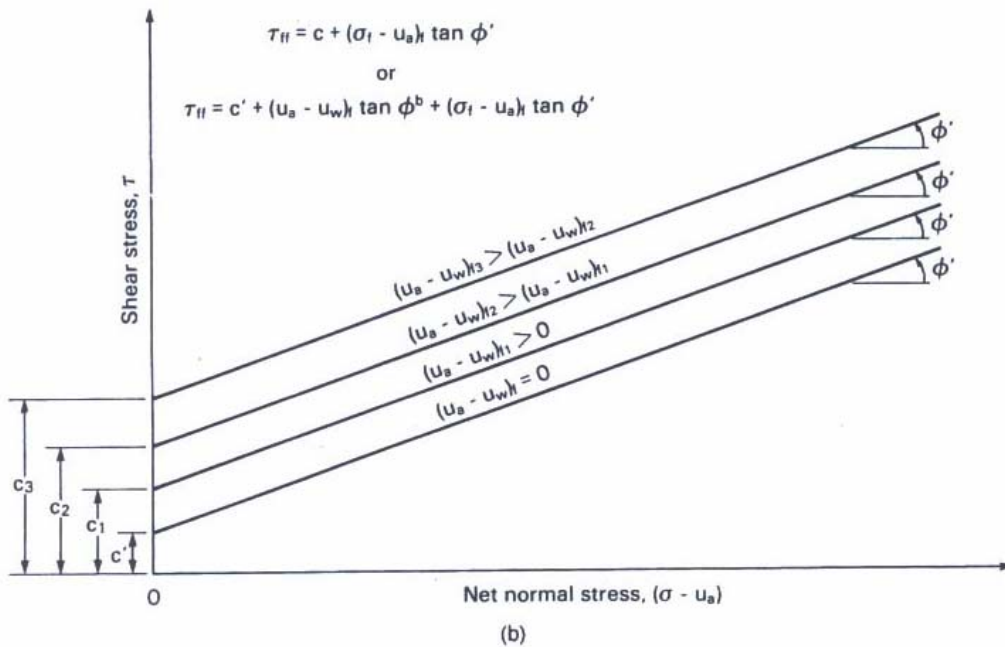


**Figure 4: Two dimensional projections of failure envelopes at various suctions. (Figure taken from Fredlund and Rahardjo, 1993).**

Equation (6) implies that shear strength is a linear function of suction. However, several studies have shown that this relationship is non-linear. Furthermore, this non-linearity is somewhat similar to the variation in  $\chi$  as a function of degree of saturation as in effective stress concept. Several different types of modifications have been proposed. Some of these modifications are based on the inclusion of a factor similar to that of degree of saturation (Vanapalli et al., 1996; Oberg & Sallfours, 1997) whereas other modifications deal with inclusion of factor related to suction (Abramento and Carvalho, 1989; Rassam and Cook, 2002). Examples of these variations are as follows:

Oberg & Sallfours (1997) :

$$\tau_f = c' + (\sigma_n - \mu_a) \tan \phi' + (S)(\mu_a - \mu_w) \tan \phi^b \quad (8)$$

Fredlund et al. (1996) and Vanapalli et al. (1996):

$$\tau_f = c' + (\sigma_n - \mu_a) \tan \phi' + (\Theta^\kappa)(\mu_a - \mu_w) \tan \phi^b \quad (9)$$

Abramento and Carvalho (1989):

$$\tau_f = c' + (\sigma_n - \mu_a) \tan \phi' + \alpha(\mu_a - \mu_w)^\beta \quad (10)$$

Rassam and Cook (2002):

$$\tau_f = c' + (\sigma_n - \mu_a) \tan \phi' + (\mu_a - \mu_w) \tan \phi - \varphi((\mu_a - \mu_w)_r - (\mu_a - \mu_w)_b)^\beta \quad (11)$$

$$\varphi = \frac{(\mu_a - \mu_w) \tan \phi - \tau_{sr}}{((\mu_a - \mu_w)_r - (\mu_a - \mu_w)_b)^\beta}$$

$$\beta = \frac{\tan \phi((\mu_a - \mu_w)_r - (\mu_a - \mu_w)_b)}{(\mu_a - \mu_w)_r \tan \phi - \tau_{sr}}$$

where S= degree of saturation;  $\Theta$ =normalized water content between saturation and residual water content;  $\alpha$ ,  $\kappa$ ,  $\beta$  are fitting constants; and  $\tau_{sr}$ =shear strength at residual suction.

Inclusions of degree of saturation or the normalized water content in Eqs. (8) and (9) by Oberg & Sallfours (1997), Fredlund et al. (1995) and Vanapalli et al. (1996) is on a conceptual basis. Like Bishop's formulation, these authors also reason that since water is present only in a fraction of the cross sectional area in unsaturated soils, the effect of soil suction needs to be reduced by the degree of saturation or the normalized water content. This also provides a mechanism to account for the variation in soil water retention

characteristics between soil types. The fitting factor “ $\kappa$ ” in Eq. (9) is based on the best fit of Eq. (9) to the experimental data.

Inclusions of the exponent function in Eqs. (10) and (11) by Abramento and Carvalho (1989) and Rassam and Cook (2002) is based on the best fit of Eq. (6) to the experimental data. Equations (10) and (11) are similar in that they are power function of suction. However, Eq. (10) starts with the shear strength at saturation and describes its increase with increase in suction whereas Eq. (11) starts with shear strength at residual water content and describes its decrease with a decrease in suction. Equations (10) and (11) imply that shear strength is not linearly related to soil suction as suggested by the original formulation by Fredlund and Morgenstern (1977). Since soil water content is related to soil suction through the water retention curves, Eqs. (10) and (11) are not different than Eqs. (8) and (9). If equations of water retention curve are substituted in Eqs. (8) and (9), it will also show a presence of non-linearity in shear strength vs. soil suction similar to that of Eqs. (10) and (11).

Recently, Garven and Vanapalli (2006) summarized 19 formulations (including four formulations listed above) that have been suggested in the literature for shear strength prediction of unsaturated soil (Table 1). These authors tested six equations that use soil moisture retention curves in their predictions. The authors assumed that if half of the predicted shear strength were within 15% of the measured value, then it was considered successful prediction. Tested equations included Eqs. (8), (9), and (11). The authors concluded that these three equations were successful 70, 17, and 7% of the times, respectively. The authors also gave the following relationship relating  $\kappa$  value in Eq. (9) to plasticity index ( $I_p$ ).

$$\kappa = 1.0 + 0.0975I_p - 0.0016I_p^2 \quad (12)$$

In all the above formulations relating shear strength to soil suction, it has been assumed that the friction angle is not influenced by soil suction or in other words it is constant. However, there have been reports that suggest that friction angle also varies with soil suction. In a suction controlled direct shear test, Feuerharmel et al. (2006) showed that internal friction angle increased with an increase in matric suction up to 150 kPa for two colluvium soils. These authors also reported that  $\phi^b$  values were higher than  $\phi'$  values thus suggesting that suction effects were more significant than that of net normal stress. Futai et al. (2006) showed that shear strength estimation based on moisture retention curve did not produce good predictions. Furthermore friction angle varied with soil suction. These authors suggested the following modification for the friction angle.

$$\phi(s) = \phi' + (\phi_{(\mu_a - \mu_w = \infty)} - \phi')(1 - 10^{b(\mu_a - \mu_w)}) \quad (13)$$

where  $\phi(s)$  is variation in friction angle with suction,  $\phi'$  is effective friction angle for saturated soil,  $\phi_{(\mu_a - \mu_w = \infty)}$  is maximum value of soil friction angle, and  $b$  is friction angle adjustment factor. Gallage and Uchimura (2006) studied the effect of hysteresis (wetting

Table 1: Relationships describing the effects of suction on shear strength. (Taken from Garven and Vanapalli, 2006).

Lamborn (1986)

$$\tau_{us} = (\mu_a - \mu_w) \theta_w \tan \phi'$$

Abramento & Carvalho (1989)

$$\tau_{us} = \alpha (\mu_a - \mu_w)^\beta$$

Lu (1992)

$$\tau_{us} = P_s \tan \phi'$$

Vanapalli et al. (1996)

$$\tau_{us} = (\mu_a - \mu_w) (\Theta)^\kappa \tan \phi'$$

Vanapalli et al. (1996)

$$\tau_{us} = (\mu_a - \mu_w) \left( \frac{\theta_w - \theta_r}{\theta_s - \theta_r} \right) \tan \phi'$$

Shen (1996)

$$\tau_{us} = \frac{(\mu_a - \mu_w)}{1 + d \cdot (\mu_a - \mu_w)} \tan \phi'$$

Oberg & Sallfours (1997)

$$\tau_{us} = (\mu_a - \mu_w) (S) \tan \phi'$$

Xu (1997)

$$\tau_{us} = k^n (\mu_a - \mu_w)^{m-n+1} \tan \phi'$$

Yu (1998)

$$\tau_{us} = \frac{(\mu_a - \mu_w) \tan \phi'}{\cot \alpha_1 + \frac{(\mu_a - \mu_w)}{\beta_1}}$$

Boa et al. (1998)

$$\tau_{us} = (\mu_a - \mu_w) \left[ \frac{\log(\mu_a - \mu_w)_r - \log(\mu_a - \mu_w)}{\log(\mu_a - \mu_w)_r - \log(\mu_a - \mu_w)_b} \right] \tan \phi'$$

Khalili & Khabbaz (1998)

$$\tau_{us} = (\mu_a - \mu_w) (\chi) \tan \phi'$$

$$\chi = \left[ \frac{(\mu_a - \mu_w)}{(\mu_a - \mu_w)_b} \right]^{-0.55}$$

Rassam and Williams (1999)

$$\tau_{us} = (\mu_a - \mu_w)^\beta$$

if  $(\mu_a - \mu_w) < AEV$ , else

$$\tau_{us} = (\gamma + \lambda(\mu_a - \mu_w)) \cdot [(\mu_a - \mu_w) - AEV]^{\beta_1} + (\mu_a - \mu_w) \tan \phi'$$

Xu and Sun (2001)

$$\tau_{us} = (\mu_a - \mu_w)_b^{1-\zeta} \cdot (\mu_a - \mu_w)^\zeta \tan \phi'; \quad \zeta = \frac{2D_s}{3} - 1$$

Rassam and Cook (2002)

$$\tau_f = c' + (\sigma_n - \mu_a) \tan \phi' + (\mu_a - \mu_w) \tan \phi - \varphi((\mu_a - \mu_w) - (\mu_a - \mu_w)_b)^\beta$$

$$\varphi = \frac{(\mu_a - \mu_w) \tan \phi - \tau_{sr}}{((\mu_a - \mu_w)_r - (\mu_a - \mu_w)_b)^\beta}$$

$$\beta = \frac{\tan \phi((\mu_a - \mu_w)_r - (\mu_a - \mu_w)_b)}{(\mu_a - \mu_w)_r \tan \phi - \tau_{sr}}$$

Miao et al. (2002)

$$\tau_{us} = \frac{a(\mu_a - \mu_w)}{1 + \frac{(1-a)}{P_{at}} \cdot (\mu_a - \mu_w)}$$

Schick (2004)

$$\tau_{us} = \frac{(\mu_a - \mu_w)}{a_1 + b_1 \cdot (\mu_a - \mu_w)} \tan \phi';$$

$$a_1 = \tan(\phi' - 90^\circ)$$

Xu (2004)

$$\tau_{us} = (\mu_a - \mu_w)_b^{1-\zeta} \cdot (\mu_a - \mu_w)^\zeta \cdot \tan \phi';$$

$$\zeta = D_s - 2$$

Tekinsoy et al. (2004)

$$\tau_{us} = \tan \phi' \left( (\mu_a - \mu_w)_b + P_{at} \right) \cdot \ln \left[ \frac{(\mu_a - \mu_w) + P_{at}}{P_{at}} \right]$$

Lee et al. (2005)

$$\tau_{us} = (\mu_a - \mu_w) \cdot \tan \phi',$$

*if*  $(\mu_a - \mu_w) < AEV$ , *else*

$$\tau_{us} = AEV \cdot (\tan \phi') + [(\mu_a - \mu_w) - AEV] (\theta^\kappa) [1 + \lambda(\sigma_3 - \mu_w)] \tan \phi'$$

$\theta_s$  - saturated water content  
 $\zeta$  - fractal dimension  
 $D_s$  - pore distribution factor  
 $P_{at}$  - atmospheric pressure (101.3 kPa)  
 $P_s$  - expansive force  
 $S$  - degree of saturation  
 $S_r$  - residual degree of saturation  
 $\kappa, \gamma, \lambda, \beta, \beta_1, \alpha$  - fitting parameters  
 $a, b_1, d, k$  - fitting parameters  
 $m, n$  - parameters related to the fractal dimensions  
 $\chi$  - Bishop's fitting parameter  
 $AEV$  - the air entry value an equivalent net normal stress

## LEGEND

$\tau_{us}$  - shear strength contribution due to suction

$\tau_{sr}$  - contributions due to shear strength at residual suction

$\phi'$  - effective angle of internal friction

$(\mu_a - \mu_w)$  - suction

$(\mu_a - \mu_w)_b$  - air entry value

$(\mu_a - \mu_w)_r$  - residual suction

$\Theta$  - normalized water content or degree of saturation

$\theta_w$  - volumetric water content

and drying) on unsaturated shear strength and found no significant effect of suction on friction angle but apparent cohesion was higher for wetting curve than for drying curve at the same suction.

### **Stiffness of Unsaturated Soils**

This section was put together by Drs. Tuncer Edil, Craig Benson, and Auckpath. Sawangsuriya of the University of Wisconsin

Stiffness of soil is an important engineering property, commonly used in geomechanical design and analysis. Moreover, the widespread adoption of mechanistic-empirical design procedures (NCHRP 1-37A 2004) and performance-based specifications for flexible pavement structures use pavement layer modulus as a key material property. Compacted soils are often used in pavement subgrades and embankments and typically are initially unsaturated. Field data suggest that most soils compacted above the water table never reach saturation and thus normally remain in an unsaturated state (Roberson, 2002). Moreover, the moisture and suction regimes of unsaturated soils can vary in response to the loading and environmental conditions while in service. The stiffness is greatly influenced by the state of stress and is also sensitive to the moisture and suction variations. As a result, the stiffness of compacted soils can be expected to change in response to changing moisture conditions. Therefore, the stiffness-suction-moisture content relationship of compacted soils is needed in order to describe their unsaturated behavior during construction and subsequently in service.

Previous studies have focused primarily on the stiffness and (or) modulus-moisture relationship of compacted soils in the as-compacted state (Li and Selig, 1994; Marinho et al., 1996; Tian et al., 1998, Muhanna et al., 1999; Butalia et al., 2003, Li and Qubain, 2003; Ooi and Pu, 2003; Yuan and Nazarian, 2003). Relatively few studies have been reported regarding such relationships corresponding to in-service moisture changes (Sauer and Monismith, 1968; Fredlund et al., 1977; Edil and Motan, 1979; Khoury and Zaman, 2004). Moreover, the relationship between modulus and suction has not been extensively explored for compacted soils either in the as-compacted or in the post-compaction states. Until recently, the dependency of modulus on suction and moisture of unsaturated soils has not yet been expressed in a quantitative relationship. In particular, a mathematical model for relating resilient modulus to the soil-water characteristic curve has not been reported in the literature. However, a recent doctoral thesis by Sawangsuriya (2006) relates small-strain modulus to the soil-water characteristic curve.

Based on the more detailed literature review (see Appendix A), it appears that the theoretical concepts and fundamental basis of stiffness and suction individually and separately have been well-established in the literature. The significant issues that emerged from the literature review are summarized as follows:

1. Use of small-strain modulus provides several benefits, e.g. most tests are simple, rapid, repeatable, and nondestructive.

2. Stiffness of particulate materials such as soils is directly related to the behavior of contacts and confining pressure.
3. Different factors that affect the modulus of soil at small strains have been extensively investigated and reported in the literature in such a way that they can be reasonably implemented to develop a relationship for the small-strain modulus of a given soil. Those factors include the current state of the soil sample (e.g. stress state, overconsolidation ratio, density, void ratio, microstructure), anisotropy, degree of saturation, aging, cementation, and temperature.
4. A general expression of the small-strain modulus for dry or saturated soils is well-established and can be adopted to form a basis for further developing a model to predict the modulus of unsaturated soils.
5. Significant factors that influence the soil-water characteristic curve are soil type and compaction conditions, such as compactive effort and initial water content.
6. The relationship between equilibrium soil suction value and average Thornthwaite climatic index value provides a basis for predicting the modulus changes caused by moisture variations under given environmental and climatic conditions while in service.
7. The unsaturated soil modulus is mainly related to the soil moisture characteristics. Most importantly, the soil suction and moisture content are two key factors that strongly influence the modulus of unsaturated soils.
8. The modulus of compacted soils is significantly impacted by suction and moisture. In addition, the modulus of compacted soils during construction is anticipated to be different from that after construction where the moisture regime tends to vary over time.
9. According to the physics of unsaturated particulate materials, the capillary menisci formed at the particle contacts creates an additional interparticle force to the particulate skeleton, resulting in an increase of modulus of contacts and the particulate skeleton. In other words, the modulus of unsaturated particulate media increases as the matric suction increases due to increased capillarity or surface tension forces between particles. Besides the capillary force, the particle surface absorptive force (i.e., water is attracted to mineral surface by electrochemical attraction) is another mechanism, especially in clayey soils.

Modulus measurements using wave propagation techniques have become a promising means to assess the small-strain modulus of compacted soils both in the laboratory and in the field (Kim and Stokoe, 1992; Kim et al., 1997; Yesiller et al., 2000; Nazarian et al., 2003). An elastic wave propagation technique called elements has been increasingly employed in a variety of geotechnical laboratory tests (Dyvik and Madshus, 1985; Thomann and Hryciw, 1990; Souto et al., 1994; Fam and Santamarina, 1995; Zeng and Ni, 1998; Fioravante and Capoferri, 2001; Pennington et al., 2001; Mancuso et al., 2002; Davich et al., 2004; Sawangsuriya et al., 2006; Swenson et al., 2006). For the field measurement of small-strain modulus, the soil stiffness gauge (SSG) can be employed as an alternative test because it provides simple, rapid, and direct means of nondestructively assessing in-place stiffness and modulus of compacted soils.

The key advantage of these techniques over conventional modulus tests is their ability to rapidly and nondestructively assess the soil modulus. Furthermore at small strain levels, soil exhibits linear and elastic behavior. Typically, the associated strain levels corresponding to many proposed geotechnical engineering structures such as pavements are however much larger (Mair, 1993; Sawangsuriya et al., 2005). For example, the strain levels of the bender element are below  $5 \times 10^{-3}\%$  and the SSG  $\sim 10^{-3} - 10^{-2}\%$ , whereas the strain levels of the resilient modulus commonly used in the design of flexible pavement structures ranges from 0.01% to 0.1% (Sawangsuriya et al., 2005). In order to correct the small-strain modulus measurements to such relevant levels of strain amplitude imposed by the proposed structure, the modulus-strain relationship (a.k.a. strain-dependent modulus degradation curve) can be employed for a given operating stress level and soil type. Sawangsuriya et al. (2005) and Sawangsuriya (2006) propose a method to correlate small-strain modulus to resilient modulus. However, this method needs to be verified by resilient modulus testing under similar conditions.

Since the modulus-suction-moisture relationship of the compacted soils at the initial conditions is different from that after they are subjected to climatic and environmental factors, the influence of moisture and suction on the resilient modulus of compacted soils need to be explored in two stages, as-compacted state (i.e., during construction) and post-compaction state (i.e., in-service state after construction subject to moisture regime changes). In the as-compacted state, the relationship of modulus, matric suction, and compaction moisture content can be investigated along the specified compaction curves. In the post-compaction state, the small-strain modulus can be evaluated under the desorption (drying) soil water characteristic curve. The literature summary is presented separately for these two stages.

**As-Compacted State:** Typical earthwork compaction acceptance criteria are currently based on the specified target dry density of the placed earthen materials achieved through appropriate moisture content and compaction energy. According to this approach, by achieving a certain dry density using an acceptable and cost-effective level of compaction energy assures attainment of an optimum level of structural properties and also minimizes the available pore space and thus limits future moisture content changes and settlement. In important projects, various laboratory and field tests are employed to relate the achieved level of compaction to mechanical properties.

Current mechanistic-empirical design procedures for structural design of flexible pavements require the mechanical properties of pavement material such as modulus. To successfully implement a mechanistic-empirical design procedure and to move toward performance-based specifications, a cost-effective, reliable, and practical means to assess the modulus of pavement layer materials rapidly and directly is of interest since the modulus of pavement layers plays a key role in the overall quality and performance of pavements.

One of the potential approaches to rapidly and directly assess soil modulus both in the laboratory and field is to employ the small-strain modulus tests. In pavement engineering, the application of small-strain modulus tests to assess the modulus of

pavement materials and structural variability for pavement performance has increased dramatically (Kim and Stokoe, 1992; Souto et al., 1994; Kim et al., 1997; Chen et al., 1999; Nazarian et al., 1999; Fiedler et al., 2000; Yesiller et al., 2000; Zeng et al., 2002; Nazarian et al., 2003; Sawangsuriya et al., 2005). The main advantage of small-strain modulus tests is the ability to non-invasively and nondestructively assess the modulus of pavement materials at the surface or under a free-field condition (i.e., near-zero confining pressure). Laboratory test methods are also available for small-strain modulus tests that can reproduce similar results to those measured in the field.

Unsaturated soil behavior plays a significant role in the mechanical properties of compacted pavement subgrades. Typical compaction specifications require that subgrade soils be compacted in the field at or near optimum water content and to a percentage of the maximum dry unit weight (i.e., relative compaction). Consequently, compacted subgrade soils are in an unsaturated state during construction. In unsaturated soil mechanics, soil suction is an important parameter which governs the state of stress. However, soil suction is not routinely quantified in geotechnical engineering practice. Furthermore, there is no unique relationship between modulus and dry unit weight alone. Similar modulus under the same stress condition can correspond to several values of dry unit weight depending on current moisture content and suction. A relationship between modulus, dry unit weight, moisture content, and suction should be developed for different soil types and compaction conditions. Understanding the influence of these factors on soil modulus will enhance the implementation of the small-strain modulus in monitoring the mechanical property quality of subgrades during earthwork construction monitoring (i.e., in the as-compacted state).

A number of studies have reported the importance of three factors affecting the modulus of compacted subgrade. Those factors include dry unit weight, moisture content or degree of saturation, and compaction conditions (i.e., compaction efforts, method of compaction) for a given soil. The influence of each factor on the modulus of soils used in highway construction has been well-documented by Shackel (1973). In general, the modulus increases with the dry unit weight but decreases as the molding moisture content increases. The difference in compaction conditions cause the alterations in soil structure and hence the modulus.

Because of its rapid and simple approach, the non-destructive evaluation using seismic waves are often employed by monitoring the P- and (or) S-wave velocities and thus corresponding to small-strain Young's and (or) shear moduli are determined if the total mass density is known. Many studies reported the correlation of wave velocities and small-strain moduli with the dry unit weight, water content, degree of saturation, and strength parameters (Sheeran et al., 1967; Marinho et al., 1996; Yesiller et al., 2000; Nazarian et al., 2003; Yuan and Nazarian, 2003; Ooi and Pu, 2003). Besides dry unit weight, moisture content or degree of saturation, and compaction conditions, matric suction also governs the modulus behavior of compacted soils, which are typically in the unsaturated state. Matric suction is the potential energy of soil water created due to curved interfaces and surface adsorptive forces and constitutes about 40-75% of total suction in fine-grained soils (Babu et al., 2005).

Both dry unit weight and moisture content reflect the current physical state of the soil, while matric suction defines the state of stress in unsaturated soils and varies with the changes in moisture content. Since modulus is sensitive to the state of stress within a subgrade and the matric suction impacts the state of stress, it is crucial to understand the influence of matric suction on modulus. Past research suggested that the modulus of unsaturated soils is strongly influenced by matric suction and a good correlation was also observed between modulus and matric suction (Sauer and Monismith, 1968; Fredlund et al., 1977; Edil et al., 1981; Khoury et al., 2003; Yang et al., 2005). The matric suction was found to be a key factor associated with the modulus of compacted soils. Appendix A-7 summarizes the findings from several investigators. In addition, Edil (1973) indicated that the matric suction is a fundamental soil parameter which controls the stress-strain response and hence the modulus of soils. Therefore, the matric suction should be treated as an independent parameter in establishing the relationship among modulus, matric suction, dry unit weight, and moisture content.

**Post-Compacted State:** Subgrade moisture is sensitive to rise in water table, infiltration, or evaporation of water. Changes in subgrade soil moisture and hence in its stiffness or modulus can occur seasonally over the service life of a pavement system in addition to the initial moisture conditions imposed during the construction period. The importance of variation in subgrade modulus with moisture and suction, however, has not been addressed systematically to reflect mechanical behavior of compacted subgrades after construction (i.e., during post-compaction state). Severe pavement damage (i.e., rutting and cracking) is often attributed to changes in subgrade modulus due to moisture and suction variations caused by climatic variations (i.e., climate-controlled moisture response of subgrade). If a pavement is constructed during wet season or an excessive amount of water is used during compaction of subgrade, a drying cycle follows the construction as the subgrade reaches moisture equilibrium with the ambient conditions. Alternatively, if a pavement is laid down during dry season or compacted dry, a wetting process begins following the construction. Both of these processes may result in significant volume change (settlement or swelling). Additionally, wetting cycle also may result in increased shear deformations in the subgrade under traffic loads.

Despite clear evidence of the unsaturated behavior in pavement subgrades, the response of compacted subgrades has rarely been explored on the basis of unsaturated soil mechanics. There has not been a widespread adoption of unsaturated soil mechanics in geotechnical profession except in some specific areas associated with collapsible and expansive soils. The long-term subgrade performance assessment also has not been based on unsaturated soil mechanics. The influences of suction and moisture must be considered in pavement subgrade performance assessment in such a way that the anticipated in-service conditions are taken into account. Laboratory test protocols and methods need to be developed for identifying and examining factors and conditions associated with the variation of soil modulus with moisture and suction in order to improve the pavement subgrade performance assessment.

The concept of soil suction provides a fundamental basis that reflects the modulus behavior of a soil (Edil, 1973; Edil and Krizek, 1976). Since the energy of a soil-water system can be expressed as a function of its soil-water characteristic curve (SWCC), soil suction, which is the difference between the free energy of the water in the soil and that of pure water in a free surface condition, represents the work required to remove an infinitesimal quantity of water from the soil. With the exception of cementation bonds, the soil suction is a measure of the combined effects of the forces holding the water in the soil and hence it can be considered to include implicitly the effects of the fundamental interaction forces that influence the deformation characteristics of the soil (Edil, 1973).

Influence of moisture and suction change on the mechanical behavior of unsaturated soils has been recognized in the geotechnical profession especially with respect to the behavior of compacted subgrade beneath the pavement. The variation of moisture and suction in pavement subgrade occurs seasonally over the service life of pavement as well as spatially, typically varying along the roadway length. For a given soil, the SWCC is often used to describe the suction changes in response to moisture changes. A number of experimental investigations have focused on the relationship of the suction and (or) moisture with modulus of soil in the post-compaction state (Fredlund et al., 1977; Edil and Motan, 1979; Edil et al., 1981; Motan and Edil, 1982; Mancuso et al., 2002; Costa et al., 2003; Inci et al., 2003; Khoury and Zaman, 2004; Sawangsuriya et al., 2005). Significant findings from these studies are summarized as the following.

Edil and Motan (1979), Edil et al. (1981), and Motan and Edil (1982) investigated the effects of compaction moisture content, degree of saturation, and suction on mechanical properties of subgrade soils in Wisconsin. Their results indicated that the resilient modulus as well as other moduli increased as the degree of saturation decreased to 75% and the soil suction increased up to approximately 800 kPa, beyond which a decrease in resilient modulus was observed. They also found that soil matric suction is a fundamental parameter in characterizing the moisture state and is proposed as a parameter to reflect the influence of soil type and fabric, compaction, climatic variation, and fluctuation of groundwater table on the mechanical behavior of soils better than compaction moisture content or degree of saturation alone. Finally, they suggested the use of the soil matric suction as the basic soil moisture parameter in addition to the compaction moisture content for pavement subgrade quality control and performance evaluation.

Mancuso et al. (2002) developed the 3-D relationship of the small-strain shear modulus ( $G_o$ ), the mean net stress, and the matric suction for the optimum and the wet of optimum compacted silty sand tested in the suction-controlled resonant column apparatus. They found that  $G_o$  measured at a constant mean net stress increased with suction for both optimum and wet of optimum compacted soils and the modulus response exhibited the typical S-shape of the SWCC. They also indicated that the difference in soil fabric due to molding water content significantly affected the  $G_o$ -matric suction relationship. The wet compaction induces a weaker soil fabric with respect to optimum compaction and thus the modulus increases with decreasing initial compaction water content (Mancuso et al. 2002).

Costa et al. (2003) evaluated the influence of matric suction on the results of plate load tests conducted in an unsaturated lateritic soil. Their results indicated that soil modulus increased substantially as suction increased. Moreover, their field test results showed the small increases in matric suction resulted in substantial increases in bearing capacity of the soil-plate system and the rate of settlement exhibited a non-linear decreasing trend with increasing matric suction. Inci et al. (2003) conducted an experimental investigation of  $G_o$  of compacted clayey soils subjected to drying after compaction as well as the effects of soil type, compaction conditions, and degree of saturation on  $G_o$ . They found that  $G_o$  increased as the plasticity and the degree of saturation of the soils decreased and  $G_o$  was significantly affected by the initial compaction conditions.

Khoury and Zaman (2004) developed correlations among resilient modulus ( $M_r$ ), moisture content, and matric suction for compacted subgrade clayey and sandy soils upon drying and wetting. Their results indicated that  $M_r$ -moisture content relationships exhibited a hysteretic behavior due to wetting and drying. The clayey soil is more susceptible to moisture variation than the sandy soil and the changes in  $M_r$  values and suction are influenced by the initial compaction water content. They also developed the 3-D relationship of  $M_r$ , moisture, and soil suction in order to understand seasonal variations in pavement performance. Sawangsuriya et al. (2005) presented a preliminary relationship between  $G_o$  and SWCC of a compacted clayey sand. Their result showed that  $G_o$  increased with increasing matric suction but decreased with increasing moisture content. Furthermore,  $G_o$  of soil compacted near optimum was greater than  $G_o$  compacted wet of optimum for a given matric suction or moisture content. They also recommended the equilibrium soil suction and moisture be incorporated into the modulus of unsaturated pavement subgrade in order to improve the prediction of the variation in modulus with moisture conditions as a result of climatic and environmental fluctuations in the long-term pavement evaluation.

Moisture changes in subgrade soils beneath pavements have been investigated by Thadkamalla and George (1995). They observed that the average moisture content at the shallow depth of the subgrade layer increased and the fluctuation of moisture content decreased over time (Thadkamalla and George, 1995). The subgrade soils beneath pavements increased its moisture content to approximately 20 to 30% higher than its plastic limit and reached equilibrium condition during the first 3 to 5 years of service (Uzan, 1998). Moreover, the moisture content of the subgrade after construction maintains a varying equilibrium moisture content with the environment (Thadkamalla and George, 1995; Uzan, 1998). Past studies (Russam and Coleman, 1961; Edil and Motan, 1979; Lytton, 1997) also indicated that soil suction is known as a fundamental soil parameter that can reflect the influence of climate on the moisture regime and it can be correlated with a climatic moisture index such as Thornthwaite moisture index (Thornthwaite, 1948).

Pavement structures are constructed over fine-grained compacted soils which are unsaturated when compacted and may not become saturated during their service life. The moisture and suction conditions can vary over time and space due to climatic and

environmental fluctuations. Consequently, the soil stiffness and (or modulus) is expected to change over time in response to temporal changes in moisture and suction conditions in addition to the initial moisture conditions imposed during construction. The modulus under unsaturated conditions has not been extensively explored for compacted soils both in the as-compacted and post-compaction states. Furthermore, the dependency of modulus on suction and moisture of unsaturated soil has not yet been expressed in a quantitative relationship.

The main conclusions from the literature review, including the recently completed doctoral thesis on the subject by Sawangsuriya (2006) are as follows:

- 1) Mathematical relationships are available to quantitatively describe the small-strain modulus of unsaturated compacted soils in both as-compacted and post-compaction states.
- 2) The modulus of compacted soils depends primarily on matric suction and to a lesser degree on compaction moisture content and dry unit weight.
- 3) Low-strain modulus normalized with initial compaction moisture content correlates semi-logarithmically with matric suction for a given compacted soil.
- 4) A generalized modulus relationship that incorporates the effect of all compaction parameters (i.e., compaction moisture content and compaction energy) and soil type as a function of matric suction has been developed. This general relationship is based on normalized modulus, normalized moisture content, and normalized dry unit weight by their values at optimum moisture content at standard Proctor effort.
- 5) Based on the well-established expression of small-strain modulus for dry or saturated soils and the measured soil-water characteristic curve, a relationship has been proposed for modulus as a function of soil type, compacted fabric, solid-water contact, and stress state. The relationship can be employed along with the fitting parameters in predicting small-strain modulus of unsaturated compacted soils.
- 6) The effect of compaction moisture content on the fitting parameters is more significant than that of compaction energy. Moreover, the fitting parameters correlate reasonably well with percent sand and fines as well as the plasticity index.

Based on the literature review on stiffness of unsaturated soils, the following recommendations are provided for future studies on this topic:

- 1) Hysteretic effects might be considered in developing the modulus-suction-moisture relationship because the in situ soil conditions can change with time due to the effects of weathering, wet-dry, and freeze-thaw conditions.
- 2) Additional test soils are recommended to confirm the proposed relationship between the fitting parameters and the soil index properties.
- 3) Higher matric suctions (i.e., greater than 1,000 kPa) might be considered to develop the modulus-suction relationship at the very low moisture contents and very high suctions.
- 4) A strain-dependent modulus degradation curve (i.e., a plot of shear modulus versus shear strain amplitude) can be developed in order to adjust the measured small-strain modulus to the modulus corresponding to larger strains such as the resilient modulus,

commonly used in the design of flexible pavement structure. To obtain such a degradation curve, the resilient modulus tests must be performed under the identical stress conditions (i.e., both matric suction and confining pressure).

## CHAPTER III: MATERIALS AND METHODS

Following Sections were put together by Drs. Satish Gupta and Andry Ranaivoson of the University of Minnesota.

### Water Retention Characteristics

Water retention characteristics curves of the four soils were measured using the Tempe Cells and the pressure plate apparatus. Procedure for water retention characterization was very similar to the procedures used by the authors and reported to Mn/DOT in our previous reports (Gupta et al., 2004; Singh et al., 2006). Briefly the procedure involved bringing the soil sample to optimal water content, packing the soil in metal cores to 100% or 105% of standard Proctor density, and then running the water retention curves. Both optimal water contents and standard Proctor density values were provided by Mn/DOT.

Since soil samples were collected under natural conditions by Mn/DOT, water content of all soil samples was greater than the optimal water content needed for packing. Thus to achieve a given level of water content, we air dried a known amount of soil on the laboratory bench. In some case, we overshot the air drying and thus to achieve the required soil water content we sprayed a known quantity of water with an atomizer. Once the soils were brought to given water content, we bagged the soils and allowed the water to distribute uniformly in the sample. This process took two to three days. After equilibration, a known quantity of soil was packed to a given density (100% or 105% of standard Proctor density) in 7.6 cm diameter and 7.6 cm high metal cores. These cores were saturated over night and then desorbed in a pressure chamber. Application of air pressure forced the excess water over and above soil's retention capacity at that pressure to drain. Once equilibrium was reached, the soil was subjected to next air pressure and the outflow was collected and measured. This process was repeated until the applied air pressure was equivalent to the air entry value of the ceramic plate. At that time, the soil core was taken out of the pressure chamber, weighed, and then oven dried at 105 °C. Water content at any pressure was then back calculated from the final water content of the soil core and the volume of outflow corresponding to each pressure step.

Drying curves covered a pressure range of 10.2 cm to 15,300 cm of water head. Several different apparatuses were used to cover the full range:

- Tempe cell apparatus: pressure range from 10.2 to 1020 cm H<sub>2</sub>O,
- 5-bar pressure plate apparatus: pressure range from 102 to 3,060 cm H<sub>2</sub>O,
- 15-bar pressure plate apparatus: pressure range from 1,020 to 15300 cm H<sub>2</sub>O.

The pressure ranges overlapped and thus helped verify the accuracy of the results obtained from three different soil cores in three different pressure apparatuses.

## Shear Strength Testing

We followed the ASTM standard test method for triaxial compression test on cohesive soil (D 2850 – 95) for shear strength measurements. The procedure involved making the specimen at given optimal water content and given density, bringing the soil specimen to a given suction, and then shearing the specimen at a given confining stress ( $\sigma_3$ ).

**Specimen Preparation:** Specimen was prepared by first air drying the bulk soil to known water content as described earlier and then packing a known quantity of soil in a cylindrical split mold to the target density (Fig. 5). The split mold was 38.1 mm in diameter and 15.2 cm long. For high clay soil (DI TH 23), the mold was 25.4 cm long. Soil packing in the split mold was done by pushing plungers at both ends of the mold. This procedure has been shown to give more uniform packing compared to top packing using one plunger (Gupta and Larson, 1979). The final dimensions of the specimen were aimed to get 2:1 ratio for length to diameter (38.1 mm in diameter and 77.0 mm in length). Quantity of the soil was calculated based on the water content of the soil and the desired density (98% or 103% of standard Proctor density). After packing, a rubber sleeve was slipped over each specimen (Fig. 6). A total of 10 specimens were prepared for shear strength measurements at any given suction. This corresponded to three replications at three confining stresses ( $\sigma_3=6.9, 27.6, \text{ and } 55.2 \text{ kPa}$ ) plus one specimen for water content measurement.

**Specimen Saturation and Desorption:** After preparation, ten specimen soil cores wrapped in a rubber sleeve were set on a pressure plate that was covered with a layer of fine soil to ensure continuity between the cores and the plate. A 15-bar pressure plate was used for specimens that will be brought to 5,000 cm suction whereas a 3-bar pressure plate was used for suction values less than 5000 cm. The ceramic plate and specimens were allowed to saturate overnight in a pressure chamber. To insure there was no trapped air in the specimens, water level in the chamber was raised to the soil core height in three stages. This step took up several hours with approximately three to four hours in between stages. The saturated cores were left overnight after which the chamber was drained by siphoning. The chamber was then closed and the compressed air at a given pressure was pumped into the chamber. The specimens were allowed to desorb for about 3 to 10 days depending upon the soil and the air pressure applied (desired suction) until there was no water flow out of the chamber and an equilibrium was reached (Fig. 6). Longer desorption time was needed for high clay soils at higher suctions.



**Figure 5: Split mold used to construct specimens. Mold diameter was 3.81 cm.**



**Figure 6: Molded soil specimens with rubber sleeves on the pressure plate in a pressure chamber. The pressure chamber was used to bring specimens to a given soil suction.**

**Triaxial Testing:** After equilibration, the specimens were taken out of the pressure chamber and specimen dimensions (length, diameter) along with weight measurements were taken. Diameters of the specimens were corrected for rubber sleeve thickness and then length and corrected diameter were entered into the computer that was hooked to the loading frame for shear testing. The specimens were placed on a plastic disc at top of the pedestal in the triaxial chamber. The rubber sleeve from the specimen was then stretched over the pedestal and secured in place with an o-ring. At top of the specimen, a plastic disc along with a metal cap was also placed and the rubber sleeve stretched to cover the cap. Again, an o-ring was used to secure the sleeve to the top cap. A ball bearing was then placed on top of the metal cap and the plunger sliding from the upper portion of the triaxial chamber was gently lowered to touch the top of the metallic ball. The whole assembly was then transferred to the loading frame where a second metallic ball was placed on top of the plunger to uniformly distribute the load from the loading frame. The chamber was then secured at its base with three locks and an o-ring, which prevented any leakage of air used to apply confining pressure on the specimen. The triaxial chamber was connected to an air compressor for supply of compressed air (Fig. 7).

Shear testing was done at three confining stresses ( $\sigma_3=6.9$  kPa, 27.5 kPa, and 55.2 kPa) at each suction. After the soil specimen was pressurized, load was applied with the cross bar of the loading frame until (i) the specimen failed, (ii) the pre-set limits of the strain were met, or (iii) the limit of the load cell was reached. The load cell used in these measurements was a 10kN load cell. Specimens were sheared at 5.8% strain per minute (Fig. 8). Applied load was recorded every tenth of a second. A loading curve was displayed on the computer screen with load values in kgf on the y-axis and vertical strain in mm on the x-axis. In shearing mode, the curve showed a peak load while in bulging mode the curve went to a maximum load. The shearing mode occurred in general with low clay soil (MnROAD and Red Wing soils) and/or at high suctions (5,000 cm and 1,000 cm) while the bulging mode occurred with high clay and/or at low suctions (100 cm, 50 cm, and saturated). Figures 9 and 10 show the variation in deviator stress ( $\sigma_1-\sigma_3$ ) vs. strain for two types of samples.

The computer output consisted of several parameters:

- Time, every tenth of a second
- Load (kgf)
- Compression stress ( $\text{kgf/cm}^2$ ); load divided by specimen cross-sectional area
- Extension (mm); movement of plunger
- Percent compression strain; percent of plunger movement relative to specimen length



**Figure 7: Equilibrated soil specimen ready for shearing in a triaxial cell.**



**Figure 8: Sheared soil specimen.**

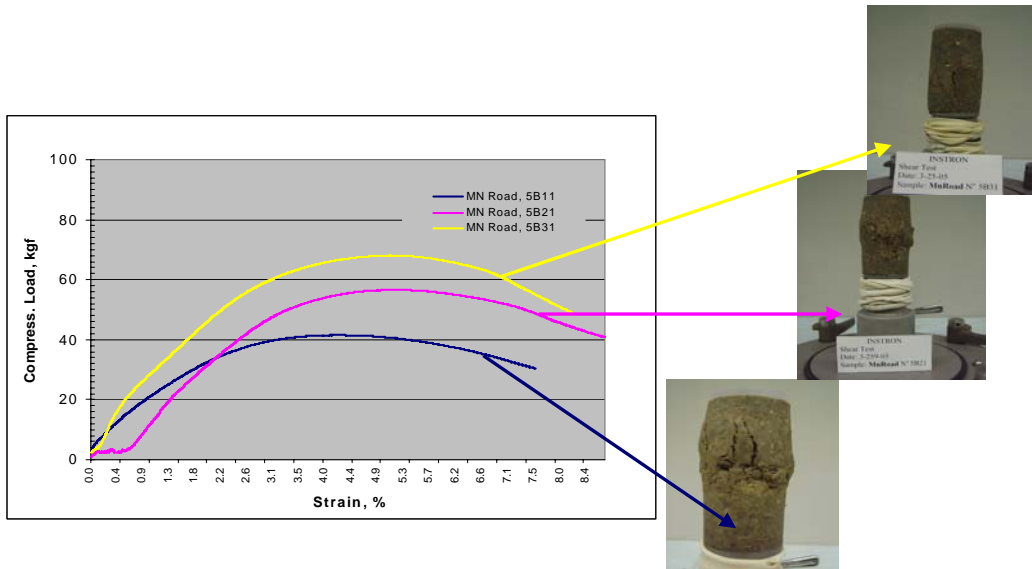


Figure 9: Variation in deviator stress as a function of strain for three MnROAD specimens at 5 kPa suction and a confining stress 6.9 kPa.

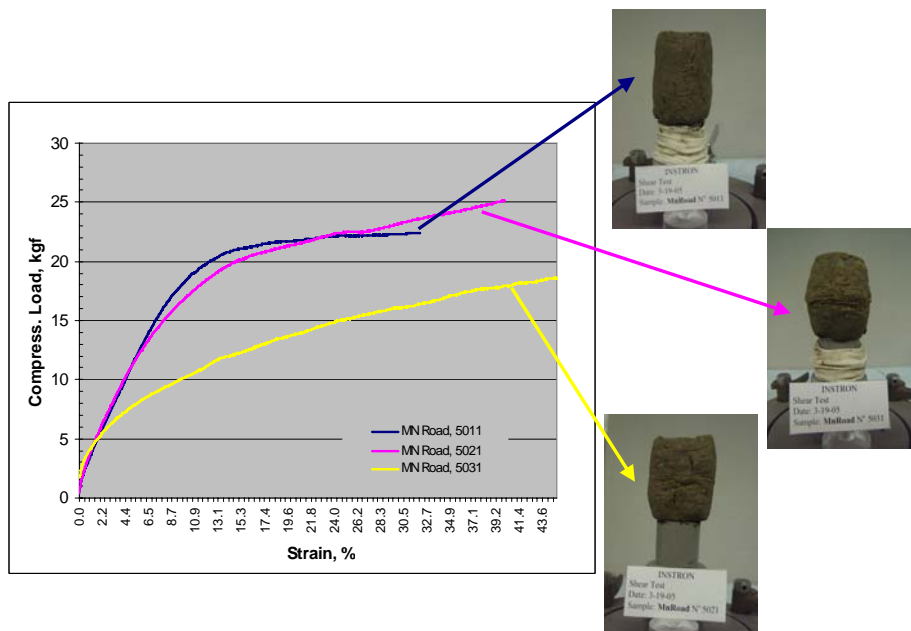


Figure 10: Variation in deviator stress as a function of strain for three MnRoad specimens at 0.5 kPa suction and a confining stress 6.9 kPa.

**Deviator Stress at 1% and 5% Strain:** One of the main objectives of this study was to see if tangent or secant modulus on the specimen at small strain can be an indicator of the resilient modulus of the specimen. We selected 1% and 5% strain to estimate the deviator stress on the specimens. These values were manually read from the computer output of deviator stress vs. strain.

### **Stiffness Testing**

This section was written by Drs. Tuncer Edil, Craig Benson, and Auckpath Sawangsuriya of the University of Wisconsin

Four subgrade soils having the plasticity index ranging between 0 and 52 are tested in this study. They include: Duluth TH23 Slopes (A-7-6(60)), Red Lake Falls (A-4(9), A-7-6(23)), Red Wing (A-4(0)), and MnROAD (A-4(3), A-6(5)). The characteristics of the soil samples are given in Table 2. All samples were collected and delivered to the University of Wisconsin-Madison Laboratories by Mn/DOT. All test soils were compacted at two specified densities (98% and 103% of the maximum density using standard Proctor) at the optimum water content. Appendix B provides the description of the specimen preparation. Three levels of matric suctions including 0, 22 psi (154 kPa), 50 psi (350 kPa) were induced in these specimens. By combining all testing parameters (density, matric suction, and soil type), a total number of specimens are 24. In order to establish the equilibrium matric suction, the compacted specimens were initially saturated and then subjected to desorption to the specified matric suctions along the soil-water characteristic curve. Time to achieve the equilibrium condition varied depending on several factors (e.g. hydraulic conductivity of soil and specimen size). After the equilibrium condition had been established, the specimens were subjected to resilient modulus ( $M_r$ ) testing. The small-strain shear modulus of the specimens measured by the wave propagation method using bender elements were conducted following the  $M_r$  test. Finally, the matric suction was measured with the thermal dissipation sensor on the specimens to obtain an independent value other than the assumed induced suction.

The flowchart of the testing program is presented in Fig. 11. The testing program is divided into three phases: (i) specimen suction conditioning, (ii) stiffness testing, and (iii) matric suction determination. Details of each phase are discussed in the following section.

**Specimen Suction Conditioning-Soil-Water Characteristic Curve:** The drying (desorption) soil-water characteristic curve (SWCC) of the compacted soil specimens was determined from a developed test apparatus under a constant net confining pressure of 35 kPa (Sawangsuriya, 2006). Additionally, 3 to 6 more data points at the dry end of the SWCC ( $> 1,000$  kPa) were also included from the chilled mirror hygrometer test assuming that there is not a substantial effect of the net confining pressure on the SWCC at very high matric suctions (see also Hoyos et al., 2005; Huat et al., 2005).

**Table 2: Properties of Test Soils**

Properties	Silt	Lean clay-1	Lean clay-2	Fat clay
Source	Red Wing	Red Lake Falls	MnROAD	DI TH23 Slopes
USCS <sup>a</sup>	ML	CL-1	CL-2	CH
AASHTO <sup>b</sup>	A-4(0)	A-7-6(23)	A-4(0)	A-7-6(60)
Liquid limit	28	42	26	85
Plastic index	11	24	9	52
Percent sand (%)	11.9	8.9	36.3	3.1
Percent silt (%)	82.4	63.8	45.3	21.2
Percent clay (%)	5.7	27.3	14.5	75.2
Percent fines (%)	88.1	91.1	59.7	96.4
Specific gravity	2.69	2.69	2.66	2.75
Optimum moisture content (%) <sup>c</sup>	13.5	22.0	16.0	27.5
Maximum dry unit weight (kN/m <sup>3</sup> ) <sup>c</sup>	17.9	15.8	17.7	14.4

<sup>a</sup>Unified Soil Classification System

<sup>b</sup>American Association of State Highway and Transportation Officials

<sup>c</sup>ASTM D 698 (Method A)

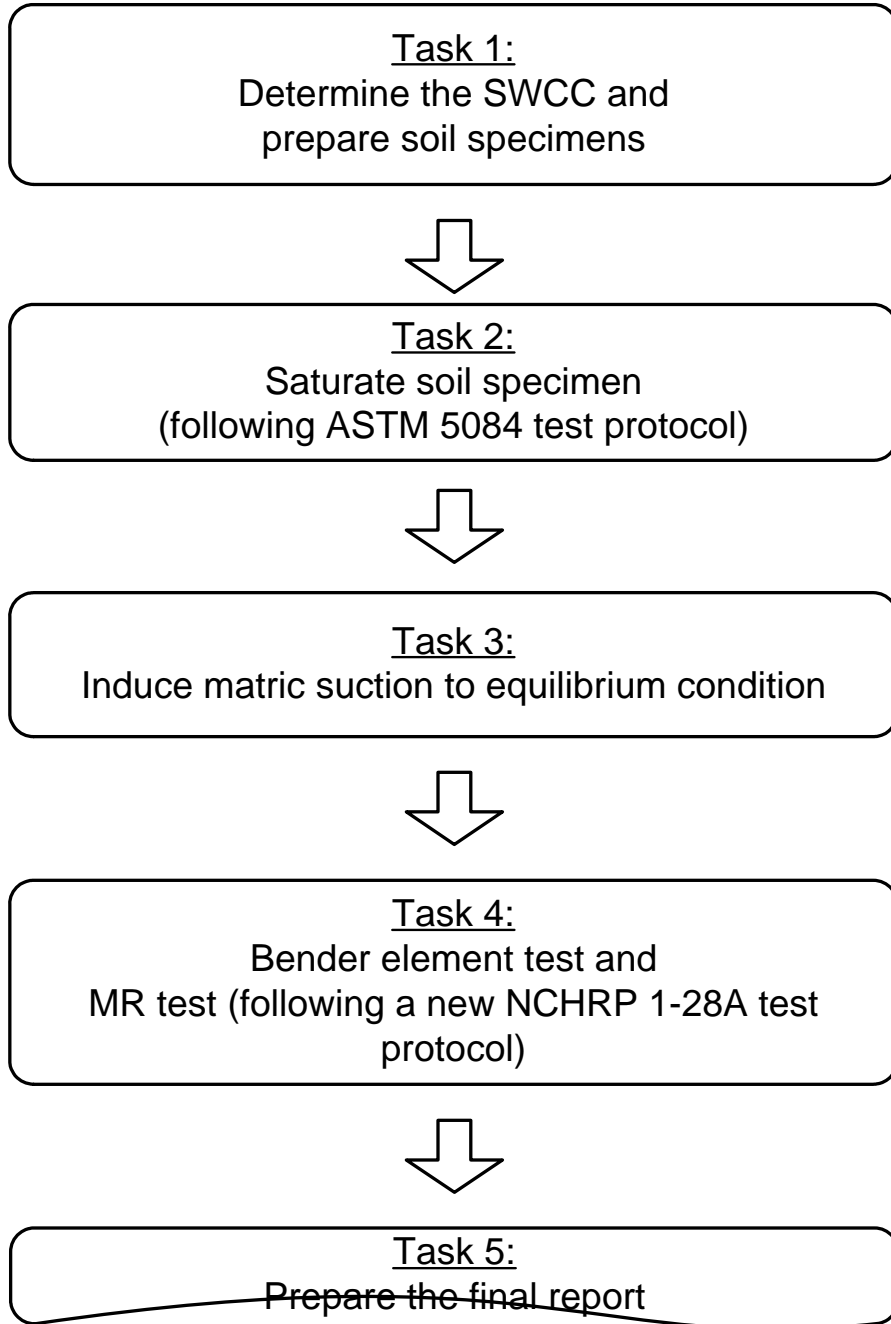


**Figure 11: Testing program flowchart.**

A number of relationships have been proposed to describe the highly nonlinear SWCC. Among these, the four-parameter relationships given by van Genuchten (1980) and Fredlund and Xing (1994) have been widely employed in engineering practice. Both equations have a similar generic form that provides a sigmoid shape of the SWCC applicable to most natural soils. These relationships are found to be the best in describing the SWCC data of a variety of soils (Leong and Rahardjo, 1997). In this study, the SWCC test data was modeled by fitting the Fredlund and Xing equation using a least-squared optimization algorithm. The Fredlund and Xing equation given below was selected because it provides a better curve-fitting for the SWCC data of a variety of soils (Leong and Rahardjo, 1997) and it also includes an additional term that allows the volumetric water content to be zero at the high suction of  $10^6$  kPa (Cronney and Coleman, 1961; Koorevaar et al., 1983), which is supported by thermodynamic theory (i.e., at a temperature of  $20^\circ\text{C}$  and a relative humidity of 0.01%, soil suction equals 1,026,289 kPa).

$$\Theta = \frac{\theta}{\theta_s} = \left[ 1 - \frac{\ln\left(1 + \frac{\psi}{\psi_r}\right)}{\ln\left(1 + \frac{10^6}{\psi_r}\right)} \right] \cdot \left[ \frac{1}{\ln(e + (\alpha\psi)^n)} \right]^m \quad (13)$$

where  $\Theta$  is the normalized volumetric water content,  $\theta$  is the volumetric water content,  $\theta_s$  is the saturated volumetric water content,  $\psi$  is the soil suction (kPa),  $\psi_r$ ,  $\alpha$ ,  $n$ , and  $m$  are the fitting parameters. This equation is similar to the van Genuchten (1980) equation. Moreover, since the pore-size distribution function used by Fredlund and Xing (1994) is a modification of the pore-size distribution function given by van Genuchten (1980), the fitting parameters in Fredlund and Xing equation (i.e.,  $\psi_r$ ,  $\alpha$ ,  $n$ , and  $m$ ) have the same meanings as those in van Genuchten (1980) and affect the shape of the SWCC in a similar fashion (Leong and Rahardjo, 1997, Yang et al., 2004). However, the only difference is that the Fredlund and Xing (1994) forces the SWCC through  $\theta = 0$  and  $\psi = 10^6$  kPa. The optimization algorithm results in a set of SWCC parameters (i.e.,  $\theta_s$ ,  $\theta_r$ ,  $\alpha$ ,  $n$ , and  $m$ ).

The specimens were prepared in accordance with NCHRP 1-28A (see Appendix B). A saturation cell was used to saturate these compacted specimens after obtaining a desired initial compaction condition. The cell can accommodate a 102-mm (4-in) diameter and 204-mm (8-in) high specimen. Four saturation cells were assembled for saturating the compacted specimen in the study. The cells used were similar to those used for the permeability testing of soils. The saturation procedure adopted in the study follows ASTM D 5084, *Standard Test Methods for Measurement of Hydraulic Conductivity of Saturated Porous Materials Using a Flexible-Wall Permeameter* (ASTM 2004). The saturation was ensured using the B-check (i.e.,  $B \geq 90\text{-}95\%$ ). The saturation took approximately 2 to 6 weeks depending on the soil sample.

A suction cell was designed and fabricated in order that the air pressure can be supplied to the cell and the pore water is allowed to drain freely from the cell. Figure 12 illustrates

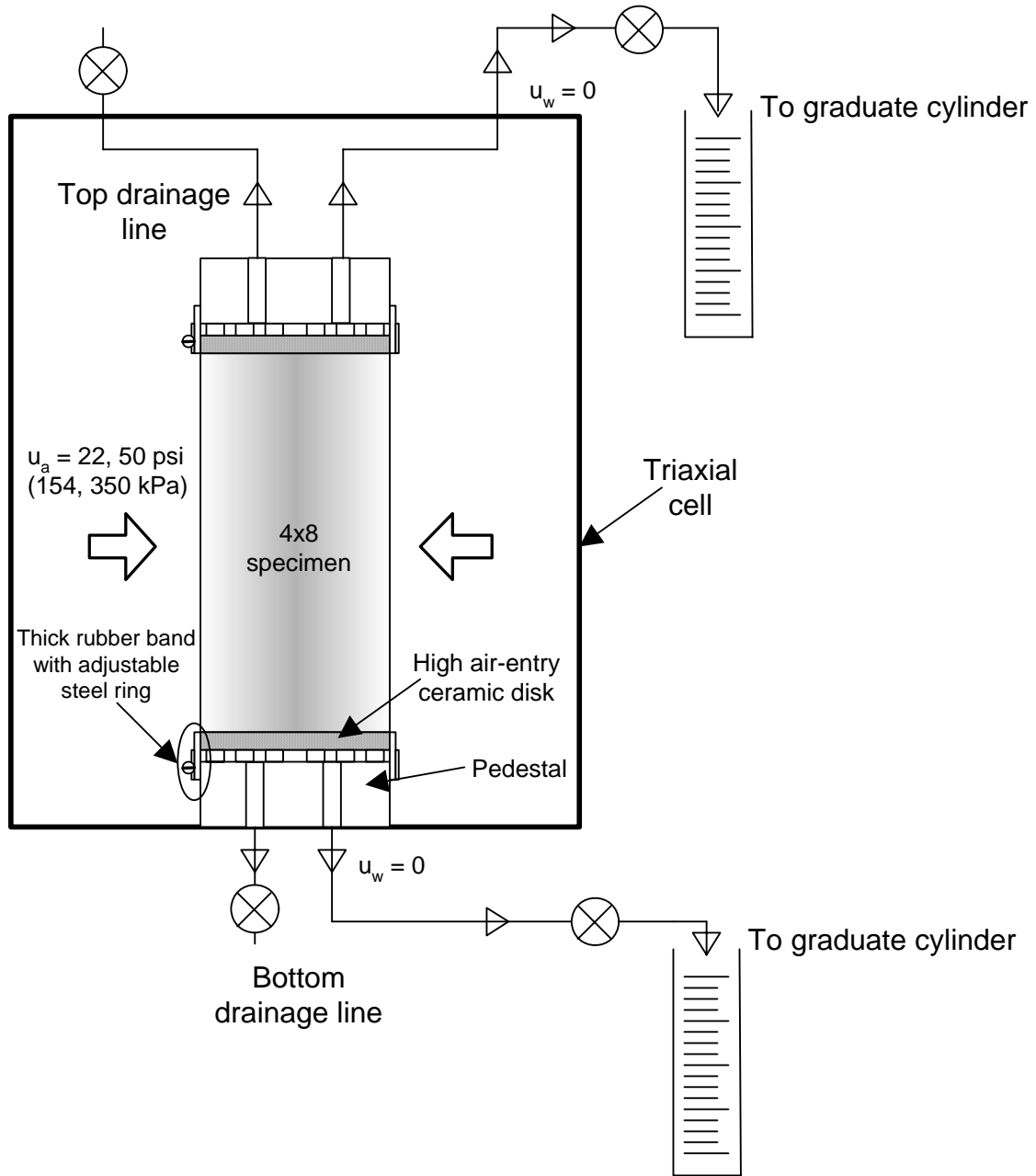


**Figure 12: Schematic of a suction cell.**

the schematic of the suction cell along with the outflow lines. The cell has the following features: (1) the controlled air pressure is applied directly on the lateral surface of the specimen and (2) the pore water can freely drain from the bottom of specimen through the pedestal fitted with a ceramic disk and also from the top of specimen through the top cap fitted with a ceramic disk. Double-drain was used in low permeable specimen to accelerate the equilibrium condition. Appendix C provides the machine drawing of this suction cell. The top cap and pedestal are designed in such a way that the water is able to flow in and out only in one direction and the air bubble can be easily flushed out of the outflow line.

An axis translation technique where the pore air pressure ( $u_a$ ) in unsaturated soil is elevated while maintaining the pore water pressure ( $u_w$ ) at atmospheric pressure was adopted so that the matric suction ( $u_a - u_w$ ) can be easily controlled and measured. This technique is achieved by separating the air and water phases of the soil through the saturated high-air-entry (HAE) ceramic disks. The specimen is placed in good contact with the saturated HAE ceramic disk. The positive air pressure is applied to the pore air on one side, while allowing the pore water to drain freely under atmospheric pressure on the other side of the disk. Separation of the air and water pressure is maintained as long as the applied air pressure is less than the air-entry pressure of the HAE ceramic disk, which is 5 bar (500 kPa) in this study.

The HAE ceramic disk has the following dimension: 10.48 cm (4.125 in) in diameter and 0.714 cm (0.281 in) high. The disk has identical diameter as the top cap and the pedestal. To avoid air leakage from the disk, a rubber membrane and a thick rubber band with a steel clamp was used to seal the disk to the cap or to the pedestal. The equilibrium condition was established when the amount of water expelled from the specimen ceased. The amount of water in the graduate cylinder was checked periodically. More details and pictures are given in Appendix C.

**Stiffness Testing-Resilient Modulus:** The resilient modulus ( $M_r$ ) test was conducted following the bender element test, which takes less than ten minutes. The  $M_r$  test was conducted in accordance with a new  $M_r$  testing protocol, NCHRP 1-28A as required by Mn/DOT. Since the soil specimens are classified as fine-grained subgrade soils (i.e., greater than 35% passing 75  $\mu\text{m}$ , No. 200) sieve, the  $M_r$  test sequence follows Procedure II. Appendix B summarizes the test sequence for NCHRP 1-28A: Procedure II. A sample test spreadsheet is given in Table 3.

The  $M_r$  testing machine used consists of a triaxial cell, a load cell located outside the chamber, two external and two internal (local) LVDTs for measuring axial deformation of the specimen. Two local LVDTs were installed on the specimen on diametrically opposite sides in the  $\frac{1}{4}$  position (where the end-friction effects are negligible). The measured axial deformations are averaged for calculating the resilient modulus.

According to NCHRP 1-28A, the load pulse for the subgrade soils has a haversine shape with a loading time of 0.2 seconds followed by a 0.8 seconds rest time. This pulse is used in the tests. Air is used as the cell pressure.

**Table 3: Example of spreadsheet for specimen and  $M_r$  test data**

Specimen ID \_\_\_\_\_ Test Date \_\_\_\_\_

<b>Specimen Property</b>	<b>Specimen Geometry</b>
<i>As-compacted state</i>	<i>As-compacted state</i>
Dry unit weight _____	Diameter _____
Moisture content _____	Height _____
<i>Post-compact state</i>	<i>Post-compact state</i>
Matric suction _____	Diameter _____
Moisture content _____	Height _____

<b>MR Test Protocol NCHRP 1-28A</b>	<b>Bender Element Test</b>
Initial specimen height _____	Tip-to-tip distance _____
Final specimen height _____	Total unit weight _____
Initial gauge length _____	S-wave travel time _____
Final gauge length _____	Shear modulus _____

Load Step	Deviator Stress (kPa)	Bulk Stress (kPa)	Confining Pressure (kPa)	Octahedral Shear Stress (kPa)	External LVDT 1 Deformation (mm)	External LVDT 2 Deformation (mm)	Internal LVDT 1 Deformation (mm)	Internal LVDT 2 Deformation (mm)	Measured MR-Ext (kPa)	Predicted MR-Ext (kPa)	Measured MR-Int (kPa)	Predicted MR-Int (kPa)
1												
2												
3												
4												
5												
6												
7												
8												
9												
10												
11												
12												
13												
14												
15												
16												

**Five-parameter log-log model**

External LVDTs	Internal LVDTs
k1 _____	k1 _____
k2 _____	k2 _____
k3 _____	k3 _____
k6 _____	k6 _____
k7 _____	k7 _____

A five-parameter log-log model will be used to represent the resilient modulus data as follows:

$$M_r = k_1 p_a \left( \frac{\sigma_b - 3k_6}{p_a} \right)^{k_2} \left( \frac{\tau_{oct}}{p_a} + k_7 \right)^{k_3} \quad (14)$$

$$[k_1, k_2 \geq 0; \quad k_3, k_6 \leq 0; \quad k_7 \geq 1]$$

where  $M_r$  is the resilient modulus,  $\sigma_b$  is the bulk stress ( $\theta = \sigma_1 + \sigma_2 + \sigma_3 = \sigma_1 + 2\sigma_3$ ),  $\tau_{oct}$  is the octahedral shear stress ( $= \frac{1}{3} \cdot \sqrt{(\sigma_1 - \sigma_2)^2 + (\sigma_1 - \sigma_3)^2 + (\sigma_2 - \sigma_3)^2} = \frac{\sqrt{2}}{3} \cdot (\sigma_1 - \sigma_3)$ ),  $\sigma_1, \sigma_2, \sigma_3$  ( $\sigma_2 = \sigma_3$ ) are the principal stresses,  $k_1, k_2, k_3, k_6$ , and  $k_7$  are the fitting constants, and  $p_a$  is the atmospheric pressure ( $\sim 100$  kPa). After the  $M_r$  test, the bender element test and suction measurement using thermal dissipation sensor were conducted on all of the specimens.

*Small-strain Shear Modulus (Bender Element Test):* After the resilient modulus test, the small-strain shear modulus was determined using the bender elements on the specimens without any applied stresses. The bender element system (Sawangsurriya et al., 2006) was installed at top and bottom ends of the specimen so that the shear wave propagating longitudinally was monitored. Knowing the travel distance ( $L$ ) and time ( $t_s$ ), the shear wave velocity can be obtained. The small-strain shear modulus ( $G_o$ ) was then calculated from the shear wave velocity ( $v_s$ ) and total mass density of the specimen ( $\rho$ ) as follows:

$$G_o = \rho \cdot v_s^2 \quad (15)$$

where  $v_s = L/t_s$ .

*Matric Suction Determination:* After the stiffness measurement, the matric suction was determined using the thermal dissipation sensor. The test took approximately 2-3 days to ensure the equilibration was established. The matric suction as measured with thermal dissipation sensor longitudinally was used to verify if the specimen met both equilibrium condition and target matric suction. The matric suction measured near the top, middle, and bottom of a specimen is shown in Fig. 13. The equilibrium matric suction obtained was close to the target matric suction ( $\sim 350$  kPa). The average matric suction as measured with the thermal dissipation sensor was approximately 204 kPa for the ML specimen and 311 kPa for the CL specimen. The measured suction is about 42% lower for the ML specimen and 11% lower for the CL specimen, implying that the equilibrium was nearly but not fully established. The gravimetric water content was also measured to ensure the moisture uniformity and homogeneity after the suction measurement. Approximately 4 to 6 measurements were taken along the soil specimen. The average and standard deviation of water content was 10.8% and 0.2 for the ML specimen and 14.6% and 0.8 for the CL specimen. However, it should be noted that water content changes may not reflect the equilibrium because changes in water content are insignificant as compared to changes in suction. Thermal dissipation sensor and suction measurement pictures are given in Appendix C.

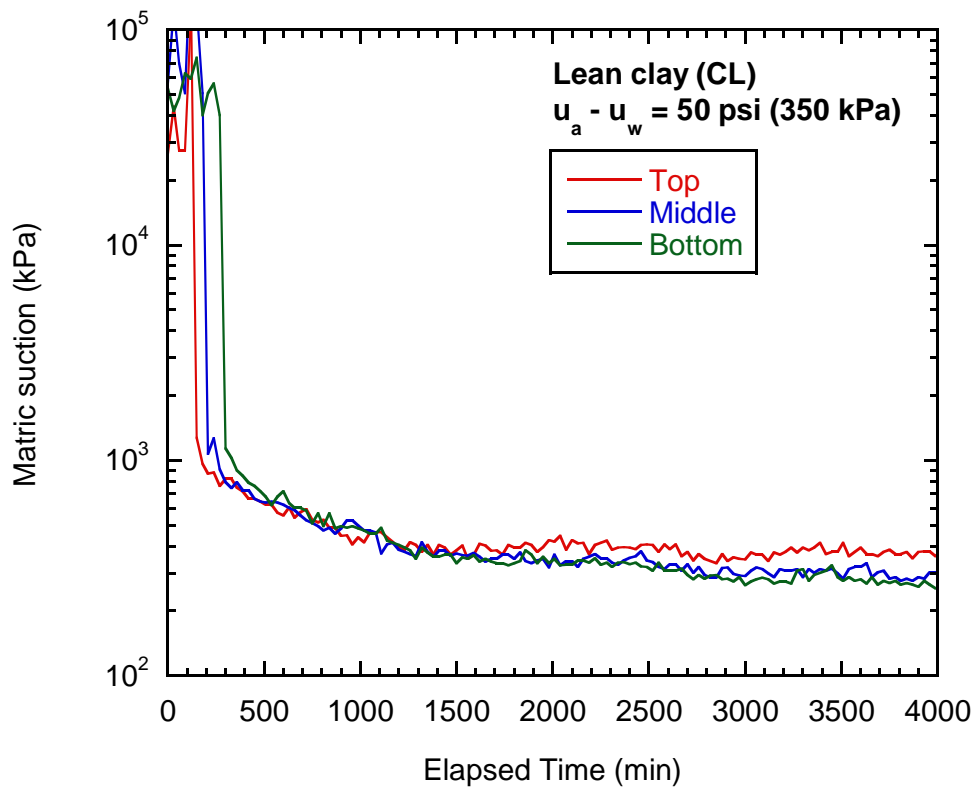
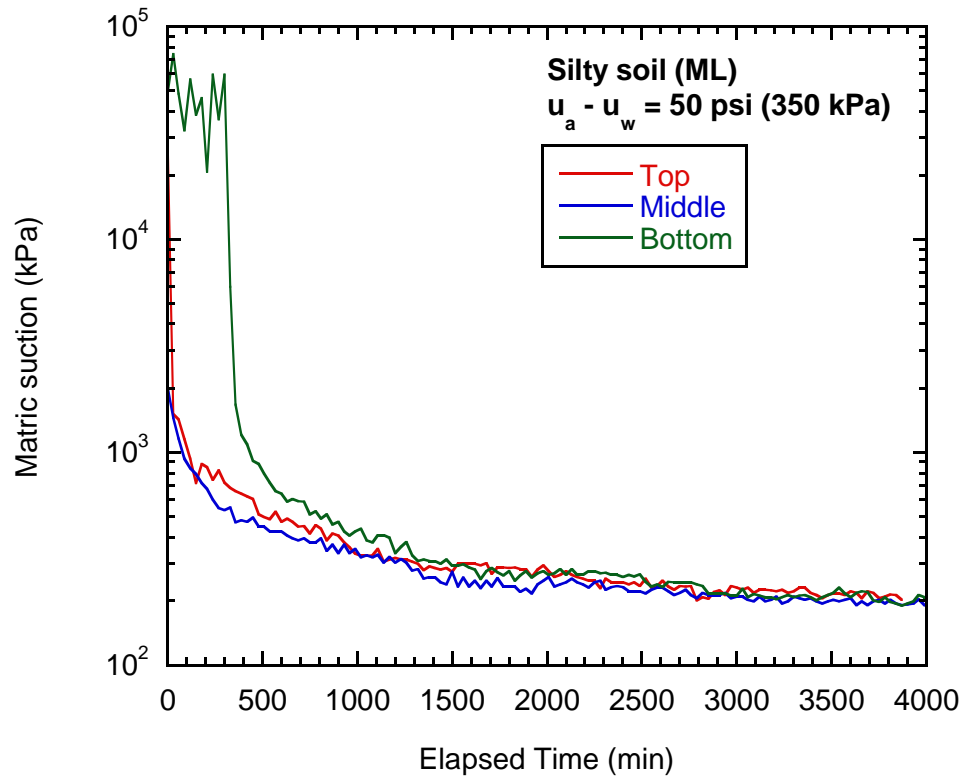


**Figure 13: Matric suction as measured with thermal dissipation sensor.**

## CHAPTER IV: RESULTS AND DISCUSSION

This section was written by Drs. Satish Gupta and Andry Ranaivoson of the University of Minnesota.

### Physical Characteristic of the Soils

Tables 4 and 5 summarize the physical characteristics of the four soils tested in this project. Red Wing soil had the least amount of clay (4.8%) whereas Duluth TH23 had the most clay (75.2%). Red Wing soils are loess soils with high silt content and represent a large area of southeastern Minnesota, southwestern Wisconsin, northeastern Iowa, and northwestern Illinois, also designated as the unglaciated region of upper Midwest. Red Lake Falls soils are formed from lake sediments of the Red River valley in northwestern Minnesota. MnROAD soil is taken from near the Mn/DOT experimental facilities near Monticello along Interstate 94. Duluth TH23 is a soil taken along Trunk Highway 23 near Duluth. Except for MnROAD soil, the initial water content of the other soils was greater than the optimal water content. Therefore in these soils, optimal water content was achieved by soil drying. In case of MnROAD soil, optimal water content was achieved by spraying additional water with an atomizer.

### Soil Water Retentions

Figures 14 thru 17 shows the water retention characteristics of all four soils packed at two densities (100% and 105% of standard Proctor density). These densities are a bit higher than the densities used in shear strength measurements partially because the Mn/DOT had initially planned to run all test at 100 and 105% of the maximum density. These plans were changed to 98% and 103% of the maximum density after we had finished part of the water retention tests. Points in Figs. 14 thru 17 are the best fit lines drawn to the experimental data using van Genuchten's function (Van Genuchten, 1980). The values of Van Genuchten parameters are given in Tables 6 thru 9. In general, there were small differences in the water retention characteristics of a given soil when packed at two different densities. With increase in density, there was a small decrease in the water content at lower suction and an increase in water content near the mid to higher suctions. This indicates that increasing compaction slightly reduced the proportion of larger pores but slightly increased the proportion of medium and smaller pores.

### Deviator Stress at 5% Strain

Figures 18 thru 21 show the variation in deviator stress ( $\sigma_1 - \sigma_3$ ) at 5% sample strain as a function of confining stress ( $\sigma_3$ ) and soil suction for four soils that were initially packed at 103% of the Proctor density. Since all samples did not shear and in many of the samples bulging occurred during compression, it was difficult to calculate the values of cohesion and friction angle for a given soil at various suctions. The bulging process indicated hardening and dilation of the specimens. Because of this limitation, we decided to use deviator stress as an indicator of shear strength in characterizing the effects of initial compaction and suction.

**Table 4: Soil name, optimum moisture, and density.**

Soil Name	%Silt	%Clay	Opt. % Moist.	Initial % Moist	Max Density, lb/ft <sup>3</sup>	Max Density, g/cm <sup>3</sup>
MnRoad	45.3	14.5	16.1	15.7	107.4	1.720
Red Wing	80.4	4.8	13.1	20.9	111.7	1.789
Duluth TH23	21.2	75.2	26.5	36.4	90.4	1.448
Red Lake Falls	67.0	24.3	16.3	29.6	107.4	1.720

**Table 5: Soil name, texture, and liquidity and plasticity parameters**

Soil Name	Textural Class	% passing #4	% passing #200	Liquid limit %	Plastic limit %.	Plasticity Index
MNRoad	L	96.9	58.6	30.5	17.4	13.1
Red Wing	Si	96.7	85.3	0.0	0.0	0.0
Duluth TH23	C	99.5	96.4	84.9	32.9	52
Red Lake Falls	SiCL	97.7	91.3	31.8	21.7	10.1

**Table 6: Value of Van Genuchten's function value for MnRoad soil at two densities.**

Density	$\theta_s$	$\theta_r$	$\alpha$	n
100%	0.3292	0.1727	0.0873	1.565
105%	0.3122	0.1659	0.3419	1.239

**Table 7: Value of Van Genuchten's function value for Red Wing soil at two densities.**

Density	$\theta_s$	$\theta_r$	$\alpha$	n
100%	0.3130	0.1009	0.00075	2.044
105%	0.3200	0.1145	0.00122	1.852

**Table 8: Value of Van Genuchten's function value for Duluth TH23 soil at two densities.**

Density	$\theta_s$	$\theta_r$	$\alpha$	n
100%	0.4852	0.3443	0.1210	1.238
105%	0.4276	0.3150	0.0145	1.370

**Table 9: Value of Van Genuchten's function value for Red Lake Falls soil at two densities.**

Density	$\theta_s$	$\theta_r$	$\alpha$	n
100%	0.3560	0.2262	0.00053	2.477
105%	0.3660	0.2544	0.00146	1.857

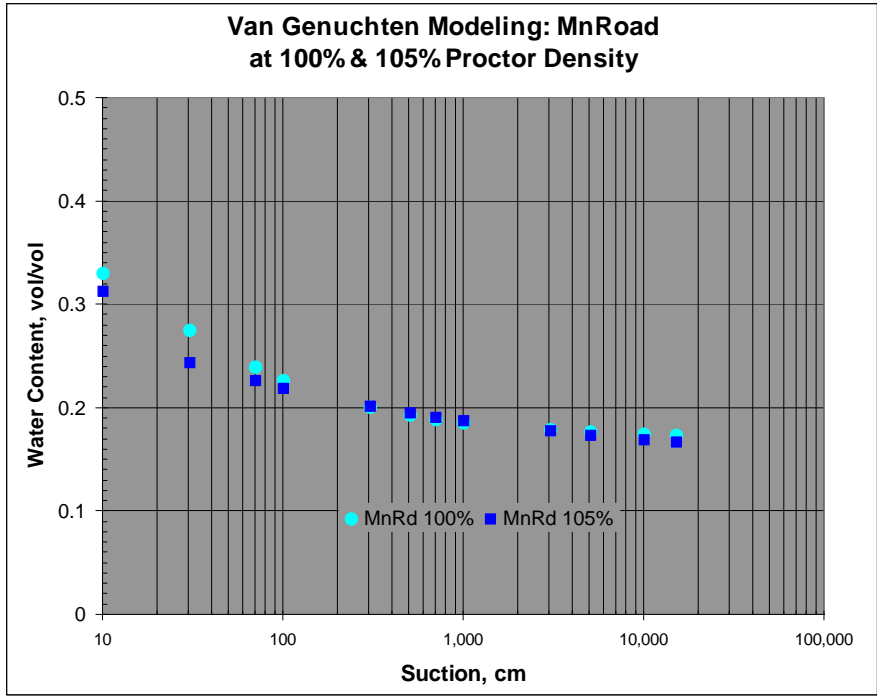


**Figure 14: Effect of compaction (100% and 105% of the Proctor Density) on water retention characteristics of the MnROAD soil.**

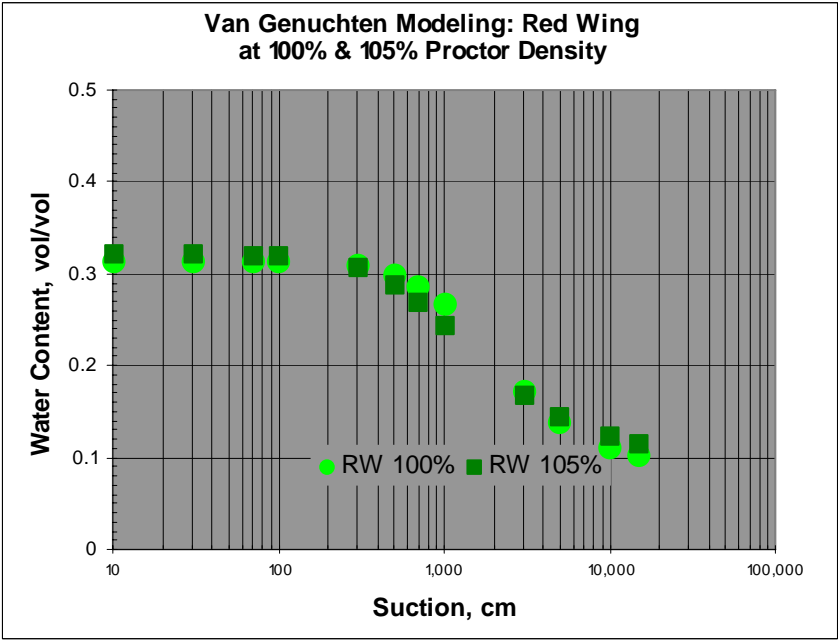


**Figure 15: Effect of compaction (100% and 105% of the Proctor Density) on water retention characteristics of the Red Wing soil.**

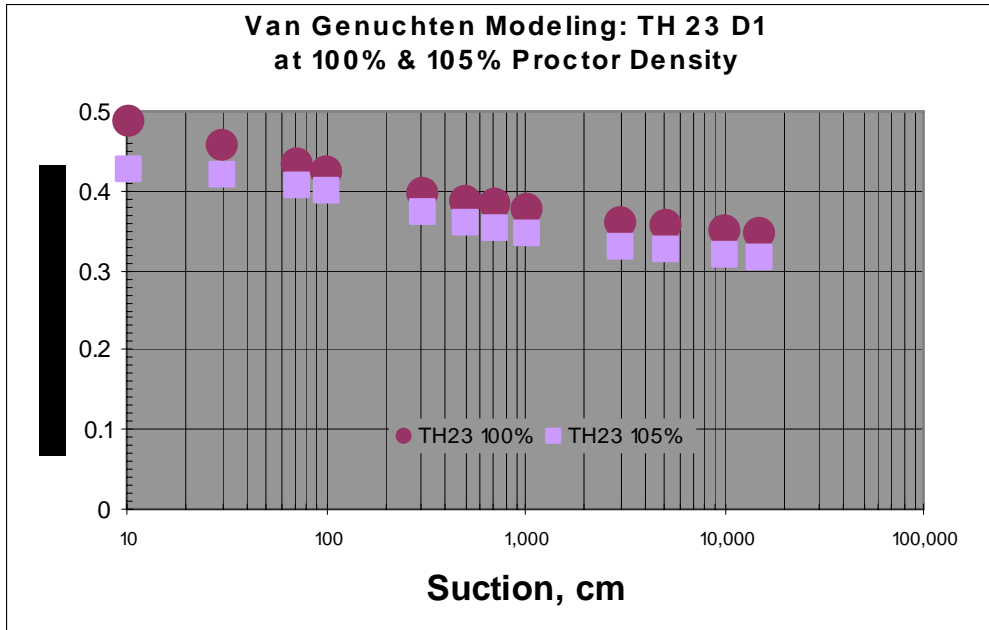


**Figure 16: Figure 16. Effect of compaction (100% and 105% of the Proctor Density) on water retention characteristics of the Duluth TH23 soil.**

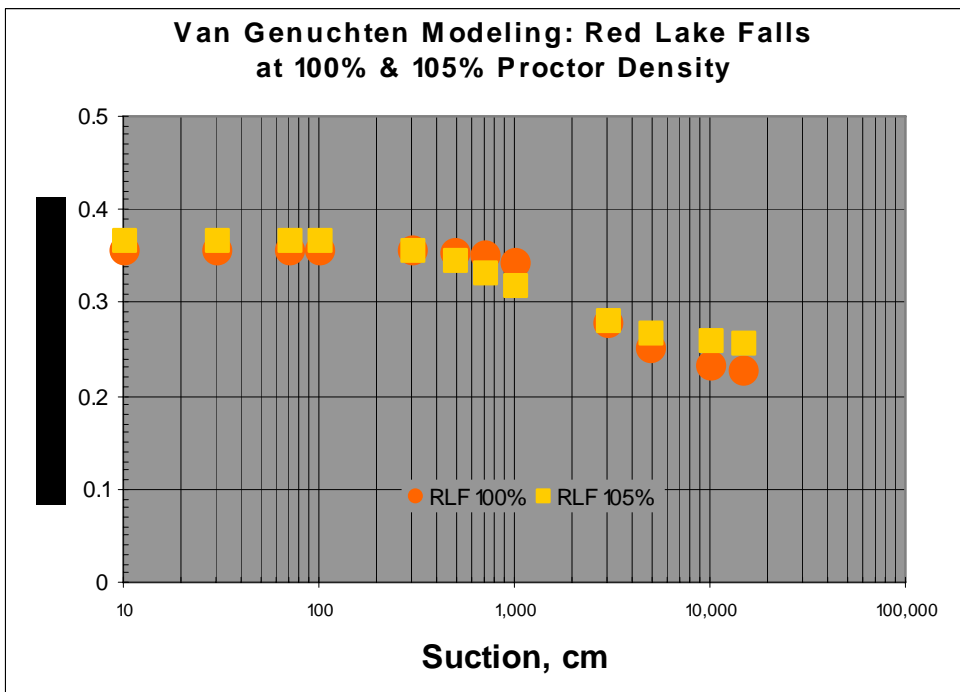


**Figure 17: Effect of compaction (100% and 105% of the Proctor Density) on water retention characteristics of the Red Lake Falls soil.**

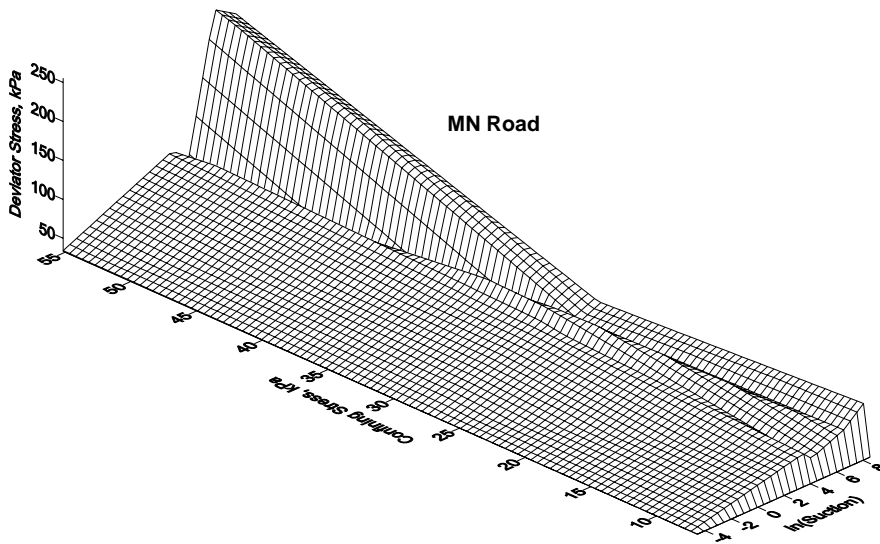


Figure 18: Variation in deviator stress ( $\sigma_1 - \sigma_3$ ) at 5% strain as a function of confining stress ( $\sigma_3$ ) and soil suction for MN Road specimens at 103% of Proctor density.

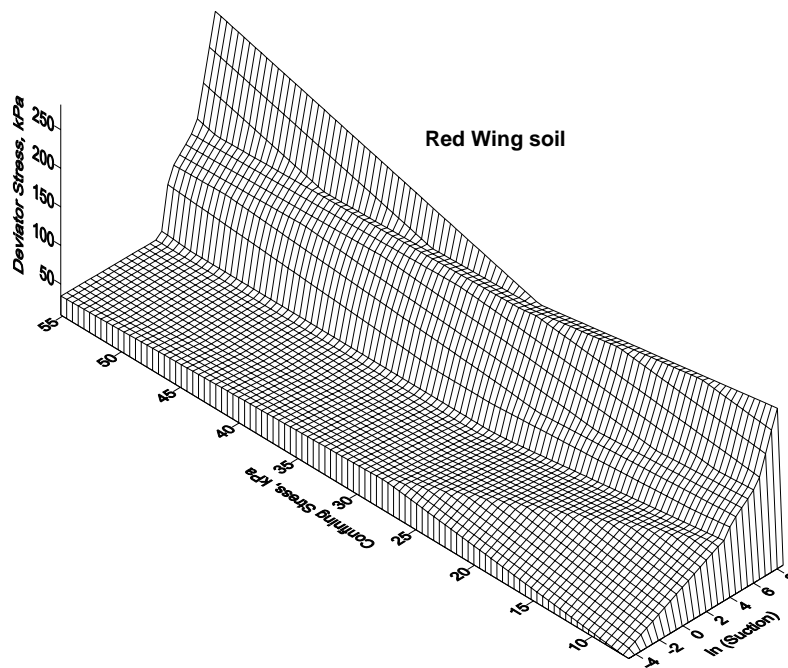


Figure 19: Variation in deviator stress ( $\sigma_1 - \sigma_3$ ) at 5% strain as a function of confining stress ( $\sigma_3$ ) and soil suction for Red Wing specimens at 103% of Proctor density.

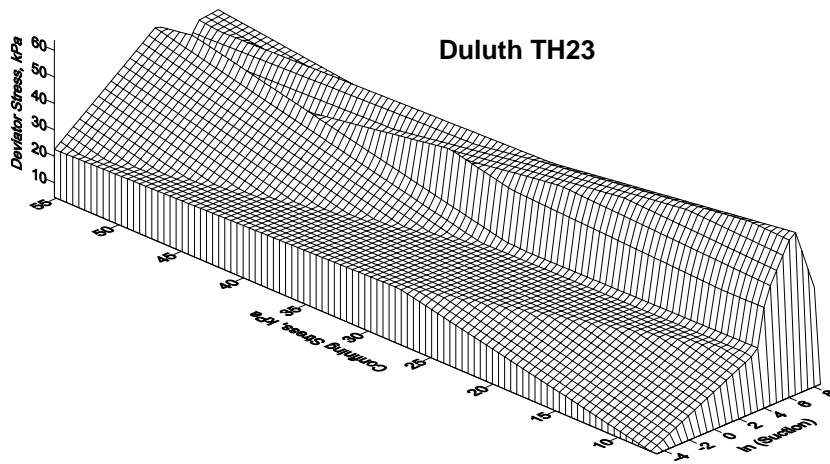


Figure 20: Variation in deviator stress ( $\sigma_1 - \sigma_3$ ) at 5% strain as a function of confining stress ( $\sigma_3$ ) and soil suction for Duluth TH23 specimens at 103% of Proctor density.

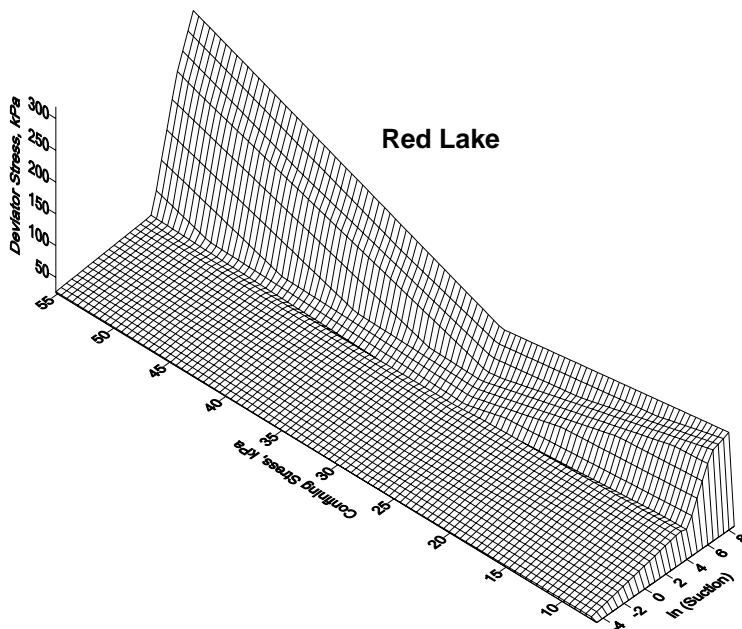


Figure 21: Variation in deviator stress ( $\sigma_1 - \sigma_3$ ) at 5% strain as a function of confining stress ( $\sigma_3$ ) and soil suction for Red Lake Falls specimens at 103% of Proctor density.

There was a greater change in deviator stress as a function of suction than the confining stress (Figs. 18-21). Also, the effect of soil suction was slightly more at higher confining stresses than at low confining stresses. Because of large variability in deviator stress between specimens, the 3-D surfaces were not smooth and they also did not show consistent trend at all suctions or confining stresses. However, the differences in deviator stresses at three confining stresses were within the range of differences observed between three replications. In other words, deviator stresses for a range of confining stresses tested in this study were nearly same especially at low suctions. Because of this trend, we assumed that deviator stress was a unique function of the soil suction for a range of confining stresses ( $\sigma_3=6.9$  to  $55.2$  kPa). Using this assumption, we plotted the deviator stress as a function of suction in a 2-D graph for all four soils (Fig. 22). The figure shows that the deviator stress is a power function of soil suction expressed as:

$$(\sigma_1-\sigma_3)=\alpha\mu_w^\beta \quad \text{for } u_w \geq 1.0 \text{ cm} \quad (15)$$

where  $\mu_w$  is soil suction (cm) and  $\alpha$  and  $\beta$  are power function constants. The coefficients of the power function for all four soils initially packed at 103% of the standard Proctor density are given in Table 10. Comparison of the best fit curves in Fig. 22 shows that there is an downward shift in the deviator stress curves with an increase in the soil clay content and the shift is nearly same at all suctions. In other words, the slope ( $\beta$ ) is nearly similar and  $\alpha$  intercept varies with soil type. At any soil suction, deviator stress needed to achieve 5% strain was minimal for DI TH23 soil (72.5% clay) and maximum for Red Wing soil (4.8% clay).

Relationship of the coefficient  $\alpha$  (intercept) with clay content shows that its value exponentially decreased with an increase in the clay content (Fig. 23). However, in case of coefficient  $\beta$ , there was a slight increase or no change with an increase in clay content (Fig. 24). We also tested relationship of  $\alpha$  or  $\beta$  coefficients to other soil properties such as percent sand, percent silt, or plastic limit (Appendix D). In general, those relationships were not that strong as indicated by  $r^2$  values.

We also tested the power function fit of deviator stress at 5% strain vs. suction on samples that had been compacted at 98% Proctor density (Figs. 25 thru 28) and found that although there was a slight change in the value of coefficients, the trends in relationships as well as in differences between soils were nearly similar. A 2-dimensional plot of the deviator stress vs. suction for four soils is plotted in Figure 29 and the corresponding coefficients of the power function are given in Table 11. Figures 30 and 31 show the relationships between the power coefficients ( $\alpha$ ,  $\beta$ ) for soils initially compacted at 98% and the clay content.

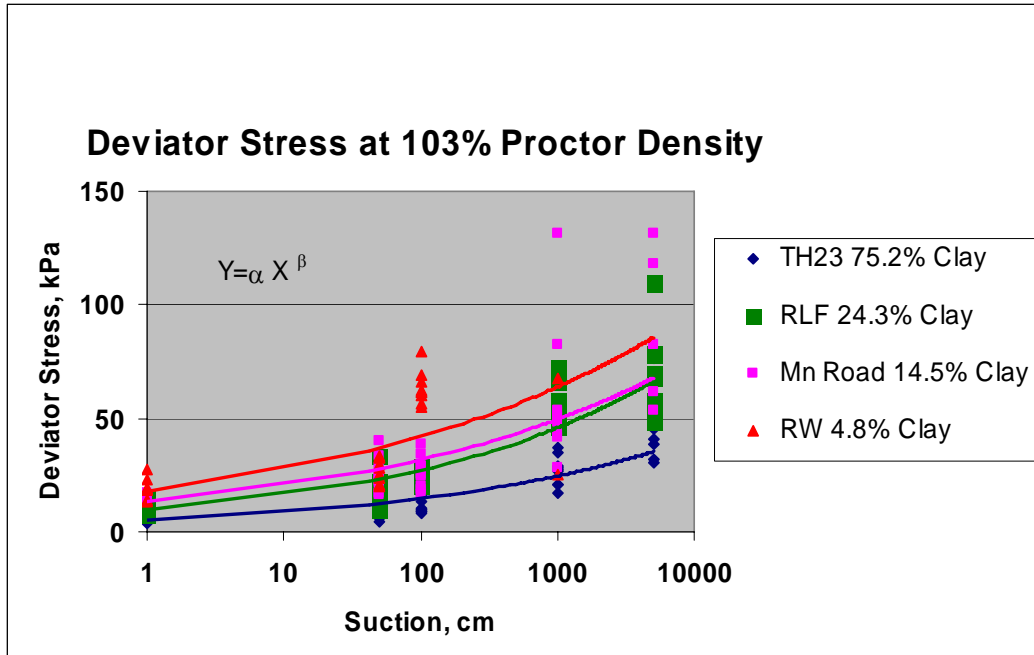


Figure 22: Variation in deviator stress as a function of soil suction for four soils. Lines are the best fit lines using the power function.

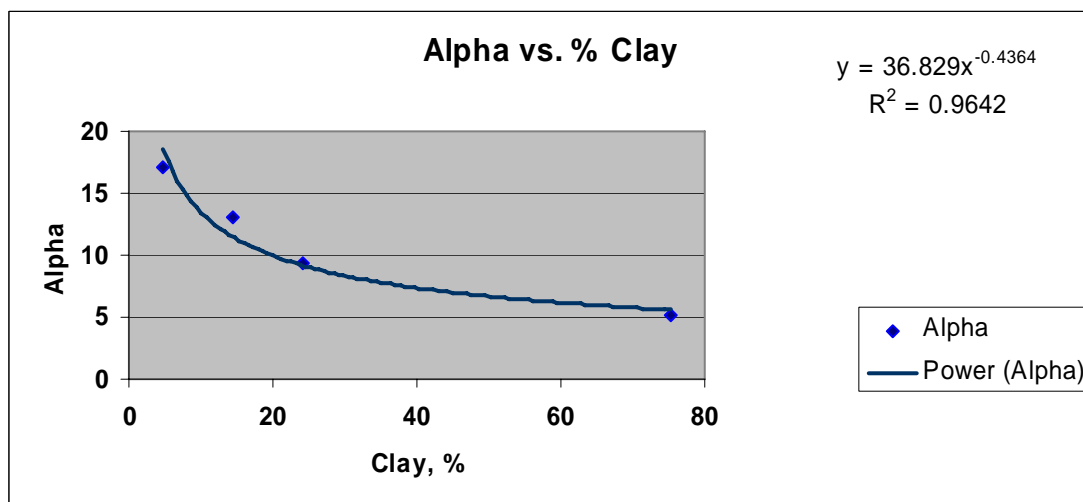
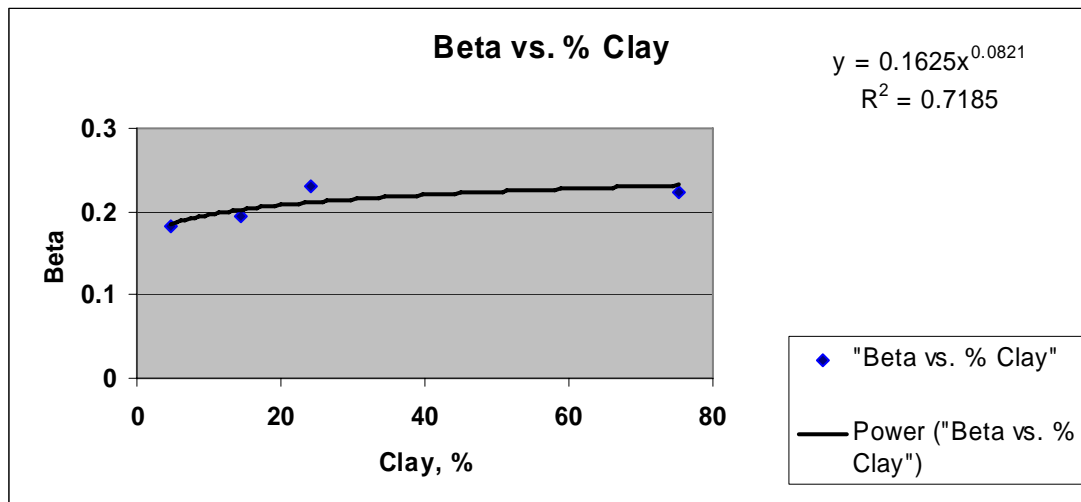


Figure 23: Variation in the power function coefficient  $\alpha$  as a function of soil clay content.



**Figure 24: Variation in the power function coefficient  $\beta$  as a function of soil clay content.**

**Table 10: Best fit value of the power function coefficients describing the change in deviator stress ( $\sigma_1 - \sigma_3$ ) at 5% strain as a function of soil suction ( $\mu_w$ ) for soils that have been compacted at 103% of Proctor density.**

Soil	Clay %	$\alpha^\dagger$	$\beta^\dagger$	R2
Duluth TH23	75.2	5.24	0.224	0.71
Red Lake Falls	24.3	9.37	0.230	0.8
MN Road	14.5	13.0	0.194	0.72
Red Wing	4.8	17.1	0.183	0.53

$$\dagger (\sigma_1 - \sigma_3) = \alpha \mu_w^\beta$$

**Table 11: Best fit value of the power function coefficients describing the change in deviator stress ( $\sigma_1 - \sigma_3$ ) at 5% strain as a function of suction ( $\mu_w$ ) for soils that have been compacted at 98% of Proctor density.**

Soil	Clay %	$\alpha^\dagger$	$\beta^\dagger$	R2
Duluth TH23	75.2	8.51	0.191	0.75
Red Lake Falls	24.3	8.35	0.238	0.58
MN Road	14.5	9.55	0.253	0.75
Red Wing	4.8	14.43	0.264	0.57

$$\dagger (\sigma_1 - \sigma_3) = \alpha \mu_w^\beta$$

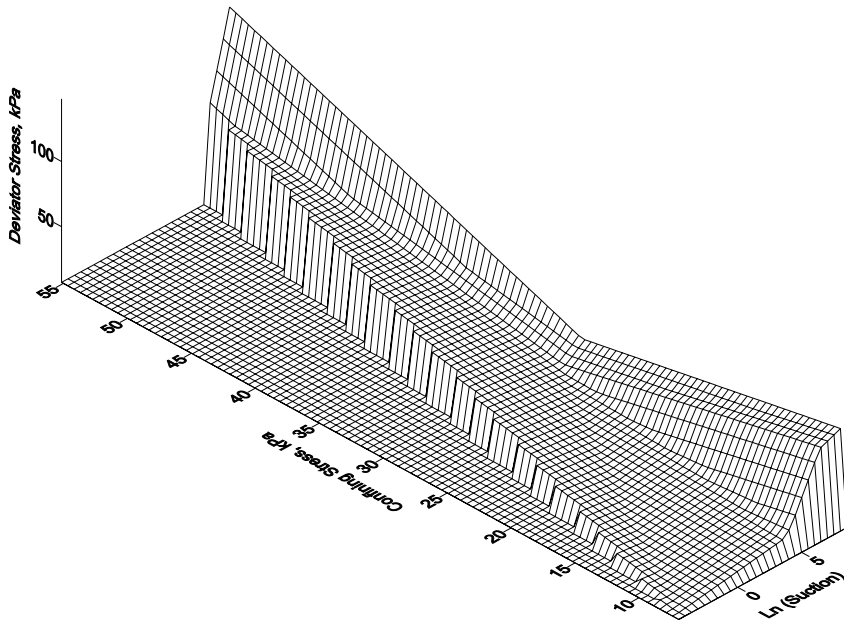


**Figure 25: Variation in deviator stress ( $\sigma_1 - \sigma_3$ ) at 5% strain as a function of confining stress ( $\sigma_3$ ) and soil suction for MN Road specimens at 98% of Proctor density.**

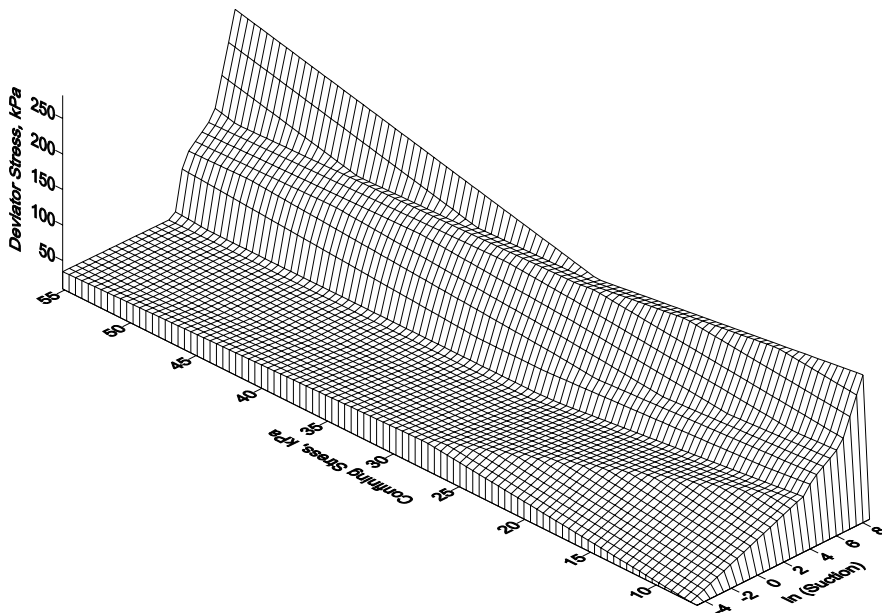


**Figure 26: Variation in deviator stress ( $\sigma_1 - \sigma_3$ ) at 5% strain as a function of confining stress ( $\sigma_3$ ) and soil suction for Red Wing specimens at 98% of Proctor density.**

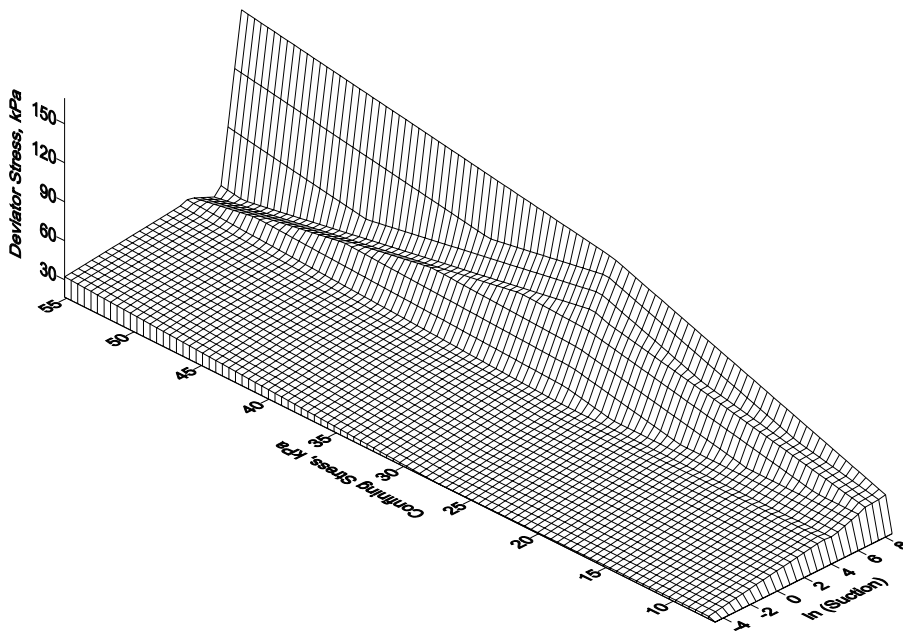


**Figure 27: Variation in deviator stress ( $\sigma_1 - \sigma_3$ ) at 5% strain as a function of confining stress ( $\sigma_3$ ) and soil suction for Duluth TH23 specimens at 98% of Proctor density.**

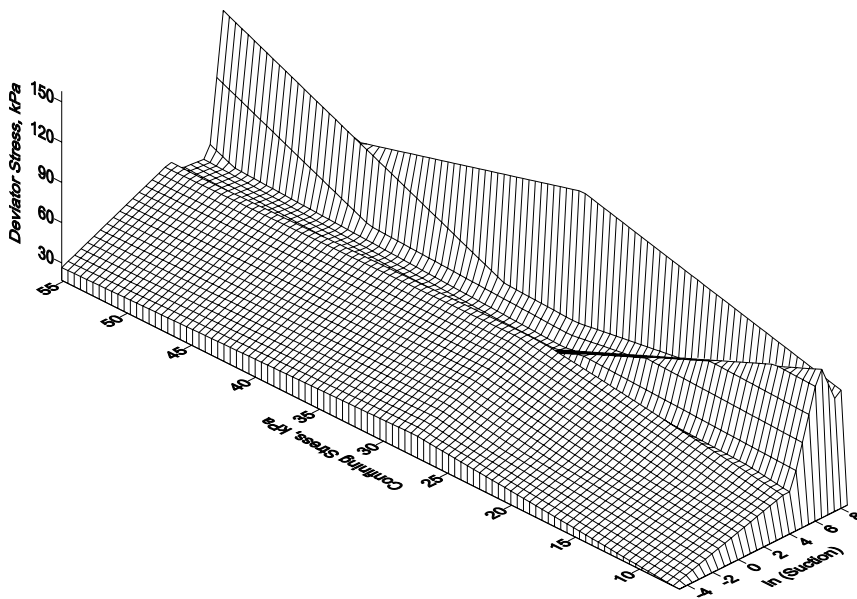


**Figure 28: Variation in deviator stress ( $\sigma_1 - \sigma_3$ ) at 5% strain as a function of confining stress ( $\sigma_3$ ) and soil suction for Red Lake Falls specimens at 98% of Proctor density.**

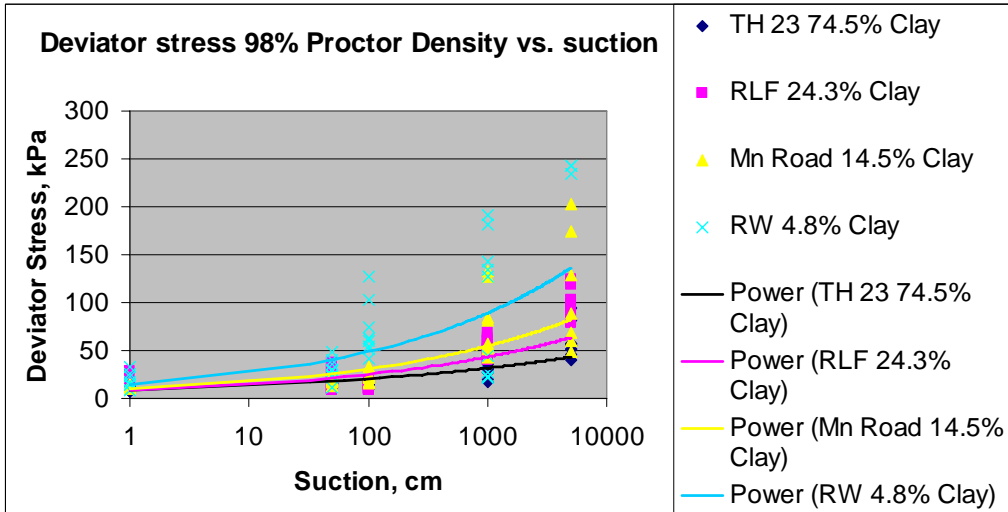


**Figure 29: Variation in deviator stress as a function of soil suction for four soils. Lines are the best fit lines using the power function.**

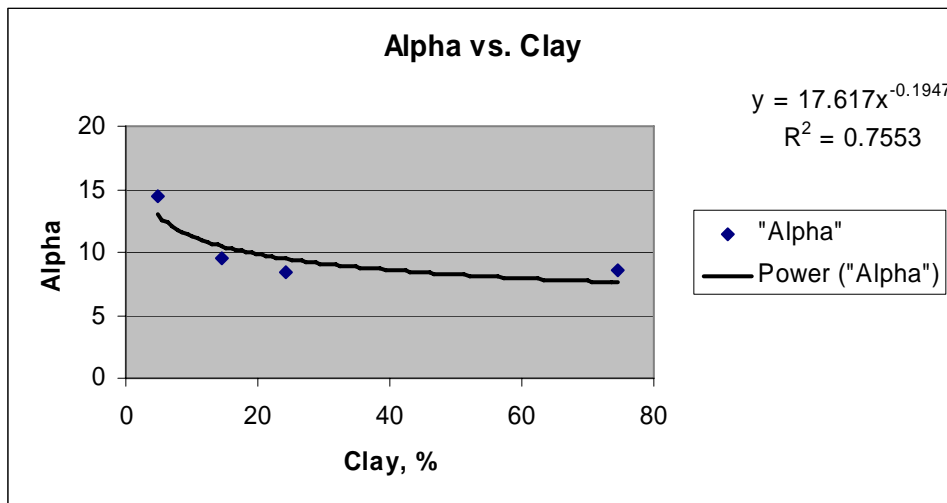


**Figure 30: Variation in the power function coefficient  $\alpha$  as a function of soil clay content.**

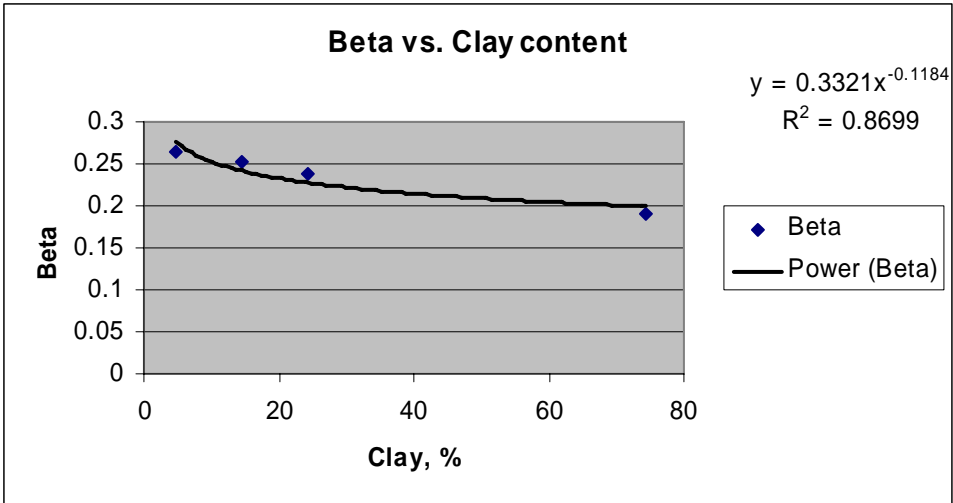


**Figure 31: Variation in the power function coefficient  $\beta$  as a function of soil clay content.**

## Deviator Stress at 1% Strain

Since in resilient modulus testing specimens are not subjected to high stresses (equivalent to stresses at failure) and the extent of strain is rather small, we further wanted to see if the above relationships between deviator stress and suction hold at 1% strain. Figures 32 and 33 show the variation in deviator stress at 1% strain as a function of suction for all four soils that have been initially packed at 103% and 98% of the standard Proctor density. These figures still show that the deviator stress is a power function of soil suction. The best fit coefficients of the power functions are summarized in Tables 12 and 13. As expected these coefficients are slightly different than the coefficients estimated for 5% strain measurements. In these relationships, both coefficients  $\alpha$  and  $\beta$  decrease with an increase in clay content (Figs. 34-37).

Like before, we also tested the relationship of  $\alpha$  and  $\beta$  coefficients at 1% strain against percent sand, percent silt and plastic limit but except for one case (103% proctor density at 1% strain),  $R^2$  values were always lower than that with clay content (Tables 14).

## Shear Strength Model for Unsaturated Soils

Since shear strength is related to deviator stress and the deviator stress can be described as a function of soil suction, one can assume that shear strength will follow some general trend as a function of soil suction similar to the relationships given in Figures 22, 29, 32, and 33. Since these figures are plotted irrespective of the confining pressure, these plots reflect the cohesion component of the shear strength parameter in Mohr-Columb law and how it varies with soil suction. Figures 22, 29, 32, and 33 also indicate that cohesion of the soil is a power function of the suction and not a linear function as suggested by Fredlund et al. (1978, 1996), and Vanapalli et al. (1996). Thus the shear strength relationship of above investigators may be modified as follows:

$$\tau_{us} = c' (\mu_a - \mu_w)^\beta + (\sigma_n - \mu_a) \tan \phi' \quad \text{for } u_w \geq 1.0 \text{ cm} \quad (16)$$

where  $\tau_{us}$  is the shear strength of an unsaturated soil,  $c'$  is the effective cohesion of the saturated soil,  $\phi'$  is the effective angle of frictional resistance of saturated soil, and  $(\mu_a - \mu_w)$  is the soil suction. Coefficient  $\beta$  will be the same or nearly similar as outlined in power function relationship of deviator stress ( $\sigma_3=6.9$  to 55.2 kPa) to suction (Figs. 22, 29, 32, and 33).

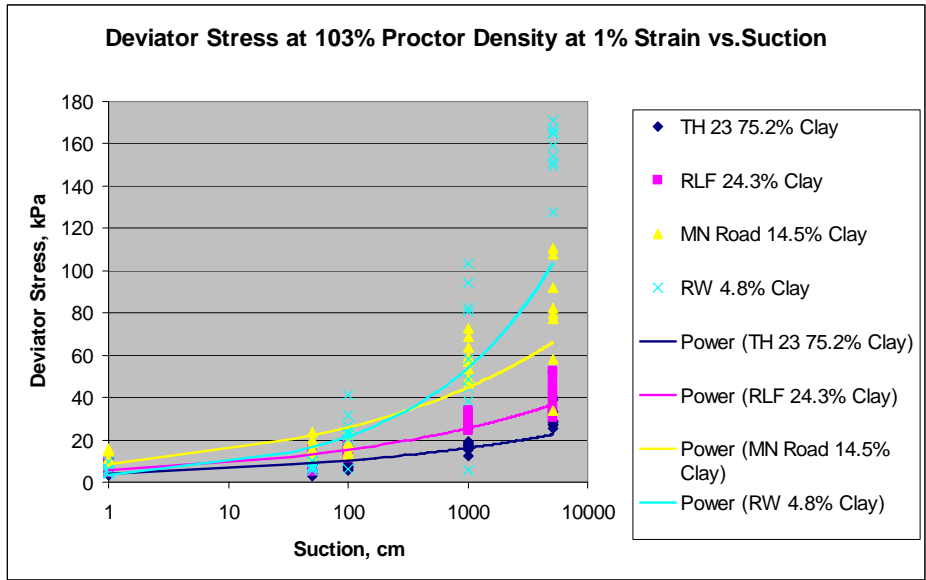


**Figure 32: Variation in deviator stress as a function of soil suction for four soils. Lines are the best fit lines using the power function.**

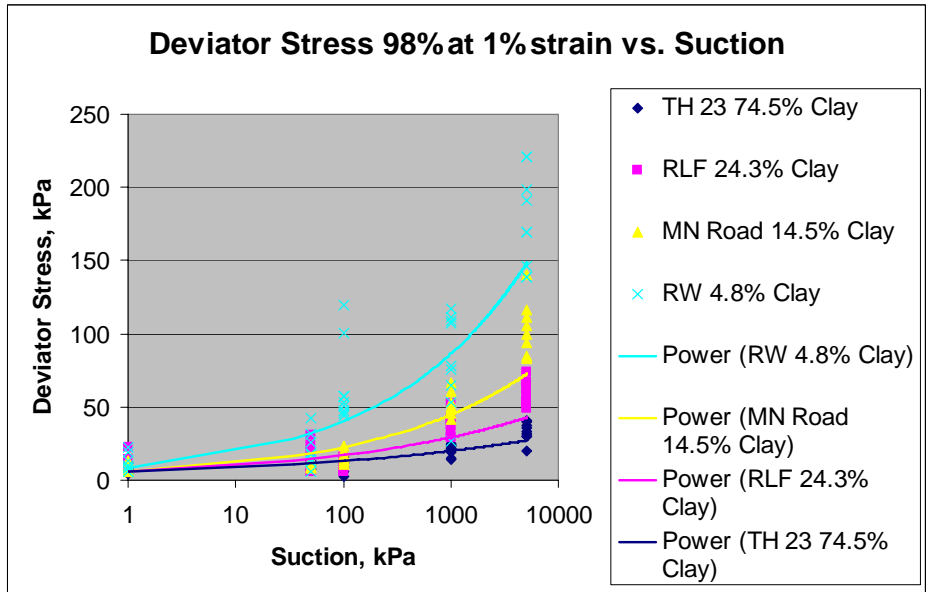


**Figure 33: Variation in deviator stress as a function of soil suction for four soils. Lines are the best fit lines using the power function.**

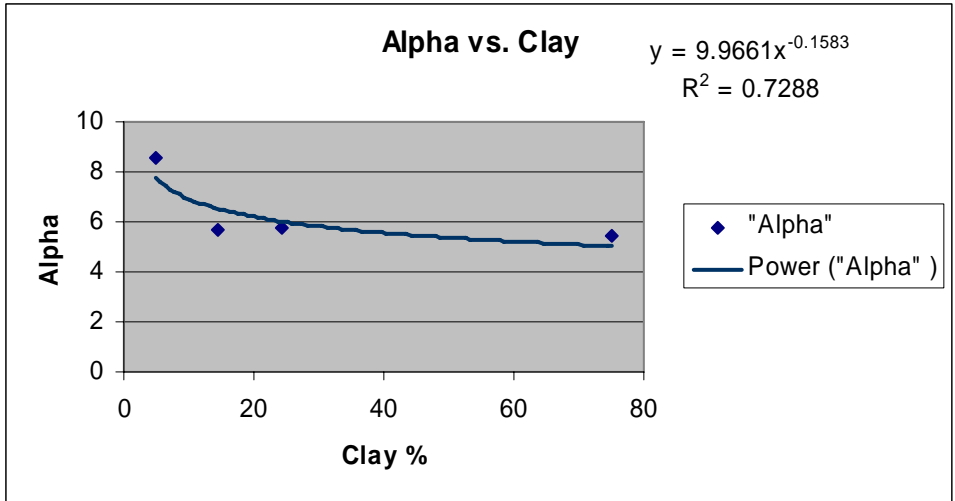


**Figure 34: Variation in the power function coefficient  $\alpha$  (103% Standard Proctor density at 1% strain) as a function of soil clay content.**

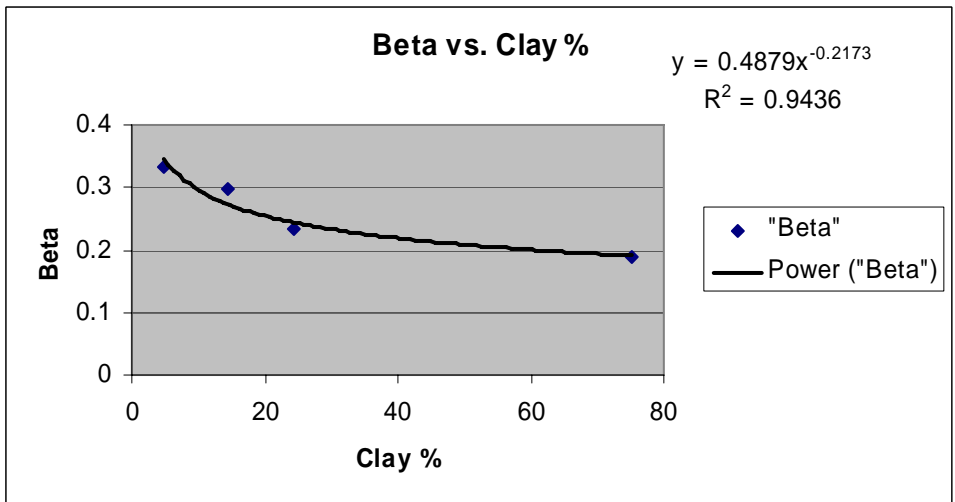


**Figure 35: Variation in the power function coefficient  $\beta$  (103% Standard Proctor density at 1% strain) as a function of soil clay content.**

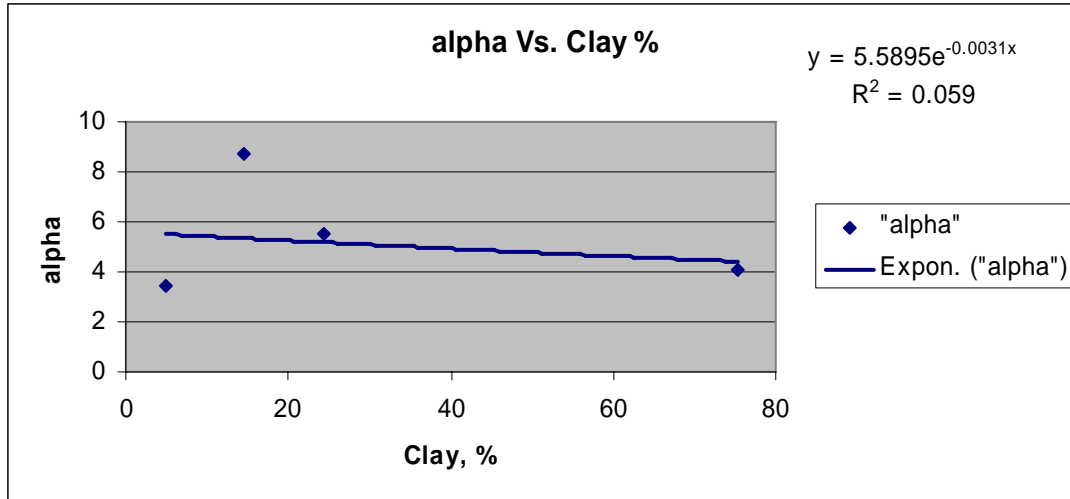


**Figure 36: Variation in the power function coefficient  $\alpha$  (98% Standard Proctor density at 1% strain) as a function of soil clay content.**

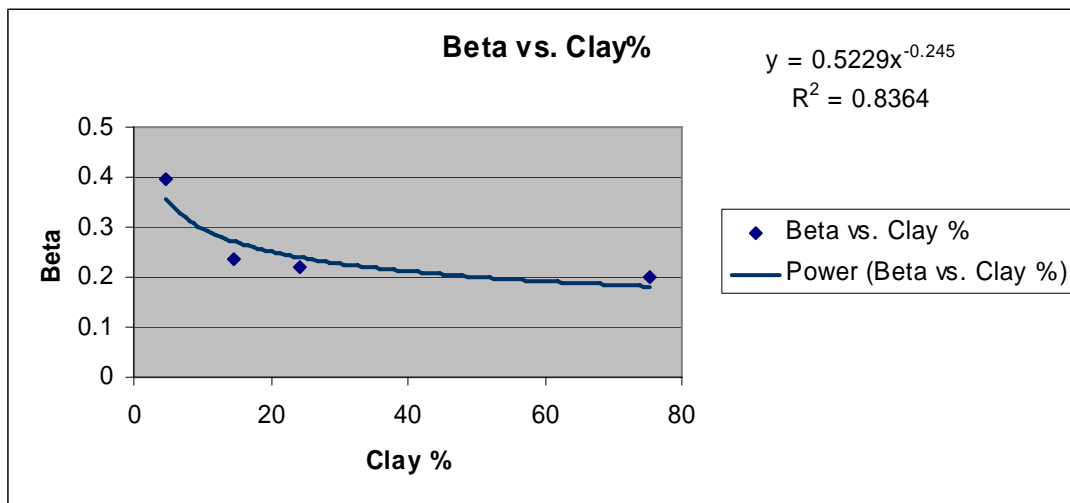


**Figure 37: Variation in the power function coefficient  $\beta$  (98% Standard Proctor density at 1% strain) as a function of soil clay content.**

**Table 12: Best fit value of the power function coefficients describing the change in deviator stress ( $\sigma_1 - \sigma_3$ ) at 1% strain as a function of suction ( $\mu_w$ ) for soils that have been compacted at 103% of Proctor density.**

Soil	Clay %	$\alpha^\dagger$	$\beta^\dagger$	R2
Duluth TH23	75.2	4.05	0.200	0.65
Red Lake Falls	24.3	5.53	0.222	0.81
MN Road	14.5	8.68	0.238	0.78
Red Wing	4.8	3.46	0.398	0.77

$$\dagger (\sigma_1 - \sigma_3) = \alpha \mu_w^\beta$$

**Table 13: Table 13: Best fit value of the power function coefficients describing the change in deviator stress ( $\sigma_1 - \sigma_3$ ) at 1% strain as a function of suction ( $\mu_w$ ) for soils that have been compacted at 98% of Proctor density.**

Soil	Clay %	$\alpha^\dagger$	$\beta^\dagger$	R2
Duluth TH23	75.2	5.55	0.188	0.70
Red Lake Falls	24.3	5.77	0.235	0.58
MN Road	14.5	5.69	0.298	0.81
Red Wing	4.8	8.58	0.334	0.77

$$\dagger (\sigma_1 - \sigma_3) = \alpha \mu_w^\beta$$

**Table 14: Correlation coefficients ( $R^2$ ) of “a” and “b” against % clay, % silt, % sand and plastic limit (PL) for soils compacted at 98% and 103% of standard Proctor density.**

Variable	1% Strain for 98% Standard Proctor Density				1% Strain for 103% Standard Proctor Density			
	Sand	Silt	Clay	PL $^\dagger$	Sand	Silt	Clay	PL
$\alpha$	0.05	0.456	0.729	0.84	0.62	0.04	0.059	0.020
$\beta$	0.683	0.6	0.944	0.89	0.137	0.5	0.836	0.894
Variable	5% Strain for 98% Standard Proctor Density				5% Strain for 103% Standard Proctor Density			
	Sand	Silt	Clay	PL $^\dagger$	Sand	Silt	Clay	PL
$\alpha$	0.125	0.34	0.755	0.84	0.326	0.665	0.94	0.954
$\beta$	0.677	0.813	0.87	0.79	0.36	0.192	0.453	0.693

$^\dagger$  Except for PL, all  $R^2$  values are for a power function. R2 values for PL are for a linear function.

## Resilient Modulus of Unsaturated Soils

This section was put together by Drs. Tuncer Edil, Craig Benson, and Auckpath Sawangsuriya of the University of Wisconsin.

The properties and the compaction characteristic of four test soils are given in Table 2 and Fig. 38. The  $M_r$  instrumentation, i.e., load cell, cell pressure, two external LVDTs, and two internal LVDTs was calibrated to ensure the accuracy of measured data. The instrumentation used was compared with the NCHRP 1-28A requirement in Table 15. The calibration of  $M_r$  instrumentation is provided in Table 16. The spreadsheet was developed to incorporate the specimen information, new  $M_r$  protocol, external and internal deformation measurements, matric suction, and bender element results. The drying (desorption) SWCCs of the compacted soil specimens were determined from the developed test apparatus under a constant net confining pressure of 35 kPa. Figure 39 shows the SWCCs of four subgrade soils compacted near optimum compaction moisture content using the standard Proctor effort. Table 17 summarizes the fitting parameters of the SWCC for each sample in accordance with the Fredlund and Xing equation. The presence of clay content significantly affects the air-entry suction of these compacted soils because these soils contain much smaller pore sizes. As shown in Fig. 39, the air-entry suction of CH soil (% clay ~ 75) is highest, whereas the ML soil (% clay ~ 6) has the lowest air-entry suction. The air-entry suction of CL-1 and CL-2 soils is approximately similar (see also Table 17). This is attributed to the fact that clays exhibit higher air-entry suction than silty soils (Tinjum et al., 1997; Miller et al., 2002). Increased clay content causes an increase in the amount of water retained at a given suction and desaturation at higher matric suction.

The summary of the resilient modulus data are given in Table 18 and the individual test data sheets are given in Appendix E, which also list the fitting parameters ( $k_1$ ,  $k_2$ ,  $k_3$ ,  $k_6$ , and  $k_7$ ). Resilient modulus was calculated at a bulk stress of 83 kPa and octahedral shear stress of 19.3 kPa as recommended by NCHRP 1-28A (2003) for typical pavement stress conditions. Figures 40 and 41 respectively show resilient modulus based on external and internal displacement measurement as a function of the measured suction. Modulus increases with increasing suction as expected, however, it is in a narrower band based on internal displacement measurement for the range of soils tested. Figure 42 shows the shear wave velocity based on bender element measurements. Specimens were free of external stresses when the bender element measurements were made. A similar trend of shear wave velocity (i.e., modulus) increase with increasing suction is observed. Figures 43, 44 and 45 shows the same parameters as a function of water content. There is a greater spread of the data when all of the soils are considered in comparison to the plots of matric suction. This implies that matric suction is a more fundamental measure of the state of moisture in partially saturated soils. The effect of density (i.e., relative compaction) appears to be relatively minor once the specimens are compacted to within 5% of the maximum dry unit weight or 98-103% of standard Proctor density. Regardless of the relative compaction (when within the range of 98-103% of standard Proctor density) and type of soil, a linear semi-logarithmic equation between resilient modulus

**Table 15: Specifications for Load and Specimen Response Measurement Instrumentation (NCHRP 1-28A, 2003).**

Instrumentation	Requirement	UW-Madison Test
<b><u>Load Cell</u></b>		
Maximum load capacity, kN (lbs)	8.9 (2000)	25 (5600)
Required accuracy, N (lbs)	$\pm 17.8 (\pm 4)$	NA
<b><u>Cell Pressure</u></b>		
Required accuracy, kPa (psi)	0.7 (0.1)	1.4 (0.2)
<b><u>On-Specimen Axial Deformation</u></b>		
Minimum range, mm (in.)	$\pm 2.54 (\pm 0.1)$	$\pm 1 (\pm 0.04)$
Minimum AC output (mV)	3.5-20	5
Typical LVDT minimum sensitivity (mV/0.001 in.)	5.4-8.4	254
<b><u>Data Acquisition</u></b>		
Resolution	12-bit	16-bit
Sampling rate	30 kS/s	Max 250 kS/s

NA = Not available

**Table 16: Calibration of Mr Instruments.**

Instrumentation	Calibration Factor
Load cell	2.224 kN/V + 0.557
Cell pressure	69.934 kPa/V
Two Internal LVDTs	0.5277 mm/V and 0.2352 mm/V
Two External LVDTs	1.0454 mm/V and 1.1078 mm/V

**Table 17: SWCC parameters of four test soils**

Specimen	$\theta_s$	$\alpha$	n	m
ML-Std-Opt	0.338	0.031	1.582	0.368
CL-1-Std-Opt	0.375	0.004	1.285	0.222
CL-2-Std-Opt	0.325	0.002	1.338	0.250
CH-Std-Opt	0.535	0.0004	1.694	0.410

Note:  $\theta_r$  is zero in all cases.

**Table 18: Summary of Resilient Modulus and Bender Element Test Results**

<u>Red Wing-Silt</u>	Target Matrix	Measured Matrix	Water	Mr-ext	Mr-int	Travel	Length	Shear Wave	Shear	Poisson's	Bender
	Suction (kPa)	Suction (kPa)	Content (%)	(kPa)	(kPa)	Time (ms)	(mm)	Vel. (m/s)	Modulus (kPa)	Ratio	Modulus (kPa)
RW-103%											
RW-103%-S0-R1	0	23	17.6	34507	48652	1653	204	123	29798	0.35	80455
RW-103%-S50-R1	345	44	11.7	42015	72489	1023	206	201	76166	0.35	205649
RW-103%-S22-R1	151.8	196	11.3	65606	149142	906	205	226	94822	0.35	256020
RW-98%											
RW-98%-S0-R1	0	9	19.6	27051	33322	2011	203	101	19679	0.35	53132
RW-98%-S50-R2	345	34	15.3	29287	50978	1292	204.25	158	46447	0.35	125406
RW-98%-S50-R1	345	83	10.7	41024	62201	1034	203	196	69001	0.35	186303
RW-98%-S22-R1	151.8	668	10.8	42117	103536	886	203	229	94074	0.35	254001
<u>MnRoad-Lean Clay</u>											
MnRd-103%											
MnRd-103%-S0-R1	0	25	16.4	21685	24504	1281	203	158	49299	0.35	133106
MnRd-103%-S22-R1	151.8	96	15.5	36657	50602	913.5	202	221	94749	0.35	255821
MnRd-103%-S50-R1	345	18949	10.3	56399	169638	339	200	590	658068	0.35	1776782
MnRd-98%											
MnRd-98%-S0-R1	0	27	17.6	13993	14890	1257	199	158	47609	0.35	128544
MnRd-98%-S22-R1	151.8	37	14.8	28370	52963	908	203.25	224	93405	0.35	252193
MnRd-98%-S50-R1	345	650	13.7	57598	104727	644	200.025	310	182867	0.35	493742
<u>Red Lake Falls-Lean Clay</u>											
RLF-103%											
RLF-103%-S0-R1	0	27	25.7	12615	13527	1983	200.75	101	18682	0.35	50442
RLF-103%-S22-R1	151.8	193	21.6	49149	94486	993.1	203	204	76162	0.35	205636
RLF-103%-S50-R1	345	2079	18.6	57378	127380	762	203	266	127307	0.35	343730
RLF-98%											
RLF-98%-S0-R1	0	59	24.5	20022	25099	1670	204	122	27435	0.35	74074
RLF-98%-S22-R1	151.8	43	27.0	10777	12217	1901	198	104	20507	0.35	55370
RLF-98%-S50-R1	345	153	19.6	40805	109534	821	202	246	104796	0.35	282948
RLF-98%-S22-R2	151.8	82	22.7	38552	54123	1262	203	160	46552	0.35	125690
<u>DI TH 23 Slopes-Fat Clay</u>											
TH23-103%											
TH23-103%-S0-R1	0	32	33.5	13424	13506.6	2120	206	97	15928	0.35	43005
TH23-103%-S22-R1	151.8	125	28.7	27275	30827	1528	208	136	32844	0.35	88678
TH23-103%-S50-R1	345	8542	21.5	62578	207451	576	199	345	207545	0.35	560370
TH23-98%											
TH23-98%-S0-R1	0	41	32.9	11163	18311	2088	184	88	12879	0.35	34773
TH23-98%-S22-R1	151.8	250	28.7	38185	66300	1350	205	152	39821	0.35	107518
TH23-98%-S50-R1_2	345	38	32.8	9781	11661	2000	194	97	14871	0.35	40153
TH23-98%-S50-R2	345	122	30.1	36096	47284	1350	205	152	39864	0.35	107633

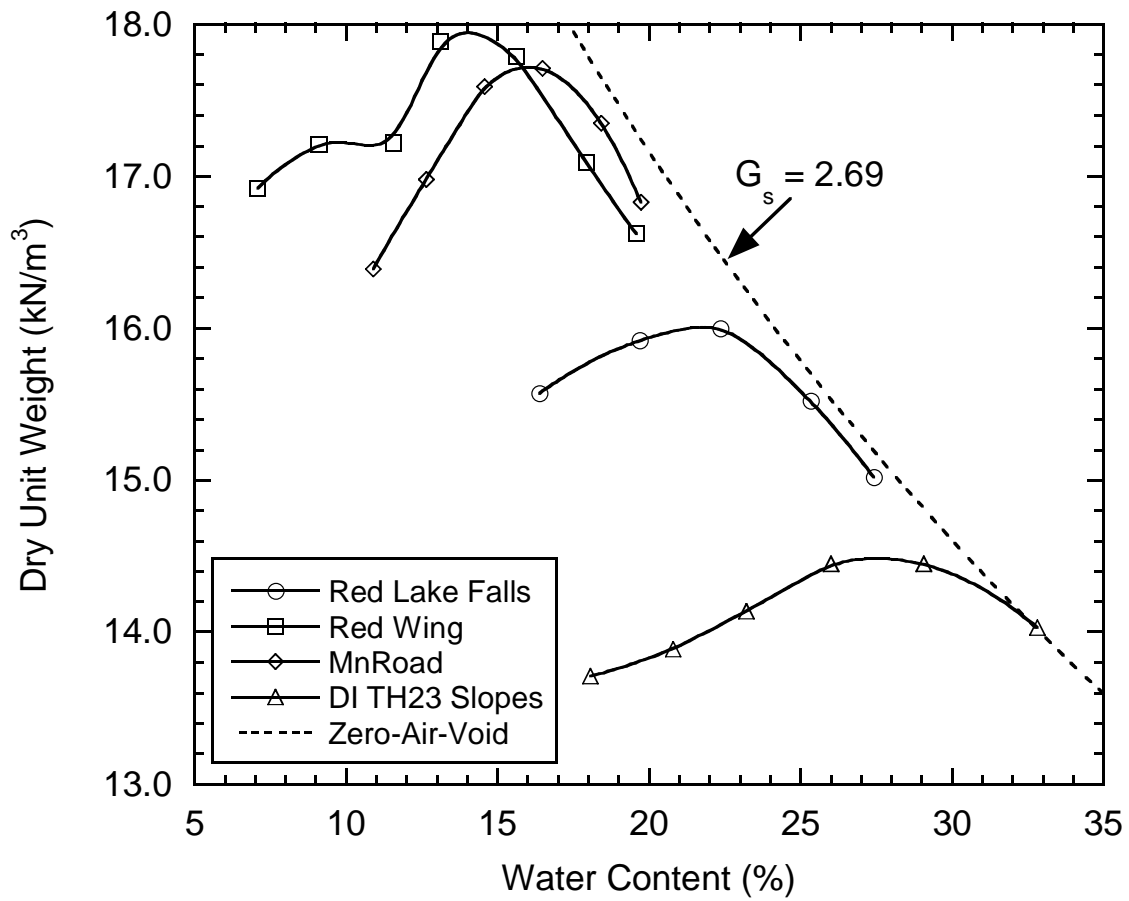


**Figure 38: Compaction characteristic of four test soils.**

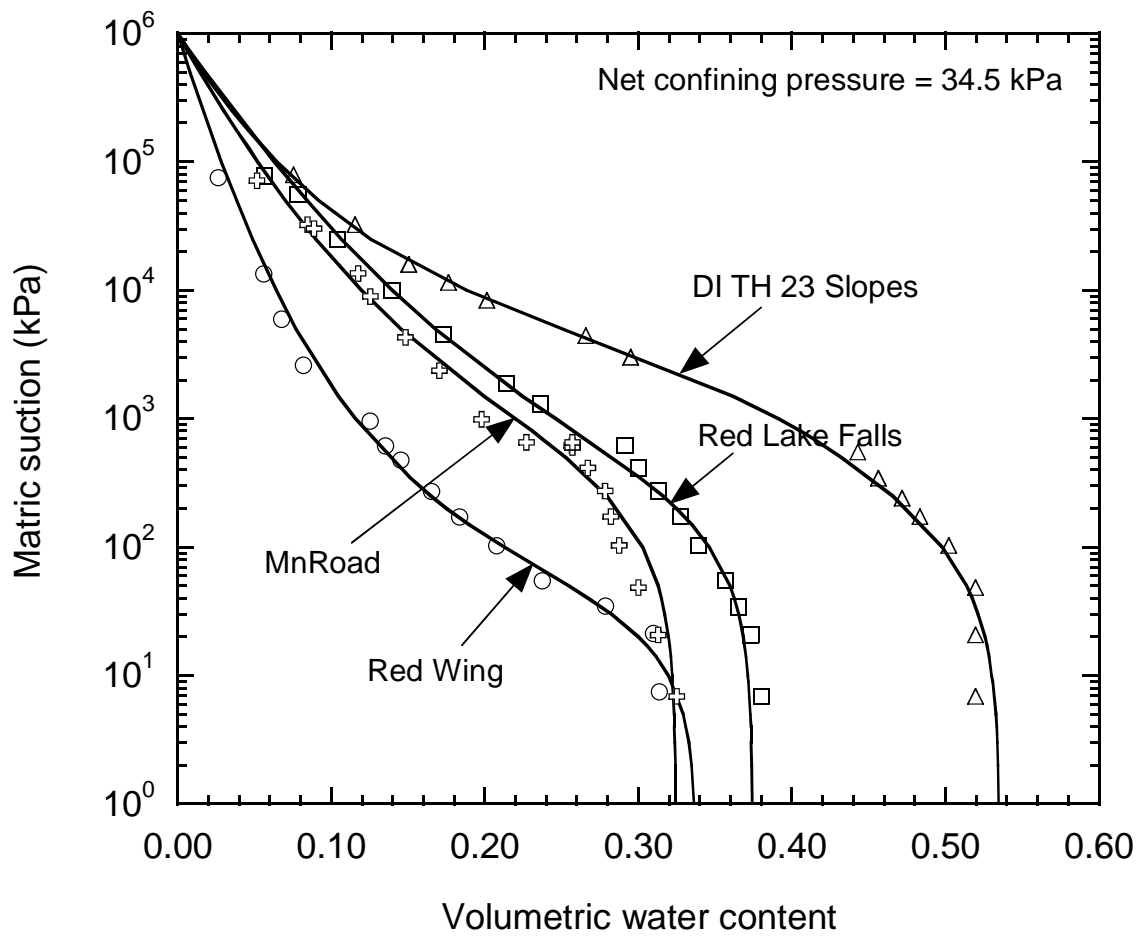


**Figure 39: SWCCs of four test soils compacted near the optimum.**

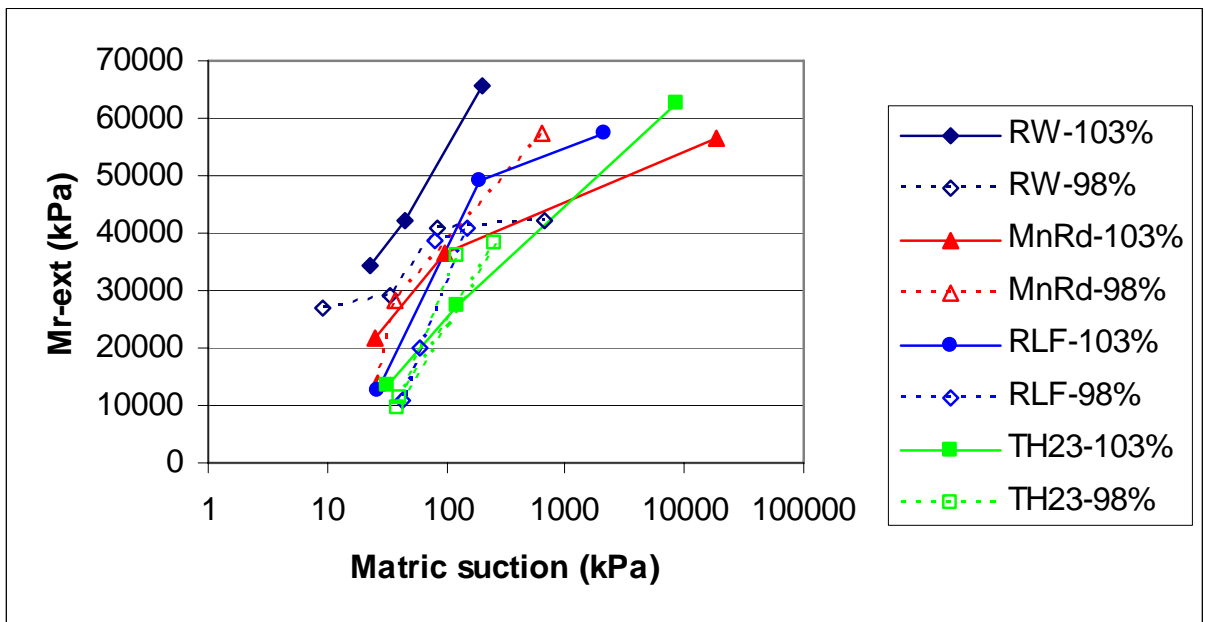


**Figure 40: Resilient Modulus (based on external displacement measurements) vs Matric Suction.**

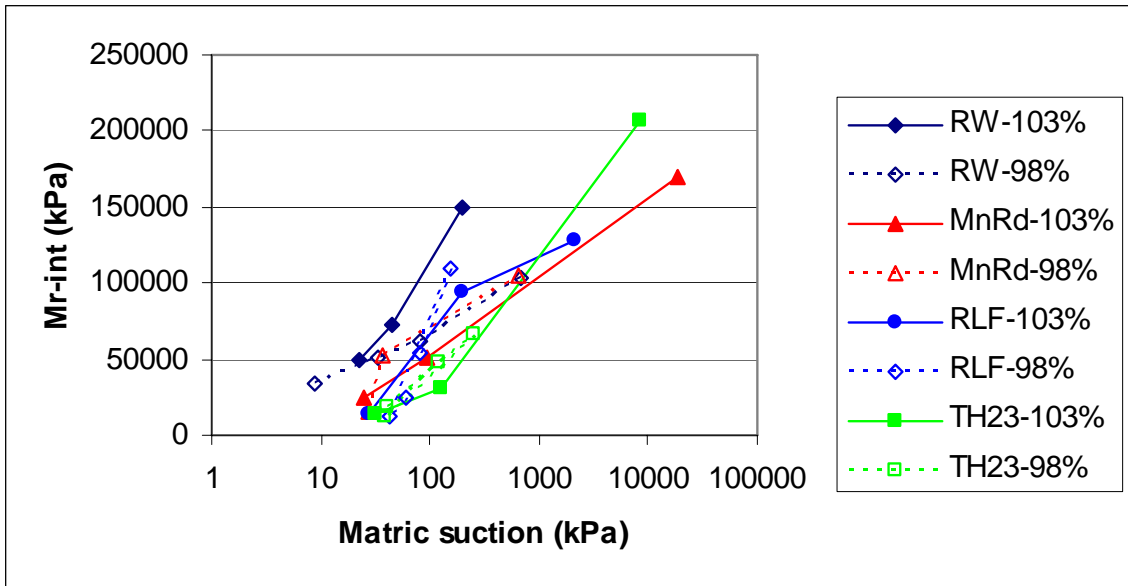


**Figure 41: Resilient Modulus (based on internal displacement measurements) vs Matric Suction.**

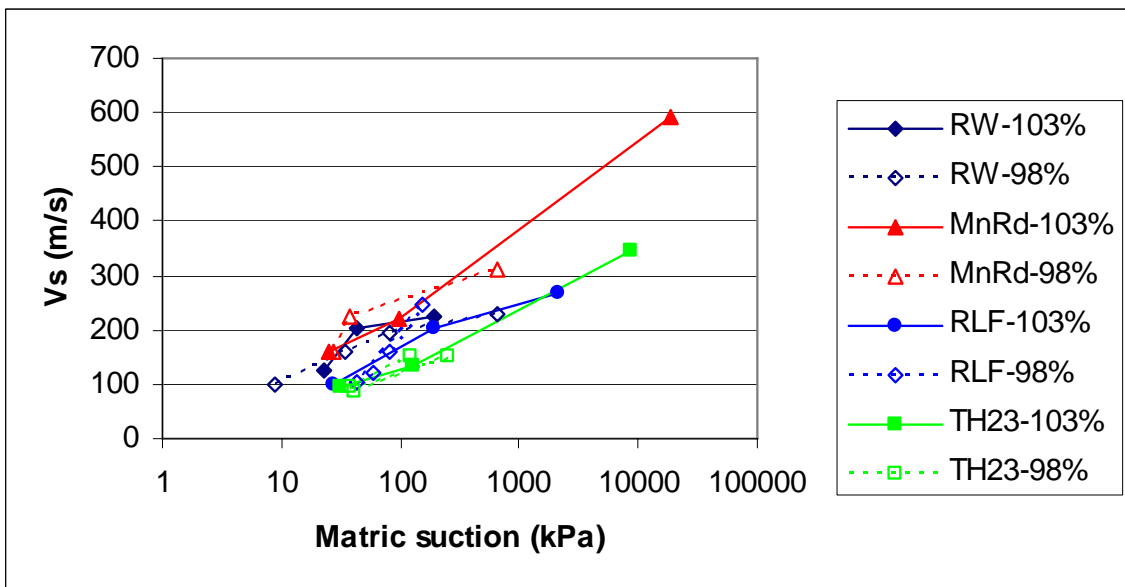


**Figure 42: Bender Element Shear Velocity vs Matric Suction.**

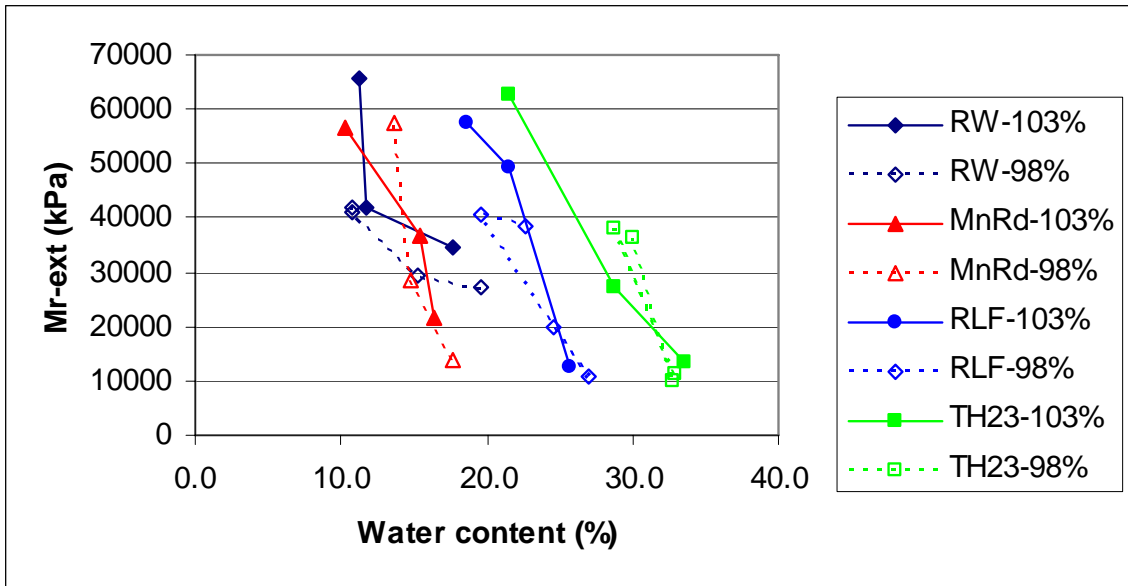


**Figure 43: Resilient Modulus (based on external displacement measurements) vs Water Content.**

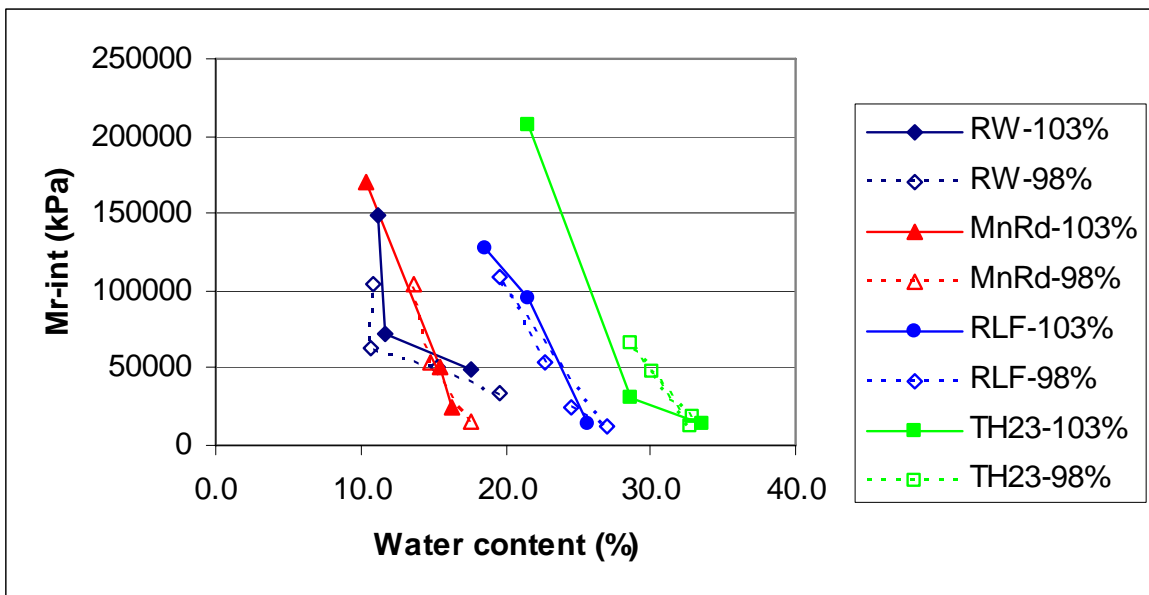


**Figure 44: Resilient Modulus (based on internal displacement measurements) vs Water Content.**

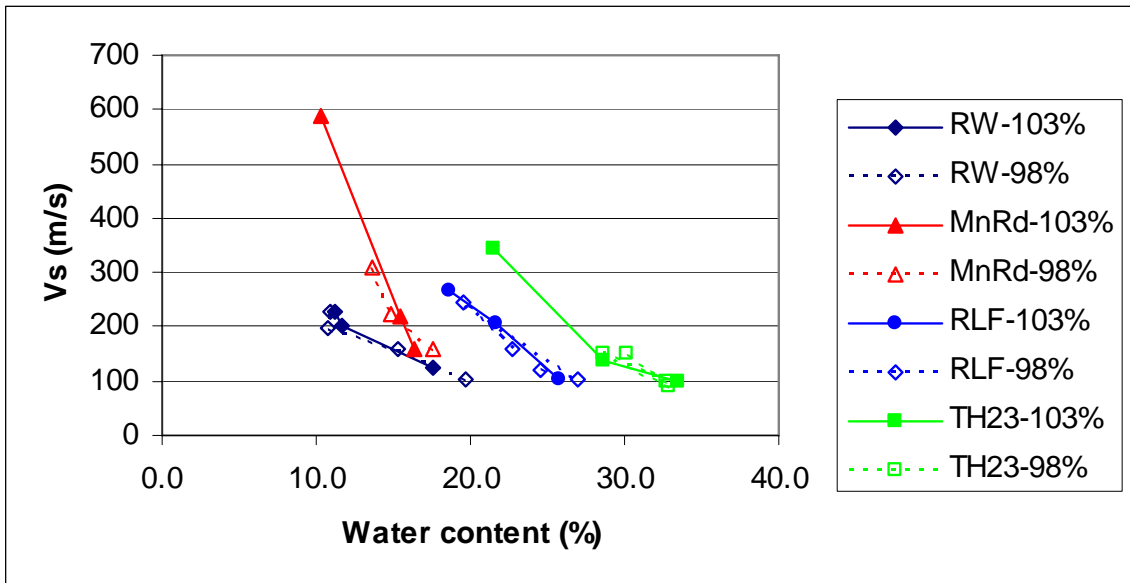


**Figure 45: Bender Element Shear Velocity vs Water Content.**

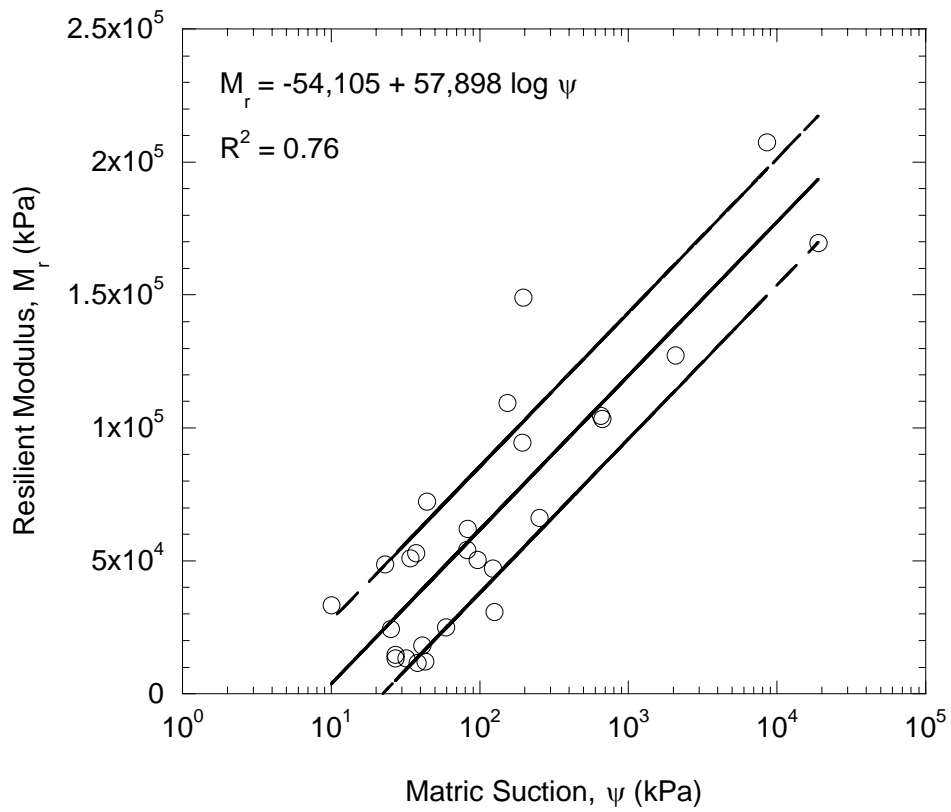


**Figure 46: A linear semi-logarithmic relationship between  $M_r$  and matric suction.**

and matric suction is developed based on the data from all of the soils tested (see Fig. 46):

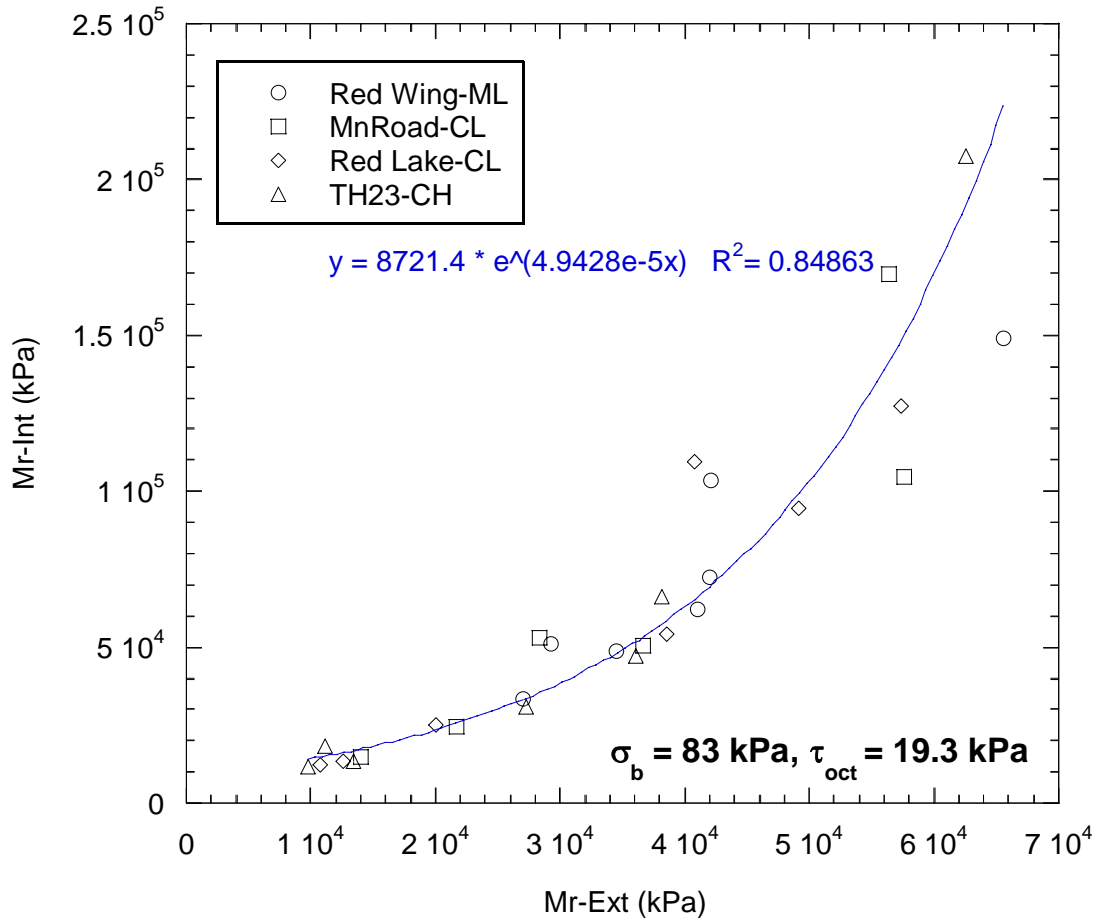
$$M_r = -54105 + 57898 \log \psi \quad (17)$$

where  $M_r$  = resilient modulus (based on internal displacement measurement and at a bulk stress of 83 kPa and octahedral shear stress of 19.3 kPa) and  $\psi$  = matric suction. The coefficient of determination ( $R^2$ ) is 0.76. The slope represents the average rate of increase of modulus with suction for any soil. Modulus at a given suction can be estimated from the modulus at a reference suction using the slope of Eq. (4) and the difference in suction for any soil within the error band represented by the upper and lower bounds.

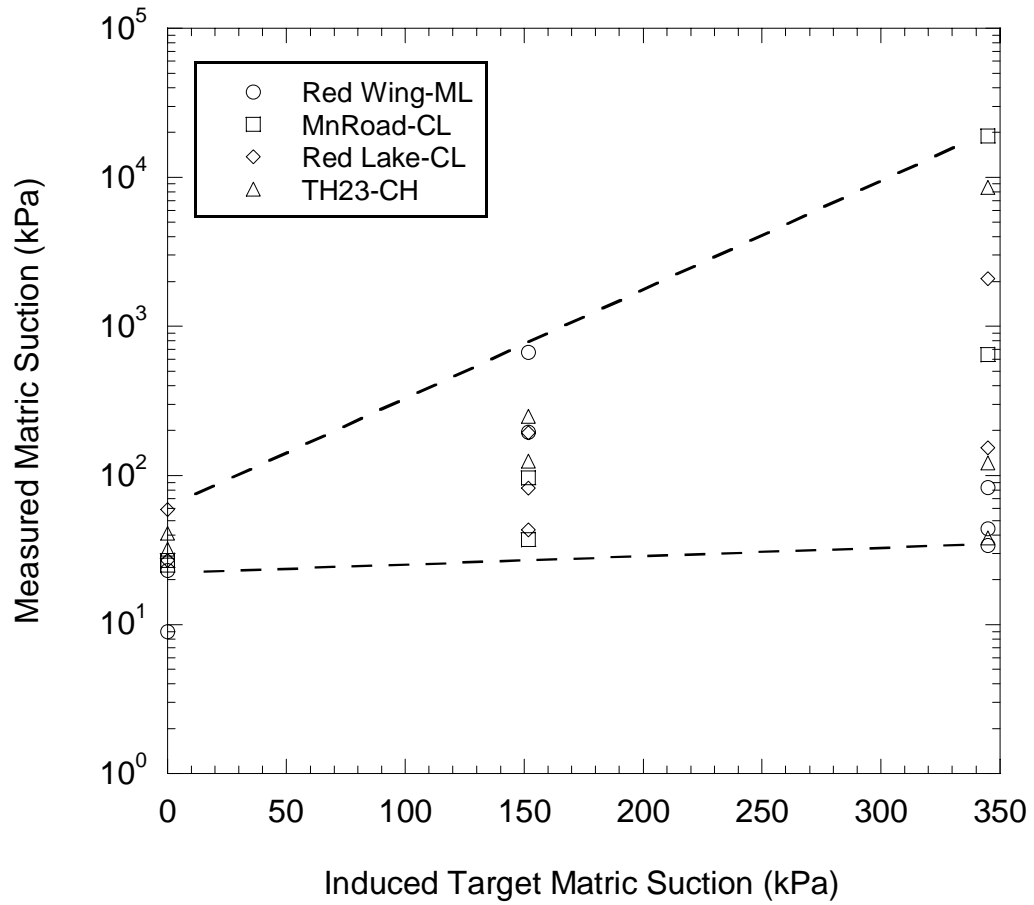
The relationship of resilient modulus based on internal displacement measurement versus that based on external displacement measurement is shown in Fig. 47. There is strong relationship between the two for all soils although the internal measurements always result in higher resilient modulus (1.7 times on average with a maximum of 3 times).

Figure 48 shows the relationship of measured suction using thermal dissipation sensor at the end of the test to the target suction during in the suction cell. The difference increases with increasing target suction. The equilibrium is difficult to ascertain in the suction cell especially at high suctions when small quantities of water is removed as the equilibrium is approached. Outflow measurements made using a horizontal capillary tube instead of a graduated cylinder would possibly reduce the discrepancy however it would also lengthen the specimen preparation period significantly.

Figures 49 and 50 compare the low-strain modulus as measured using bender elements with the resilient modulus based on external and internal displacement measurements. It is noted that bender element measurements were made with no external stress and the resilient moduli are calculated at a bulk stress of 83 kPa and octahedral shear stress of 19.3 kPa. There appears to be a much clearer correlation with the resilient modulus based on internal displacement measurements.



**Figure 47: Resilient Modulus Based on Internal versus External Displacement Measurement.**



**Figure 48: Matrix Suction Measured by Thermal Dissipation versus Induced Target Matrix Suction.**

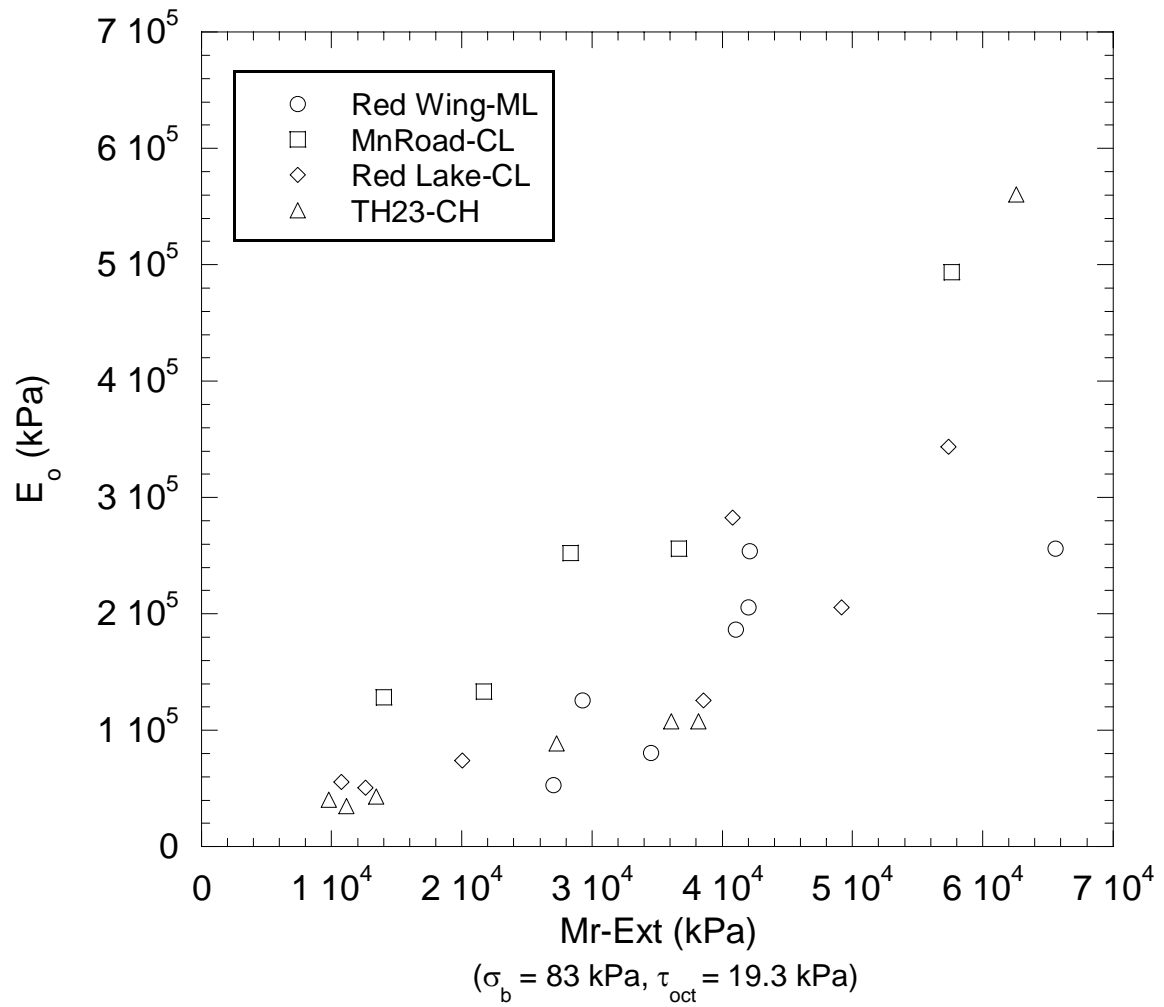


**Figure 49: Low-Strain Modulus from Bender Element versus Resilient Modulus based on External Displacement Measurement.**

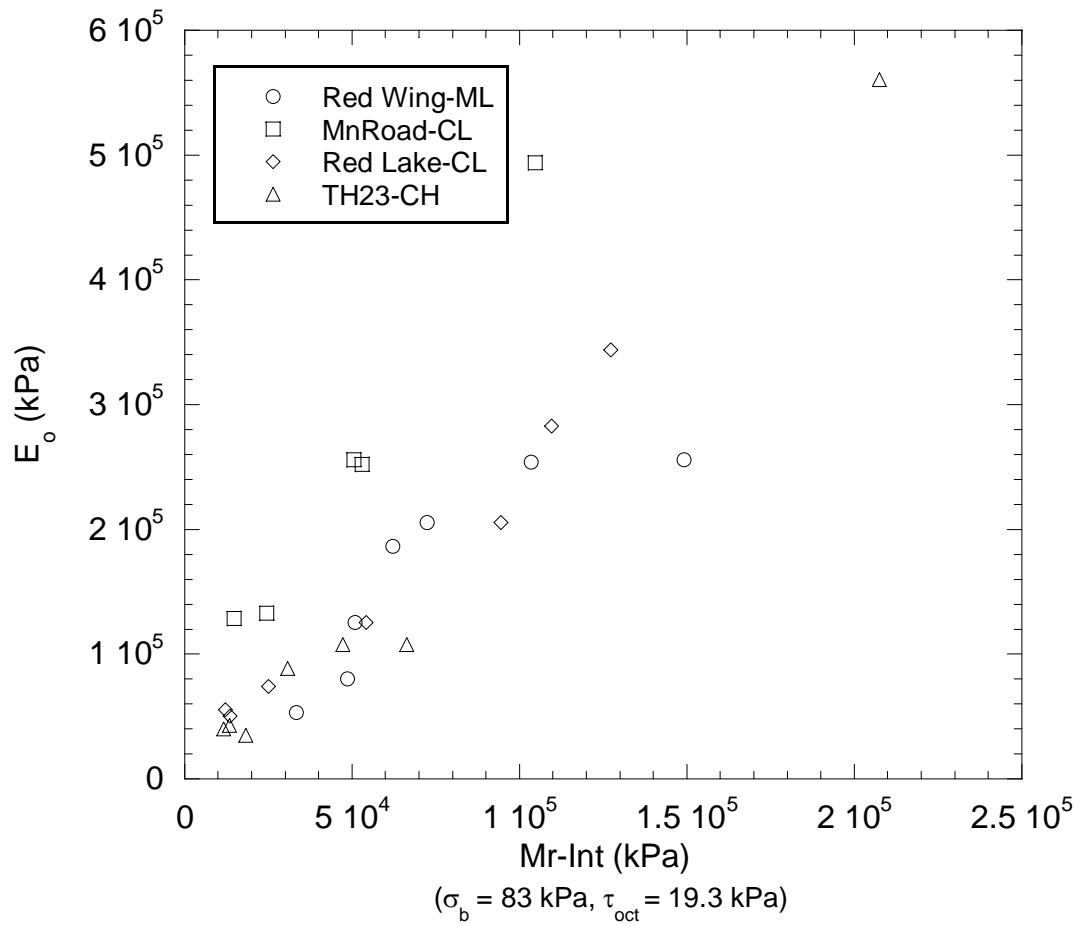


**Figure 50: Low-Strain Modulus from Bender Element versus Resilient Modulus based on Internal Displacement Measurement.**

## Resilient Modulus–Suction and Resilient Modulus–Moisture Relationships

The relationships between resilient modulus ( $M_r$ ) (based on internal or external displacement measurement and at a bulk stress of 83 kPa and octahedral shear stress of 19.3 kPa as recommended by NCHRP 1-28A, 2003) and matric suction for the ML, CL-1, CL-2, CH specimens compacted at 98% and 103% relative compaction near optimum moisture content are shown in Figs. 51-54. In general,  $M_r$  increases with increasing matric suction in the range of matric suctions measured (i.e., from 0 to ~10 MPa). This is consistent with  $M_r$  increase with matric suction as reported by Edil and Motan (1979), Edil et al. (1981), and Motan and Edil (1982).

The influence of relative compaction is not significant on the relationship. This might be explained by the fact that all the specimens were compacted near the optimum moisture content. As reported in Sawangsuriya (2006), the initial compaction moisture content plays a key role on the small-strain modulus-matric suction relationship, whereas the effect of compaction energy is minor (i.e., specimen compacted near optimum using the enhanced Proctor effort is comparable to that compacted near optimum using the standard Proctor effort). Sawangsuriya also indicated the difference in soil fabric or microstructure due to the difference in the initial compaction moisture content has a greater impact on small-strain shear modulus. A similar observation is also made in this study. The influence of relative compaction on  $M_r$ -matric suction relationship is insignificant since specimens were compacted near the optimum moisture content.

The variation of  $M_r$  with respect to matric suction for the ML, CL-1, CL-2, CH soils compacted near optimum indicated that at any given matric suction, the ML specimen tends to have the highest  $M_r$ , whereas the CH specimens tends to have lowest  $M_r$ . This might be attributed to the index properties and composition of the tested soils (e.g. plasticity index, fine fraction, and clay content). Further discussion will be given in the following section.  $M_r$  of the specimens measured at zero induced suction (or at saturation) increases approximately two to three times at  $10^3$  kPa suction. Larger increase in  $M_r$  was observed for the  $M_r$  measured with internal LVDTs .

The relationships between the resilient modulus ( $M_r$ ) and the volumetric water content for the ML, CL-1, CL-2, and CH specimens compacted at 98% and 103% relative compaction near optimum moisture content are illustrated in Figs. 55-59. In general,  $M_r$  increases as the volumetric water content decreases (i.e., following the drying curve) for the range of volumetric water contents measured. Consistent tendency were also observed for the resilient modulus-equilibrium water content relationship (Edil and Motan 1979) and small-strain shear modulus-volumetric water content (Sawangsuriya 2006).

The effect of relative compaction on  $M_r$ -volumetric water content relationship is similar to that of the  $M_r$ -matric suction relationship and hence no additional discussion is provided herein. The greater increase in  $M_r$  with volumetric water content is observed in the CH specimen, while gradual changes in  $M_r$  are obtained in the ML specimen. Percent increase in  $M_r$  is not directly proportional to the percent decrease in the amount of

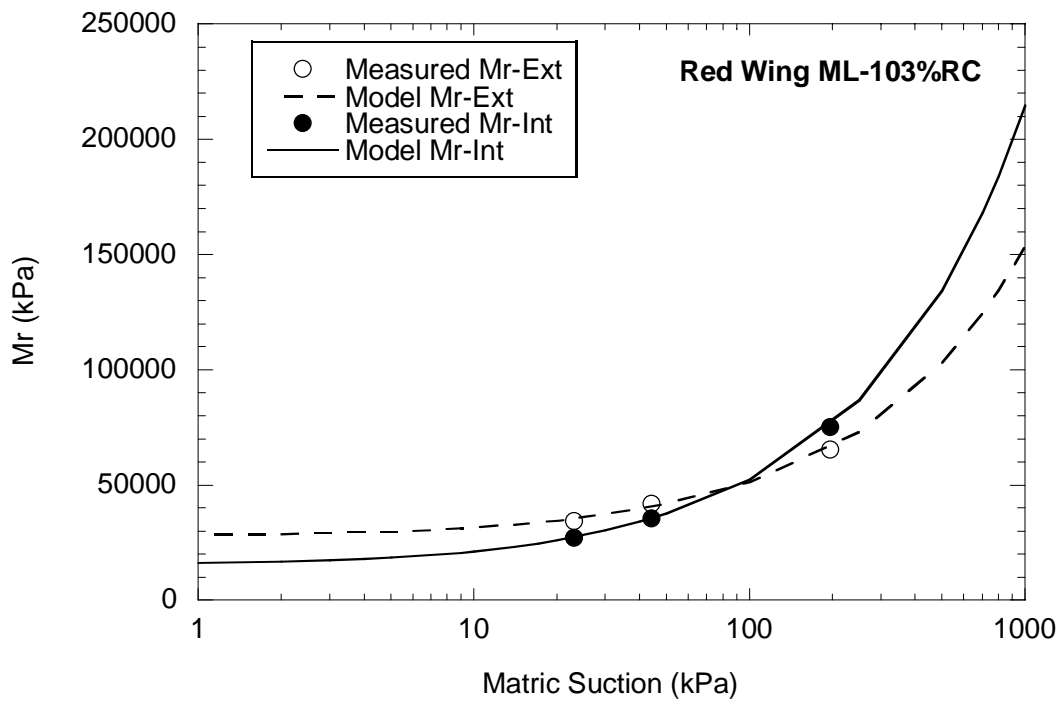
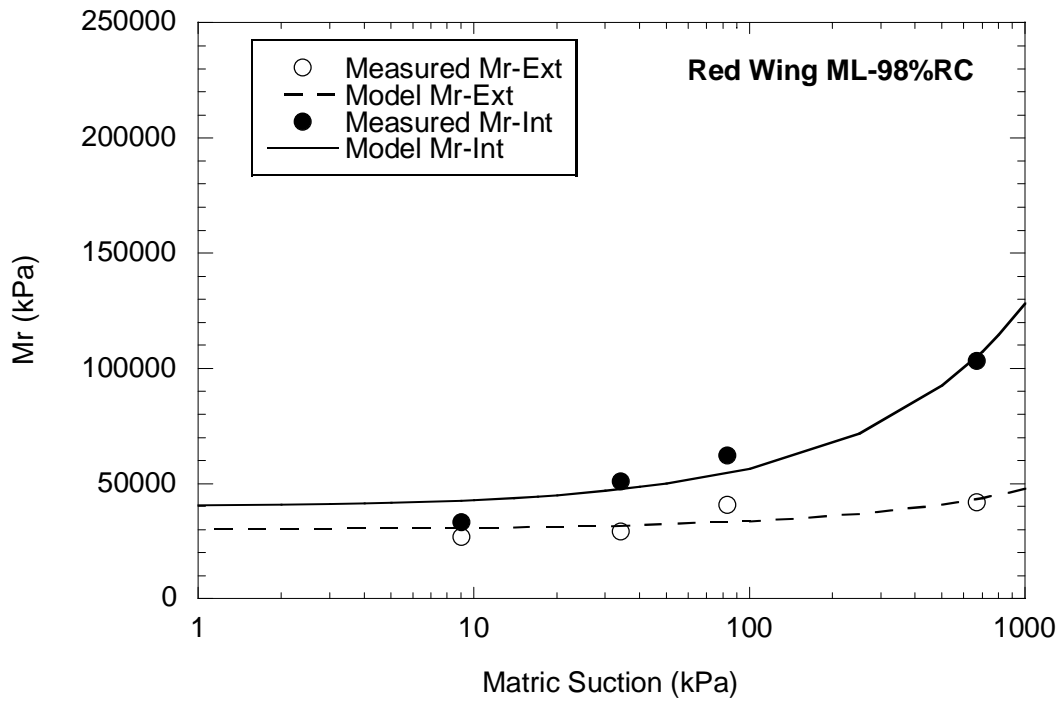


**Figure 51: Mr-matric suction relationship for the ML specimens compacted with 98% and 103% relative compaction.**

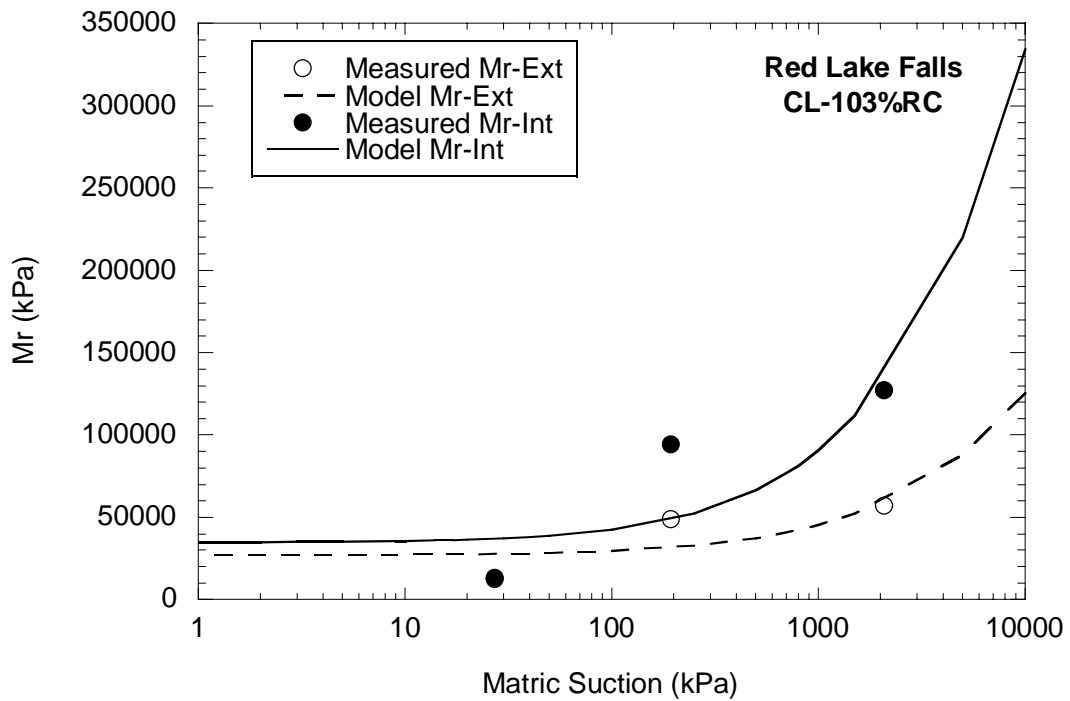
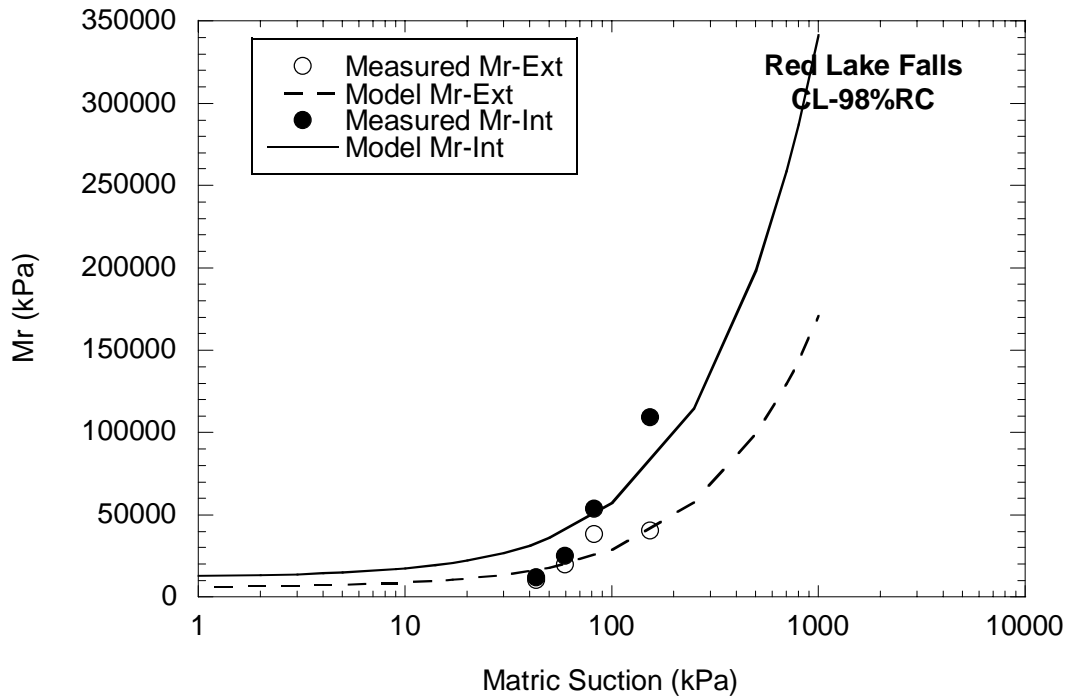


**Figure 52: Mr-matric suction relationship for the CL-1 specimens compacted with 98% and 103% relative compaction.**

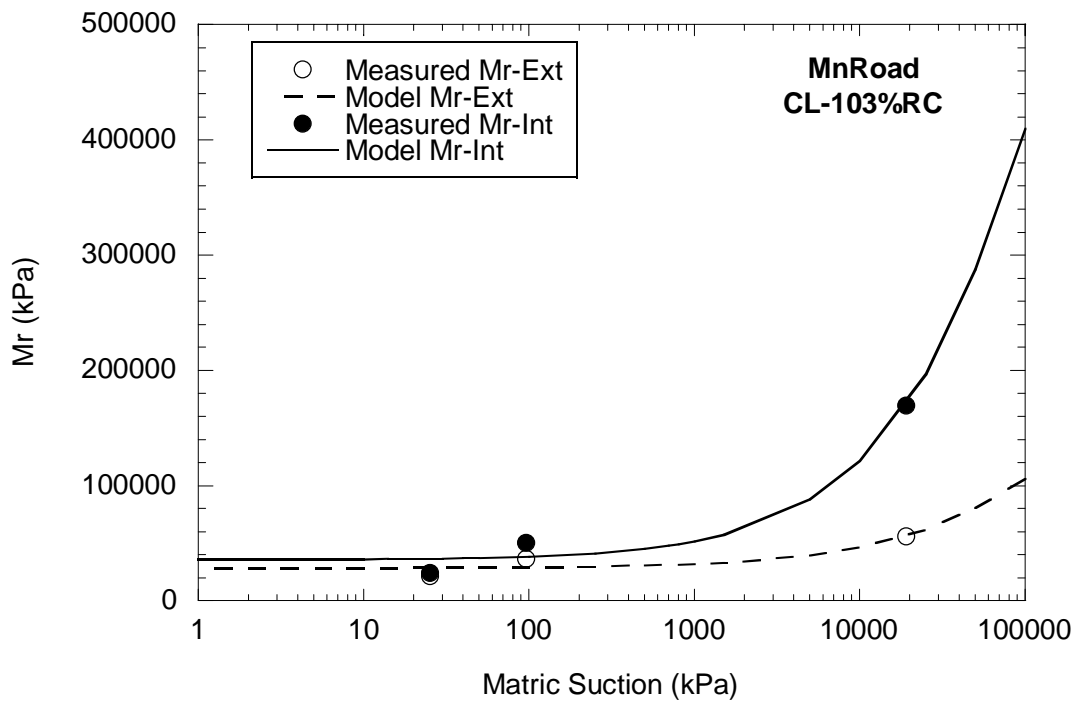
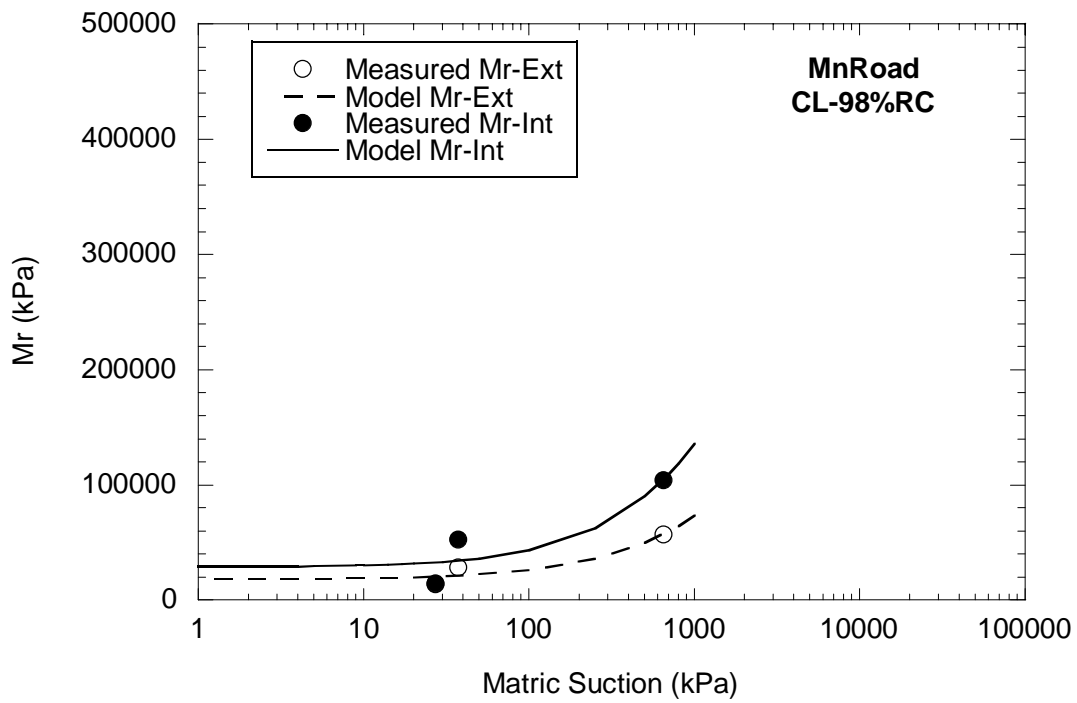


**Figure 53: Mr-matric suction relationship for the CL-2 specimens compacted with 98% and 103% relative compaction.**

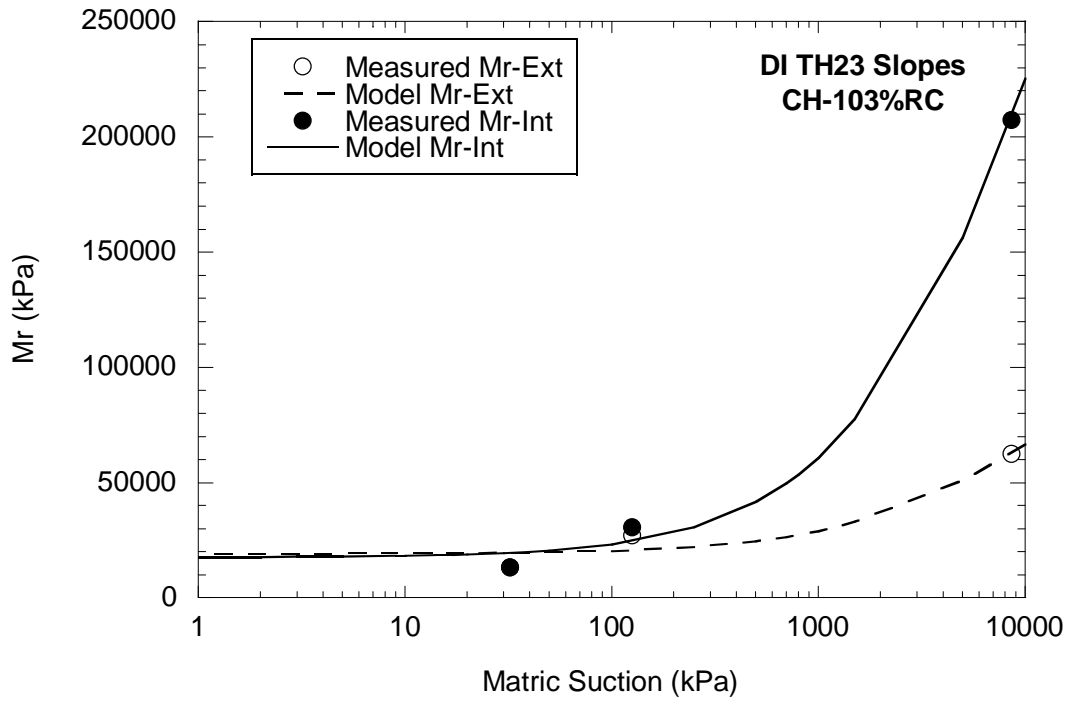
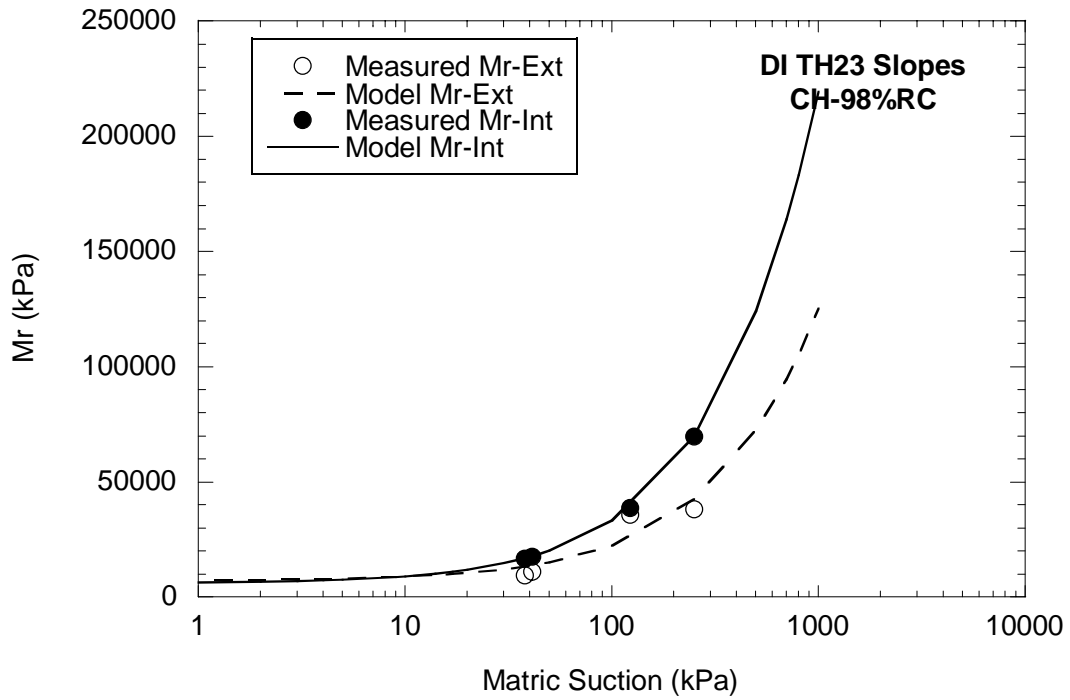


**Figure 54: Mr-matric suction relationship for the CH specimens compacted with 98% and 103% relative compaction.**

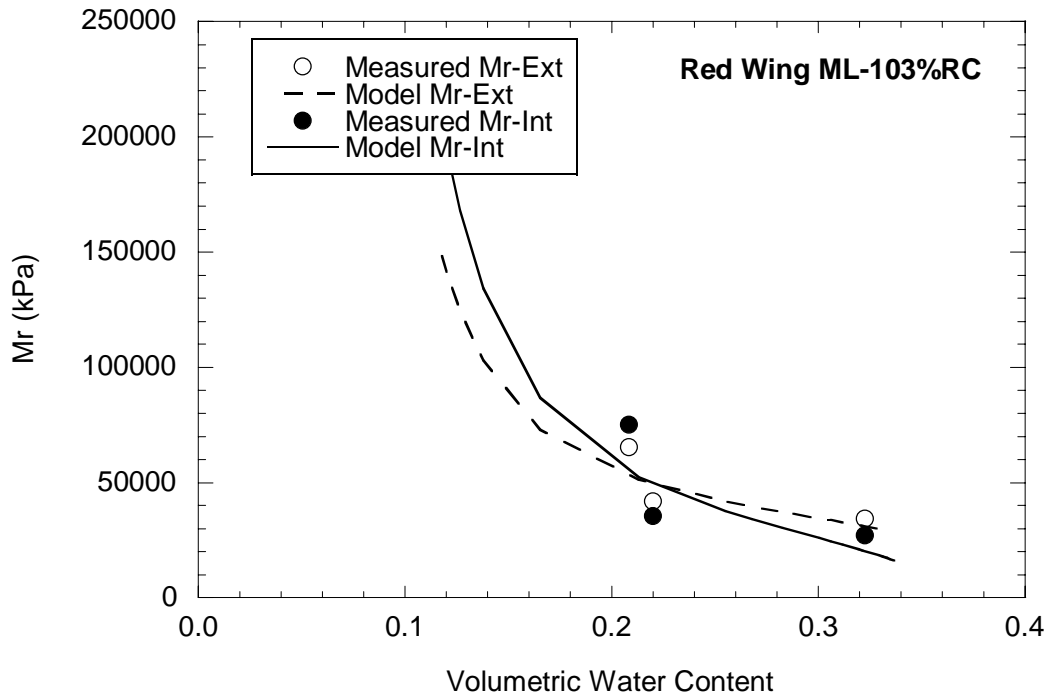
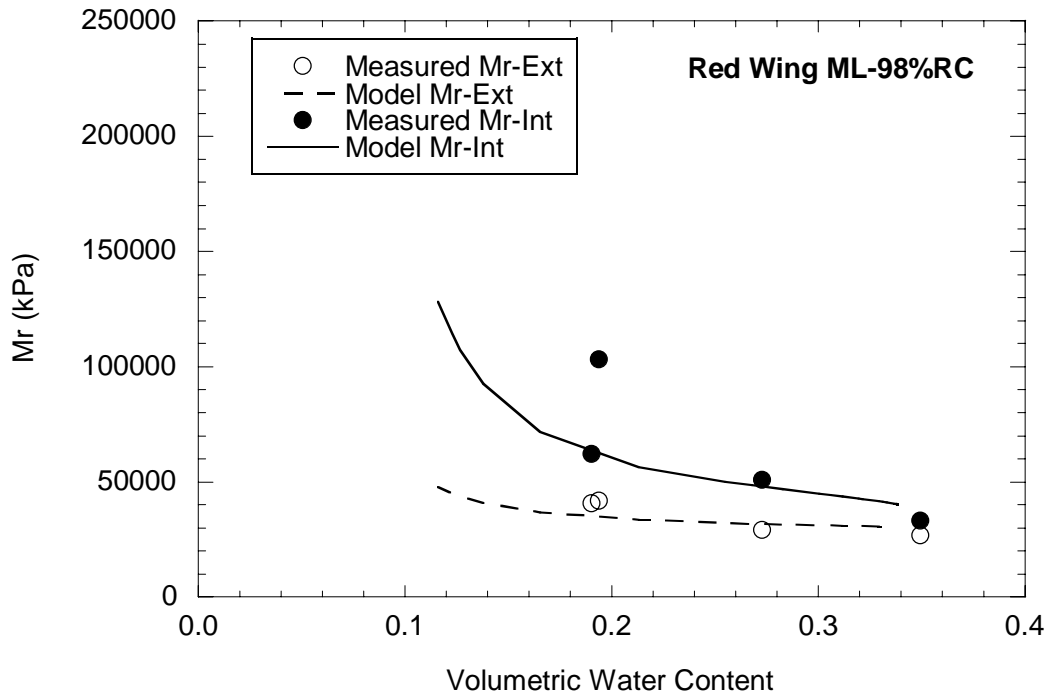


**Figure 55: Mr-volumetric water content relationship for the ML specimens compacted with 98% and 103% relative compaction.**

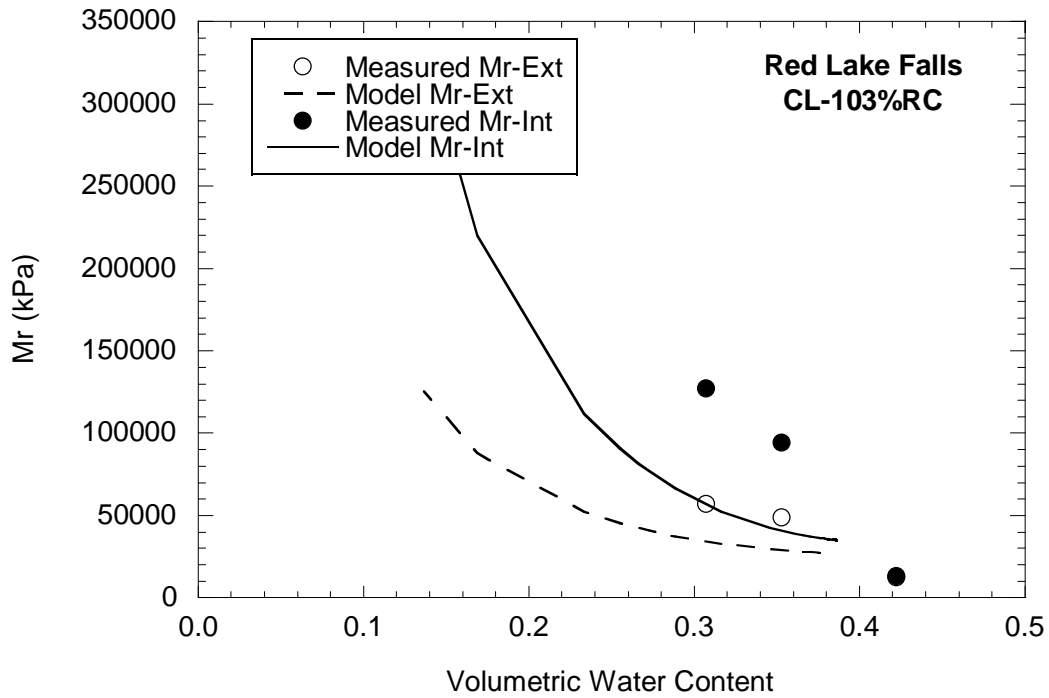
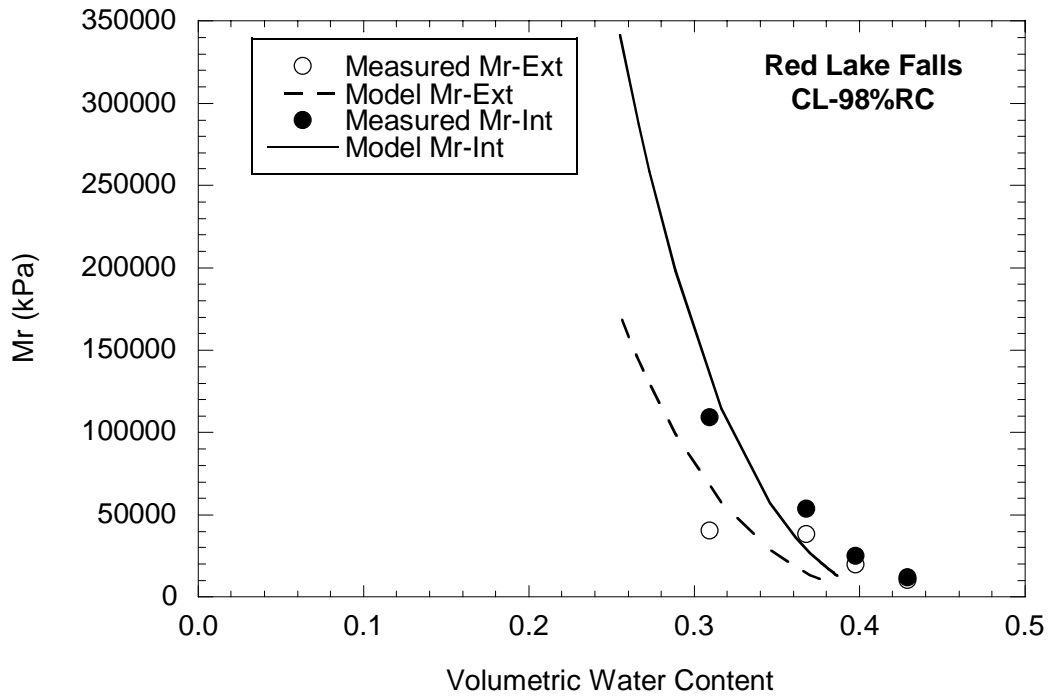


**Figure 56: Mr-volumetric water content relationship for the CL-1 specimens compacted with 98% and 103% relative compaction.**

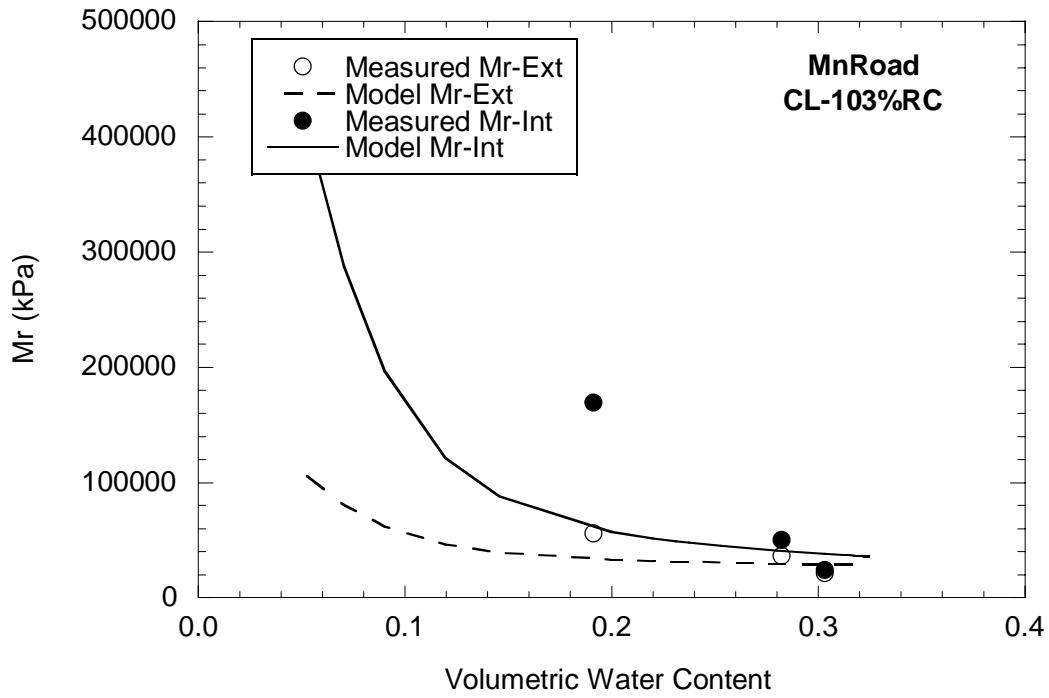
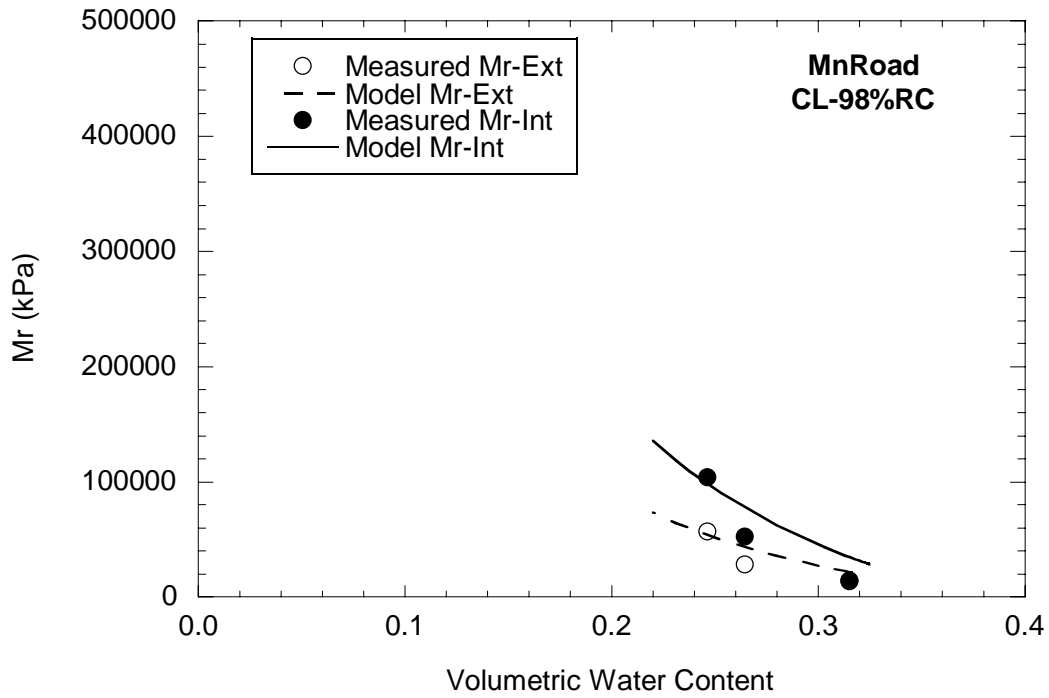


**Figure 57: Mr-volumetric water content relationship for the CL-2 specimens compacted with 98% and 103% relative compaction.**

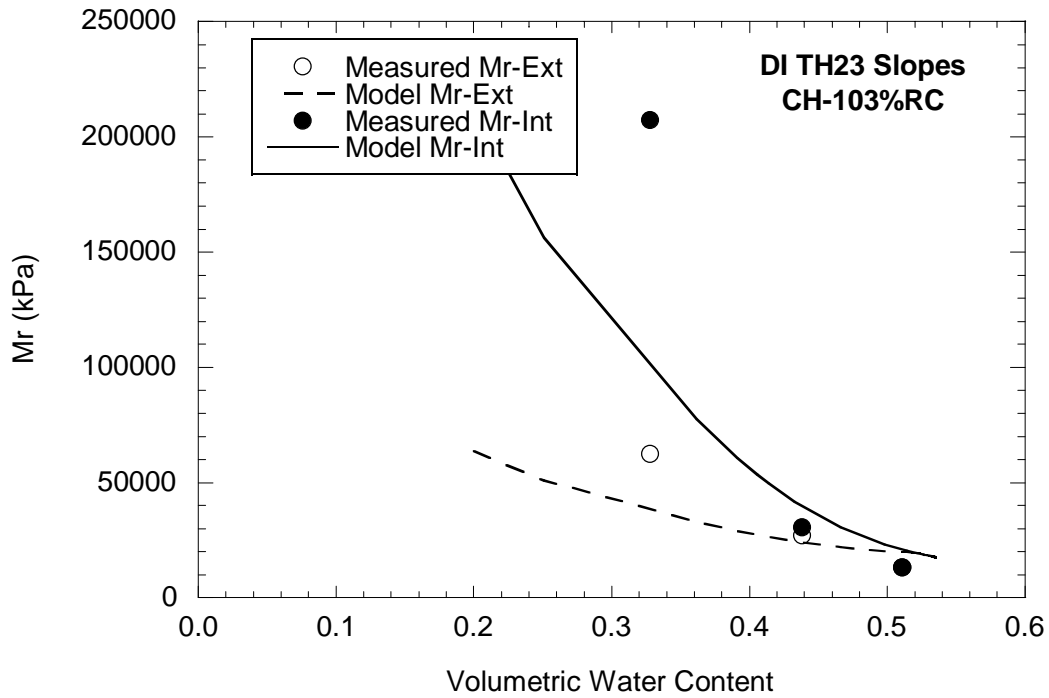
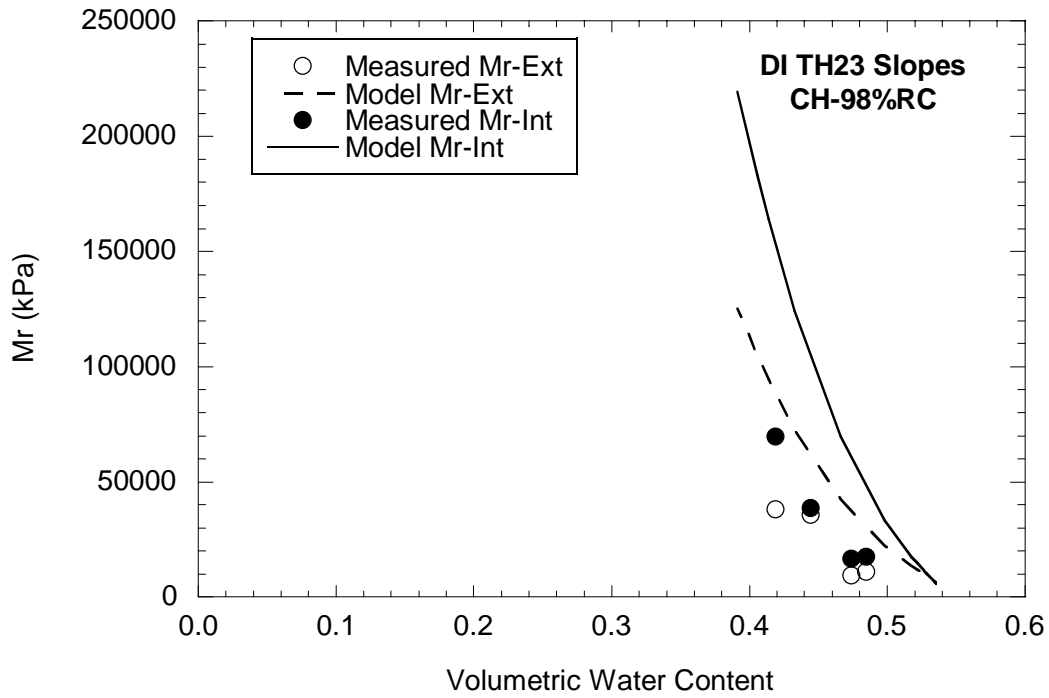


**Figure 58: Mr-volumetric water content relationship for the CH specimens compacted with 98% and 103% relative compaction.**

volumetric water content. In other words, higher increase in  $M_r$  tend to occur for small decreases in volumetric water content.

### Development of Mathematical Model

To describe the shear strength, deformation, and volume change behavior of unsaturated soils, a mathematical relationship should incorporate the two independent stress variables: net normal stress ( $\sigma_n - u_a$ ) and matric suction ( $u_a - u_w$ ) (Fredlund and Morgenstern 1977). Fredlund et al. (1978) proposed a relationship to explain the shear strength of unsaturated soils in terms of the two independent stress variables:

$$\tau_{us} = c' + (\sigma_n - u_a) \tan \phi' + (u_a - u_w) \tan \phi^b \quad (18)$$

where  $\tau_{us}$  is the shear strength of an unsaturated soil,  $c'$  is effective cohesion of saturated soil,  $\phi'$  is the effective angle of frictional resistance for a saturated soil, and  $\phi^b$  is the angle of frictional resistance defining the rate of increase in shear strength with respect to matric suction. The first part of Eq. (18) is related to the dry or saturated shear strength. This part of the equation is a function of normal effective stress as the shear strength parameters  $c'$  and  $\phi'$  are constant for a dry or saturated soil. The second part of Eq. (18) is the shear strength contribution due to matric suction. Equation (18) has been further modified by Vanapalli et al. (1996) in order to predict the shear strength of an unsaturated soil using the entire SWCC (i.e., 0 to 1,000,000 kPa). Vanapalli et al. modified the shear strength contribution due to matric suction (i.e., the second part of Eq. (18)) in terms of the normalized volumetric water content or effective saturation ( $\Theta$ ), which reflects the amount of water in the soil and varies from unity at saturation to a small value under residual moisture state conditions, and zero when the soil becomes dry. Since the wetted area of contact between the soil particles decreases with an increase in the soil suction and the decrease or increase in wetted area of water contact between the soil particles is related to the rate at which shear strength changes in unsaturated conditions, there is a strong relationship between the shear strength of unsaturated soils and the SWCC (Vanapalli et al. 1996). The modified equation is written as (Vanapalli et al. 1996, Fredlund et al. 1996):

$$\tau_{us} = c' + (\sigma_n - u_a) \tan \phi' + (u_a - u_w) (\Theta^\kappa \tan \phi') \quad (19)$$

where  $\kappa$  is a fitting parameter,  $\Theta = \frac{\theta}{\theta_s}$ ,  $\theta$  is the volumetric water content, and  $\theta_s$  is the saturated volumetric water content. Vanapalli and Fredlund (2000) examined different equations developed for predicting the shear strength of unsaturated soils and suggested that Eq. (19) provides better predictions in comparison to other equations.

Using a similar approach, the resilient modulus of unsaturated soils ( $M_r$ )<sub>us</sub> can be expressed as a function of three stress variables, the bulk stress ( $\sigma_b$ ), matric suction ( $u_a - u_w$ ), and deviator stress ( $\sigma_d$ ) (Fredlund et al., 1975). The relationship between resilient

modulus and the stress variables has been later confirmed by Fredlund et al. (1977). Oloo and Fredlund (1998) suggested such relationship be represented as follows:

$$\text{For coarse-grained soils,} \quad (M_r)_{us} = k\sigma_b^n + k_s(u_a - u_w) \quad (20)$$

For fine-grained soils,

$$\text{For } k_1 > \sigma_d \quad (M_r)_{us} = k_2 - k_3(k_1 - \sigma_d) + k_s(u_a - u_w) \quad (21)$$

$$\text{For } k_1 < \sigma_d \quad (M_r)_{us} = k_2 + k_4(\sigma_d - k_1) + k_s(u_a - u_w) \quad (22)$$

where  $k$ ,  $k_1$ ,  $k_2$ ,  $k_3$ ,  $k_4$ , and  $n$  are material constants determined experimentally,  $\sigma_b$  is the bulk stress (i.e., the summation of all three principle stresses), and  $k_s$  is a parameter that defines the rate of change of  $(M_r)_{us}$  with matric suction ( $u_a - u_w$ ). Note that the parameter  $k_s$  is soil dependent and is similar in definition to  $(\tan\phi^b)$  for the case of shear strength of unsaturated soils (Fredlund et al. 1978).

To provide a theoretical basis for the use of the SWCC in predicting  $(M_r)_{us}$ , the normalized volumetric water content ( $\Theta$ ) is included in the model to reflect the amount of water in the soil from the saturated to dry condition as suggested by Vanapalli et al. (1996). In the case of the shear strength of unsaturated soils, Vanapalli et al. (1996) related a parameter  $\tan\phi^b$  with  $\Theta^k \tan\phi'$ . This implies a simple linear relationship between  $\tan\phi^b$  and  $\Theta^k$  by having  $\tan\phi'$  as a linear fitting coefficient since the contribution of matric suction on shear modulus is similar to that on shear strength (i.e., increase or decrease the particle contact points). By having a constant  $k_{us}$  as a linear fitting coefficient, the parameter  $k_s$  can be rewritten as:

$$k_s = k_{us} \Theta^k \quad (23)$$

NCHRP 1-28A recommends the use of a five-parameter log-log model to represent the resilient modulus as a function of stress state as follows:

$$M_r = k_1 p_a \left( \frac{\sigma_b - 3k_6}{p_a} \right)^{k_2} \left( \frac{\tau_{oct} + k_7}{p_a} \right)^{k_3} \quad (24)$$

$$[k_1, k_2 \geq 0; \quad k_3, k_6 \leq 0; \quad k_7 \geq 1]$$

where  $\sigma_b$  is the bulk stress ( $\sigma_b = \sigma_1 + \sigma_2 + \sigma_3 = \sigma_1 + 2\sigma_3$ ),  $\tau_{oct}$  is the octahedral shear stress ( $= \frac{1}{3} \cdot \sqrt{(\sigma_1 - \sigma_2)^2 + (\sigma_1 - \sigma_3)^2 + (\sigma_2 - \sigma_3)^2} = \frac{\sqrt{2}}{3} \cdot (\sigma_1 - \sigma_3)$ ),  $\sigma_1$ ,  $\sigma_2$ ,  $\sigma_3$  ( $\sigma_2 = \sigma_3$ ) are the principal stresses,  $k_1$ ,  $k_2$ ,  $k_3$ ,  $k_6$ , and  $k_7$  are the fitting constants, and  $p_a$  is the atmospheric pressure ( $\sim 100$  kPa).

Based on the formulations published in the literature as presented in Eq. (20) through Eq. (24), a mathematical model for the resilient modulus of unsaturated soils ( $M_r$ )<sub>us</sub> can be rewritten as follows:

$$(M_r)_{us} = k_1 p_a \left( \frac{\sigma_b}{p_a} \right)^{k_2} \left( \frac{\tau_{oct}}{p_a} + 1 \right)^{k_3} + k_{us} p_a \Theta^\kappa (u_a - u_w) \quad (25)$$

$$[k_1, k_2 \geq 0; \quad k_3 \leq 0; \quad k_{us} \geq 0]$$

where  $k_1$ ,  $k_2$ ,  $k_3$ , and  $k_{us}$  are fitting parameters optimized to obtain a best-fit between the measured and the predicted values,  $\Theta$  is the normalized volumetric water content,  $\kappa$  is the fitting parameter,  $(u_a - u_w)$  is the matric suction, and  $p_a$  is the atmospheric pressure (~100 kPa). The second term incorporates  $M_r$ -matric suction relationship of unsaturated soils. Note that the fitting parameters  $k_6$  and  $k_7$  are respectively close to 0 and 1 according to the experimental results. In addition, the fitting parameter  $\kappa$  of 1.0 appears to be appropriate within the measured suction range (< 10 MPa) when it is used to fit all of the data.

The model consists of two terms that incorporate two independent stress variables. The first term incorporates  $M_r$ -stress relationship of dry or saturated soils where the state of stress is expressed in terms of bulk stress and octahedral stress. The representative stress state can be selected for an appropriate design  $M_r$  for the subgrade soil. NCHRP 1-28A (2003) recommends using a deviator stress of 41 kPa and a confining pressure of 14 kPa for calculating the design  $M_r$  for the subgrade soils for typical pavement stress conditions. Based on these stresses, the corresponding bulk stress and octahedral shear stress are calculated to be 83 kPa and 19 kPa, respectively.  $M_r$  is calculated at a bulk stress ( $\sigma_b$ ) of 83 kPa and octahedral shear stress ( $\tau_{oct}$ ) of 19 kPa as recommended by NCHRP 1-28A (2003).

Since equilibrium is difficult to ascertain during suction inducement especially at higher suctions when small quantities of water is removed as the equilibrium is approached, the measured volumetric water content might be a misleading basis to establish equilibrium. If the equilibrium matric suction used in the model is independently measured such as with a thermal dissipation sensor (TDS), it can be used to obtain the corresponding equilibrium volumetric water content ( $\theta$ ) from the SWCC, and hence the normalized volumetric water content  $\Theta$ . In this study, the SWCC was used as determined separately using the pressure plate extractor and smaller specimens prepared near the optimum compaction moisture content. The test procedure for the SWCC determination is given in Sawangsuriya (2006). Therefore for a given soil, the corresponding normalized volumetric water content can be obtained if the equilibrium matric suction as measured with TDS is known.

### Model Validation

The measured  $M_r$  data at different induced suctions obtained experimentally were best-fitted with the proposed mathematical model along with the curve-fitting parameters obtained as shown in Figs. 51 to 58. Table 19 summarizes the fitting parameters of the

**Table 19: Summary of the fitting parameters of the mathematical model.**

Soil Type	Fitting parameters	98% RC		103% RC	
		External LVDTs	Internal LVDTs	External LVDTs	Internal LVDTs
Red Wing	$k_1$	305	405	282	158
Silt	$k_{us}$	0.5	2.6	3.7	5.8
MnROAD	$k_1$	186	288	289	362
Lean Clay	$k_{us}$	0.8	1.6	0	0.2
Red Lake	$k_1$	65	126	272	350
Falls Lean Clay	$k_{us}$	2.5	5.0	0.3	0.9
DI TH23	$k_1$	74	62	193	178
Slopes Fat Clay	$k_{us}$	1.6	2.9	0.1	0.6

RC = Relative Compaction

$k_2$  and  $k_3 = 0.0$

mathematical model. The model fitted the measured data reasonably well within the range of measured suctions (i.e., 0 to 10 MPa) as demonstrated in Figs. 51 to 58. It appears that the proposed model is able to capture the suction effect and quantitatively describe the behavior of  $M_r$  of the unsaturated soils tested.

The fitting parameter  $\kappa$  of 1.0 was used to fit all of the data and appeared to be appropriate within the measured suction range. Sawangsuriya (2006) studied different values of  $\kappa$  in the mathematical model for the small-strain shear modulus ( $G_0$ ) of unsaturated soils. That study indicated that larger  $\kappa$  resulted in smaller  $G_0$  at high suctions. In this study, different values of  $\kappa$  may need to be used at very high suctions; however, the curve-fitting model was not significantly impacted by the parameter  $\kappa$  for the range of the measured suctions.

The parameter  $k_1$  is the main material parameter that typically reflects the effects of soil type, soil fabric, and density that characterize the microstructure of the dry or the saturated soil. When soil becomes unsaturated, the contact force distribution in the particle assembly becomes dependent on pore size and its distribution as well as particle arrangement (or soil fabric) (Mitchell and Soga, 2005). Therefore, the parameter  $k_{us}$  reflects the contribution of matric suction (e.g. capillary force and surface attractive forces) on the contact between the soil particles in the unsaturated state. It should be noted that in this study every specimen was prepared at or near the optimum moisture content so there is no basis to expect significant soil fabric effect due to compaction moisture content variation. In addition, the relative compaction used for the compacted specimens was within a narrow range (i.e., between 98% and 103%). Consequently, the density does not play a major role in controlling modulus. A t-test analysis was performed in order to verify if there is a significant difference between  $M_r$  at 98% and  $M_r$  at 103% relative compaction irrespective of soil type and suction. Based on t-test comparison, there is a not significant difference between  $M_r$  at 98% and  $M_r$  at 103% relative compaction at a 95% confidence level irrespective of soil type and suction. The t-value ( $\sim 1.6$ ) is less than the critical t ( $\sim 1.7$ ).

It has been shown that for soil samples compacted to 90% or higher relative compaction, the density effect on modulus is small and negligible within experimental variability (Edil and Sawangsuriya, 2005). Of course, this is not true for an uncompacted natural deposit where there may be large variations in density. Consequently, the developed model is considered valid only for properly compacted soils at optimum moisture content. It is recommended that further study should be conducted to investigate the specimens compacted on the dry and wet side of the line of optimum (i.e., different compaction moisture contents, compaction energies, and (or) densities) for a more generalized model.

In the model,  $k_1$  captures the effect of soil type, whereas  $k_{us}$  captures the effect of matric suction along with normalized volumetric water content.  $k_1$  varied relatively less than  $k_{us}$ . The range of  $k_1$  for  $M_r$  based on internal displacement measurements varied from 62 to 405 (less than 10 times) for all soils, whereas  $k_{us}$  varied from 0.2 to 5.8 (more than an order of magnitude). To understand the physical meanings of the curve-fitting parameters ( $k_1$  and  $k_{us}$ ), the fitting parameters obtained from the proposed model are

plotted against the test soil characteristics. The relationships with four type of soils tested (Figs. 59 and 60) indicate that the parameter  $k_1$  exhibits some trends with liquid limit and plasticity index. The parameter  $k_1$  decreases as liquid limit and plasticity index increase. In contrast, no particular trend was observed for the relationship between parameter  $k_{us}$  and liquid limit and plasticity index. Therefore, it can be seen that  $k_{us}$  does not depend heavily on soil characteristics for this range of soil types tested in this study (i.e., primarily fine-grained soils) but somewhat dispersed in a band. A t-test was run on both  $k_1$  and  $k_{us}$  at 98% and 103% relative compaction. The results suggested that the difference in both  $k_1$  and  $k_{us}$  at 98% and 103% relative compaction is not statistically significant at 95% confidence level. The t-values for  $k_1$  and  $k_{us}$  based on internal displacement measurement are respectively 0.4 and 0.8 and the t-values for  $k_1$  and  $k_{us}$  based on external displacement measurement are respectively 1.7 and 0.3, which are less than the critical t ( $\sim 2$ ). The statistical analyses indicate that the relative compaction used in the study has no significant impact on parameters  $k_1$  and  $k_{us}$  and thus correspondingly on unsaturated  $M_r$ .

The relationship of parameters  $k_1$  and  $k_{us}$  with group index (a composite parameter that reflects the effects of Atterberg limits and percent fines) suggests that parameter  $k_1$  exhibits a slight decreasing trend, whereas parameter  $k_{us}$  is dispersed in a band as shown in Fig. 61 for the soils tested.

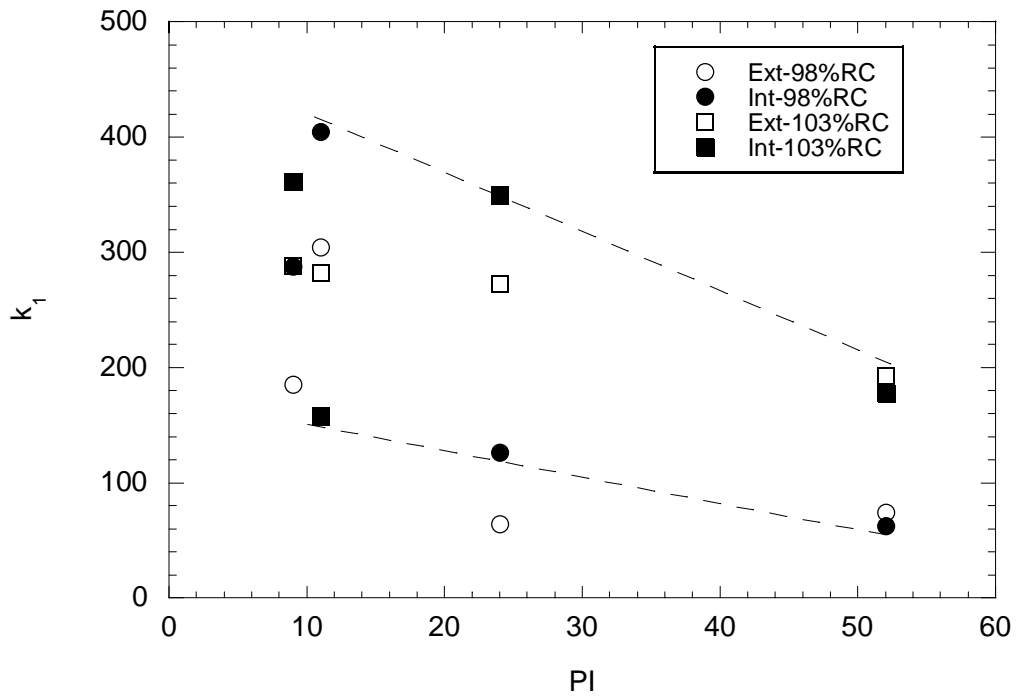
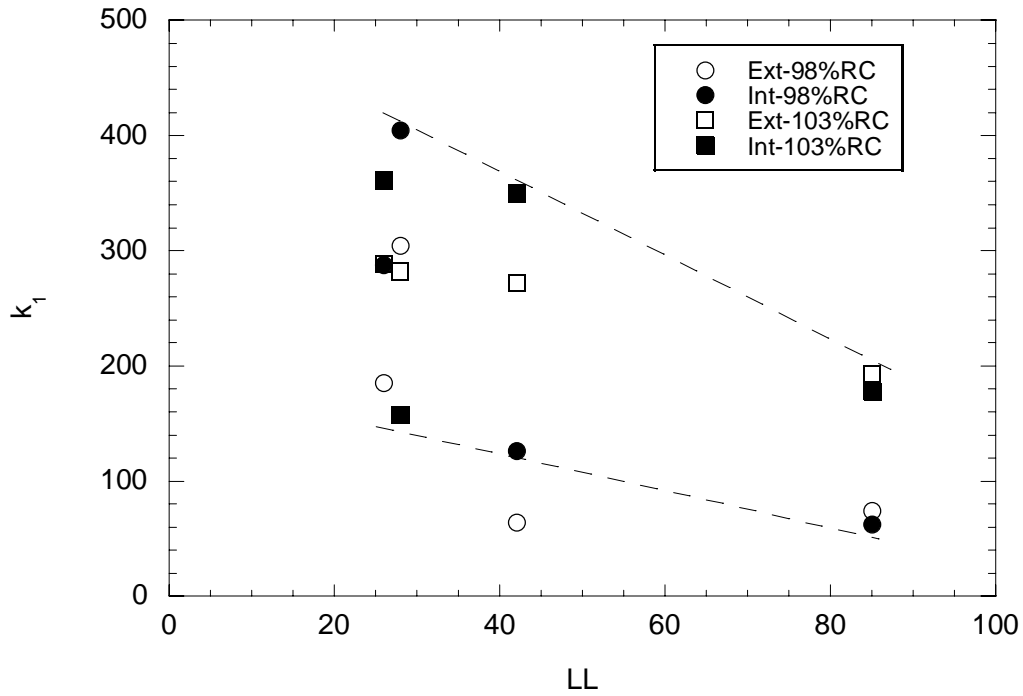


**Figure 59: Relationship of parameter k1 with liquid limit and plasticity index.**

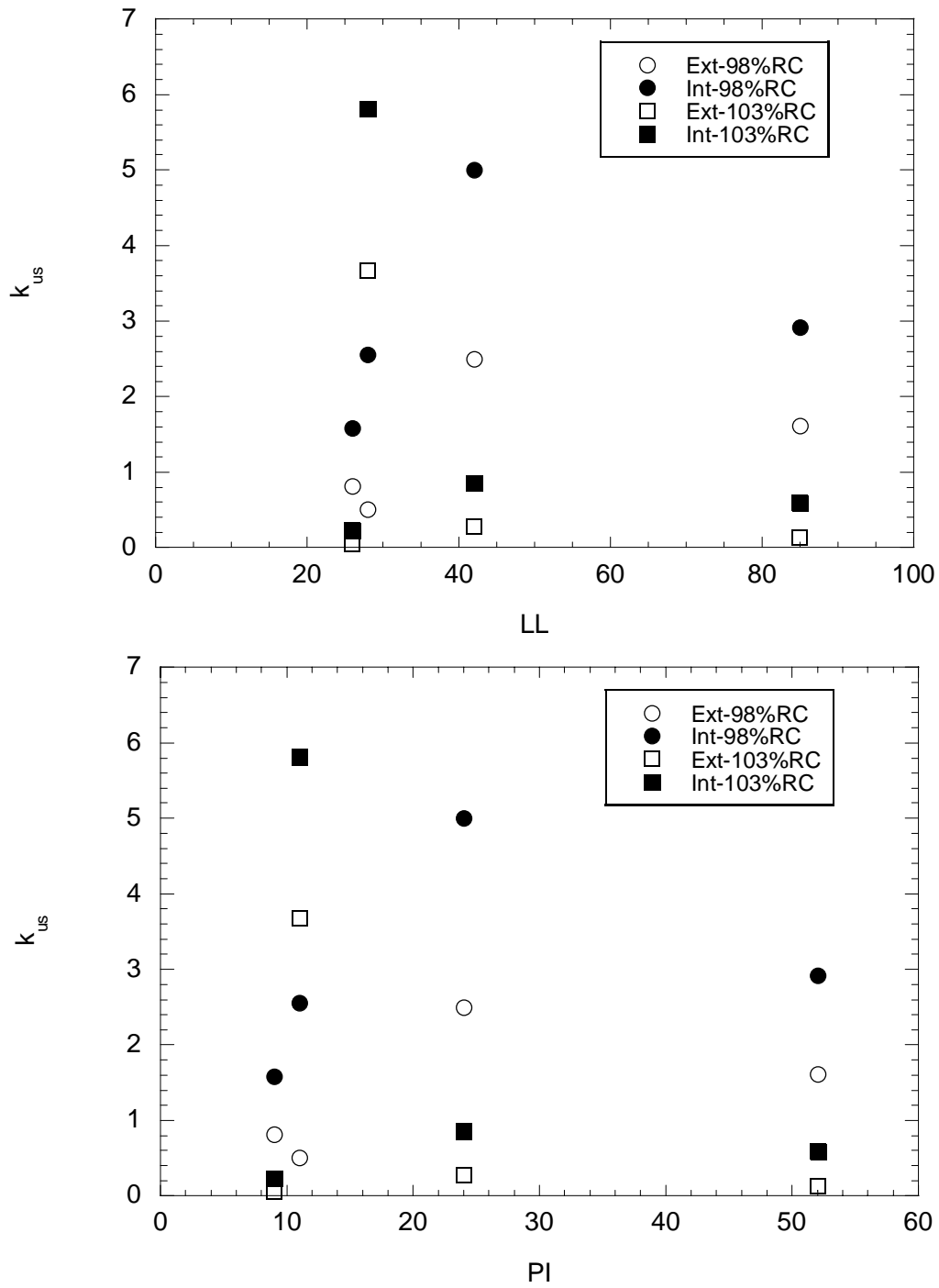


**Figure 60: Relationship of parameter  $k_{US}$  with liquid limit and plasticity index.**

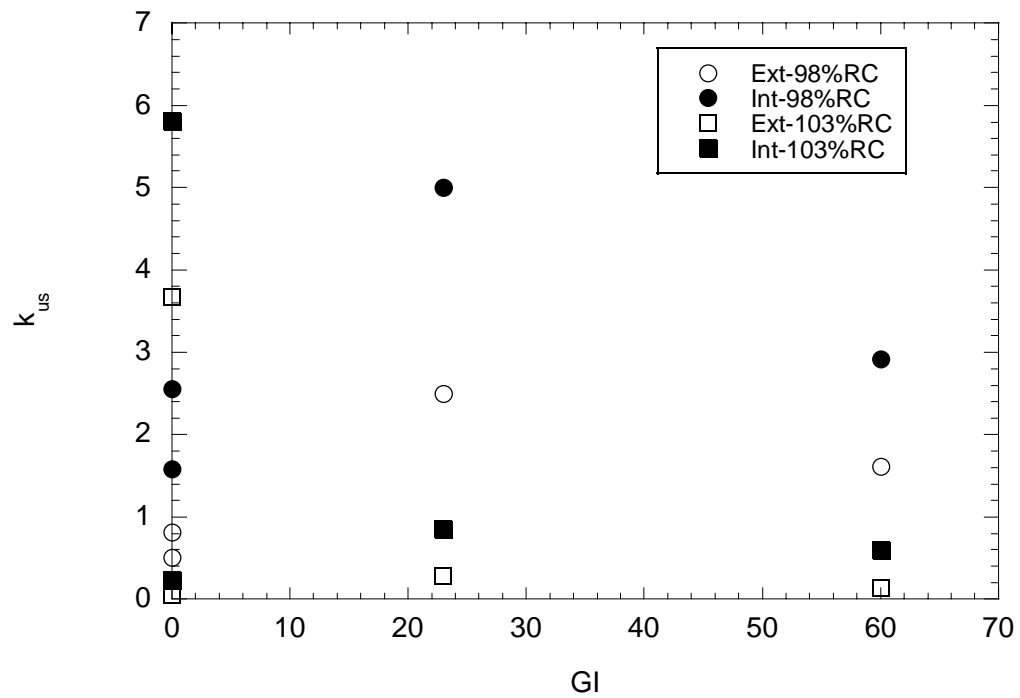
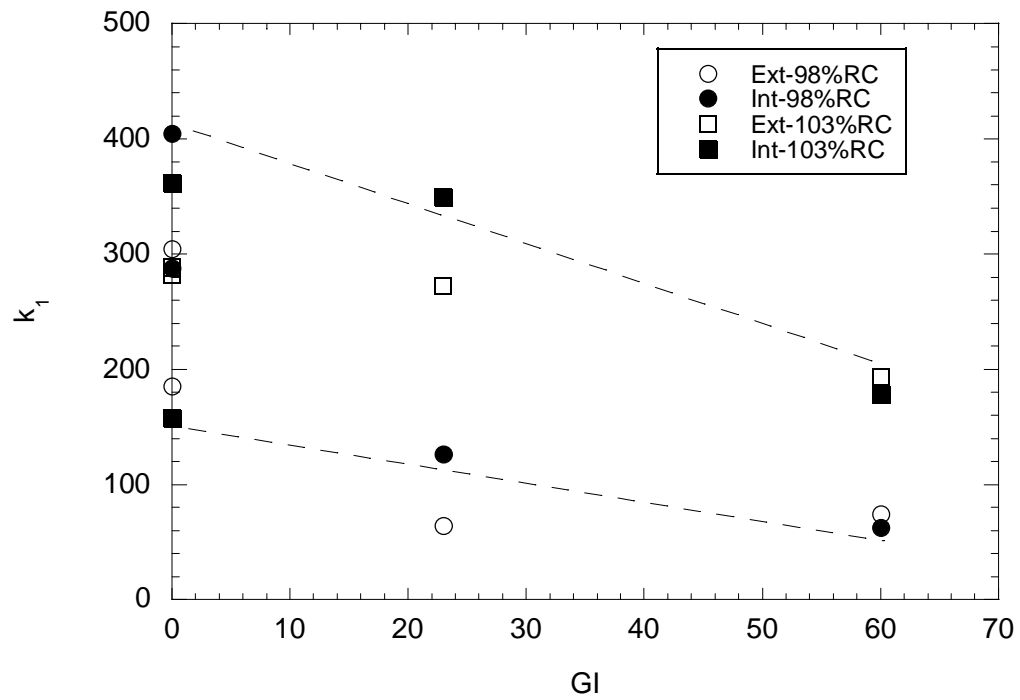


Figure 61: Relationship of parameters  $k_1$  and  $k_{us}$  with group index.

## CHAPTER V: LINKING SHEAR STRENGTH MEASUREMENTS TO RESILIENT MODULUS

This section was compiled by Drs. Satish Gupta and Andry Ranaivoson based on their results on shear strength and stiffness measurements by Drs. Tuncer Edil, Craig Benson, Auckpath Sawangsuriya of the University of Wisconsin.

### Power Function Model for Resilient Modulus of Unsaturated Soils

In the resilient behavior characterization of the present report, Edil et al. (2007) suggest two formulations that can form the basis of a model for predicting resilient modulus of unsaturated soils. In one formulation, the authors used the relationship suggested by Oloo and Fredlund (1998) between deviator stress ( $\sigma_d$ ) and resilient modulus ( $M_r$ ) as the basis and added a component similar to the component of unsaturated cohesion in shear strength model of Fredlund and Morgenstern (1977) as modified by Vanapalli (1996). The final forms of the relationships were:

$$\text{For coarse-grained soils:} \quad (M_r)_{us} = k\sigma_b^n + k_{us}\Theta^\kappa(\mu_a - \mu_w) \quad (26)$$

For fine-grained soils:

$$\text{For } k_1 > \sigma_d \quad (M_r)_{us} = k_2 - k_3(k_1 - \sigma_d) + k_{us}\Theta^\kappa(\mu_a - \mu_w) \quad (27)$$

$$\text{For } k_1 < \sigma_d \quad (M_r)_{us} = k_2 + k_4(\sigma_d - k_1) + k_{us}\Theta^\kappa(\mu_a - \mu_w) \quad (28)$$

where  $k_1$ ,  $k_2$ ,  $k_3$ ,  $k_4$ ,  $k_{us}$ , and  $n$  are material constants determined experimentally,  $\sigma_b$  is bulk stress ( $\sigma_b = \sigma_1 + \sigma_2 + \sigma_3 = \sigma_1 + 2\sigma_3$ ), and  $\kappa$  is a fitting coefficient.

The other formulation suggested by Edil et al. (2007) for resilient modulus is a modification of a five-parameter log-log model recommended by NCHRP 1-28A (2003). To account for unsaturated effects, Edil et al. (2000) again used Vanapalli et al. (1996) modification of Fredlund and Morgenstern (1977) equation for unsaturated shear strength. The new model for resilient modulus is thus written as:

$$M_r = k_1 p_a \left( \frac{\sigma_b - 3k_6}{p_a} \right)^{k_2} \left( \frac{\tau_{oct}}{p_a} + k_7 \right)^{k_3} + k_{us} p_a \Theta^\kappa(\mu_a - \mu_w) \quad (29)$$

where  $k_1$ ,  $k_2$ ,  $k_3$ ,  $k_6$ ,  $k_7$  are the fitting constants with  $k_1$  and  $k_2 \geq 0$ ,  $k_3$  and  $k_6 \leq 0$ , and  $k_7 \geq 1$ ;  $p_a$  is atmospheric pressure ( $\sim 100$  kPa); and  $\tau_{oct}$  is octahedral shear stress defined as:

$$\tau_{oct} = \frac{1}{3} \sqrt{(\sigma_1 - \sigma_2)^2 + (\sigma_1 - \sigma_3)^2 + (\sigma_2 - \sigma_3)^2} = \frac{\sqrt{2}}{3} (\sigma_1 - \sigma_3) \quad (30)$$

where  $\sigma_1$ ,  $\sigma_2$ , and  $\sigma_3$  are principal stresses with  $\sigma_2=\sigma_3$ .

As mentioned in the literature review section of shear strength, Vanapalli et al. (1996) modification of Fredlund and Morgenstern (1977) equation explicitly include soil water retention characteristics in the shear strength relationship. Use of  $\kappa$  in Vanapalli et al. (1996) equation is mainly to match predicted shear strength to measured values.

$$\tau_f = c' + (\sigma_n - \mu_a) \tan \phi' + (\Theta^\kappa)(\mu_a - \mu_w) \tan \phi^b \quad (31)$$

However, if any of the water retention functions (Brooks and Corey, 1964; van Genuchten, 1980; Fredlund and Xing, 1994) are explicitly included in Eq. (31), this relationship will look like a power function relationship of shear strength to soil suction.

$$\tau_f = (\sigma_n - \mu_a) \tan \phi' + c'(\mu_a - \mu_w)^\beta \quad (32)$$

where  $c'$  is imbedded in the  $\alpha$  value defined in the power function relationship of deviator stress to suction. The advantage of Eq. (32) over Eq. (31) is that water retention curve is implicitly included in the shear strength relationship and there is no need to have two independent variables ( $\theta$  and  $u_w$ ) in the shear strength equation. The above equation will be valid for soil suction greater than the air entry value.

Now similar argument can be made for modification of resilient modulus equations (Eqs. 26-29) proposed by Edil et al. (2007) in this report. Thus the new formulations for Oloo and Fredlund (1998) model will be:

$$\text{For coarse-grained soil} \quad (M_r)_{us} = (k\sigma_b^n) + \alpha_1(\mu_a - \mu_w)^{\beta_1} \quad (33)$$

For fine-grained soils:

$$\text{For } k_1 > \sigma_d \quad (M_r)_{us} = (k_2 - k_3(k_1 - \sigma_d)) + \alpha_1(\mu_a - \mu_w)^{\beta_1} \quad (34)$$

$$\text{For } k_1 < \sigma_d \quad (M_r)_{us} = (k_2 + k_4(\sigma_d - k_1)) + \alpha_1(\mu_a - \mu_w)^{\beta_1} \quad (35)$$

The corresponding formulations for NCHRP 1-28A (2003) model will be:

$$(M_r)_{us} = \left( k_1 p_a \left( \frac{\sigma_b - 3k_6}{p_a} \right)^{k_2} \left( \frac{\tau_{oct}}{p_a} + k_7 \right)^{k_3} \right) + \alpha_1(\mu_a - \mu_w)^{\beta_1} \quad (36)$$

where  $(M_r)_{us}$  is resilient modulus of an unsaturated soil and  $\alpha_1$  and  $\beta_1$  are intercept and slope of the  $(M_r)_{us}$  at a given  $\sigma_b$  and  $\tau_{oct}$  vs. suction relationship.

The proposed relationships (Eqs. 33-36) have advantage over the relationships in Eqs. (26-29) that these do not require measurements of both water content and suction to estimate resilient modulus. Furthermore, the experience of the authors of this section suggests that exponent ( $\kappa$ ) in Vanapalli et al. (1996) and Fredlund et al. (1996) equations is not constant over the whole suction range. Comparatively, the shear strength measurements suggest that for most practical purposes,  $\beta$  and  $\beta_1$  are constant values over a large range suctions varying from saturation to 500 kPa for shear strength and saturation to 193 kPa for  $M_r$ .

### Testing for Suction Effects on Resilient Modulus

Above concepts on suction effects were tested on the  $M_r$  data of Edil et al. (2006). Figures 62 and 63 show the relationships between  $M_r$  values vs. suction for both external and internal LVDT, respectively.  $M_r$  values are estimated at a bulk stress of 83 kPa and octahedral stress of 19 kPa (Edil et al., 2006). Since there was no statistical difference in  $M_r$  values between samples that had been compacted to 98% and 103% of the maximum density, data for both these compaction levels were combined during regression. Like shear strength-suction relationship, these figures also show that  $M_r$  varies with soil suction as a power function relationship.

$$M_r = \alpha_1 (\mu_a - \mu_w)^{\beta_1} \quad (37)$$

where  $\alpha_1$  and  $\beta_1$  are empirical constants. Tables 20 and 21 list the value of these coefficients for various soils.

Although the relationships between  $M_r$  vs. soil suction for various soils fall within a narrow range, it appears that there are some differences between soil types. In general,  $\alpha_1$  values decrease whereas  $\beta_1$  values increase with an increase in clay content (Figs. 64 thru 67).  $\alpha_1$  and  $\beta_1$  values were also regressed with other physical constants such as % sand, % silt, and plastic limit but their correlation coefficients were generally low and/or not consistent over both parameters (Table 22, Appendix F).

### Relationship between Resilient Modulus and Shear Strength

One of the objectives of this study was to see if deviator stress at small strains (an indicator of shear strength) can be used to predict resilient modulus of unsaturated soils. Discussions in Chapter 1 and here show that both deviator stress at 1% strain and resilient modulus increase with an increase in soil suction and that increase is a power function relationship (Table 23). This suggests that there is a definite positive relationship between the shear strength indicator (deviator stress at 1% strain) and resilient modulus at any given suction for any given soil. The question is: can this relationship be generalized over different soil types ranging in particle size distribution and indirectly on varying water retention characteristics. Data in Table 23 shows that for any given soil, the rate of increase of  $M_r$  with soil suction ( $\beta_1$ ) is different than the rate of increase in deviator stress with soil suction ( $\beta$ ). Furthermore, it shows that  $\beta_1$  value increases with clay content and

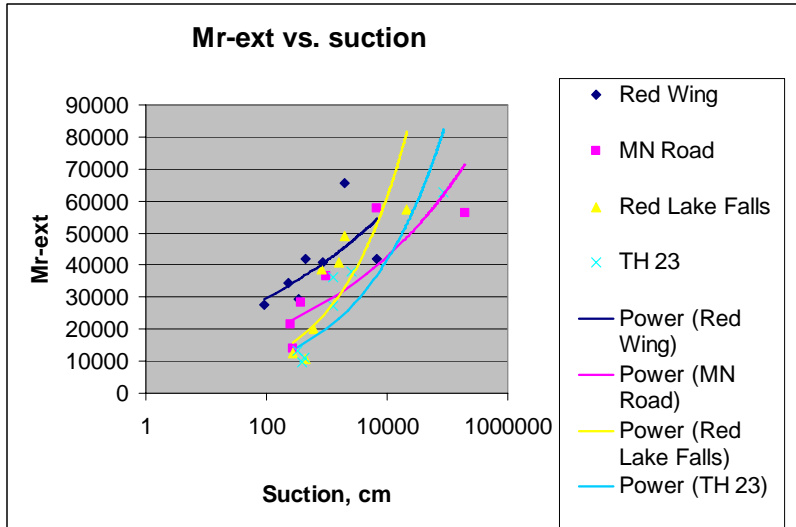


**Figure 62: Relationship between resilient modulus at (measured using external LVDT) as a function of soil suction. Resilient modulus values correspond to bulk stress of 83 kPa and octahedral stress of 19 kPa. Data taken from Edil et al. (2007).**

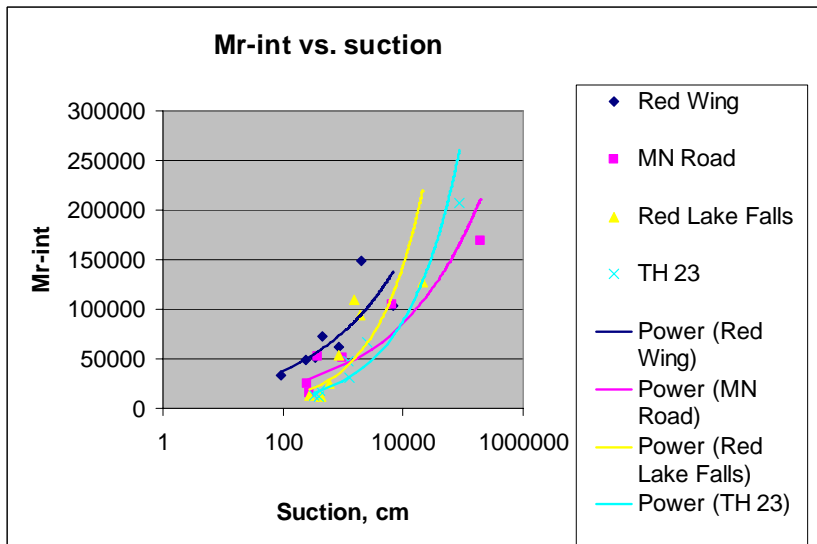


**Figure 63: Relationship between resilient modulus at (measured using internal LVDT) as a function of soil suction. Resilient modulus values correspond to bulk stress of 83 kPa and octahedral stress of 19 kPa. Data taken from Edil et al. (2007).**

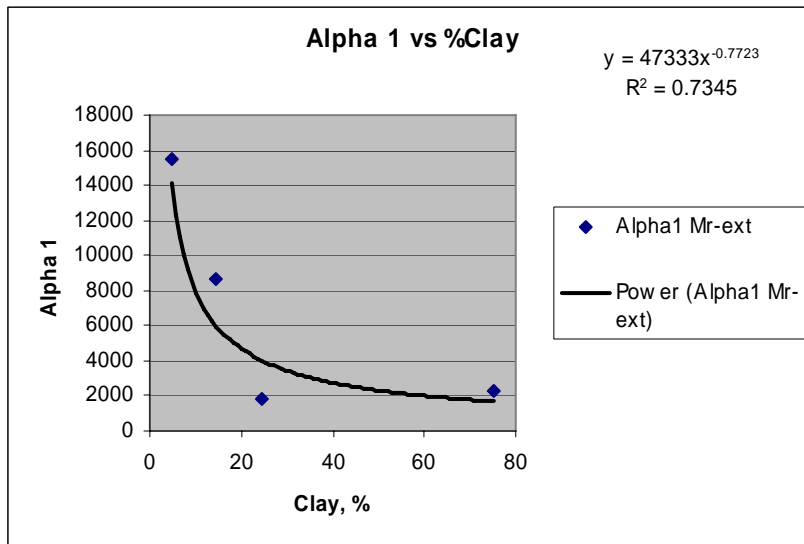


**Figure 64: Relationship between  $\alpha_1$  vs. clay content.  $\alpha_1$  values are for Mr data measured with external LVDT.**

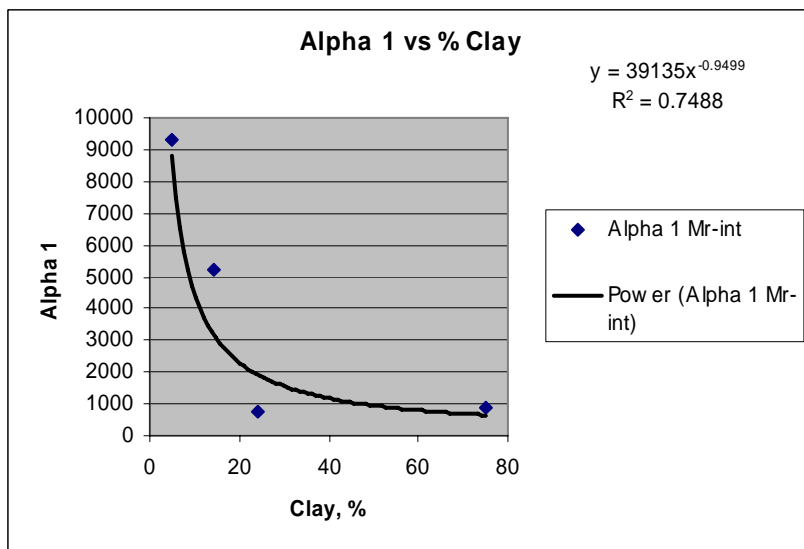


**Figure 65: Relationship between  $\alpha_1$  vs. clay content.  $\alpha_1$  values are for Mr data measured with internal LVDT.**

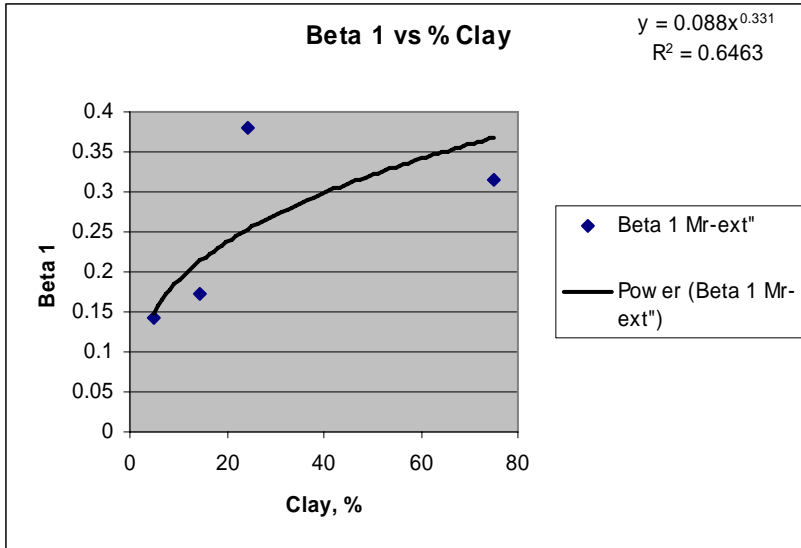


**Figure 66: Relationship between  $\beta_1$  vs. clay content.  $\beta_1$  values are for Mr data measured with external LVDT.**

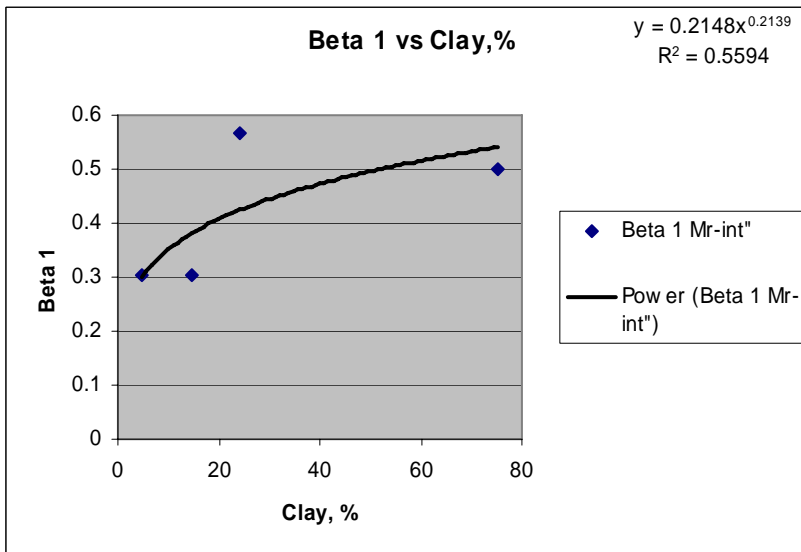


**Figure 67: Relationship between  $\beta_1$  vs. clay content.  $\beta_1$  values are for Mr data measured with internal LVDT.**

**Table 20: Best fit value of the power function coefficients describing the change in resilient modulus (Mr) as a function of suction ( $\square w$ ) for four soils. Mr values correspond to values measured using external LVDT.**

Soil	Clay %	$\alpha_1^\dagger$	$\beta_1^\dagger$	R <sup>2</sup>
Duluth TH23	75.2	2294	0.3148	0.74
Red Lake Falls	24.3	1853	0.3799	0.65
MN Road	14.5	8683	0.173	0.66
Red Wing	4.8	15545	0.1413	0.79

$$\dagger M_r = \alpha_1 \mu_w^{\beta_1}$$

**Table 21: Best fit value of the power function coefficients describing the change in resilient modulus (Mr) as a function of suction ( $\square w$ ) for four soils. Mr values correspond to values measured using internal LVDT.**

Soil	Clay %	$\alpha_1^\dagger$	$\beta_1^\dagger$	R <sup>2</sup>
Duluth TH23	75.2	888	0.4993	0.91
Red Lake Falls	24.3	770	0.5678	0.67
MN Road	14.5	5220	0.3039	0.78
Red Wing	4.8	9310	0.3051	0.76

$$\dagger M_r = \alpha_1 \mu_w^{\beta_1}$$

**Table 22: Correlation coefficients (R2) of  $\square_1$  and  $\square_1$  against % clay, % silt, % sand and plastic limit (PL) for Mr values measured using external and internal LVDT.**

Variable	M <sub>r</sub> measured using external LVDT				M <sub>r</sub> measured using internal LVDT			
	Sand	Silt	Clay	PL <sup>†</sup>	Sand	Silt	Clay	PL
	-----R <sup>2</sup> -----							
$\alpha_1$	0.48	0.22	0.73	0.85	0.54	0.24	0.75	0.86
$\beta_1$	0.48	0.15	0.65	0.55	0.60	0.11	0.56	0.49

<sup>†</sup>Except for PL, all R<sup>2</sup> values are for a power function. R2 values for PL are for a linear function.

**Table 23: Table 23: Slope of the power function describing deviator stress ( $\sigma_1 - \sigma_3$ ) vs. suction and slope of the power function describing resilient modulus ( $M_r$ ) vs. suction for four soils.**

		98% of maximum density	103% of maximum density	Mr-ext	Mr-int
Soil	Clay, %	$\beta^\dagger$ for 1% strain	$\beta^\dagger$ for 1% strain	$\beta_1^\S$	$\beta_1^\S$
TH 23	75.2	0.1882	0.2003	0.3148	0.4993
RLF	24.3	0.2349	0.2215	0.3799	0.5678
Mn Road	14.5	0.2984	0.2376	0.173	0.3039
RW	4.8	0.334	0.398	0.1419	0.3051

$$\dagger (\sigma_1 - \sigma_3) = \alpha u_w^\beta$$

$$\S M_r = \alpha_1 u_w^{\beta_1}$$

levels off at clay content of about 30%. Comparatively,  $\beta$  value decreases with clay content and also levels off at about 30% clay content. Threshold of 30% clay content indicates that soils above this level of clay content essentially behave as a clay matrix with coarser particles imbedded in that matrix. This is similar to the observations of Larson et al. (1980) and Larson and Gupta (1980) who found that soils with clay content greater than 33% essentially behaved as clays. Regression between  $\beta_1$  and  $\beta$  value shows that there exist an inverse relationship between these parameters irrespective whether  $M_r$  is measured using external (Fig. 68) or internal (Fig. 69) LVDT. However, the correlation coefficients for these relationships appear to be somewhat small. For practical purposes, these relationships (Figs. 68 and 69) may be used for estimating slope of resilient modulus vs. suction curves from the slope of deviator stress at 1% strain vs. suction. However, a better way may be to directly estimate slope ( $\beta_1$ ) of the resilient modulus vs. suction curve from clay content using relationships given in Figs. 66 and 67.

## CHAPTER VI: FRAMEWORK FOR DEVELOPING MnPAVE FACTORS FOR SUCTION EFFECTS

Currently, the MnPAVE resistance factors are given for different seasons but these values are based on limited data set. Field measurements by Ovik (1998) and Roberson et al. (2004) show that soil water content (in turn soil suction) under pavement varies with season and is not saturated most of the time. Therefore adjustments are needed to account for increased strength and stiffness of the material as a result of unsaturated soil conditions. These adjustments will not only reflect the realistic field conditions but will result in more accurate prediction of performance compared to the current design.

As a start, a simple procedure to develop resistance factors that account for suction effects will be to estimate the range of suctions/water contents that might exist in sub grade soils for different seasons. These estimates will be needed for different soils in various parts of Minnesota. Generally, these measurements are not readily available for a wide variety of soils. In that case, simulation models could be used to generate variation in soil suction in various parts of Minnesota based on long-term climate. These suctions can then be used in Eq. (37) to estimate  $M_r$  values of a given sub grade soil for different seasons. Equation (37) assumes a bulk stress of 83 kPa and an octahedral stress of 19 kPa. If the bulk and octahedral stresses are different than that suggested by NCHRP 1-28A (2003) then Eq. (36) may be used to estimate  $M_r$  values of a given sub grade soil for various seasons. Estimate of  $\alpha_1$  and  $\beta_1$  can be obtained using the soil clay content and the corresponding relationships (Eqs. 38-41) given in this report.

$$M_{r-ext} \quad \alpha_1 = 47333(\% \text{ clay})^{-0.7723} \quad R^2=0.73 \quad (38)$$

$$M_{r-int} \quad \alpha_1 = 39135(\% \text{ clay})^{-0.9499} \quad R^2=0.75 \quad (39)$$

$$M_{r-ext} \quad \beta_1 = 0.088(\% \text{ clay})^{0.313} \quad R^2=0.65 \quad (40)$$

$$M_{r-int} \quad \beta_1 = 0.2148(\% \text{ clay})^{0.2139} \quad R^2=0.56 \quad (41)$$

The resistance factors of a given soil for various seasons will then be a ratio of  $M_r$  values in different seasons to  $M_r$  value in fall. This method assumes  $M_r$  value in fall as a reference (Roberson et al., 2004). If bulk stress and octahedral stress are same among various seasons then resistance factor for a given season will be equal to

$$R_{season} = \frac{(M_r)_{season}}{(M_r)_{fall}} = \left( \frac{(\mu_a - \mu_w)_{season}}{(\mu_a - \mu_w)_{fall}} \right)^{\beta_1} \quad (42)$$

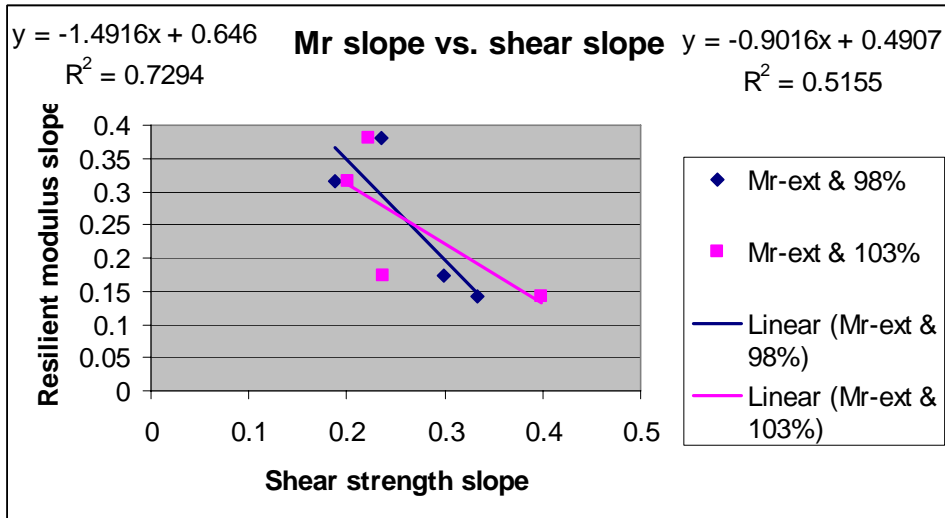


**Figure 68: Relationship between slope of Mr -ext vs. suction ( $\beta_i$ ) and slope of deviator stress at 1% strain vs. suction ( $\beta$ ).**

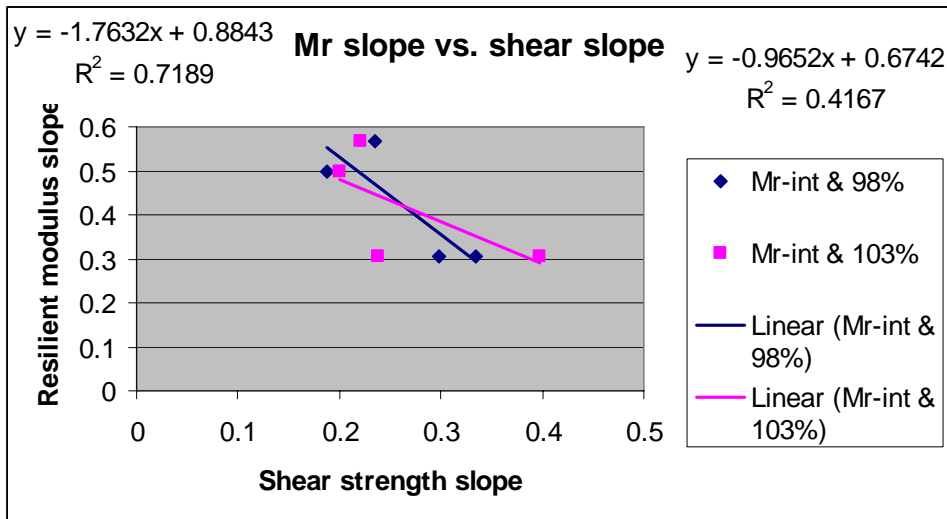


**Figure 69: Relationship between the slope of Mr-int vs. suction ( $\beta_i$ ) and slope of deviator stress at 1% strain vs. suction ( $\beta$ ).**

## **CHAPTER VII: EXPECTED BENEFITS AND FUTURE RESEARCH NEEDS**

Since soil water content and the resulting soil suction under the pavement varies with season and is not saturated most of the time, adjustments are needed to account for increased strength and stiffness of the material as a result of unsaturated soil conditions. The data and the Pedo-transfer function provided in this report will be useful in developing a frame work for adjusting the effects of suction in the resistance factors of MnPAVE. These adjustments will not only reflect the more realistic field conditions but will result in more reliable performance predictions than the current pavement design method. Furthermore, these data bases will be valuable in assessing the effect of variation in material properties on variation on pavement properties. This kind of assessment can be probably linked with intelligent compaction and performance based specifications (White et al., 2007) to separate the variation in pavement performance from machinery effects and material variation.

Proposed relationships for shear strength, resilient modulus, and resistance factors to account for unsaturated conditions have not been tested. A thorough testing of these relationships should be undertaken either based on the data from the literature or a set of new measurements on soils other than those on which these relationships have been developed. Furthermore, efforts should be directed to estimate variation in soil suction/soil water contents in sub grade soils across Minnesota either through measurements or through model simulations using long-term climate data.

## CHAPTER VIII: REFERENCES

- Abramento, M., and Carvalho, S. (1989), "Goetechnical parameters for study of slope insatbilization at Serra do Mar-Brazillan Southeast," *Proceedings of the 12<sup>th</sup> International Conference on Soil Mechanics and Foundation Engineering*, Rio de Janeiro, 3: 1599-1602.
- Acar, Y. B., and EL-Tahir, E. A. (1986), "Low Strain Dynamic Properties of Artificially Cemented Sand," *Journal of Geotechnical Engineering*, ASCE, Vol. 112, No. 11, pp. 1001-1015.
- Alonso, E.E., and Delage, P. (1995), *Proceedings 1<sup>st</sup> International Conference on Unsaturated Soils*, Paris, Balkema.
- ASTM (2004), *Annual Book of Standards*, Vol. 04.09, ASTM, West Conshohocken, PA, USA
- Atkinson, J. H. (2000), "Non-Linear Soil Stiffness in Routine Design," *Geotechnique*, 40<sup>th</sup> Rankine Lecture, pp. 487-508.
- Babu, G. L., Peter, J., Mukesh, M. D., and Gartung, E. (2005), "Significance of Soil Suction and Soil Water Characteristic Curve Parameters," *Geotechnical Testing Journal*, Vol. 28, No. 1, pp. 102-107.
- Bao, C. G., Gong, B., and Zhan, L. (1998), "Properties of Unsaturated Soils and Slope Stability of Expansive Soil," Keynote Lecture, *Proceedings of the 2<sup>nd</sup> International Conference on Unsaturated Soils*, Beijing.
- Bishop, A. W. (1959), "The Principle of Effective Stress," *Teknisk Ukeblad I Samarbeide Med Teknikk*, Oslo, Norway, Vol. 106, No. 39, pp. 859-863.
- Bishop, A.W., I, Alan, G.E. Blight, and I.B. Donald. (1960), "Factors controlling the strength of partially saturated cohesive soils," *Proc. Res. Conf. Shear Strength Cohes. Soils*. ASCE, pp 503-532.
- Bishop, A.W. and Blight, G.E. (1963), "Some aspects of effective stress in saturated and unsaturated soil", *Geotechnique* 13: 177-197.
- Blight, G. E. (1965). "A study of effective stress for volume change," *Proc. Symposium on Moisture Equilibria and Moisture Change in the Soils Beneath Covered Areas*, Butterworths, Sydney, Australia, 259-269.
- Bouwer, H. (1966), "Rapid Field Measurement of Air Entry Value and Hydraulic Conductivity of Soil as Significant Parameters in Flow System Analysis," *Water Resources Research*, Vol. 2, No. 4, pp. 729-738.

- Briaud, J-L, Li, Y., and Rhee, K. (2006), "BCD: A Soil Modulus Device for Compaction Control," *Journal of Geotechnical and Geoenvironmental Engineering*, ASCE, Vol. 132, No. 1, pp. 108-115.
- Brooks, R.H., and Corey, A.T. (1964), "Hydraulic properties of porous media," Hydrol. Paper. 3, *Colorado State University*, Fort Collins, CO.
- Butalia, T. S., Huang, J., Kim, D.-G., and Croft, F. (2003), "Effect of Moisture Content and Pore Water Pressure Buildup on Resilient Modulus of Cohesive Soils," *Resilient Modulus Testing for Pavement Components, ASTM STP 1437*, West Conshohocken, PA, pp. 70-84.
- Chandler, R. J., Crilly, M. S., and Montgomery-Smith, G. (2002), "A Low Cost Method of Assessing Clay Desiccation for Low-Rise Buildings," *Proceedings of the Institution of Civil Engineers*, Vol. 92, No. 2, pp. 82-89.
- Chen, D.-H., Wu, W., He, R., Bilyeu, J., and Arrelano, M. (1999), "Evaluation of In-Situ Resilient Modulus Testing Techniques," *Recent Advances in the Characterization of Transportation Geo-Materials*, Geotechnical Special Publication, No. 86, ASCE, Reston, VA., pp. 1-11.
- Chiang, I-B. (1998), "Effect of Fines and Gradation on Soil Water Characteristics Curves of Sands," *M.S. Thesis*, The University of Wisconsin-Madison, Madison, WI.
- Croney, D. and Coleman, J. D. (1961), "Pore Pressure and Suction in Soils," *Proceedings of the Conference of Pore Pressure and Suctions in Soils*, Butterworths, London, UK, pp. 31-37.
- Coleman, J. D. (1962), "Stress-Strain Relations for Partially Saturated Soils," *Geotechnique*, Vol. 12, No. 4, pp. 348-350.
- Costa, Y. D., Cintra, J. C., and Zornberg, J. G. (2003), "Influence of Matric Suction on the Results of Plate Load Tests Performed on a Lateritic Soil Deposit," *Geotechnical Testing Journal*, ASTM, Vol. 26, No. 2, pp. 1-9.
- Cui, Y.J., and Delage, P. (1996), "Yielding and plastic behaviour of an unsaturated compacted silt," *Geotechnique* 46: 291-311.
- Das, B.M. (1979), *Introduction to Soil Mechanics*, The Iowa State University Press, Ames, IA.
- Davich, P., Labuz, J., Guzina, B., and Drescher, A. (2004), "Small Strain and Resilient Modulus Testing of Granular Soils," Final Report 2004-39, Minnesota Department of Transportation, St. Paul, MN

- Drumright, E.E. (1989), "The contribution of matric suction to the shear strength of unsaturated soils," *Ph.D. Dissertation*, Colorado State University, 449p.
- Drumright, E.E., and Nelson, J.D. (1995), "The shear strength of unsaturated tailings sand", *In* Alonso and Delage (eds.). *Proceedings 1<sup>st</sup> International Conference on Unsaturated Soils*, Paris, Balkema, pp 45-50.
- Dyvik, R. and Madshus, C. (1985), "Lab Measurements of  $G_{max}$  Using Bender Elements," *Proceedings of the Geotechnical Engineering Division: Advances in the Art of Testing Soil Under Cyclic Conditions*, ASCE, Detroit, MI, pp. 186-196.
- Edil, T. B. (1973), "Influence of Fabric and Soil-Water Potential on Stress-Strain Response of Clay," *Ph.D. Thesis*, Northwestern University, Evanston, IL.
- Edil, T. B., and Krizek, R. J. (1976), "Influence of Fabric and Soil-Water Potential on the Mechanical Behavior of Kaolinitic Clay," *Geoderma*, Vol. 15, pp. 831-840.
- Edil, T. B. and Motan, S. E. (1979), "Soil-Water Potential and Resilient Behavior of Subgrade Soils," *Transportation Research Record*, No. 705, Washington, D.C., pp. 54-63.
- Edil, T. B., Motan, S. E., and Toha, F. X. (1981), "Mechanical Behavior and Testing Methods of Unsaturated Soils," *Laboratory Shear Strength of Soil, ASTM STP 740*, Philadelphia, PA, pp. 114-129.
- Edil, T. B., and Sawangsuriya, A. (2005), "Earthwork Quality Control Using Soil Stiffness," *Proceedings of the 16<sup>th</sup> International Conference on Soil Mechanics and Geotechnical Engineering*, Osaka, Japan, pp. 1689-1692.
- Edit, T. B., Benson, C., and Sawangsuriya, A. (2006), "Resilient modulus of unsaturated soils." A report submitted to the University of Minnesota as part of the subcontract on the Mn/DOT project "Pavement design Using Unsaturated technology", St. paul, MN.
- Fam, M., and Santamarina, J. C. (1995), "Study of Geoprocesses with Complementary Wave Measurements in an Oedometer," *Geotechnical Testing Journal*, Vol. 18, No. 3, pp. 307-314.
- Feng, M., Fredlund, D. G., and Shuai, F. (2002), "A Laboratory Study of the Hysteresis of a Thermal Conductivity Soil Suction Sensor," *Geotechnical Testing Journal*, Vol. 25, No. 3, pp. 303-314.
- Feuerharmel, C., Pereira, S.L., Gehling, W.Y.Y., and Bica, A.V.D. (2006), "Determination of shear strength parameters of two unsaturated colluvium soils using direct shear test," *In* Miller et al. (eds.). *Unsaturated soils. Proceedings of the 4<sup>th</sup> International Conference on Unsaturated Soils*, Carefree, AZ, 2-6 April 2006. ASCE. Geotechnical Special Publication no. 147. pp 1181-1190.

- Fiedler, S. A., Main, M., and DiMillio, A. F. (2000), "In-Place Stiffness and Modulus Measurements," *Proceedings of Sessions of ASCE Specialty Conference on Performance Confirmation of Constructed Geotechnical Facilities*, Geotechnical Special Publication, No. 94, ASCE, Amherst, MA, pp. 365-376.
- Fioravante, V., and Capoferri, R. (2001), "On the Use of Multi-Directional Piezoelectric Transducers in Triaxial Testings," *Geotechnical Testing Journal*, Vol. 24, No. 3, pp. 243-255.
- Flint, A. L., Campbell, G. S., Ellett, K. M., and Calissendorff, K. M. (2002). "Calibration and Temperature Correction of Heat Dissipation Matric Potential Sensors." *Soil Science Society of America Journal*, Vol. 66, pp. 1439-1445.
- Fleureau, J.M., Kheirbek-Saoud, S., Soemitro, R., and Taibi, S. (1993), "Behaviour of clayey soils on drying-wetting paths," *Can. Geotech. J.* 30: 287-296.
- Fredlund, D.G., and Morgenstern, N.R., (1976), "Constitutive relations for volume change in unsaturated soils," *Can. Geotech. J.* 13: 261-276.
- Fredlund, D.G., and Morgenstern, N.R., (1977), "Stress state variables for unsaturated soils," *ABB Rev.*, 103(5), 447-466.
- Fredlund, D. G., Bergan, A. T., and Sauer, E. K. (1975), "The Deformation Characteristics of Subgrade Soils for Highways and Runways in Northern Environments," *Canadian Geotechnical Journal*, Vol. 12, No. 2, pp. 213-223.
- Fredlund, D. G., Bergan, A. T., and Wong, P. K. (1977), "Relation between Resilient Modulus and Stress Conditions for Cohesive Subgrade Soils," *Transportation Research Record*, No. 642, Washington, D.C., pp. 73-81.
- Fredlund, D. G., Morgenstern, N. R., and Widger, R. A. (1978), "The Shear Strength of Unsaturated Soils," *Canadian Geotechnical Journal*, Vol. 15, No. 3, pp. 316-321.
- Fredlund, D. G., and Morgenstern, N. R. (1977), "Stress State Variables for Unsaturated Soils," *Journal of Geotechnical Engineering*, ASCE, Vol. 103, No. GT5, pp. 447-466.
- Fredlund, D. G., Sattler, P. J., and Gan, J. K-M. (1992), "In Situ Suction Measurements using Thermal Sensors," *Proceedings of the 7<sup>th</sup> International Conference on Expansive Soils*, Dallas, TX, pp. 325-330.
- Fredlund, D. G., and Rahardjo, H. (1993), *Soil Mechanics for Unsaturated Soils*, John Wiley & Sons, Inc., New York, NY.

- Fredlund, D. G., and Xing, A. (1994), "Equations for the Soil-Water Characteristic Curve," *Canadian Geotechnical Journal*, Vol. 31, No. 4, pp. 521-532.
- Fredlund, D.G. (1996), "The scope of unsaturated soil mechanics," An overview. In Alonso and Delage (eds.). *Proceedings 1<sup>st</sup> International Conference on Unsaturated Soils*, Paris, France. Balkema Press.
- Fredlund, D. G., Xing, A., Fredlund, M. D., and Barbour, S. L. (1996), "The Relationship of the Unsaturated Soil Shear Strength to the Soil-Water Characteristic Curve," *Canadian Geotechnical Journal*, Vol. 33, No. 3, pp. 440-448.
- Futai, M.M., Almeida, M.S.S., and Lacerda, W.A. (2006), "The shear strength of unsaturated tropical soils in Ouro Preto, Brazil," In Miller et al. (eds.). *Unsaturated soils. Proceedings of the 4<sup>th</sup> International Conference on Unsaturated Soils*, Carefree, AZ, 2-6 April 2006. ASCE. Geotechnical Special Publication no. 147. pp 1201-1211.
- Gallage, C.P.K., and Uchimura, T. (2006), "Effects of wetting and drying on unsaturated shear strength of silty sand under low suction," In Miller et al. (eds.) *Proceedings of the 4th International Conference on Unsaturated Soils*. 2-6 April 2006, Carefree, AZ. ASCE Geotechnical Special Publication no. 147. pp 1247-1258.
- Garven, E. A., and Vanapalli, S.K. (2006), "Evaluation of empirical procedures for predicting the shear strength of unsaturated soils", In Miller et al. (eds.) *Proceedings of the 4th International Conference on Unsaturated Soils*. 2-6 April 2006, Carefree, AZ. ASCE Geotechnical Special Publication no. 147. pp 2570-2581.
- Geiser, F. (1999), Comportement mécanique d'un limon non saturé: Étude expérimentale et modélisation constitutive, *Ph.D. thesis Swiss Federal Institute of Technology*, Lusanne, Switzerland.
- Graham, J., Blatz, J. A., Alfaro, M. C., and Sivakumar, V. (2001), "Behavioral Influence of Specimen Preparation Methods for Unsaturated Plastic Compacted Clays," *Proceedings of the 15<sup>th</sup> International Conference on Soil Mechanics and Geotechnical Engineering*, Istanbul, Turkey, Vol. 1, pp. 633-638.
- Gupta, S. C., and Larson, W. E. (1979), "Estimating soil water retention characteristics from particle size distribution, organic matter percent, and bulk density," *Water Resources. Res.* 1633-1635.
- Gupta, S.C., Singh, A., and Ranavivoson, A. (2004), "Moisture Retention Characteristics Of Base and Sub-base Materials," A report submitted to *Minnesota department of Transportation*, 36p. St. Paul, MN.
- Hamblin, A. P. (1981), "Filter-Paper Method for Routine Measurement of Field Water Potential," *Journal of Hydrology*, Vol. 53, pp. 355-360.

- Hardin, B. O. (1978), "The Nature of Stress-Strain Behavior of Soils," *Proceedings of the Geotechnical Engineering Division Specialty Conference on Earthquake Engineering and Soil Dynamics*, ASCE, Pasadena, CA, Vol. 1, pp. 1-90.
- Hardin, B. O., and Blandford, G. E. (1989), "Elasticity of Particulate Materials," *Journal of Geotechnical Engineering*, ASCE, Vol. 115, No. GT6, pp. 788-805.
- Hillel, D. (1982), *Introduction to Soil Physics*, Academic Press, NY.
- Houlsby, G. T. (1997), "The Work Input to an Unsaturated Granular Material," *Geotechnique*, Vol. 47, No. 1, pp. 193-196.
- Houston, S. L., Houston, W. N., and Wagner, A. M. (1994), "Laboratory Filter Paper Suction Measurements," *Geotechnical Testing Journal*, Vol. 17, No. 2, pp. 185-194.
- Houston, S., and Fredlund, D.G. (1997), "Unsaturated soil engineering practice", *ASCE Geotechnical special publication no. 68*.
- Hoyos, L. R., Takkabutr, P., and Puppala, A. J. (2005), "A Pressure Plate Extractor Device for Assessment of SWCC under Net Radial Confinement," *Proceedings of International Conference on Problematic Soils*, Famagusta, N. Cyprus, Vol. 1, pp. 123-130.
- Huat, B. B. K., Ali, F.H., and Abdullah, A. (2005), "Field and Laboratory Suction-Soil Moisture Relationship of Unsaturated Residual Soils," *American Journal of Environmental Sciences*, Vol. 1, No. 1, pp. 34-40.
- Inci, G., Yesiller, N., and Kagawa, T. (2003), "Experimental Investigation of Dynamic Response of Compacted Clayey Soils," *Geotechnical Testing Journal*, ASTM, Vol. 26, No. 2, pp. 125-141.
- Kawaguchi, T., Mitachi, T., Shibuya, S. (2001), "Evaluation of Shear Wave Travel Time in Laboratory Bender Element Test," *Proceedings of the 15<sup>th</sup> International Conference on Soil Mechanics and Geotechnical Engineering*, Istanbul, Turkey, pp. 155-158.
- Khalili, N., and Khabbaz, M. H. (1998), "A Unique Relationship for  $\chi$  for the Determination of the Shear Strength of Unsaturated Soils," *Geotechnique*, Vol. 48, No. 5, pp. 681-687.
- Khalili, N., Geiser, F., and Blight, G. E. (2004), "Effective Stress in Unsaturated Soils: Review with New Evidence," *International Journal of Geomechanics*, ASCE, Vol. 4, No. 2, pp. 115-126.

- Khoury, N. N., Zaman, M. M., Nevels, J. B., and Mann, J. (2003), "Effect of Soil Suction on Resilient Modulus of Subgrade Soil Using the Filter Paper Technique," *Transportation Research Board 82<sup>nd</sup> Annual Meeting*, Washington, D.C. (CD-ROM)
- Khoury, N. N., and Zaman, M. M. (2004), "Correlation between Resilient Modulus, Moisture Variation, and Soil Suction for Subgrade Soils," *Transportation Research Record*, No. 1874, Washington, D.C., pp. 99-107.
- Kim, D.-S., and Stokoe, K. H., II (1992), "Characterization of Resilient Modulus of Compacted Subgrade Soils Using Resonant Column and Torsional Shear Tests," *Transportation Research Record*, No. 1369, Washington, D.C., pp. 83-91.
- Kim, D.-S., Kweon, G.-C., and Lee, K.-H. (1997), "Alternative Method of Determining Resilient Modulus of Compacted Subgrade Soils Using Free-Free Resonant Column Test," *Transportation Research Record*, No. 1577, Washington, D.C., pp. 62-69.
- Koorevaar, P., Menelik, G., and Dirksen, C. (1983), *Elements of Soil Physics*, Elsevier Science Publishers B. V., Amsterdam, The Netherlands
- Lamborn, M.J. (1986), "A micromechanical approach to modeling partly saturated soils," *M.Sc. Thesis Texas A & M University*, College Station, TX.
- Larson, W.E., Gupta, S.C., and Useche, R.A. (1980), "Compression of agricultural soils from eight soil orders," *Soil Sci. Soc. Am. J.* 44:450-457.
- Larson, W.E., and Gupta, S.C. (1980), "Estimating critical stress in unsaturated soils from changes in pore water pressure during confined compression," *Soil Sci. Soc. Am. J.* 44:1127-1132.
- Lee, I.-M., Sung, S.-G., and Cho, G.-C. (2005), "Effect of stress state on the unsaturated shear strength of a weathered granite," *Canadian Geotechnical J.* 42: 624-631.
- Lee, J.-S., and Santamarina, J. C. (2005). "Bender Elements: Performance and Signal Interpretation," *Journal of Geotechnical and Geoenvironmental Engineering*, ASCE, Vol. 131, No. 9, pp. 1063-1070.
- Leong, E. C., and Rahardjo, H. (1997), "Review of Soil-Water Characteristic Curve Equations," *Journal of Geotechnical and Geoenvironmental Engineering*, ASCE, Vol. 123, No. 12, pp. 1106-1117.
- Leong, E. C., He, L., and Rahardjo, H. (2002), "Factors Affecting the Filter Paper Method for Total and Matric Suction Measurement," *Geotechnical Testing Journal*, Vol. 25, No. 3, pp. 322-333.

- Li, A. G., Tham, L. G., Yue, Z. Q., Lee, C. F., and Law, K. T. (2005), "Comparison of Field and Laboratory Soil-Water Characteristic Curves," *Journal of Geotechnical and Geoenvironmental Engineering*, ASCE, Vol. 131, No. 9, pp. 1176-1180.
- Li, D., and Selig, E. T. (1994), "Resilient Modulus for Fine-Grained Subgrade Soils," *Journal of Geotechnical Engineering*, ASCE, Vol. 120, No. 6, pp. 939-957.
- Li, J., and Qubain, B. S. (2003), "Resilient Modulus Variations with Water Content," *Resilient Modulus Testing for Pavement Components*, ASTM 1437, West Conshohocken, PA, pp. 59-69.
- Li, X. S. (2005), "Modeling of Hysteresis Response for Arbitrary Wetting/Drying Paths," *Computer and Geotechnics*, Vol. 32, No. 2, pp. 133-137.
- Lu, N., and Griffiths, D. V. (2004), "Profiles of Steady-State Suction Stress in Unsaturated Soils," *Journal of Geotechnical and Geoenvironmental Engineering*, ASCE, Vol. 130, No. 10, pp. 1063-1076.
- Lu, N., and Likos, W. J. (2004), *Unsaturated Soil Mechanics*, John Wiley & Sons, Inc., Hoboken, NJ.
- Lu, Z. (1992), "The relationship of shear strength to swelling pressure for unsaturated soils," *Chinese J. Geotechnical Engineering*. 143: 1-8. [in Chinese]
- Lytton, R. L. (1997), "Engineering Structures in Expansive Soils," Keynote Address, *Proceedings of the 3<sup>rd</sup> International Symposium on Unsaturated Soils*, Rio de Janeiro, Brazil, Vol. 2, pp. 333-354.
- Mair, R. J. (1993), "Developments in Geotechnical Engineering Research: Application to Tunnels and Deep Excavations," Unwin Memorial Lecture 1992, *Proceedings of the Institution of Civil Engineers, Civil Engineering*, Vol. 97, No. 1, pp. 27-41.
- Mancuso, C., Vassallo, R., and d'Onofrio, A. (2002), "Small Strain Behavior of a Silty Sand in Controlled-Suction Resonant Column-Torsional Shear Tests," *Canadian Geotechnical Journal*, Vol. 39, No. 1, pp. 22-31.
- Marinho, F. A. M., Chandler, R. J., and Crilly, M. S. (1996), "Stiffness Measurements on an Unsaturated High Plasticity Clay Using Bender Elements," *Proceedings of the 1<sup>st</sup> International Conference on Unsaturated Soils*, Paris, France, Vol. 1, pp. 1179-1200.
- Maâtouk, A., Leroueil, S., and La Rochelle, P. (1995), "Yielding and critical state of collapsible unsaturated silty soil," *Geotechnique* 45: 465-477.
- Melgarejo, M. L., Ridley, A. M., and Dineen, K. (2002), "A Comparison of the Soil Water Characteristic Curves for Reconstituted and Undisturbed Samples of a

- Colluvium from Rio de Janeiro,” *Proceedings of the Third International Conference on Unsaturated Soils*, Recife, Brazil, pp. 313-316.
- Miao, L., Liu, S., and Lai, Y. (2002), “Research of soil-water characteristics and shear strength features on Nanyang expansive soil,” *Engineering Geology*. 65(4): 261-267.
- Miller, C. J., Yesiller, N., Yaldo, K., and Merayyan, S. (2002), “Impact of Soil Type and Compaction Conditions on Soil Water Characteristic,” *Journal of Geotechnical and Geoenvironmental Engineering*, ASCE, Vol. 128, No. 9, pp. 733-742.
- Miller, G.A., Zapata, C.E., Houston, S.L., and Fredlund, D.G. (2006), “Unsaturated Soils,” *Proceedings of the 4<sup>th</sup> International Conference on Unsaturated Soils*, Carefree, AZ, 2-6 April 2006. ASCE. Geotechnical Special Publication no. 147.
- Mitchell, J. K., and Soga, K. (2005), *Fundamentals of Soil Behavior*, John Wiley and Sons, Inc., NJ.
- Motan, S. E., and Edil, T. B. (1982), “Repetitive-Load Behavior of Unsaturated Soils,” *Transportation Research Record*, No. 872, Washington, D.C., pp. 41-48.
- Muhanna, A. S., Rahman, M. S., and Lambe, P. C. (1999), “Resilient Modulus Measurement of Fine-Grained Subgrade Soils,” *Transportation Research Record*, No. 1687, Washington, D.C., pp. 3-12.
- Mualem, Y. (1977), “Extension of the Similarity Hypothesis Used for Modeling the Soil Water Characteristics,” *Water Resources Research*, Vol. 13, No. 4, pp. 773-780.
- Mualem, Y. (1984), “Prediction of the Soil Boundary Wetting Curve,” *Journal of Soil Science*, Vol. 137, No. 6, pp. 379-390.
- Nazarian, S., Yuan, D., and Tandon, V. (1999), “Structural Field Testing of Flexible Pavement Layers with Seismic Methods for Quality Control,” *Transportation Research Record*, No. 1654, Washington, D.C., pp. 50-60.
- Nazarian, S., Yuan, D., and Arellano, M. (2002), “Quality Management of Base and Subgrade Materials with Seismic Methods,” *Transportation Research Record*, No. 1786, Washington, D.C., pp. 3-10.
- Nazarian, S., Yuan, D., and Williams, R. R. (2003), “A Simple Method for Determining Modulus of Base and Subgrade Materials,” *Resilient Modulus Testing for Pavement Components*, ASTM STP 1437, West Conshohocken, PA, pp. 153-164.
- NCHRP 1-28A (2003), *Harmonized Test Method for Laboratory Determination of Resilient Modulus for Flexible Pavement Design*, Final Report, National Cooperative Highway Research Program, Transportation Research Board, National Research Council, Washington, DC., 414 pages.

- NCHRP 1-37A (2004), *Guide for Mechanistic-Empirical Design of New and Rehabilitated Pavement Structures, Final Report, Part 2, Design Inputs*, National Cooperative Highway Research Program, Transportation Research Board, National Research Council, Washington, DC.
- Nichol, C., Smith, L., and Beckie, R. (2003), "Long-Term Measurement of Matric Suction using Thermal Conductivity Sensors," *Canadian Geotechnical Journal*, Vol. 40, pp. 587-597.
- Nimmo, J. R. (1992), "Semi-Empirical Model of Soil Water Hysteresis," *Soil Science Society of America Journal*, Vol. 56, pp. 1732-1730.
- Oberg, A. and Sallfors, G. (1997), "Determination of Shear Strength Parameters of Unsaturated Silts and Sands Based on the Water Retention Curve," *Geotechnical Testing Journal*, Vol. 20, No. 1, pp. 40-48.
- Oloo, S. Y., and Fredlund, D. G. (1998). "The Application of Unsaturated Soil Mechanics Theory to the Design of Pavements," *Proceedings of the 5<sup>th</sup> International Conference on the Bearing Capacity of Roads and Airfields*, Trondheim, Norway, pp. 1419-1428.
- Olson, R. E. and Langfelder, L. J. (1965), "Pore Water Pressures in Unsaturated Soils," *Journal of the Soil Mechanics and Foundations Division*, ASCE, Vol. 91, No. SM4, pp. 127-150.
- Ooi, P. S. K. and Pu, J. (2003), "Use of Stiffness for Evaluating Compactness of Cohesive Pavement Geomaterials," *Transportation Research Record*, No. 1849, Washington, D.C., pp. 11-19.
- Ooi, P. S. K., Archilla, A. R., and Sandefur, K. G. (2004), "Resilient Modulus Models for Compacted Cohesive soils," *Transportation Research Record*, No. 1874, Washington, D.C., pp. 115-124.
- Parlange, J.-Y. (1976), "Capillary Hysteresis and the Relationship between Drying and Wetting Curves," *Water Resources Research*, Vol. 12, No. 2, pp. 224-228.
- Pennington, D. S., Nash, D. F. T., and Lings, M. L. (1997), "Anisotropy of  $G_0$  Shear Stiffness in Gault Clay," *Geotechnique*, Vol. 47, No. 3, pp. 391-398.
- Pennington, D. S., Nash, D. F. T., and Lings, M. L. (2001), "Horizontally Mounted Bender Elements for Measuring Anisotropic Shear Moduli in Triaxial Clay Specimens," *Geotechnical Testing Journal*, Vol. 24, No. 2, pp. 133-144.

- Perera, Y. Y., Zapata, C. E., Houston, W. N., Houston, S. L. (2004), "Moisture Equilibria beneath Highway Pavements," *Transportation Research Board 83<sup>rd</sup> Annual Meeting*, Washington, D.C. (CD-ROM)
- Pham, Q. H., Fredlund, D. Q., and Barbour, S. L. (2003), "A Practical Hysteresis Model for the Soil-Water Characteristic Curve for Soils with Negligible Volume Change," *Geotechnique*, Vol. 53, No. 2, pp. 293-298.
- Pham, Q. H., Fredlund, D. Q., and Barbour, S. L. (2005), "A Study of Hysteresis Models for Soil-Water Characteristic Curves," *Canadian Geotechnical Journal*, Vol. 42, No. 6, pp. 1548-1568.
- Phene, C. J., Clark, D. A., Cardon, G. E., and Mead, R. M. (1992). "Soil Matric Potential Sensor: Research and Applications," *Advances in Measurement of Soil Physical Properties: Bringing Theory into Practice*, SSSA SP 30, San Antonio, TX, pp. 263-280.
- Rassam, D.W., and Cook, F.J. (1999), "A relationship describing the shear strength of unsaturated soils," *Geotechnical testing J.* 28: 215-220.
- Rassam, D.W., and Cook, F.J. (2002), "Predicting the shear strength envelope of unsaturated soils," *Geotechnical Testing J.* 28: 215-220.
- Rassam, D.W., and Williams, D. J. (1999), "A relationship describing the shear strength of unsaturated soils," *Canadian Geotechnical J.* 36: 363-368.
- Russam, K. (1965), "The Prediction of Subgrade Moisture Conditions for Design Purposes," *Moisture Equilibria and Moisture Changes in Soils beneath Covered Areas*, Butterworth, Sydney, Australia.
- Russam, K., and Coleman, J. D. (1961), "The Effect of Climatic Factors on Subgrade Moisture Conditions," *Geotechnique*, Vol. 11, No. 1, pp. 22-28.
- Roberson, R. (2002), "Material Moisture Characterization," *Seminar on Unsaturated Soil Engineering: Applications in Pavements*, Minnesota Department of Transportation, MN.
- Sanchez-Salinerio, I., Roesset, J. M., and Stokoe, K. H., II (1986), *Analytical Studies of Body Wave Propagation and Attenuation, Report GR 86-15*, University of Texas, Austin, TX.
- Sauer, E. K. and Monismith, C. L. (1968), "Influence of Soil Suction on Behavior of a Glacial Till Subjected to Repeated Loading," *Highway Research Record*, No. 215, Washington, D.C., pp. 18-23.

- Santamarina, J. C., Klein, K. A., and Fam, M. A. (2001), *Soils and Waves*, John Wiley & Sons, Chichester, UK.
- Sawangsurriya, A., Edil, T. B., and Bosscher, P. J. (2005), "Stiffness Behavior of an Unsaturated Pavement Subgrade Soil," *Proceedings of International Conference on Problematic Soils*, Famagusta, N. Cyprus, pp. 209-217.
- Sawangsurriya, A., Bosscher, P. J., and Edil, T. B. (2005), "Alternative Testing Techniques for Modulus of Pavement Bases and Subgrades," *Proceedings of the 13<sup>th</sup> Annual Great Lakes Geotechnical and Geoenvironmental Engineering Conference, Geotechnical Applications for Transportation Infrastructure*, ASCE, Geotechnical Practice Publication, No. 3, Milwaukee, WI, pp. 108-121.
- Sawangsurriya, A., (2006), "Stiffness-Suction-Moisture Relationship for Compacted Soils," Ph. D. *Thesis*, Department of Civil and Environmental Engineering, University of Wisconsin, Madison, WI.
- Sawangsurriya, A., Biringen, E., Fratta, D., Bosscher, P. J. and Edil, T. B. (2006), "Dimensionless Limits for the Collection and Interpretation of Wave Propagation Data in Soils," *GeoShanghai Conference, Site and Geomaterial Characterization, ASCE, Geotechnical Special Publication*, Shanghai, China (accepted for publication).
- Schick, P. (2004), "Scherfestigkeit durch Kapillarität in unzementierten ungesättigten bindigen Boden (Capillary strength of uncemented and unsaturated cohesive soils in direct shear)," *Bautechnik*, 81(1) 31-37.
- Shackel, B. (1973), "Repeated Loading of Soils—A Review," *Australian Road Research*, Vol. 5, No. 3, pp.22-49.
- Shackelford, C.D., Houston, S.L., and Chang, N-Y. (2000), "Advances in Unsaturated Geomechanics," *Proceedings of sessions of Geo-Denver 2000*. ASCE Geotechnical Special Publication no. 99.
- Sheeran, D. E., Baker, W. H., and Krizek, R. J. (1967), "Experimental Study of Pulse Velocities in Compacted Soils," *Highway Research Record*, No. 177, Washington, D.C., pp. 226-238.
- Shen, Z. (1996), "The problem in the present studies on mechanics for unsaturated soils" *Proceedings of the Symposium on Geotechnical Aspects of Regional Soils*, Nanjing, China, [in Chinese].
- Shuai, F., and Fredlund, D. G. (2000), "Use of a New Thermal Conductivity Sensor to Measure Soil Suction," *Proceedings of Sessions of Geo-Denver 2000, Advances in Unsaturated Geotechnics*, Geotechnical Special Publication, No. 99, ASCE, Denver, CO, pp. 1-12.

- Singh, A., Roberson, R., Ranaivoson, A., Siekmeier, J., and Gupta, S.C. (2006), "Water Retention Characteristics of Aggregate and Granular Materials," *4th International Conf. on Unsaturated Soils*. ASCE. Phoenix, AZ. 2-6 April 2006, pp 1326-1337.
- Souto, A., Hartikainen, J., and Özüdoğru, K. (1994), "Measurement of Dynamic Parameters of Road Pavement Materials by the Bender Element and Resonant Column Tests," *Geotechnique*, Vol. 44, No. 3, pp. 519-526.
- Swenson, J., Guzina, B., Labuz, J., and Drescher, A. (2006), "Moisture Effects on PVD and DCP Measurements," Final Report 2006-26, Minnesota Department of Transportation, St. Paul, MN.
- Tan, E., Fredlund, D. G., and Marjerison, B. (2004), "Long Term Measurements of Matric Suction and Soil Temperature using Thermal Conductivity Sensors," *Transportation Research Board 83<sup>rd</sup> Annual Meeting*, Washington, D.C. (CD-ROM).
- Tekinsoy, M.A., Kayadelen, C., Keskin, M.S., and Soylemez, M. (2004), "An equation for predicting shear strength envelope with respect to matric suction," *Computers and Geotechnics*, 3(7): 589-593.
- Terzaghi, K. (1936). "The shear resistance of unsaturated soil," Proc., 1<sup>st</sup> Int. Conf. on *Soil Mechanics and Foundation Engineering*, Harvard Printing Office, Cambridge, Mass., 54-56.
- Tian, P., Zaman, M. M., and Laguros, J. G. (1998), "Gradation and Moisture Effects on Resilient Moduli of Aggregate Bases," *Transportation Research Record*, No. 1619, Washington, D.C., pp. 75-83.
- Thadkamalla, G. B., and George, K. P. (1995), "Characterization of Subgrade Soils at Simulated Field Moisture," *Transportation Research Record*, No. 1481, Washington, D.C., pp. 21-27.
- Thakur, V. K. S., Sreedeeep, S., and Singh, D. N. (2005), "Parameters Affecting Soil-Water Characteristic Curves of Fine-Grained Soils," *Journal of Geotechnical and Geoenvironmental Engineering*, ASCE, Vol. 131, No. 4, pp. 521-524.
- Thomann, T. G., and Hryciw, R. D. (1990), "Laboratory Measurement of Small Strain Shear Modulus under  $K_0$  Conditions," *Geotechnical Testing Journal*, Vol. 13, No. 2, pp. 97-105.
- Thompson, M. R., and Robnett, Q. L. (1979), "Resilient Properties of Subgrade Soils," *Transportation Engineering Journal*, ASCE, Vol. 105, No. 1, pp. 71-89.
- Thornthwaite, C. W. (1948), "An Approach toward a Rational Classification of Climate," *Geographical Review*, Vol. 38, No. 1, pp. 55-94.

- Tinjum, J. M., Benson, C. H., and Blotz, L. R. (1997), "Soil-Water Characteristic Curves for Compacted Clays," *Journal of Geotechnical and Geoenvironmental Engineering*, ASCE, Vol. 123, No. 11, pp. 1060-1069.
- Topp, G. C. and Miller E. E. (1966), "Hysteretic Moisture Characteristics and Hydraulic Conductivities for Glass-Bead Media," *Soil Science Society of America Journal*, Vol. 30, pp. 156-162.
- van Genuchten, M. (1980), "A Closed-Form Equation for Predicting the Hydraulic Conductivity of Unsaturated Soils," *Soil Science Society of America Journal*, Vol. 44, pp. 892-898.
- Vanapalli, S. K., and Fredlund, D. G. (2000), "Comparison of Different Procedures to Predict Unsaturated Soil Shear Strength," *Proceedings of Sessions of Geo-Denver 2000, Advances in Unsaturated Geotechnics*, ASCE, Geotechnical Special Publication, No. 99, Denver, CO, pp. 195-209.
- Vanapalli, S. K., Fredlund, D. G., and Pufahl, D. E. (1999), "The Influence of Soil Structure and Stress History on the Soil-Water Characteristics of a Compacted Till," *Geotechnique*, Vol. 49, No. 2, pp. 143-159.
- Vanapalli, S. K., Fredlund, D. G., and Pufahl, D. E. (1996a), "The Relationship between the Soil-Water Characteristic Curve and the Unsaturated Shear Strength of a Compacted Glacial Till," *Geotechnical Testing Journal*, Vol. 19, No. 3, pp. 259-268.
- Vanapalli, S. K., Fredlund, D. G., Pufahl, D. E., and Clifton, A. W. (1996b), "Model for the Prediction of Shear Strength with Respect to Soil Suction," *Canadian Geotechnical Journal*, Vol. 33, No. 3, pp. 379-392.
- Viggiani, G., and Atkinson, J. H. (1995), "Interpretation of Bender Element Tests," *Geotechnique*, Vol. 45, No. 1, pp. 149-154.
- Vanapalli, S. K., Fredlund, D. G., Pufahl, D. E., and Clifton, A. W. (1996), "Model for the Prediction of Shear Strength with Respect to Soil Suction," *Canadian Geotechnical Journal*, Vol. 33, No. 3, pp. 379-392.
- Vanapalli, S. K., and Fredlund, D. G. (2000), "Comparison of Different Procedures to Predict Unsaturated Soil Shear Strength," *Proceedings of Sessions of Geo-Denver 2000, Advances in Unsaturated Geotechnics*, ASCE, Geotechnical Special Publication, No. 99, Denver, CO, pp. 195-209.
- Viggiani, G., and Atkinson, J. H. (1995), "Interpretation of Bender Element Tests," *Geotechnique*, Vol. 45, No. 1, pp. 149-154.

- Wan, A. W.-L., Gray, M. N., and Graham, J. (1995), "On the Relations of Suction Moisture Content and Soil Structure in Compacted Clays," *Proceedings of the 1<sup>st</sup> International Conference on Unsaturated Soils*, Paris, France, pp. 215-222.
- Wang, X., and Benson, C. H. (2004), "Leak-Free Pressure Plate Extractor for Measuring the Soil Water Characteristic Curve," *Geotechnical Testing Journal*, Vol. 27, No. 2, pp. 1-10.
- Watson, K. K., Reginato, R. J., and Jackson, R. D. (1975), "Soil Water Hysteresis in a Field Soil," *Soil Science Society of America Journal*, Vol. 39, pp. 242-246.
- Wheeler, S. J. and Sivakumar, V. (1995), "An Elasto-Plastic Critical State Framework for Unsaturated Soils," *Geotechnique*, Vol. 45, No. 1, pp. 35-53.
- White, D.J., Thompson, M.J., and Vennapusa, P.K.R. (2007), "Field monitoring of Intelligent Compaction Monitoring Technology for Unbound Materials," a report submitted to *Mn/DOT*, Iowa State University, Ames, IA.
- Xu, Y. (1997), "Mechanical properties of unsaturated expansive soils and its application in engineering," *Ph. D. Thesis, HoHai University*, Nanjing, China, [in Chinese].
- Xu, Y.F., and Sun, D. (2001), "Determination of unsaturated shear strength using a fractal model," *Fractals* 91: 51-60.
- Xu, Y.F. (2004), "Fractal approach to unsaturated shear strength," *J. Geotechnical and Geoenvironmental Engineering*, 130(3): 264-273.
- Yang, H., Rahardjo, H., Leong, E.-C., and Fredlund, D. G. (2004), "Factors Affecting Drying and Wetting Soil-Water Characteristic Curves of Sandy Soils," *Canadian Geotechnical*.
- Yang, S.-R., Huang, W.-H., and Tai, Y.-T. (2005), "Variation of Resilient Modulus with Soil Suction for Compacted Subgrade Soils," *Transportation Research Record*, No. 1913, Washington, D.C., pp. 99-106.
- Yesiller, N., Inci, G., and Miller, C. J. (2000), "Ultrasonic Testing for Compacted Clayey Soils," *Proceedings of Sessions of Geo-Denver 2000, Advances in Unsaturated Geotechnics*, ASCE, Geotechnical Special Publication, No. 99, Denver, CO, pp. 54-68.
- Yong, R.N., and Warkintin, B.P. (1975), "Soil properties and behaviour," *Elsevier*, Amsterdam.

## **APPENDIX A: REVIEW OF STIFFNESS AND SUCTION**

Appendices A, B, C, and E were put together by Drs. Tuncer Edil, Craig Benson, and Auckpath Sawangsuriya of the University of Wisconsin.

## A-1 Stiffness of Soil at Small Strains

Stiffness of soil at small strains is an important and fundamental soil property for a variety of geotechnical design applications and can be applied to all kinds of static (monotonic) and dynamic geotechnical problems at small strains (Richart et al. 1970, Jardine et al. 1986, Burland 1989). It is generally denoted by a small-strain (elastic) shear modulus of soil ( $G_0$ ), which is typically in the shear strain range below the elastic threshold strain ( $\sim 10^{-3}\%$ - $10^{-2}\%$ ). Within the small strain range where the deformations or strains are purely elastic and fully recoverable, the shear modulus is independent of strain amplitude and reaches a nearly constant limiting value of the maximum shear modulus. In this strain region, the soil exhibits linear-elastic behavior.

The small-strain stiffness of soil can be determined using dynamic techniques both in the field and the laboratory tests of which the deformation characteristics of the soils are related to elastic shear wave velocities. Measurements of shear wave velocities and corresponding small-strain shear modulus using dynamic techniques have several advantages:

1. Most dynamic techniques are relatively simple, rapid, repeatable, and nondestructive.
2. Good agreement between  $G_0$  measured in the laboratory and in the field is made when the laboratory specimens are at the same conditions as those in the field (Anderson and Woods 1976, Viggiani and Atkinson 1995a, Nazarian et al. 1999, Atkinson 2000).
3. Load repetition, strain rate, and loading frequency have only minor influence in the small-strain range (Iwasaki et al. 1978, Ni 1987, Bolton and Wilson 1989, Tatsuoka and Shibuya 1991, Jardine 1992, Shibuya et al. 1992, 1995, Ishihara 1996).
4.  $G_0$  of soils is unique for both static (monotonic) and dynamic (cyclic) loading conditions (Georgiannou et al. 1991, Jamiolkowski et al. 1994, Tatsuoka et al. 1997).
5. Little or no hysteresis (stress-strain loop) exists in both slow repetitive and dynamic cyclic loading tests (Silvestri 1991).
6. Volumetric and shear deformations (or strains) are fully recoverable and the tendency of soils to dilate or to contract during drained shear does not occur (Ishihara 1996).
7. Magnitude of  $G_0$  is independent of drainage since the induced strain levels are too small to cause pore water pressure to build up during undrained shear test (Ohara and Matsuda 1988, Dobry 1989, Georgiannou et al. 1991, Silvestri 1991). Pore water pressure does not build up if the shear strain amplitude is smaller than  $10^{-2}\%$  for sands (Dobry 1989) and  $0.1\%$  for clays (Ohara and Matsuda 1988).

## A-2 Stiffness of Particulate Materials-Microscale Behavior

Soils are particulate materials which assemble of discrete elastic soil particles. Some aspects of the mechanic behavior of particulate media are useful in examining small-strain stiffness model. In particulate materials, the small-strain stiffness is strongly determined by the behavior of contacts because at small strains, particle deformation depends mainly on the interparticle contact response and elastic properties of material. Cascante and Santamarina (1996) indicated that shear waves directly reflects the behavior of the particle contacts and the state of assembly since it propagates exclusively through the soil skeleton.

Preliminary observations and analyses indicated that small-strain stiffness depends on packing conditions (i.e., coordination number, contact behavior), confining pressure, and cementation (Petraakis and Dobry 1987, Acar and El-Tahir 1986). The exponent  $n$  of the power relationship between stiffness and confining pressure (i.e.,  $G \propto \sigma_o^n$ ) represents the type of contact. For similar fabric conditions,  $n$  equals to  $1/3$  for spherical contacts between linear-elastic materials, whereas  $n$  equals to  $1/2$  for cone-to-plane contacts. Goddard (1990) showed that the increase in coordination number among spherical particles due to buckling of particle chains can justify an exponent  $n = 1/2$ . Chang et al. (1991) showed that the shear modulus is proportional to the coordination number to the power  $2/3$  for a random packing of spheres with Mindlin contacts.

The most simple and idealized contact characteristic is known as elastic Hertzian contact. Hertz's theory (Hertz 1881) describes the behavior of identical and linear elastic spheres of radius ( $R$ ) compressed against each other by a normal contact force ( $N$ ) and is expressed as (Timoshenko and Goodier 1951):

$$N = \frac{2\sqrt{2}GR^{3/2}}{3(1-\nu)} \delta_N^{3/2} \quad (\text{A-1})$$

where  $G$  is the shear modulus and  $\nu$  is the Poisson's ratio of the material that makes the spheres, and  $\delta_N$  is the center-to-center displacement of the two spheres in contact (Fig. A-1). The stiffness ( $k$ ) of two elastic spheres in contact can be computed from the Hertzian relationship as:

$$k = \frac{dN}{d\delta_N} = 3 \left[ \frac{G}{3(1-\nu)} \right]^{2/3} N^{1/3} \quad (\text{A-2})$$

This relationship can be extended to determine the tangent elastic modulus ( $E_T$ ) of a simple cubic packing with Hertzian contacts. The normal contact force ( $N$ ) transferred through the contact can be expressed in terms of the average normal stress ( $\sigma$ ). For a simple cubic packing, the contribution area for one sphere is  $4R^2$ . Therefore, the average normal stress for a cubically packed array of spheres loaded along one of the packing axes (Fig. A-2) is obtained by dividing the normal contact force by its tributary area.

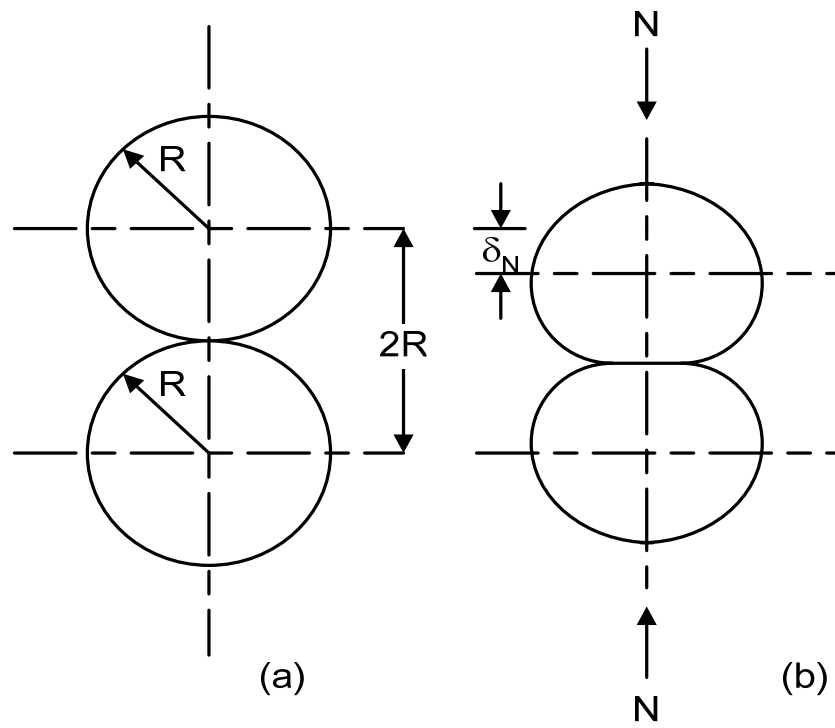


Fig. A-1. Behavior of equal spheres in contact: (a) spheres just touching (b) deformation by normal force.

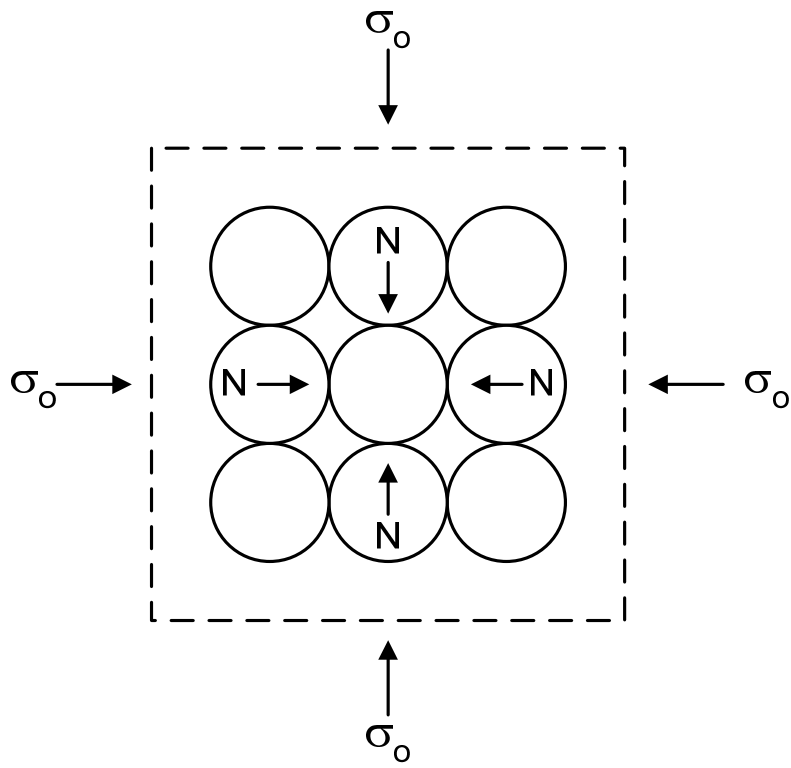


Fig. A-2. Cubically packed array of spheres subjected to average normal confining stress ( $\sigma_o$ ) that produce inter-particle contact force (N).

$$\sigma = \frac{N}{(2R)^2} = \frac{N}{4R^2} \quad (\text{A-3})$$

Therefore, the tangent elastic modulus ( $E_T$ ) or Young's modulus ( $E$ ) of a simple contact packing with Hertzian contacts of the particulate media subjected to uniaxial loading is (Richart et al. 1970):

$$E_T = \frac{d\sigma}{d\varepsilon} = \frac{dN/4R^2}{d\delta_N/2R} = \frac{1}{2R} \frac{dN}{d\delta_N} = \frac{3}{2} \left[ \frac{2G}{3(1-\nu)} \right]^{2/3} \sigma^{1/3} \quad (\text{A-4})$$

where  $\varepsilon$  is uniaxial strain. Eq. (A-4) can be rewritten in terms of  $G$  using the standard relation between  $E$  and  $G$  for isotropic materials. In general, the applied normal stress ( $\sigma$ ) is orders of magnitude smaller than the shear modulus of the sphere ( $G$ ). Therefore, Eq. (A-4) suggests very low  $E_T$  of the particulate material relative to the modulus of the material that composes the particles and that  $E_T$  theoretically vary with the cube root of the normal stress. The variation of elastic modulus with confining pressure to the power 1/3 applies to other regular packings (Duffy and Mindlin, 1957; Deresiewicz, 1973; Petrakis and Dobry, 1987). Note that the particulate behavior in terms of the simple cubic packing of identical and elastic spheres as given in Eq. (A-4) benefits from clarity and simplicity. The relationship is valid as long as only normal forces are developed at the points of contact between the spheres along the principle axes. Eq. (A-4) also leads to an expression for the modulus of volume compression or bulk modulus ( $B$ ), which relates the confining pressure or hydrostatic pressure ( $\sigma_o$ ) to volumetric strain ( $\varepsilon_v$ ). Since  $\sigma_o = \sigma_1 = \sigma_2 = \sigma_3$ ,  $\varepsilon_v$  is three times the uniaxial strain ( $\varepsilon$ ) given in Eq. (A-4) and  $B$  becomes:

$$B = \frac{1}{2} \left[ \frac{2G}{3(1-\nu)} \right]^{2/3} \sigma_o^{1/3} \quad (\text{A-5})$$

Knowing the deformation of spheres in contact is a local phenomenon, the behavior described by Eq. (A-4) and (A-5) could be superposed in any order as long as only normal forces are developed at the points of contact between the spheres (Richart et al., 1970). In general, the soil existing in the ground is subjected to a certain amount of confining pressure ( $\sigma_o$ ) due to its own weight, known as geostatic stress, in the "at-rest" condition. If an additional stress is induced to any of the principle axes, the elastic modulus corresponding to this stress can be expressed in Eq. (A-4) by substituting  $\sigma_o$  for  $\sigma$ . An additional theory is required to take the effects of shearing forces when both normal shearing forces are developed at the points of contact, i.e., stresses are applied along a diagonal direction (Richart et al., 1970). The studies by Duffy and Mindlin (1957) on a face-centered cubic packing suggested that tangential forces have an important effect on the stiffness of particulate materials.

The variation of stiffness with normal force for a conical contact was studied by Goddard (1990). The stiffness ( $k$ ) is given by:

$$k = \frac{dN}{d\delta_N} = \left[ \frac{8G}{\pi(1-\nu)\alpha} \right]^{1/2} N^{1/2} \quad (\text{A-6})$$

where  $\alpha$  is the angle between the cone and the normal plane. Note that the exponent of the normal contact force is 1/2 in comparison with 1/3 for the Hertzian contact. Goddard (1990) suggests that conical contacts can explain the common observation that the stiffness on dry sands varies with isotropic confining pressure with exponents close to 1/2, instead of the 1/3 predicted for Hertzian contacts.

### A-3 Factors Affecting Stiffness of Soil at Small Strains

**Current State:** The current state of a soil sample relative to small-strain stiffness is defined by: (i) existing normal stresses in the soil which is also known as the mean effective principle stress or confining pressure ( $\sigma_o'$ ), (ii) the overconsolidation ratio (OCR), and (iii) the void ratio ( $e$ ) or the density of the soil ( $\rho$ ). By taking all parameters into account, a general expression as proposed by different investigators for the small-strain shear modulus ( $G_o$ ) of soils is of the following form:

$$G_o = A(\text{OCR})^k f(e) \rho_a^{(1-n)} (\sigma_o')^n \quad (\text{A-7})$$

where  $A$  is a dimensionless material constant coefficient,  $k$  is a overconsolidation ratio exponent,  $f(e)$  is a void ratio function,  $p_a$  is the reference stress or atmospheric pressure (~100 kPa) expressed in the same units as  $G_o$  and  $\sigma_o'$ , and  $n$  is a stress exponent. A number of studies have been conducted to estimate these parameters by relating with other physical soil properties as summarized in Table A-1 and Table A-2.

**Anisotropy:** Anisotropic small-strain stiffness of soils is generally described in terms of stress-induced anisotropy and inherent anisotropy (Stokoe et al., 1985). The stress-induced anisotropy results from the anisotropy of the current stress condition and is independent of the stress and strain history of the soil. The inherent or fabric anisotropy results from structure or fabric of the soil that reflects the deposition or forming process (such as aging, cementation). Both stress-induced anisotropy and fabric anisotropy of small-strain stiffness of soils depend on the direction of loading (Mitchell and Soga, 2005). For example,  $G_o$  is a function of the principal effective stresses in the directions of wave propagation and particle motion and is independent of the out-of-plane principal stress (Stokoe et al., 1995). The inherent anisotropy can be evaluated by measuring body wave velocities propagating through the soil specimen subjected to isotropic states of stress (i.e., mean effective stress). For the stress-induced anisotropy, the measurements are taken from specimen subjected to anisotropy states of stress (i.e., changes in vertical stress while maintaining average principal stresses).

Table A-1. Parameters describing a current state of soil sample for  $G_o$

Parameter	Dependency	Typical value	References
A	Grain characteristics or nature of grains, soil fabric or microstructure	Determined by regression analysis for individual soil test	See Table A-2
k	Plasticity index (PI)	Vary from 0 to 0.5 (for $PI < 40$ , $k = 0$ ; $PI > 40$ , $k = 0.5$ )	Hardin and Black (1968), Hardin and Drnevich (1972)
f(e)	Properties of packing and density	See Table A-2	See Table A-2 Hardin and Richart (1963), Hardin and Black (1966, 1968), Drnevich et al. (1967), Seed and Idriss (1970), Silver and Seed (1971), Hardin and Drnevich (1972), Kuribayashi et al. (1975), Kokusho (1980)
n	Contact between particles and strain amplitude	Approximately 0.5 at small strains	

Table A-2. Function and constants in proposed empirical equations on  $G_o$

$$G_o = A \cdot f(e) \cdot (\sigma_o')^n$$

Soil	A	f(e)	n	References
Round-grained Ottawa sand	6,900	$(2.17 - e)^2 / (1 + e)$	0.5	Hardin and Black (1968)
Angular-grained crushed quartz	3,270	$(2.97 - e)^2 / (1 + e)$	0.5	
Clean sand	41,600	$0.67 - e / (1 + e)$	0.5	Shibata and Soelarno (1975)
Clean sand ( $C_u < 1.8$ )	14,100	$(2.17 - e)^2 / (1 + e)$	0.4	Iwasaki and Tatsuoka (1977)
Clean sand	9,000	$(2.17 - e)^2 / (1 + e)$	0.4	Iwasaki et al. (1978)
Toyoura sand	8,400	$(2.17 - e)^2 / (1 + e)$	0.5	Kokusho (1980)
Clean sand	7,000	$(2.17 - e)^2 / (1 + e)$	0.5	Yu and Richart (1984)
Ticino sand	7,100	$(2.27 - e)^2 / (1 + e)$	0.4	Lo Presti et al. (1993)
Clean sand	9,300	$1/e^{1.3}$	0.45	Lo Presti et al. (1997)
Reconstituted NC Kaolinite (PI = 20) and undisturbed NC clays	3,270	$(2.97 - e)^2 / (1 + e)$	0.5	Hardin and Black (1968)
Reconstituted NC Kaolinite (PI = 35)	4,500	$(2.97 - e)^2 / (1 + e)$	0.5	Marcuson and Wahls (1972)
Reconstituted NC Bentonite (PI = 60)	445	$(4.4 - e)^2 / (1 + e)$	0.5	
Remolded clay (PI = 0~50)	2,000~4,000	$(2.97 - e)^2 / (1 + e)$	0.5	Zen et al. (1978)
Undisturbed NC clay (PI = 40~85)	90	$(7.32 - e)^2 / (1 + e)$	0.6	Kokusho et al. (1982)
Clay deposits (PI = 20~150)	5,000	$1/e^{1.5}$	0.5	Shibuya and Tanaka (1996) <sup>†</sup>
Remolded clay (PI = 20~60)	24,000	$1/(1+e)^{2.4}$	0.5	Shibuya et al. (1997) <sup>†</sup>
Sand and clay	6,250	$1/(0.3+0.7e^2)$	0.5	Hardin (1978)
Several soils	5,700	$1/e$	0.5	Biarez and Hicher (1994)

Note:  $G_o$  and  $\sigma_o'$  are in kPa, <sup>†</sup> using  $\sigma_v'$  instead of  $\sigma_o'$

Under anisotropic states of stress, the representative stiffness values can be different, depending on the measurement conditions and the sample preparation procedures. The anisotropy of the stress state induces anisotropy of small-strain stiffness. An empirical equation for  $G_o$  under anisotropic stress conditions is expressed as (Roesler 1979, Stokoe et al. 1985):

$$G_o = A(\text{OCR})^k F(e) p_a^{1-n} \sigma_i^{n_i} \sigma_j^{n_j} \quad (\text{A-8})$$

where  $\sigma_i'$  is the effective normal stress in the direction of wave propagation,  $\sigma_j'$  is the effective normal stress in the direction of particle motion, and  $n = n_i + n_j$ .

**Degree of Saturation:** Early studies on the influence of the degree of saturation on  $G_o$  described a coupled motion of the solid particles and the fluid (Biot 1956, Hardin and Richart 1963, Richart et al. 1970). According to Biot's theory, no structural coupling exists between the solid particle and the fluid (the fluid has no shearing stiffness), the coupling in the shearing mode is only developed by the relative motions of the solid and fluid as indicated by the term involving the apparent additional mass density and thus  $G_o$  can be expressed as:

$$G_o = v_s^2 \left( \rho + \frac{\rho_f \rho_a}{\rho_f + \rho_a} \right) \quad (\text{A-9})$$

where  $\rho$  is the mass density of the solid particles,  $\rho_f$  is the mass density of fluid, and  $\rho_a$  is the mass density of an additional apparent mass. In a real soil,  $\rho_a$  varies with the grain size and permeability; however, the total mass density of the saturated soil could be substituted into the mass density term of Eq. (A-9) to take into account the coupling effect of the mass of the fluid. The shear wave velocity of saturated soil is therefore less than that of dry soil because the added apparent mass of water moving along with the soil skeleton (i.e., the drag of the water in the pores). Recent studies by Santamarina et al. (2001) and Inci et al. (2003) indicated that the response of  $G_o$  by varying the degree of saturation demonstrates three phases of behavior and is attributed to contact-level capillary forces or suction. The effect of soil suction on  $G_o$  will be discussed later in this chapter. A sharp increase in  $G_o$  is observed at the beginning of the drying process, followed by a period of gradual increase in measured  $G_o$ , and a final sharp increase in  $G_o$  at the end of the drying period.

**Aging:** A time-dependent nature of  $G_o$  of soils has been reported by several investigators (Afifi and Woods 1971, Marcuson and Wahls 1972, Afifi and Richart 1973, Stokoe and Richart 1973, Trudeau et al. 1974, Anderson and Woods 1975, Anderson and Woods 1976, Anderson and Stokoe 1978, Isenhower and Stokoe 1981, Athanasopoulos 1981, Kokusho 1987). Results of these investigations indicate that  $G_o$  tends to increase with the duration of time under a constant confining pressure after the primary consolidation is complete due to a time effect results from strengthening of particle bonding. The time dependency of  $G_o$  increase can be characterized by two phases: (i) an initial phase due to primary consolidation and (ii) a second phase in which  $G_o$  increases about linearly with

the logarithm of time and occurs after completion of primary consolidation, also referred as the long-term time effect (Fig. A-3). The second phase of secondary consolidation occurs after primary phase when  $G_o$  increases continuously with time. The rate of secondary increase in  $G_o$  is related to thixotropic changes in the clay structure and is determined to be linear when plotted versus the logarithm of time. To incorporate this long-term time effect, the change in  $G_o$  with time can be expressed by:

$$\Delta G = N_G G_{1000} \quad (\text{A-10})$$

and

$$N_G = \left( \frac{1}{G_{1000}} \right) \left( \frac{\Delta G}{\log_{10}(t_2/t_1)} \right) \quad (\text{A-11})$$

where  $\Delta G$  is the increase in  $G_o$  over one logarithm cycle of time,  $G_{1000}$  is the value of  $G_o$  measured after 1,000 minutes of application of constant confining pressure following the primary consolidation, and  $N_G$  is the aging increment coefficient, which indicates an increase of  $G_o$  within one logarithmic cycle of time.

The duration of primary consolidation and the magnitude of the secondary increase, as defined by change in  $G_o$  per logarithmic cycle of time, vary with soil types and stress conditions (i.e., confining pressure). For sands, the rate of increase in  $G_o$  is relatively small (1 to 3% per log cycle of time) but for clays the effect is quite remarkable as illustrated in Fig. A-4.

**Cementation:** Cementation occurs either naturally due to the precipitation or formation of salts, calcite, alumina, iron oxides, silicates, and aluminates or artificial soil stabilization processes produced by adding lime, cement, asphalt, fly ash, or other bonding agents to natural soils. The effect of cementation on  $G_o$  have been evaluated by Clough et al. (1981), Acar and El-Tahir (1986), Saxena et al. (1988), Lade and Overton (1989), Baig et al. (1997), Fernandez and Santamarina (2001), Yun and Santamarina (2005).  $G_o$  of cemented soils increases with increasing cement content and confining pressure (Fig. A-5). Additionally at low confinement, the stiffness behavior of cemented soils is controlled by the cementation and the soils become brittle, whereas at high confinement the behavior is controlled by the state of stress and resembles an uncemented material, which becomes more ductile.

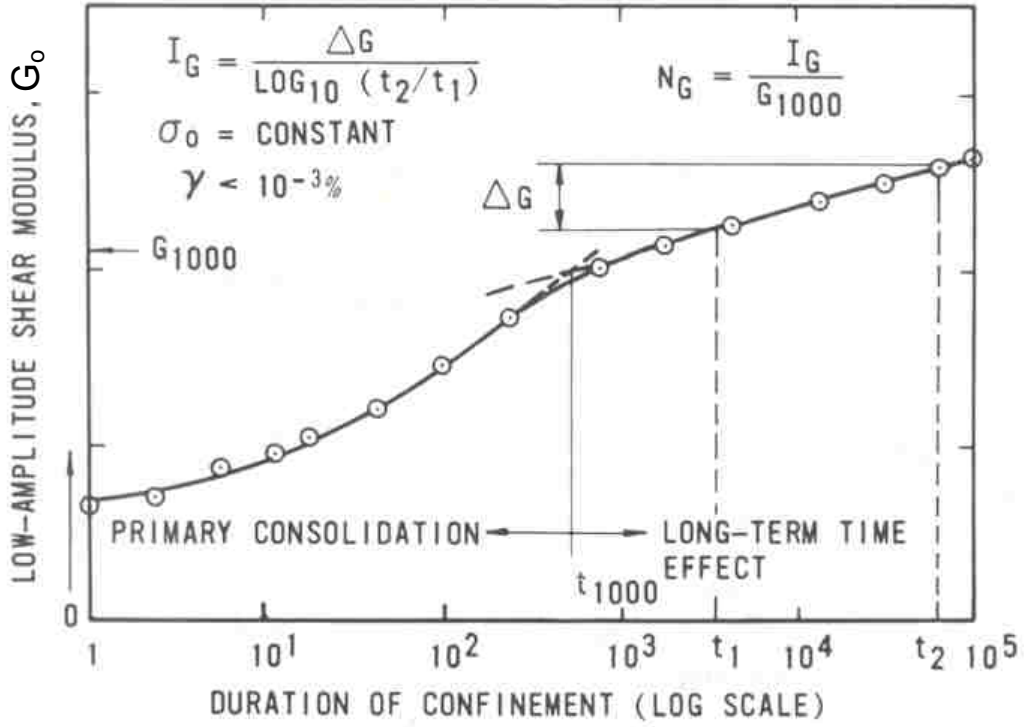


Fig. A-3. Phases of  $G_0$  versus confinement time (Anderson and Stokoe 1978).

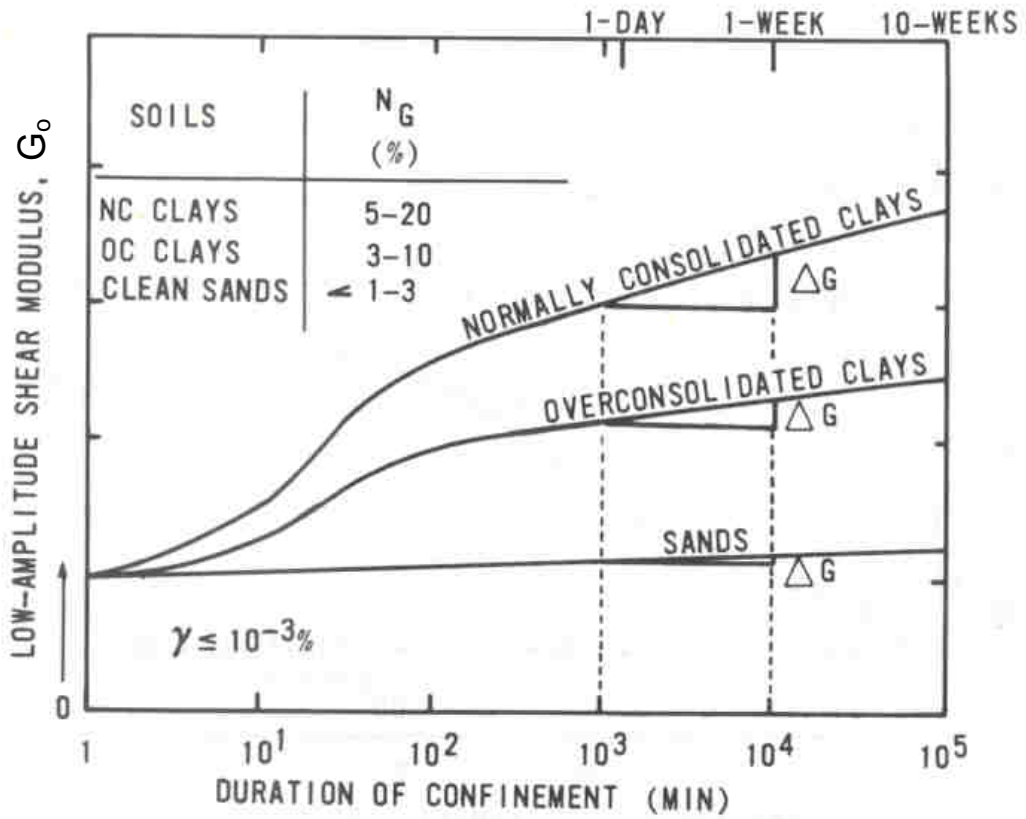


Fig. A-4. Effect of aging on  $G_0$  (Anderson and Stokoe 1978).

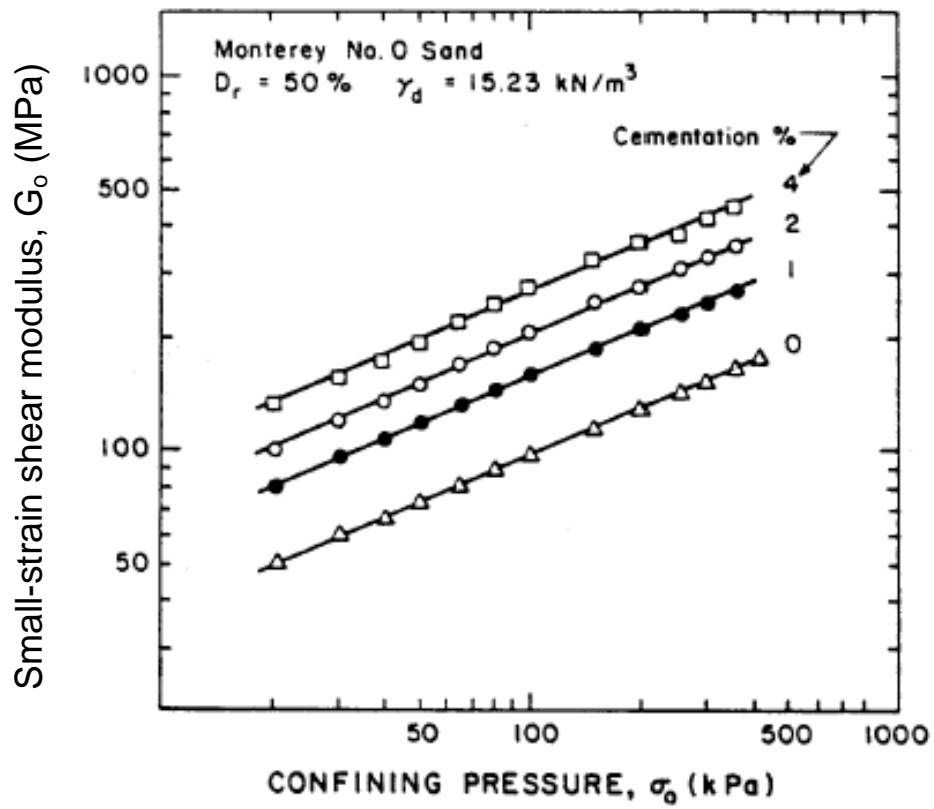


Fig. A-5. Effect of cementation on  $G_0$  (Acar and El-Tahir 1986).

**Temperature:** Effect of temperature on time-dependent changes in  $G_0$  was reported in Bosscher and Nelson (1987), Fam et al. (1998). The dependency of  $G_0$  on temperature suggests that higher temperatures cause the stiffness increase with time. Fam et al. (1998) presented the evolution in velocity with time for coarse-grained granular salt specimen under a constant effective stress and subjected to a temperature step (heating-cooling cycle) as illustrated in Fig. A-6. The rate of increase in velocity with time increases at higher temperatures (Fam et al. 1998). Bosscher and Nelson (1987) studied  $G_0$  of frozen Ottawa 20-30 sand as a function of the confining pressure, the degree of ice saturation, the relative density, and the temperature. They found that  $G_0$  of frozen sand is higher than that of non-frozen state. At temperatures near the melting point of ice,  $G_0$  can be significantly influenced by the confining pressure, the degree of ice saturation, and the relative density (Bosscher and Nelson 1987).

#### **A-4 Measurements of Soil Stiffness at Small Strains**

Different stiffness measurement techniques have different applied stress (or strain levels) and different loading frequencies, which in turn affect the response of test materials. This section involves only the stiffness measurements at small strains (below  $10^{-3}$ - $10^{-2}\%$ ) both in the laboratory and in the field in such a way that the stiffness obtained is independent of strain amplitude, the effect of loading frequency is insignificant, and the soil exhibits completely linearly elastic behavior. Table A-3 summarizes the existing measurement techniques used by the geotechnical engineering community in the U.S.

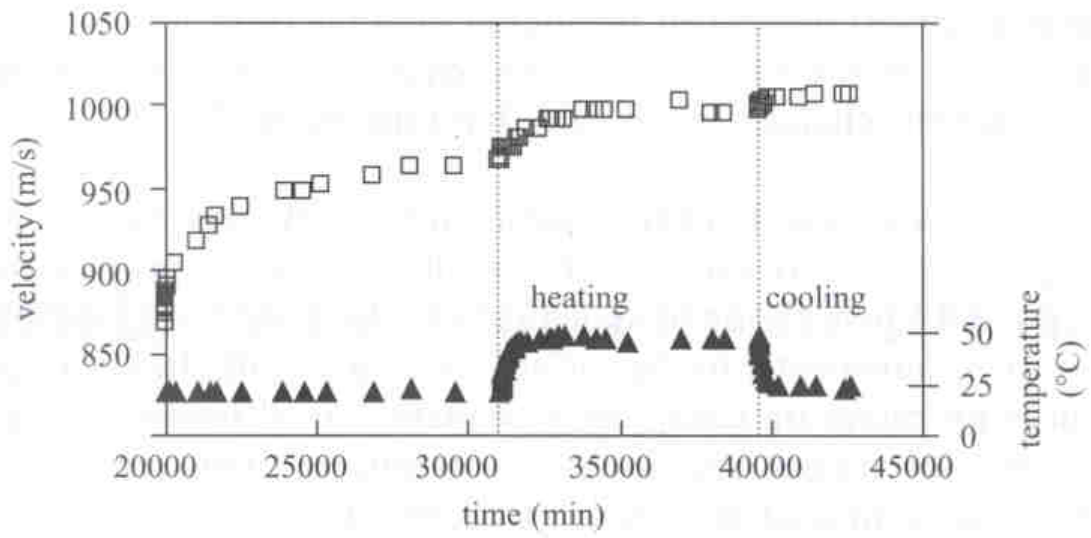


Fig. A-6. Effect of temperature on time-dependent changes in velocity for a coarse-grained granular salt specimen under a constant vertical load (Fam et al. 1998).

Table. A-3.  $G_0$  measurement techniques

Test Methods	Standard	Test Principle	References
Soil Stiffness Gauge (SSG)	ASTM D 6758	A small dynamic force generated inside the device is applied through a ring-shaped foot resting on the surface and a deflection is measured using velocity sensors. The surficial soil stiffness is then determined as the ratio of the applied force to the measured deflection.	Wu et al. (1998), Humboldt (1999, 2000a, 2000b), Fiedler et al. (1998, 2000), Nelson and Sondag (1999), Chen et al. (1999), Siekmeir et al. (1999), Hill et al. (1999), Sargand et al. (2000a), Weaver et al. (2001), Lenke et al. (2001, 2003), Sargand (2001), Peterson et al. (2002), Sawangsuriya et al. (2002, 2003, 2004)
Bender Element	None	Shear wave velocity is determined by measuring the travel time of shear wave and the tip-to-tip distance of piezoceramic bender elements. The corresponding shear modulus is calculated by knowing the shear wave velocity and mass density of soil.	Dyvik and Madshus (1985), Thomann and Hryciw (1990), Hryciw and Thomann (1993), Souto et al. (1994), Fam and Santamarina (1995), Nakagawa et al. (1996), Viggiani and Atkinson (1995b, 1997), Jovicic and Coop (1998), Zeng and Ni (1998), Fioravante and Capoferri (2001), Santamarina et al. (2001), Davich et al. (2004), Swenson et al. (2006)
Resonant Column	ASTM D 4015	Resonant frequency is measured and is related to the shear wave velocity and the corresponding shear modulus.	Wilson and Dietrich (1960), Hardin and Music (1965), Hardin (1970), Drnevich (1977), Drnevich et al. (1978), Edil and Luh (1978), Isenhower (1980), Drnevich (1985), Ray and Woods (1988), Morris (1990), Lewis (1990), Cascante

Ultrasonic Pulse	ASTM C 597	Elastic wave velocity is determined from the travel time of either compression or shear wave arrivals and the distance between ultrasonic transducers. The soil stiffness is calculated based on the elastic theory.	et al. (1998) Lawrence (1963), Nacci and Taylor (1967), Sheeran et al. (1967), Woods (1978), Nakagawa et al. (1996), Yesiller et al. (2000)
Seismic Reflection	None	Travel time of seismic waves reflected from subsurface interfaces is measured. The wave propagation velocity and soil stiffness is calculated based on the elastic theory.	Kramer (1996), Sharma (1997), Frost and Burns (2003)
Seismic Refraction	ASTM D 5777	Travel time of seismic refracted waves when they encounter a stiffer material (higher shear wave velocity) in the subsurface interface following the law of refraction (Snell's law) is measured so that the elastic wave propagation velocity and the corresponding soil stiffness are determined.	Kramer (1996), Sharma (1997), Frost and Burns (2003)
Spectral Analysis of Surface Waves (SASW)	None	Surface (Rayleigh) wave velocity varied with frequency is measured by utilizing the dispersion characteristics of surface wave and the fact that surface waves propagate to depths that are proportional to their wavelengths or frequencies in order to determine the stiffness of subsurface profiles.	Nazarian and Stokoe (1987), Sanchez-Salinerio et al. (1987), Rix and Stokoe (1989), Campanella (1994), Nazarian et al. (1994), Wright et al. (1994), Mayne et al. (2001)
Seismic Cross-Hole	ASTM D 4428	Measurement of wave propagation velocity either compressional or shear wave from one subsurface boring to other adjacent subsurface borings in a linear array. The seismic wave is	Stokoe and Woods (1972), Stokoe and Richart (1973), Anderson and Woods (1975), Hoar and Stokoe (1978), Campanella (1994), Mayne et al.

		generated by various means so that the elastic waves propagate in the horizontal direction through the soil and are detected by the geophones located in the other hole.	(2001), Frost and Burns (2003)
Seismic Down-Hole or Up-Hole	None	Compressional and/or shear waves propagating vertically in soil deposits in a single borehole are monitored. The travel time of compressional and/or shear waves from the source to receiver(s) is measured. The wave propagation velocity at any depths is obtained from a plot of travel time versus depth.	Richart (1977), Campanella (1994), Ishihara (1996), Mayne et al. (2001), Frost and Burns (2003)
Seismic Cone Penetration	None	Similar to the seismic down-hole test, except that no borehole is required. The profile of shear wave velocity is obtained in a same manner as the seismic down-hole test. The receiver is located in the cone	Campanella et al. (1986), Robertson et al. (1986), Baldi et al. (1988), Campanella (1994), Kramer (1996), Mayne (2001), Frost and Burns (2003)

## A-5 Soil Water Characteristics Curve

Behavior of unsaturated soils is highly dependent on the magnitude of soil suction (i.e., soil pore water is under tension), which in turn is influenced by soil moisture content for a given soil. Soil suction is defined as the potential difference between the soil pore water and water outside the soil pores, per volume of water and is also referred to as free energy state of soil water (Fredlund and Rahardjo 1993). Water in soil pores is held in place by the potential energy of the tensile forces created due to curved interfaces and surface adsorptive forces (matric suction) and potential differences due to solute concentrations (osmotic suction). In most engineering problems where the matric suction component largely governs the behavior of unsaturated soils (such as mechanical problems), the osmotic suction is not commonly determined and is relatively not very important. The relationship between water content and the associated matric suction (i.e., negative pressure or tension) in the pore water can be empirically described by the soil water characteristic curve (SWCC), which is defined as the water storage capacity of a soil at a given soil suction.

A typical SWCC that defines the relationship between volumetric water content and matric suction is illustrated in Fig. A-7. The graph consists of two curves: (i) a drying or desorption curve and (ii) a wetting or sorption curve. These different curves exhibit hysteresis, which can be explained by the complex nature of soil pore structure. This phenomenon is caused by size differences between the primary pores and the interconnecting pore throats, changes in the contact angle during drying and wetting, and trapped air (Hillel 1980, Fredlund and Rahardjo 1993, Tinjum et al. 1997). For standard practice, only the drying (desorption) portion of the curve is usually measured because of experimental difficulties associated with measurement of the wetting (sorption) curve (Hillel 1980). Physically, the curve indicates (at any given moisture content) how much energy (per unit quantity of water removed) is required to remove a small quantity of water from the soil. Several defining parameters of the SWCC including saturated volumetric water content ( $\theta_s$ ), air-entry suction ( $\psi_a$ ), residual volumetric water content ( $\theta_r$ ) are also presented in Fig. A-7. The matric suction corresponding to the break in the curve (near the saturated volumetric water content  $\theta_s$ ) is referred to as the air-entry suction ( $\psi_a$ ). The air-entry suction corresponds to the matric suction required to remove water from the largest pores (Brook and Corey, 1966). The water content corresponding to the asymptotical increase in suction to infinity along the SWCC as the degree of saturation approaches the residual state (i.e., approximately a constant value) is defined as the residual volumetric water content ( $\theta_r$ ). The shape of the curve is a function of soil type. Soils with smaller pores have higher  $\psi_a$ . Soils with a wider range of pore sizes exhibit greater changes in matric suction with water content and thus the slope of the SWCC becomes steeper (Hillel, 1980; Fredlund and Rahardjo, 1993).

A typical SWCC for the entire range of suction values (i.e., from 0 to 1,000,000 kPa) and water content (i.e., from fully saturated condition to completely dry condition) is illustrated in Fig. A-8 (Vanapalli et al., 1999). As discussed in Vanapalli et al. (1999),

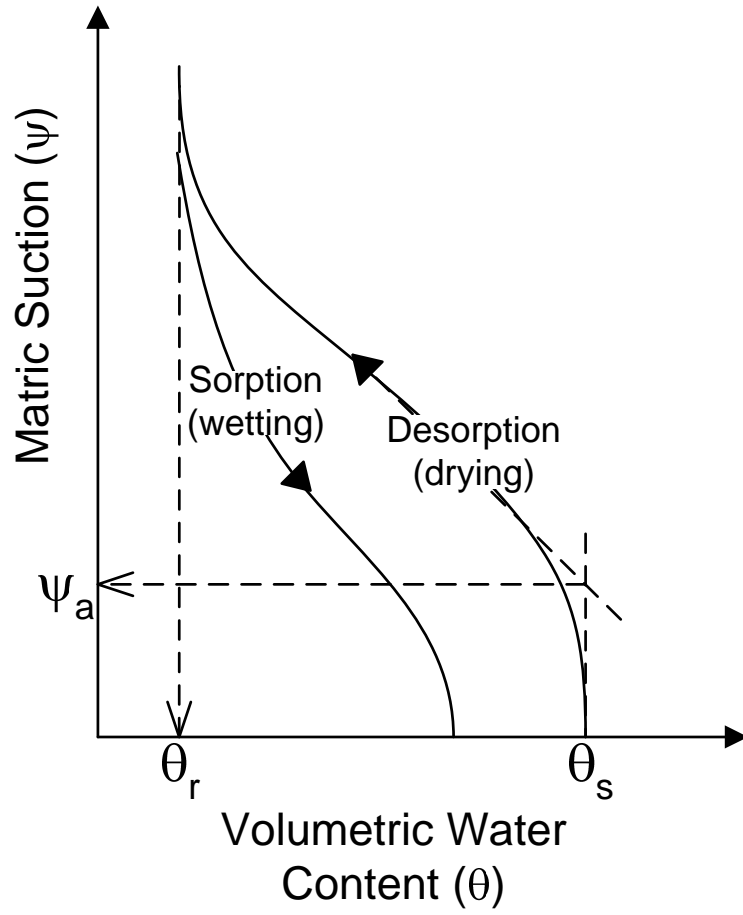


Figure A-7. Typical soil water characteristic curve for desorption and sorption.

this maximum suction value of 1,000,000 kPa is a common value of suction at which all soils approach zero water content (Croney et al., 1958; Russam, 1958; Fredlund, 1964; Vanapalli, 1994) and also supported by thermodynamic principles (Richards, 1965). The SWCC over the entire suction range has two key features: (i) the air-entry suction value and (ii) the residual state of unsaturation. Vanapalli (1994) described three identifiable stages of desaturation (Fig. A-8): the boundary effect stage, the transition stage (i.e., primary and secondary), and the residual stage of unsaturation. In the boundary effect stage, almost all of the soil pores are filled with water. The soil desaturates at the air-entry suction value in the transition stage. In this stage, the flow of water is in the liquid phase as the applied suction increases and the soil dries rapidly with increasing suction. The connectivity of the water in the voids or pores continues to reduce with increased values of suction, and eventually large increases in suction lead to relatively small changes in the degree of saturation. The residual state of saturation is considered to be the degree of saturation at which the liquid phase becomes discontinuous. Consequently, the residual state of saturation represents the degree of saturation value beyond which it becomes increasingly difficult to remove water from a specimen by drainage. The point at which residual state of saturation is reached is not always clearly defined.

Fig. A-9 illustrates the typical SWCCs for four Canadian soils (Vanapalli et al., 1999). A coarse-grained soil such as a gravel or sand has large interconnected pores and shows a tendency to change in degree of saturation at a fast rate as values of suction increase. The rate of drying decreases with an increase of fines. The water storage capacity of a soil that corresponds to a particular value of suction is higher for a soil with a higher percentage of fines. The air-entry value is also higher for soils which have more fines. Similarly, the residual state of saturation also increases with the increase in fines.

Two most common models used to fit to the experimental data and to describe the SWCC are the Brooks-Corey model (Brooks and Corey 1966) and the van Genuchten model (van Genuchten 1980). The Brooks-Corey model is:

$$\Theta = \left( \frac{\Psi_a}{\Psi} \right)^\lambda \quad (\text{A-12})$$

where  $\Theta$  = effective saturation or normalized volumetric water content =  $(\theta - \theta_r)/(\theta_s - \theta_r)$ ; and  $\Psi_a$  and  $\lambda$  = curve-fitting parameters. The parameter  $\lambda$  is also called the pore size distribution index, which is a function of the distribution of pores in the soil. If  $\theta_r = 0$ , then  $\Theta$  = degree of saturation (S). The van Genuchten model is:

$$\Theta = \left[ \frac{1}{1 + (\alpha\Psi)^n} \right]^m \quad (\text{A-13})$$

where  $\alpha$ ,  $n$ , and  $m$  = curve-fitting parameters. The stability of the curve-fitting process is improved by equating the parameter  $m$  to  $1-1/n$  (van Genuchten et al. 1991). The parameters in Eq. (A-12) and (A-13) describe the shape of the SWCC. The parameters  $\Psi_a$  and  $\alpha$  are related to the value of air-entry suction. Higher air-entry suction (i.e., soils with smaller pores) is characterized by greater  $\Psi_a$  in Eq. (A-12) or smaller  $\alpha$  in Eq. (A-

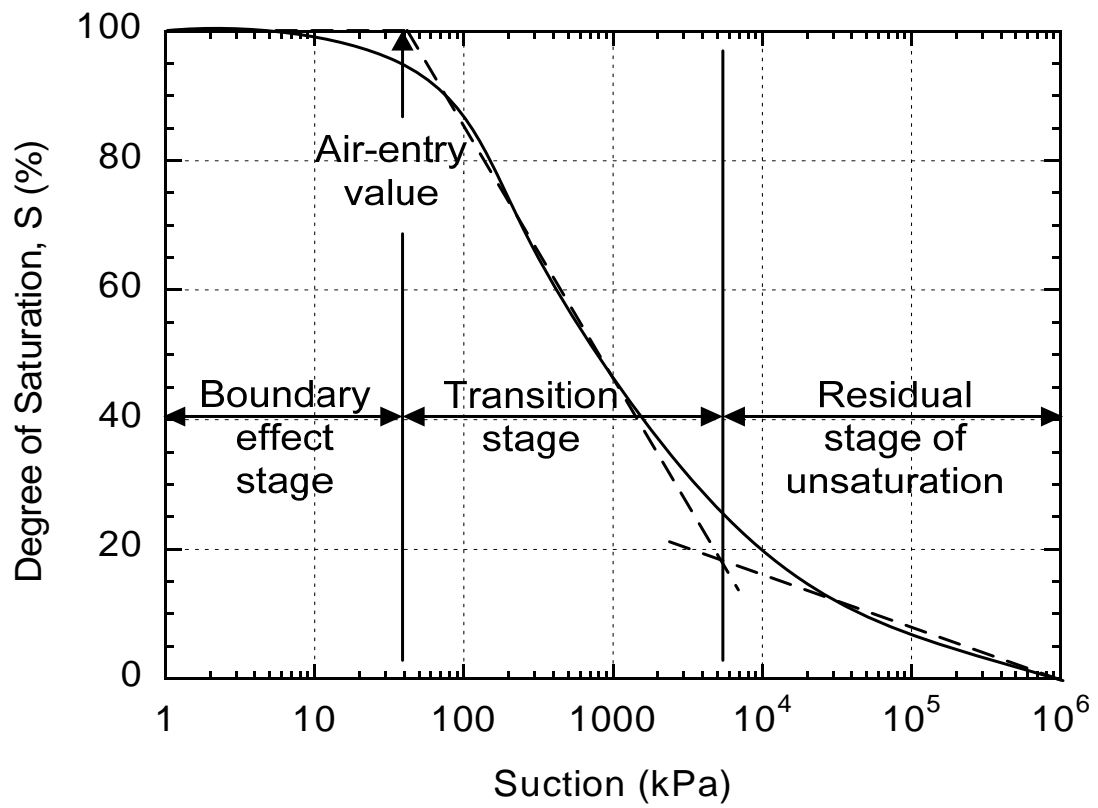


Fig. A-8. Three identifiable stages of a typical SWCC for the entire range of suction values (Vanapalli et al. 1999).

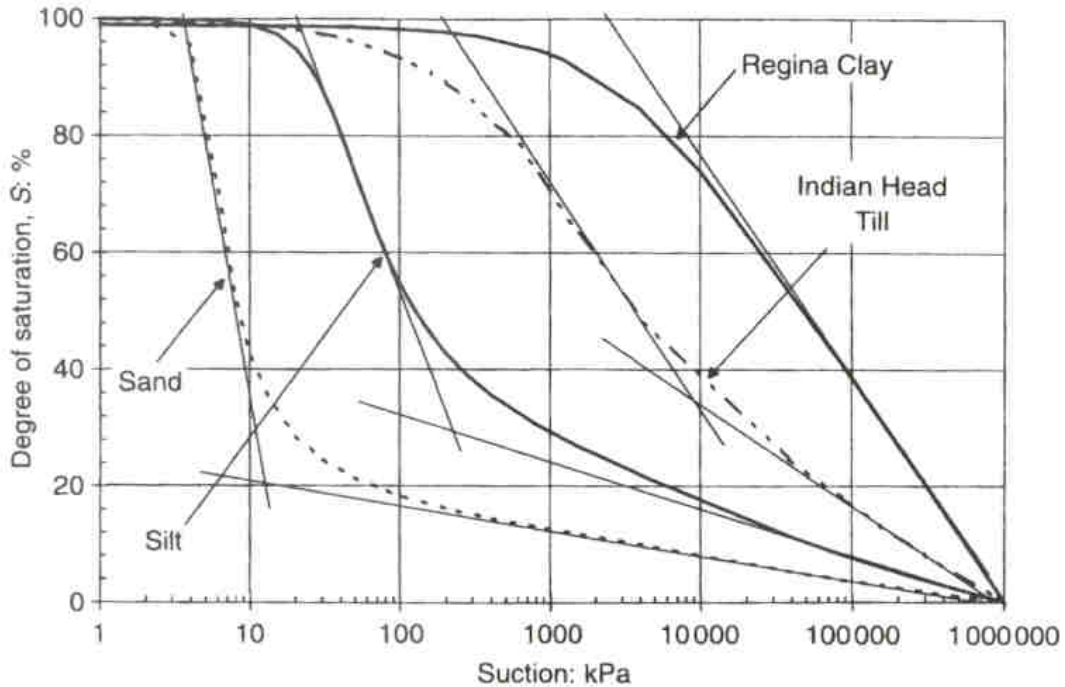


Fig. A-9. Typical SWCCs for four Canadian soils (Vanapalli et al. 1999).

13). Soils with a steeper SWCC (i.e., wider range of pore sizes) are characterized by smaller  $\lambda$  or  $n$ . In other words,  $\psi_a$  and  $\alpha$  are inversely related, whereas  $\lambda$  and  $n$  are directly related. Soils with smaller pore size typically have greater  $\psi_a$  or smaller  $\alpha$ , and soils with a broader range of pore sizes have smaller  $\lambda$  or  $n$  (Corey 1994). Factors affecting the SWCCs have been reported by various investigators as summarized in Table A-4.

In summary, the distinguishing features of the SWCC depend on several factors such as soil structure (and aggregation), compaction conditions (i.e., compaction water content, compactive effort, and method of compaction), dry unit weight (or void ratio), soil type (i.e., mineralogy and texture), and stress history (or stress state). The four most important factors: soil type, compactive effort, compaction water content, and stress history, have the most influence on the nature of the SWCC for fine-grained soils. Specimens of a particular soil, in spite of having the same texture and mineralogy, can exhibit different SWCCs if they are prepared at different compaction conditions and possess different stress histories.

Table A-4. Influencing factors on the SWCC

Investigator	Influencing factors	Significance Findings
Olson and Langfelder (1965)	Type of compaction (static and kneading) and initial dry unit weight	<ol style="list-style-type: none"> <li>1) Influence of initial dry unit weight on the compaction water content and suction relationship is negligible.</li> <li>2) Kneading compaction produces different compaction water content and suction relationship from the static compaction.</li> </ol>
Vanapalli et al (1996)	Shear strength and compaction water content	<ol style="list-style-type: none"> <li>1) Shear strength of the unsaturated soil and the SWCC depend on the soil structure, which in turn depend on the compaction water content and the method of compaction.</li> <li>2) Specimens compacted wet of optimum water content develop higher shear strength and start to desaturate at higher suctions when compared to specimens compacted at optimum or dry of optimum.</li> </ol>
Tinjum et al. (1997)	Compaction water content, compactive efforts (standard and modified Proctor), and soil types	<ol style="list-style-type: none"> <li>1) Clays with higher plasticity index, clays compacted wet of optimum water content, or clays compacted at greater compactive effort results in higher air-entry suction.</li> <li>2) SWCCs depend on compaction conditions and soil types.</li> <li>3) Influence of compaction water content on the SWCC is more significant than that of compactive effort.</li> <li>4) Shape of the SWCC is independent of dry unit weight.</li> </ol>
Vanapalli et al. (1999)	Compaction water content, soil structure, and stress history	<ol style="list-style-type: none"> <li>1) Compaction water content has a considerable influence on soil structure and thus the SWCC.</li> <li>2) SWCC depends mainly on soil structure and stress history, rather than void ratio.</li> <li>3) Air-entry value and residual state of saturation increase with increasing stress history for specimens compacted dry of optimum.</li> <li>4) Specimens wet of optimum have higher air-entry values and higher values of residual state of saturation than those compacted at optimum or dry of optimum.</li> <li>5) SWCCs are significantly influenced by the stress history for specimens compacted dry of optimum; however, SWCCs of specimens compacted wet of optimum are not significantly</li> </ol>

NG and Pang (2000)	Stress state	<p>influenced by the stress history.</p> <p>6) SWCCs of specimens compacted at optimum lies in between those of specimens compacted dry and wet of optimum water content.</p> <p>7) In high suction ranges, the soil structure and stress history have insignificant effect on the SWCC.</p> <p>1) At zero suction, specimens loaded to a higher net normal stress exhibit a lower initial volumetric water content.</p> <p>2) Volumetric water content decreases with increasing matric suction for all specimens but at different rates.</p> <p>3) Applied load increases with decreasing rate of reduction in volumetric water content.</p> <p>4) Specimen subjected to higher stress has larger air-entry value due to the presence of a smaller average pore size distribution under the higher applied load.</p> <p>5) Upon wetting, the volumetric water content for specimen subjected to smaller stress increases more rapidly than that from specimen subjected to higher stress.</p> <p>6) Size of hysteresis loops tends to be independent of the applied stress.</p>
Marinho and Stuermer (2000)	Compactive effort and compaction water content	<p>1) At a particular compactive effort, the compaction water content affects the SWCC.</p> <p>2) SWCC of specimen compacted at optimum or dry of optimum always lie below that of specimen compacted wet of optimum.</p> <p>3) Air-entry value is not greatly affected by the compaction water content.</p> <p>4) Compactive effort affects the air-entry value.</p>
Graham et al. (2001)	Compaction water content and drying process	<p>1) Compaction water content and suction plot shows significantly lower suction than the SWCC for specimens at the same water prepared by drying following compaction.</p> <p>2) Microstructure of the specimens was affected by the compaction water content.</p> <p>3) Curve from specimens in which suction was measured by varying the compaction water contents does not form a SWCC such that each compaction water content generates a unique structure which in turn has its own SWCC.</p> <p>4) Specimens compacted at varying water contents do not belong to a single SWCC but are</p>

Miller et al. (2002)	Soil type, compactive effort, and compaction water content	<p>points on a series of separate SWCCs that are unique for each compaction water content.</p> <p>5) SWCC is not a unique relationship for a specific material but is intimately related to the microstructure, which is related to the compaction water content.</p> <p>1) SWCCs are more sensitive to the changes in compactive effort than changes in compaction water content.</p> <p>2) At similar water contents, the suction increases with increasing compactive effort for each compaction condition and soil type.</p> <p>3) For all compaction conditions, the lowest plasticity soils retain the smallest water content and the highest plasticity soils retain the highest water content at a specified suction.</p>
-------------------------	---	---

### A-6 Climate and Soil-Suction Relationship

The magnitude of suction underneath the ground, which is significantly influenced by the amount of water in the soil, is mainly associated with climatic factors (Coleman 1965, Russam and Coleman 1961, De Bruijn 1965). These climatic factors can be given in terms of a climatically controlled Thornthwaite climatic (moisture) index ( $I_m$  or TMI), which is an index that indicates the relative aridity or humidity of a soil-climate system of a given site (Thornthwaite 1948). A dimensionless value of  $I_m$  indicates the amount of net water surplus or the relative soil-water balance between water entering the soil as precipitation and evapotranspiration of water from the ground surface and is used to characterize the cyclic nature of climatic wetting and drying of soils on an annual basis, which represents characteristic of a site's climatic influences over a distinct period. The method basically compares potential precipitation and evapotranspiration on an annual basis, and then averages the  $I_m$  values to obtain an average  $I_m$  for a period of time, which can be subsequently used as a climatic rating for a given site. The value of  $I_m$  for a year (y) is calculated by:

$$I_m = \frac{100(R_y) - 60(DF_y)}{(PE_y)} \quad (A-14)$$

where  $R_y$  is runoff in cm of water for year (y),  $DF$  is deficit in cm of water for year (y), and  $PE_y$  is potential evapotranspiration in cm of water for year (y). A detailed procedure for calculating  $I_m$  for a given site is given by McKeen and Johnson (1990). Note that positive values of  $I_m$  indicate humid (wet) climates, whereas negative values represents sub-humid to arid (dry) climates. In addition to Eq. (A-14), the average  $I_m$  values for a given site can be also estimated from the  $I_m$  contour map. Fig. A-10 illustrates contours of the average  $I_m$  value for the U.S.

The equilibrium water contents in subgrades do not typically reach saturation. Under given environmental and climatic conditions, water contents in subgrades reach equilibrium values (Russam 1965). An estimated equilibrium (constant) soil suction value, commonly used in the climatic design of the pavement and foundation systems (PTI 1996), is used to represent the suction in subgrades. This equilibrium soil suction value is the soil suction below the depth of climatic moisture variation (i.e., active zone depth) (Mitchell 1979) and is also correlated to average  $I_m$  value. Many investigators have studied a climate factor in term of  $I_m$  and equilibrium soil suction value relationship.

Russam and Coleman (1961) and PTI (1996) provided a correlation between the average value of  $I_m$  and the equilibrium soil suction value, which was measured at depths away from the influence of climatic moisture variation (i.e., the water table is below 7.5 m) for different soil types. Fig. A-11 shows the variation of soil suction with the average  $I_m$  value for different soil types. Using Fig. A-11, the soil suction expected to develop beneath a pavement can be estimated in any specified climate. Note that the soil suction units in Fig. A-11 are pF (logarithm to the base 10 of the suction in centimeters of water).

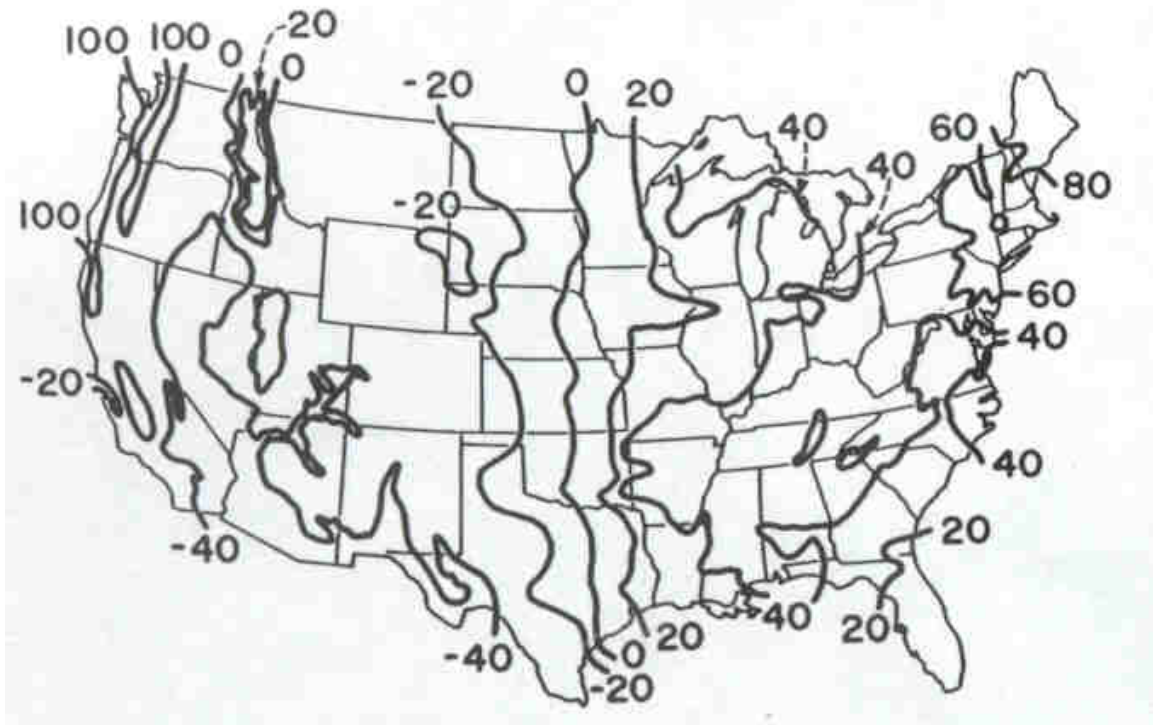


Fig. A-10. Average Thornthwaite climatic index ( $I_m$ ) distribution in the U.S. (Thornthwaite 1948)

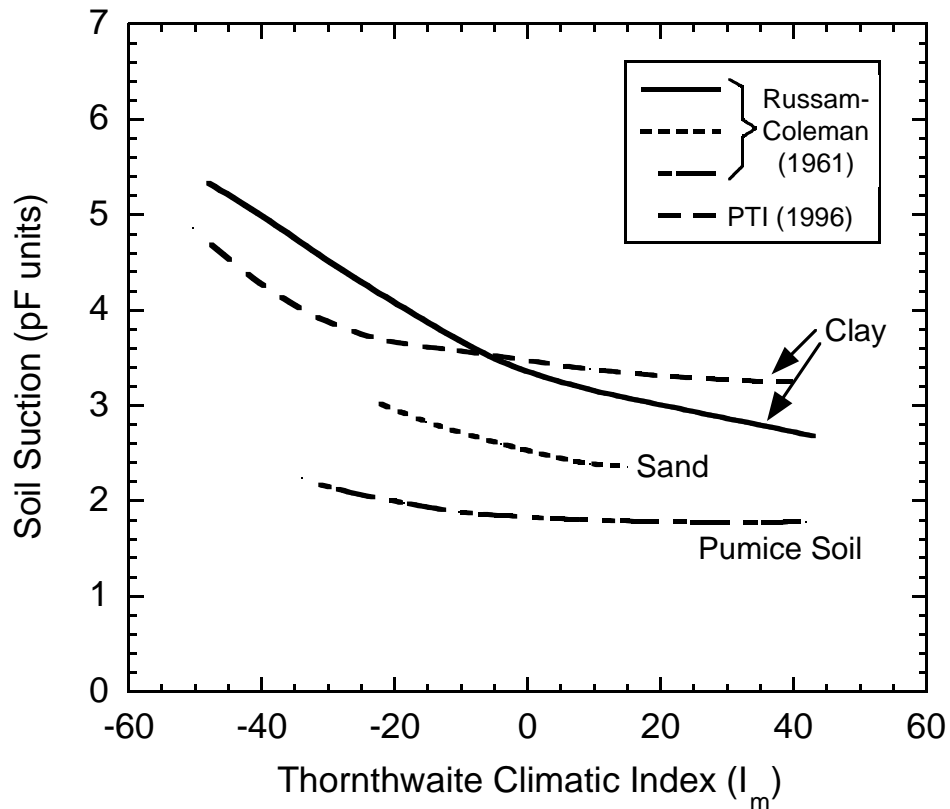


Fig. A-11. Variation of equilibrium soil suction with average  $I_m$ .

Brayant (1998) studied the variation of soil suction with depth in Dallas and Fort Worth, Texas from 1995 to 1997. Brayant indicated that the range of total soil suction values was the greatest at the surface and decreased with depth. Moreover, the average measured total soil suction values are substantially higher than those predicted by Russam-Coleman and PTI. Lytton (1997) found discrepancies between the Russam-Coleman relation and the measured suction value in the field. Lytton recommended the use of the soil water characteristic curve (SWCC) on any given site to determine the equilibrium soil suction on a more fundamental basis and to provide an equilibrium soil suction value routinely.

Reed and Kelly (2000) indicated that the addition of irrigation increases the average calculated  $I_m$  value. PTI design parameters used for the PTI analysis based on average  $I_m$  values can be significantly different from values calculated using a site-specific  $I_m$ , where  $I_m$  is calculated by including the influence of irrigation. Stanculescu and Fodor (1975) compared the equilibrium soil suction value determined by the average value of  $I_m$  based on the Russam-Coleman relation and that determined by phreatic level during the time of investigations. They indicated that by taking the equilibrium conditions into consideration, the equilibrium soil suction values obtained from both approaches do not essentially change the presumptive value of the subgrade water content. However, the

equilibrium condition established cannot be extended over the whole width of the pavement.

Perera et al. (2004) investigated a number of climatic parameters including data from the National Climatic Data Center, the NCHRP 2002 Design Guide database, the Long-Term Pavement Performance (LTPP) database, the United States Geological Survey (USGS) database, the depth of groundwater table (GWT), the average  $I_m$  values, and the soil index properties for correlation with the equilibrium soil suction value beneath highway pavements from the 18 sites located throughout the U.S. Knowing the in situ degree of saturation, the soil suction underneath the pavement systems is obtained by laboratory SWCC. They found that the equilibrium soil suction value is best-correlated with the average  $I_m$  value obtained from the  $I_m$  contour map (Fig. A-10) and soil index properties, i.e., percent passing No. 200 ( $P_{200}$ ) and plasticity index (PI). Additionally, they proposed two prediction models to estimate the equilibrium soil suction values beneath pavements located in arid and semi-arid zones when the GWT is more than 0.9 m from the ground surface. The first model is named the  $I_m$ - $P_{200}$  model for granular base materials:

$$\psi = \alpha + e^{[\beta + \gamma(I_m + 10^1)]} \quad (\text{A-15})$$

where  $\psi$  is soil suction,  $\alpha$ ,  $\beta$ , and  $\gamma$  are fitting constants. Table A-5 provides the values of these constants corresponding to  $P_{200} = 4, 6, 8, 10,$  and  $12$ . The second model is named the  $I_m$ - $P_{200}$ /wPI model for subbase and subgrade materials:

$$\psi = \alpha \left\{ e^{[\beta / (I_m + 10^1) + \gamma]} + \delta \right\} \quad (\text{A-16})$$

where  $\psi$  is soil suction,  $\alpha$ ,  $\beta$ ,  $\gamma$ , and  $\delta$  are fitting constants. The values of these four constants are given along with  $P_{200} = 10, P_{200} = 50/\text{wPI} = 0.5$  or less,  $\text{wPI} = 5, 10, 20,$  and  $50$  as shown in Table A-6. Note that wPI is the weighted PI and is obtained as the product of  $P_{200}$  in decimal and PI in percentage.

### **A-7 Stiffness Behavior of Unsaturated Soils**

Unsaturated soil mechanics addresses the more general condition in which soils comprise a matrix of solids, water, and air. Due to the existence of air and water together in the pore space, factors that do not exist in two-phase systems, such as the surface tension of water at air-water interfaces, affect the soil behavior. Although stresses can still be partitioned into effective stress and pore pressure components, these components no longer act over equal areas. In unsaturated soils, the area over which the pore water pressure (or tension) acts is a fraction of the total cross-sectional area and is not easily quantifiable. Two stress state variables: matric suction ( $u_a - u_w$ ) and net normal stress ( $\square - u_a$ ), which are related to the geometry of the pore water, are often employed to characterize unsaturated soil behavior (Fredlund and Rahardjo 1993).

Interests in examining the influence of moisture changes on the mechanical behavior of unsaturated soils have increased since soil suction, which is a stress state variable that governs the mechanical behavior of unsaturated soils, varies with moisture. Suction can

vary significantly from one soil to another. For a given soil, suction varies with changes in moisture content as described by the SWCC. Since the soil moisture is sensitive to a rise in the water table, infiltration of water, or evaporation of water, the effects of moisture content and matric suction along with other influencing factors on the mechanical behaviors of unsaturated soils must be well-established. The behavior of unsaturated soil stiffness can be described with respect to two soil groups: fine-grained soils and coarse-grained soils.

**Fine-Grained Soils:** A number of previous studies were conducted to evaluate changes in moisture content and soil suction with respect to the stiffness of fine-grained soils. Table A-7 presents the summary of previous studies reported by different investigators.

**Coarse-Grained Soils:** Significant differences in behavior between unsaturated and saturated coarse-grained soils can be described by the effect of capillarity in unsaturated soils. Capillary action induces the development of tension (or suction) in the pore water. The capillary menisci (negative pressures) developed in the pore spaces influence intergranular stress development by producing additional effective stress acting on the soil particle and structure, which in turn increase the soil stiffness. Changes in the water content of natural deposit or compacted coarse-grained soil in response to wetting, drying, and inundation can alter the capillary contribution to intergranular stresses, and therefore the soil stiffness (Wu et al. 1984). Previous studies reported the factors affecting the stiffness behavior of unsaturated coarse-grained soils and are listed in Table A-8.

Table A-5. Regression constants for  $I_m$ - $P_{200}$  model (Perera et al. 2004)

$P_{200}$	$\alpha$	$\beta$	$\gamma$
4	5.285	3.473	-0.04004
6	6.877	4.402	-0.03726
8	8.621	5.379	-0.03836
10	12.180	6.646	-0.04688
12	15.590	7.581	-0.04904

Table A-6. Regression constants for  $I_m$ - $P_{200}$ /wPI model (Perera et al. 2004)

$P_{200}$ or wPI	$\alpha$	$\beta$	$\gamma$	$\delta$
$P_{200} = 10$	0.300	419.07	133.45	15.00
$P_{200} = 50$ / wPI = 0.5 or less	0.300	543.48	144.22	14.36
wPI = 5	0.0113	1461.60	193.97	870.94
wPI = 10	0.010	1759.00	206.00	1290
wPI = 20	0.010	2003.00	210.28	2210
wPI = 50	0.300	1060.80	148.80	72.00

Table A-7. Stiffness behavior of unsaturated fine-grained soils

Investigator(s)	Test Variables	Summary of the Findings
Sauer and Monismith (1968)	Soil suction, resilient modulus, and residual deformation	<ol style="list-style-type: none"> <li>1) Soil suction has significant effect on resilient modulus and residual deformation.</li> <li>2) Pavement deflection decreases with increasing soil suction and higher soil suction produces higher resilient modulus.</li> </ol>
Shackel (1973)	Repetitive load and soil suction	<ol style="list-style-type: none"> <li>1) Soil suction decreases with increasing the number of stress cycles.</li> <li>2) Specimens with a higher degree of saturation exhibit more reduction in soil suction.</li> <li>3) Effect of stress history on soil suction is important.</li> </ol>
Fredlund et al. (1977)	State of stress variables (deviator stress, net confining pressure, and matric suction), compaction water content, and resilient modulus	<ol style="list-style-type: none"> <li>1) Good correlation between the resilient modulus and the state of stress variables.</li> <li>2) Among the state of stress variables, deviator stress and matric suction have the most significant effect on the resilient modulus.</li> <li>3) Relationship between resilient modulus and compaction water content is not as clear as the relationship between resilient modulus and matric suction.</li> </ol>
Edil and Motan (1979), Edil et al. (1981), Motan and Edil (1982)	Compaction moisture content, degree of saturation, total and matric suction, and resilient modulus	<ol style="list-style-type: none"> <li>1) Resilient modulus increases with increasing degree of saturation from 65% to 75%, beyond which a decrease is noticed.</li> <li>2) Resilient modulus increases with soil suction up to approximately 800 kPa, beyond</li> </ol>

		<p>which a decrease is observed.</p> <p>3) Soil suction is the fundamental parameter in characterizing moisture state and also reflects the effects of soil type, soil structure, compaction, climatic variation, and fluctuation of groundwater table on mechanical behavior of soils better than compaction water content or degree of saturation alone.</p> <p>1) Resilient modulus decreases with increasing compaction water content.</p> <p>2) Resilient modulus of specimens compacted dry of optimum are greater than that of specimens compacted at optimum and the resilient modulus of specimens compacted wet of optimum are lower than that of specimens compacted at optimum.</p> <p>3) Resilient modulus of fully saturated soil specimen is approximately 50% lower than that measured at optimum water content for each deviator stress; however, for cohesive soils containing slightly granular soils, their resilient moduli at saturation are only 10 to 30% lower than the resilient moduli at optimum.</p>
Li and Selig (1994), Tian et al. (1998), Muhanna et al. (1999), Butalia et al. (2003), Li and Qubain (2003)	Compaction water content and resilient modulus	
Marinho et al. (1996)	Degree of saturation and small-strain modulus using bender elements	Stiffness peaks at degree of saturation between 75% and 85%, which is less than the degree of saturation for the line of optimums.
Mancuso et al. (2002)	Net confining stress, matric suction, compaction water content, and small-strain shear modulus ( $G_o$ ) using a resonant column test	<p>1) <math>G_o</math> measured at a constant net confining stress show an S-shaped increase with suction for both optimum and wet of optimum compacted soils.</p> <p>2) Stiffness response complies with the typical S-shape of the SWCC.</p> <p>3) Relationship between <math>G_o</math> and matric suction is explained by three zones. <u>Zone 1</u> starts in saturated conditions (low suction). In this zone, bulk water effects govern the soil behavior because the amount of air present in the soil is negligible and the variations in matric suction are equivalent to changes in mean effective stress. <u>Zone 2</u> starts where a progressive shift of stiffness response occurs from bulk water dominated behavior to menisci water dominated</p>

Khoury et al. (2003)	Total suction, matric suction, osmotic suction, compaction water content, and resilient modulus	<p>behavior. In this zone, the amount of air present in the pore space becomes more significant as suction increases. <u>Zone 3</u>, the suction is high so that the menisci water dominates the soil response and the <math>G_o</math> increases with suction.</p> <p>4) Compaction water content has significant effect on soil response. The wet compaction induces a weaker soil fabric with respect to optimum compaction</p> <p>1) Resilient modulus increases as total and matric suctions increase.</p> <p>2) Variation of resilient modulus with total and matric suctions reveals the same trends and the osmotic suction has less significant effect on resilient modulus.</p> <p>3) No specific trend between resilient modulus and compaction water content, since different compaction water contents may produce same matric suction depending on the SWCC, and thus same state of stress that governs resilient modulus.</p> <p>4) Resilient modulus correlates better with soil suction than with compaction water content.</p>
Yuan and Nazarian (2003)	Compaction water content and small-strain modulus using a free-free resonant column test	<p>1) Modulus-compaction water content relationship exhibits two patterns: for compaction water contents greater than the value at which the maximum modulus occurs, the modulus decreases with an increase in compaction water content. A sharp drop in modulus due to cracking of the specimen for compaction water contents less than that of maximum modulus is observed.</p> <p>2) Maximum modulus occurs at a compaction water content lower than the optimum compaction water content.</p> <p>3) Difference between the optimum compaction water content and the compaction water content at which the maximum modulus occurs depends on the fine content of soil.</p>
Ooi and Pu (2003)	Compaction water content, degree of saturation, and small-strain stiffness using	<p>1) SSG stiffness peaks dry of optimum and decreases upon wetting.</p> <p>2) All SSG stiffness values peak within a range of degree of saturation from 66% to</p>

Costa et al. (2003)	the Soil Stiffness Gauge (SSG) Matric suction, settlement, stiffness, and bearing capacity from a plate load test	89%, which is less than the degree of saturation for the line of optimums. 1) Settlement increases considerably as suction decreases for a given stress level, that is, increasing suction lead to a substantial increase in soil stiffness. 2) Small increases in matric suction lead to substantial increases in bearing capacity of the soil-plate system. 3) Rate of settlement shows a non-linear decreasing trend with increasing matric suction.
Inci et al. (2003)	Soil type, compaction conditions, degree of saturation, and small-strain shear modulus ( $G_o$ ) using the ultrasonic method	1) $G_o$ increases as soil plasticity decreases. 2) $G_o$ increases significantly at the early stages of drying and gradually increases as drying progressed. 3) Variations in $G_o$ are high for soils compacted with low compaction energy and high compaction water content.
Khoury and Zaman (2004)	Moisture, drying and wetting cycles, soil suction, and resilient modulus	1) Resilient modulus-moisture relationship exhibits a hysteretic behavior due to drying and wetting. 2) Clayey soil is more susceptible to moisture variation than the sandy soil. 3) Changes in resilient moduli and suction are influenced by compaction water content.
Sawangsurriya et al. (2005)	Soil water characteristic, and small-strain shear modulus ( $G_o$ ) using the bender elements	1) $G_o$ increases with increasing matric suction but decreasing moisture content. 2) $G_o$ of soil compacted at optimum is greater than $G_o$ compacted wet of optimum for a given matric suction or moisture content.

Table A-8. Stiffness behavior of unsaturated coarse-grained soils

Investigators	Influencing Factors	Summary of the Findings
Lane and Washburn (1946), Lambe and Whitman (1969)	Effective grain diameter ( $D_{10}$ )	Equilibrium height of capillary rise (representing maximum pore water tension or capillary action) in a soil depends mainly on $D_{10}$ .
Wu et al (1984)	Degree of saturation, confining pressure, effective grain diameter ( $D_{10}$ )	<ol style="list-style-type: none"> <li>1) Soils with the smallest <math>D_{10}</math> and the lowest confining pressure have the greatest maximum increase in shear moduli (<math>G</math>).</li> <li>2) <math>D_{10}</math> correlates well with the ratio of maximum <math>G</math> in a moist condition to <math>G</math> in a completely dry condition and the degree of saturation corresponding to the maximum <math>G</math>.</li> <li>3) Maximum capillary influence occurs at a degree of saturation between 5% and 20%.</li> <li>4) Capillary effects are absent for dry and completely saturated specimens.</li> </ol>
Qian et al. (1993)	Degree of saturation, void ratio, confining pressure, grain shape, and grain size distribution	<ol style="list-style-type: none"> <li>1) Capillary action significantly increase shear modulus.</li> <li>2) Soil granulometry is an important factor affecting shear modulus of unsaturated sands.</li> <li>3) Effects of capillary are absent for dry and saturated sands.</li> <li>4) Capillary effects are more pronounced for soils with low void ratios and low confining pressures.</li> <li>5) A linear relationship exists between the ratio of maximum <math>G</math> in a moist condition to <math>G</math> in a completely dry condition and void ratio and its slope depends on the grain shape.</li> <li>6) Degree of saturation corresponding to the maximum <math>G</math> increases with increasing void ratio.</li> <li>7) Grain size significantly affects the ratio of maximum <math>G</math> in a moist condition to <math>G</math> in a completely dry condition of unsaturated sand.</li> </ol>

## A-8 Physics of Unsaturated Particulate Materials

In unsaturated soils, the negative pore-water pressure in menisci (i.e., capillary or suction) at particle contacts adds local particulate contact (interparticle) forces to the particulate skeleton and hence increases the stiffness of contacts and the particulate skeleton. As water evaporates from saturated soils upon gradual drying, the air-water interface starts to curve due to the pressure difference between the air pressure ( $u_a$ ) and the water pressure ( $u_w$ ). A pressure difference ( $\Delta u$ ), also referred to as matric suction, is related to the curvature of the interface characterized by radii  $r_1$  and  $r_2$ , and the surface tension ( $T_s$ ) according to Laplace's equation:

$$\Delta u = u_a - u_w = T_s \left( \frac{1}{r_1} + \frac{1}{r_2} \right) \quad (\text{A-17})$$

To clarify the physics of unsaturated particulate media, two spherical particles of radius  $R$  in contact (Fig. A-12) are considered. The water meniscus between them is bound by the two particles and by an imaginary torus. The small radius of this doughnut-shaped torus is  $r_1$  and the distance from the center to the inside wall of the torus is  $r_2$ . Therefore, the local contact force ( $F$ ), which the meniscus imposes on the particles, contributing by the pressure of the fluid acting on the cross-sectional area of the meniscus and the surface tension acting along the perimeter of the meniscus can be expressed as (Cho and Santamarina 2001):

$$F = \Delta u (\pi r_2^2) + T_s (2\pi r_2) \quad (\text{A-18})$$

To understand the behavior of stiffness increased due to matric suction and how a water-air meniscus affects the stress state of the unsaturated particulate media, a simple model by Fisher (1926) is shown in Fig. A-13(a). The meniscus water at the spherical particle contact induces a force ( $F$ ) normal to the plane passing through the contact point and orthogonal to the line connecting the particles centers. This force is the only one arising from menisci water and increases as suction increases. Therefore, the effects of matric suction ( $u_a - u_w$ ) result in a greater normal force holding the particles together and greater limiting slippage strength. As the results, the unsaturated particulate media show a stiffer and more resistant to load response (i.e., higher shear strength) with respect to that of dry contacts or fully saturated particles. Depending on the size of the particulate media and thus their corresponding pore size, the stiffness and strength of unsaturated particulate media increase with increasing matric suction. However, this effect does not increase infinitely since the contact force ( $F$ ) tends towards a limiting value due to the progressive reduction in the meniscus radius as suction increases as shown in Fig. A-13(b)

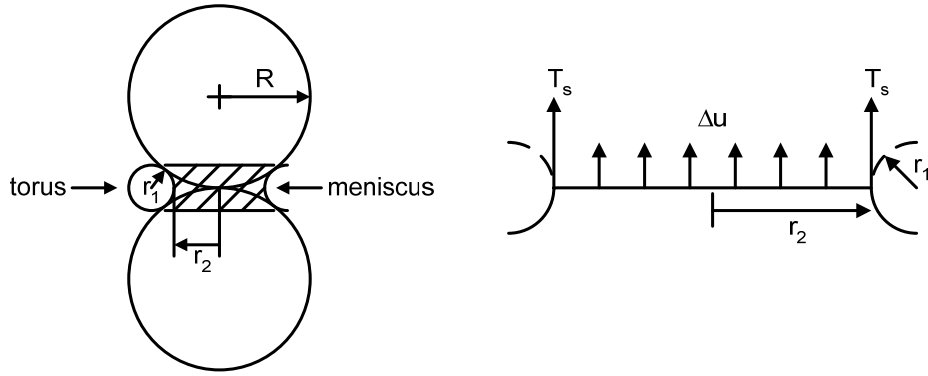


Fig. A-12. Microscale models—schematic of unsaturated spherical particles (Cho and Santamarina 2001).

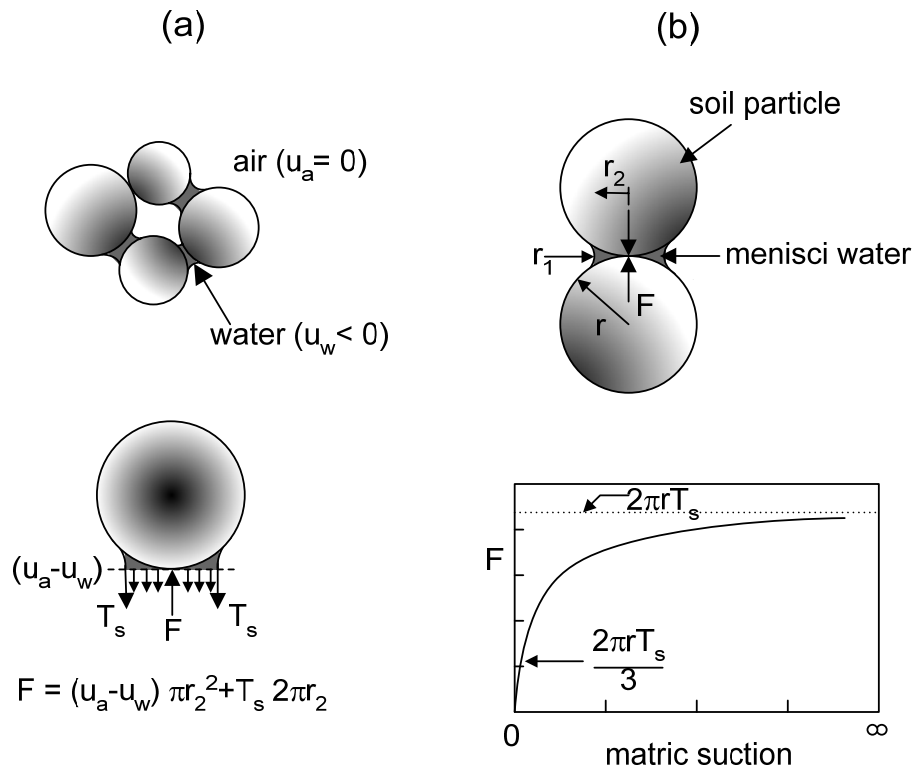


Fig. A-13. Water-air menisci between two solid sphere: (a) effect of suction on the normal force ( $F$ ) between the spheres and (b) induced  $F$  versus suction (Mancuso et al. 2002).

Mancuso et al. (2002) described the behavior of unsaturated particulate media on the basis of the role of menisci water and bulk water as illustrated by a simplified model in Fig. A-14. In the case of bulk water (Fig. A-14), the principles of saturated soil mechanics govern the soil behavior. Changes in suction correspond to pore-water pressure reductions. This can be represented by a contact force ( $F$ ) between the particles, which varies linearly with variations in matric suction ( $u_a - u_w$ ). This linear behavior continues until the air-entry value is reached. The particulate behavior moving from a saturated to an unsaturated condition can be described by the increase of  $F$  along the bulk water curve (Fig. A-14):

$$F = (u_a - u_w)\pi r^2 \quad (\text{A-19})$$

where  $r$  is the radius of the spherical particle. Beyond the air-entry value, the particulate behavior tends toward the menisci water curve defined in Fig. A-14, which illustrates the way in which a real soil moves from bulk water dominated behavior to menisci water dominated behavior.

Cho and Santamarina (2001) evaluate stiffness of particulate medium or soil skeleton by the shear wave velocity and the mass density of the soil mass which is related to the degree of saturation as shown in Fig. A-15. At constant confinement, the stiffness of the soil skeleton increases with decreasing degree of saturation due to contact-level capillary forces (or suction) and reaches a peak at dry conditions due to salt precipitation and clay buttress formation at contacts. Fig. A-16 shows different stages of unsaturated conditions, which can apply to most natural soils subjected to drying (Cho and Santamarina 2001). As water begins drying or draining from a saturated soil, the outside menisci at boundaries pull inward and the suction pressure according to Laplace's equation. While the change in water content is very small at the early stage of drying, the change in pore water pressure has an important global effect on the soil mass, which remains saturated away from the boundary. The pressure when the air phase breaks into the pore structure is called the air-entry value. The air-entry value depends on the pore size; therefore, the finer particles with smaller pore throats have higher air-entry values. Air entry generally occurs at degrees of saturation ( $S$ ) between 0.9 and 1.0. Once air breaks in, the soil mass becomes unsaturated, yet the water still forms a continuous phase. This is called the funicular stage (Newitt and Conway-Jones 1958, Pietsch 1991, Levenson and Lohnes 1995). As drying proceeds, the suction pressure increases gradually with decreasing degree of saturation, following a quasi-linear trend. Any local change in water pressure is rapidly homogenized throughout the mass by pressure diffusion within the continuous water phase. The drying rate is relatively constant in this region.

The pendular stage begins when water becomes disconnected. Water rings form around particle contacts and only an adsorbed film may be present on particle surfaces (Levenson and Lohnes 1995). Since the radii of menisci are small, the suction pressure increases significantly. Because this is only a contact-level effect, a change in suction within a meniscus is felt at other menisci through the corresponding change in vapor pressure and thus the total suction as expressed in Kelvin's equation (Fredlund and Rahardjo 1993).

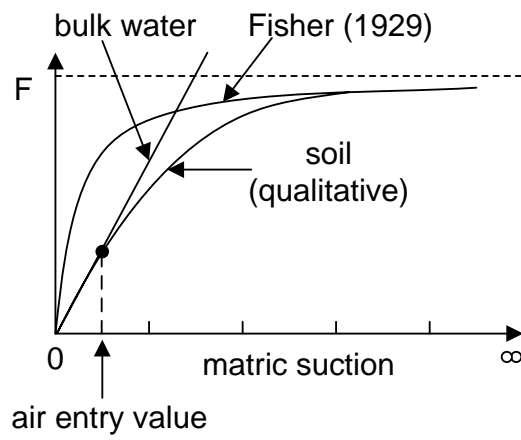
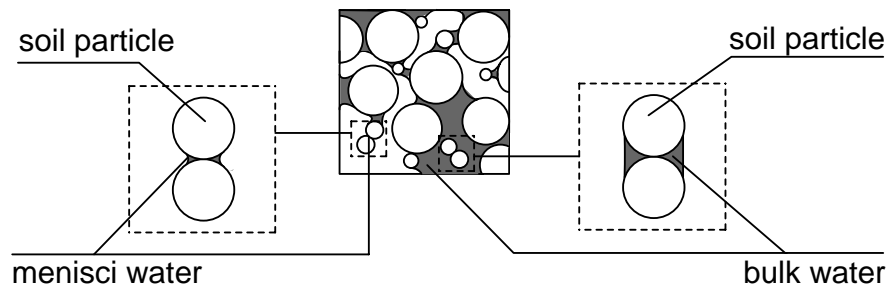


Fig. A-14. Effect of suction on the normal force ( $F$ ) between two spherical particles for bulk and menisci water (Mancuso et al., 2002).

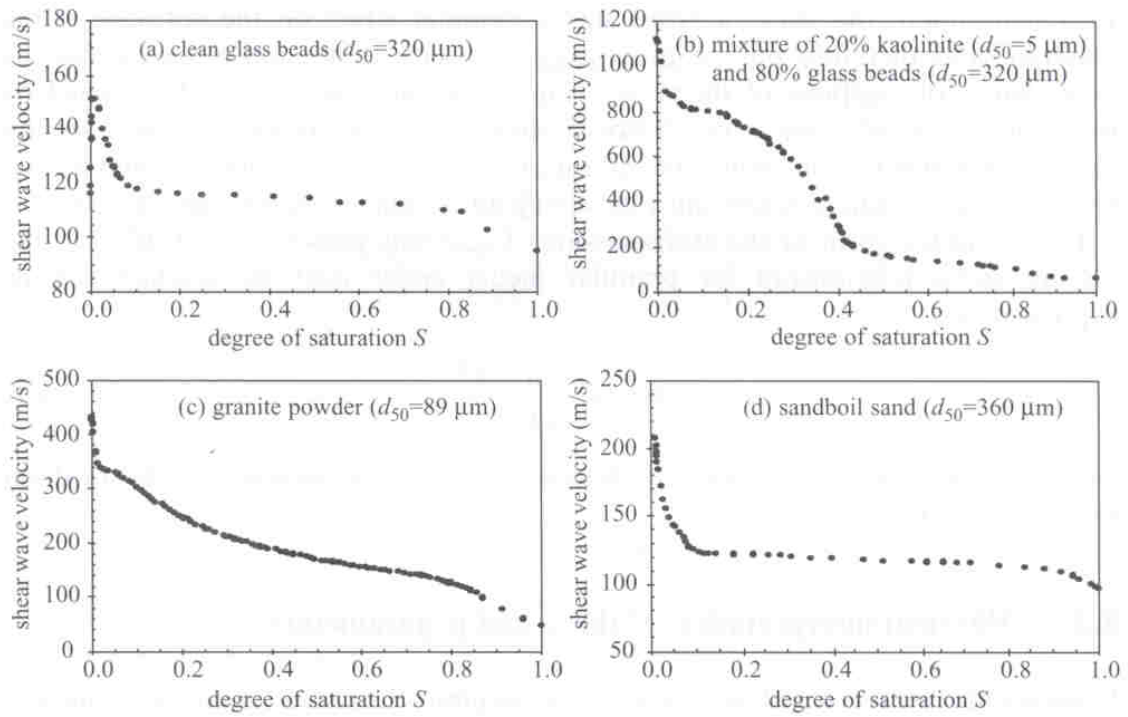
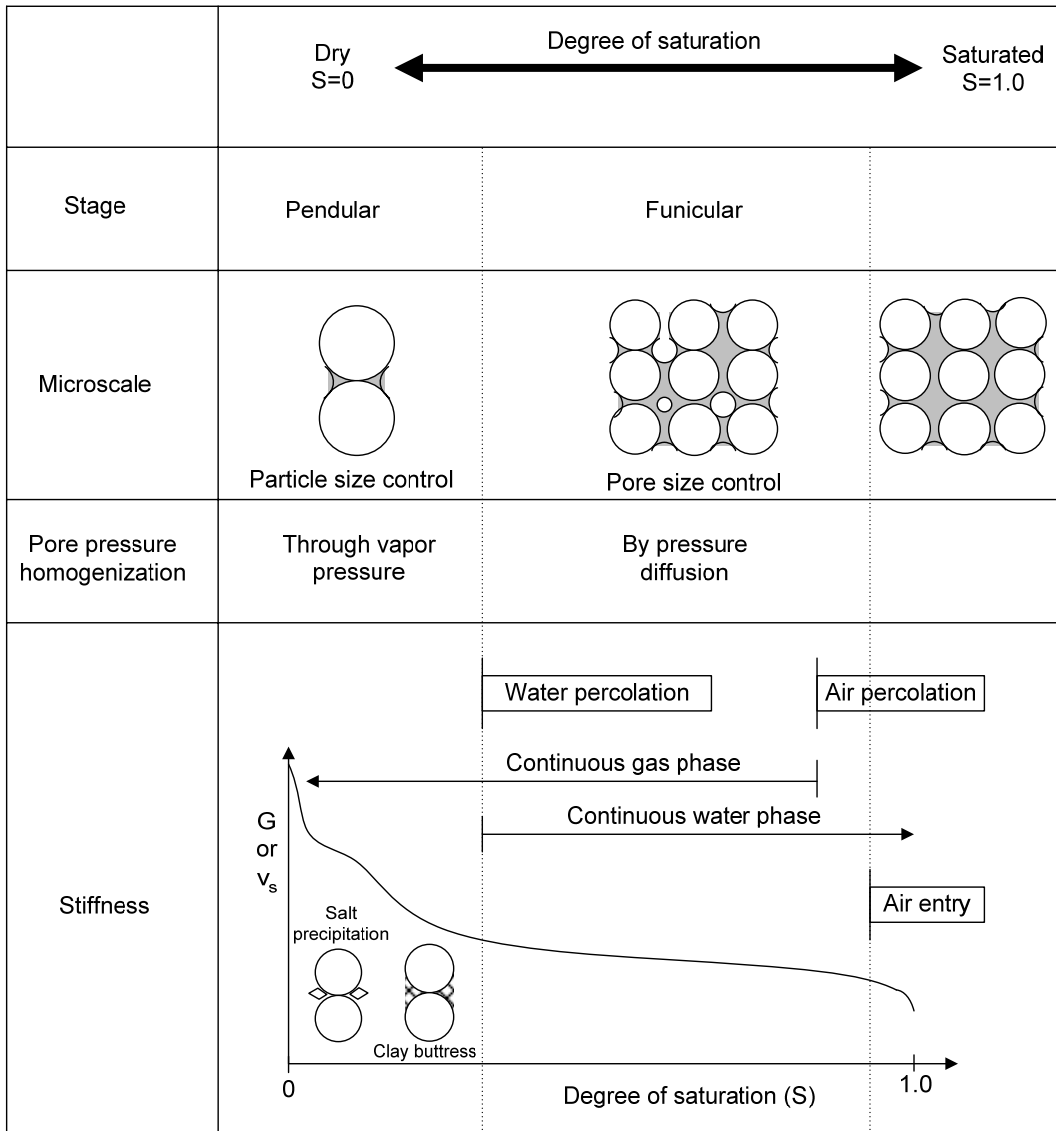


Fig. A-15. Shear wave velocity versus degree of saturation (Cho and Santamarina, 2001).



Note:  $G$  is small-strain shear modulus,  $v_s$  is shear wave velocity

Fig. A-16. Stages of unsaturated conditions and related phenomena (Cho and Santamarina, 2001).

This is a slow homogenization process. The drying rate in this stage is increasingly slower.

As the soil dries, fines migrate to contacts, and form buttresses between larger particles. These buttresses increase the stiffness of the particulate material formed by the coarser grains. At the same time, the ionic concentration in the pendular water increases and eventually reaches saturation causing the precipitation of salt crystals between the two contacting particles. Salt precipitation also increases the stiffness of the particulate skeleton (Cho and Santamarina, 2001). The stiffness increases as explained by these two phenomena is similar to the cementation effect (Rinaldi et al., 1998).

## A-9 References

- Acar, Y. B. and EL-Tahir, E. A. (1986), "Low Strain Dynamic Properties of Artificially Cemented Sand," *Journal of Geotechnical Engineering*, ASCE, Vol. 112, No. 11, pp. 1001-1015.
- Afifi, S. S., and Richart, F. E., Jr. (1973), "Stress-History Effects on Shear Modulus of Soils," *Soils and Foundations*, Vol. 13, No. 1, pp. 77-95.
- Afifi, S. S., and Woods, R. D. (1971), "Long-Term Pressure Effects on Shear Modulus of Soils," *Journal of the Soil Mechanics and Foundations Division*, ASCE, Vol. 97, No. SM10, pp. 1445-1460.
- Anderson, D. G., and Woods, R. D. (1975), "Comparison of Field and Laboratory Shear Moduli," *Proceedings of the Conference on In Situ Measurement of Soil Properties*, Raleigh, NC, Vol. 1, pp. 69-92.
- Anderson, D. G., and Woods, R. D. (1976), "Time-Dependent Increase in Shear Modulus of Clay," *Journal of the Geotechnical Engineering Division*, ASCE, Vol. 102, No. GT5, pp. 525-537.
- Anderson, D. G., and Stokoe, K. H., II (1978), "Shear Modulus: A Time-Dependent Soil Property," *Dynamic Geotechnical Testing, ASTM STP 654*, Philadelphia, PA, pp. 66-90.
- Athanasopoulos, G. A. (1981), "Time Effects on Low-Amplitude Shear Modulus of Cohesive Soils," *Report UMEE 81R1*, The University of Michigan, Ann Arbor, MI.
- Atkinson, J. H. (2000), "Non-Linear Soil Stiffness in Routine Design," *Geotechnique*, 40<sup>th</sup> Rankine Lecture, pp. 487-508.
- Baig, S., Picornell, M., and Nazarian, S. (1997), "Low Strain Shear Moduli of Cemented Sands," *Journal of Geotechnical Engineering*, ASCE, Vol. 123, pp. 540-545.

- Baldi, G., Bruzzi, D., and Superbo, S. (1988), "Seismic Cone in Po River Sand," *Proceedings of the 1<sup>st</sup> International Symposium on Penetration Testing*, Balkema, Vol. 1, pp. 643-650.
- Bergan, A. T., and Monosmith, C. L. (1973), "Characterization of Subgrade Soils in Cold Regions for Pavement Design Purposes," *Highway Research Record*, No. 431, Washington, D.C., pp. 25-37.
- Benson, C. H., and Gribb, M. M. (1997), "Measuring Unsaturated Hydraulic Conductivity in the Laboratory and Field," *Proceedings of Sessions on Unsaturated Soils at Geo-Logan'97, Unsaturated Soil Engineering Practice*, Logan, Utah, pp. 113-168.
- Biarez, J., and Hicher, P.-Y. (1994), *Elementary Mechanics of Soil Behaviour-Saturated Remoulded Soils*, Balkema.
- Biot, M. A. (1956), "Theory of Propagation of Elastic Waves in a Fluid-Saturated Porous Solid," *Journal of the Acoustic Society of America*, Vol. 28, No. 2, pp. 168-191.
- Bolton, M. D., and Wilson, J. M. R. (1989), "An Experimental and Theoretical Comparison between Static and Dynamic Torsional Soil Tests," *Geotechnique*, Vol. 39, No. 4, pp. 585-599.
- Bosscher, P. J., and Nelson, D. L. (1987), "Resonant Column Testing of Frozen Ottawa Sand," *Geotechnical Testing Journal*, ASTM, Vol. 10, No. 3, pp. 123-134.
- Brayant, J. T. (1998), "Variation of Soil Suction with Depth in Dallas and Forth Worth, Texas," *Transportation Research Record*, No. 1615, Washington, D.C., pp. 100-104.
- Brooks, R. H., and Corey, A. T. (1964), "Hydraulic Properties of Porous Medium," *Hydrology Paper No. 3*, Colorado State University, Fort Collins, CO.
- Brooks, R. H., and Corey, A. T. (1966), "Properties of Porous Media Affecting Fluid Flow," *Journal of the Irrigation and Drainage Division*, ASCE, Vol. 92, No. 2, pp. 61-88.
- Burland, J. B. (1989), "The Ninth Lauritis Bjerrum Memorial Lecture: 'Small is Beautiful'- the Stiffness of Soils at Small Strains," *Canadian Geotechnical Journal*, Vol. 26, pp. 499-516.
- Butalia, T. S., Huang, J., Kim, D.-G., and Croft, F. (2003), "Effect of Moisture Content and Pore Water Pressure Buildup on Resilient Modulus of Cohesive Soils," *Resilient Modulus Testing for Pavement Components, ASTM STP 1437*, West Conshohocken, PA, pp. 70-84.

- Campanella, R. G. (1994), "Field Methods for Dynamic Geotechnical Testing: An Overview of Capabilities and Needs," *Dynamic Geotechnical Testing II, ASTM STP 1213*, Philadelphia, PA, pp. 3-23.
- Campanella, R. G., Robertson, P. K., and Gillespie (1986), "Seismic Cone Penetration Test," *Proceedings of Sessions on In Situ 86, ASCE Specialty Conference on Use of In Situ Tests in Geotechnical Engineering*, Blackburg, VA, pp. 116-130.
- Cascante, G., and Santamarina, J. C. (1996), "Interparticle Contact Behavior and Wave Propagation," *Journal of Geotechnical Engineering*, ASCE, Vol. 122, No. 10, pp. 831-839.
- Cascante, G., Santamarina, J. C., and Yassir, N., (1998), "Flexural Excitation in a Standard Resonant Column Device," *Canadian Geotechnical Journal*, Vol. 35, No. 3, pp. 488-490.
- Chamberlain, E. J., Cole, D. M., and Johnson, T. C. (1979), "Resilient Response of Two Frozen and Thawed Soils," *Journal of the Geotechnical Engineering Division*, ASCE, Vol. 105, No. 2, pp. 257-271.
- Chang, C. S., Misra, A., and Sundaram, S. S. (1991), "Properties of Granular Packings under Low Amplitude Cyclic Loading," *Soil Dynamics and Earthquake Engineering*, Vol. 10, No. 4, pp. 201-211.
- Chen, D.-H., Wu, W., He, R., Bilyeu, J., and Arrelano, M. (1999), "Evaluation of In-Situ Resilient Modulus Testing Techniques," *Recent Advances in the Characterization of Transportation Geo-Materials*, Geotechnical Special Publication, No. 86, ASCE, Reston, VA., pp. 1-11.
- Cho, G. C., and Santamarina, J. C. (2001), "Unsaturated Particulate Materials-Particle-Level Studies," *Journal of Geotechnical and Geoenvironmental Engineering*, ASCE, Vol. 127, No. 1, pp. 84-96.
- Clough, G. W., Sitar, N., Bachus, R. C., and Rad, N. S. (1981), "Cemented Sands under Static Loading," *Journal of the Geotechnical Engineering Division*, ASCE, Vol. 107, pp. 799-817.
- Corey, A. (1994), "Mechanics of Immiscible Fluids in Porous Media," *Water Resources Publications*, Highlands Ranch, CO.
- Costa, Y. D., Cintra, J. C., and Zornberg, J. G. (2003), "Influence of Matric Suction on the Results of Plate Load Tests Performed on a Lateritic Soil Deposit," *Geotechnical Testing Journal*, ASTM, Vol. 26, No. 2, pp. 1-9.

- Croney, D., Coleman, J. D., and Black, W. P. M. (1958), "The Movement and Distribution of Water in Soil in Relation to Highway Design and Performance," *Road Research Laboratory*, Research Note 3209, pp. 1-14.
- Culley, R. W. (1971), "Effect of Freeze-Thaw Cycling on Stress-Strain Characteristics and Volume Change of a Till Subjected to Repetitive Loading," *Canadian Geotechnical Journal*, Vol. 8, No. 3, pp. 359-371.
- Davich, P., Labuz, J., Guzina, B. and Drescher, A. (2004), "Small Strain and Resilient Modulus Testing of Granular Soils," Final Report 2004-39, Minnesota Department of Transportation, St. Paul, MN.
- Deresiewicz, H. (1973), "Bodies in Contact with Applications to Granular Media," *R. D. Mindlin and Applied Mechanics*, Pergamon Press, NY, pp. 105-145.
- Dobry, R. (1989), "Some Basic Aspects of Soil Liquefaction during Earthquakes," *Earthquake Hazards and the Design of Constructed Facilities in the Eastern United States*, Annual of the New York Academy of Sciences, No. 558, pp. 172-182.
- Drnevich, V. P. (1977), "The Resonant Column Test," *Report to the U.S. Army Corps of Engineers*, Soil Mechanics Series, No. 23, Department of Civil Engineering, The University of Kentucky.
- Drnevich, V. P. (1985), "Recent Developments in Resonant Column Testing," *Richart Commemorative Lectures, Proceedings of the ASCE Specialty Session*, Detroit, MI, pp. 79-107.
- Drnevich, V. P., Hall, J. R., and Richart, F. E. (1967), "Effects of Amplitude of Vibration on the Shear Modulus of Sand," *Proceedings of the International Symposium on Wave Propagation and Dynamic Properties of Earth Materials*, Albuquerque, NM, pp. 189-199.
- Drnevich, V. P., Hardin, B. O., and Shippy, D. J. (1978), "Modulus and Damping of Soils by the Resonant-Column Method," *Dynamic Geotechnical Testing, ASTM STP 654*, Philadelphia, PA, pp. 91-125.
- Duffy, J., and Mindlin, R. D. (1957), "Stress-Strain Relations of a Granular Medium," *Journal of the Applied Mechanics*, Vol. 24, No. 4, pp. 585-593.
- Dyvik, R., and Madshus, C. (1985), "Lab Measurements of  $G_{max}$  Using Bender Elements," *Proceedings of the Geotechnical Engineering Division: Advances in the Art of Testing Soil Under Cyclic Conditions*, ASCE, Detroit, MI, pp. 186-196.
- Edil, T. B., and Luh, G.-F. (1978), "Dynamic Modulus and Damping Relationships for Sands," *Proceedings on the Specialty Conference on Earthquake Engineering and Soil Dynamics*, ASCE, Pasadena, CA, pp. 394-409.

- Edil, T. B., and Motan, S. E. (1979), "Soil-Water Potential and Resilient Behavior of Subgrade Soils," *Transportation Research Record*, No. 705, Washington, D.C., pp. 54-63.
- Edil, T. B., Motan, S. E., and Toha, F. X. (1981), "Mechanical Behavior and Testing Methods of Unsaturated Soils," *Laboratory Shear Strength of Soil, ASTM STP 740*, Philadelphia, PA, pp. 114-129.
- Edil, T.B., Benson, C., and Sawangsuriya, A. 2007, "Resilient modulus of unsaturated soils." A report submitted to the University of Minnesota as part of the subcontract on the Mn/DOT project "Pavement Design using Unsaturated Technology, St. Paul, MN.
- Edris, V. E., and Lytton, R. L. (1977), "Climatic Materials Characterization of Fine-Grained Soils," *Transportation Research Record*, No. 642, Washington, D.C., pp. 39-44.
- Egorov, K. E. (1965), "Calculation of Bed for Foundation with Ring Footing," *Proceedings of the 6<sup>th</sup> International Conference of Soil Mechanics and Foundation Engineering*, Vol. 2, pp. 41-45.
- Fam, M., and Santamarina, J. C. (1995), "Study of Geoprocesses with Complementary Wave Measurements in an Oedometer," *Geotechnical Testing Journal*, ASTM, Vol. 18, No. 3, pp. 307-314.
- Fam, M., Santamarina, J. C., and Dusseault, M. (1998), "Wave-Based Monitoring Processes in Granular Salt," *Journal of the Environmental and Engineering Geophysics*, Vol. 3, pp. 15-26.
- Fernandez, A., and Santamarina, J. C. (2001), "Effect of Cementation on the Small-Strain Parameters of Sands," *Canadian Geotechnical Journal*, Vol. 38, No. 1, pp. 191-199.
- Fiedler, S. A., Nelson, C. R., Berkman, E. F. and DiMillio, A. F. (1998), "Soil Stiffness Gauge for Soil Compaction Control," *Public Roads*, U.S. Department of Transportation, Federal Highway Administration, Washington, DC, Vol. 61, No. 4.
- Fiedler, S. A., Main, M., and DiMillio, A. F. (2000), "In-Place Stiffness and Modulus Measurements," *Proceedings of Sessions of ASCE Specialty Conference on Performance Confirmation of Constructed Geotechnical Facilities*, Geotechnical Special Publication, No. 94, ASCE, Amherst, MA, pp. 365-376.
- Fioravante, V., and Capoferri, R. (2001), "On the Use of Multi-Directional Piezoelectric Transducers in Triaxial Testings," *Geotechnical Testing Journal*, ASTM, Vol. 24, No. 3, pp. 243-255.

- Fisher, R. A. (1926), "On the Capillary Forces in an Ideal Soil," *Journal of Agricultural Science*, Vol. 16, pp. 492-505.
- Fredlund, D. G. (1964), "Comparison of Soil Suction and One-Dimensional Consolidation Characteristics of a Highly Plastic Clay," *M.S. Thesis*, The University of Alberta, Edmonton, Alberta, Canada.
- Fredlund, D. G., Bergan, A. T., and Wong, P. K. (1977), "Relation between Resilient Modulus and Stress Conditions for Cohesive Subgrade Soils," *Transportation Research Record*, No. 642, Washington, D.C., pp. 73-81.
- Fredlund, D. G., and Rahardjo, H. (1993), *Soil Mechanics for Unsaturated Soils*, John Wiley & Sons, Inc., New York, NY.
- Frost J. D., and Burns, S. E. (2003), "In Situ Subsurface Characterization," *The Civil Engineering Handbook*, 2<sup>nd</sup> Edition by W. F. Chen and J. Y. Richard, CRC Press LLC.
- Georgiannou, V. N., Rampello, S., and Silvestri, F. (1991), "Static and Dynamic Measurement of Undrained Stiffness of National Overconsolidated Clays," *Proceedings of the 10<sup>th</sup> European Conference Soil Mechanics*, Florence, Italy, Vol. 1, pp. 91-96.
- Goddard, J. D. (1990), "Nonlinear Elasticity and Pressure-Dependent Wave Speeds in Granular Media," *Proceedings of the Royal Society of London*, London, England, Vol. 430, pp. 105-131.
- Goto, S., Tatsuoka, F., Shibuya, S., and Sato, T. (1991), "A Simple Gauge for Local Strain Measurements in the Laboratory," *Soils and Foundations*, Vol. 31, No. 1, pp. 169-180.
- Graham, J., Blatz, J. A., Alfaro, M. C., and Sivakumar, V. (2001), "Behavioral Influence of Specimen Preparation Methods for Unsaturated Plastic Compacted Clays," *Proceedings of the 15<sup>th</sup> International Conference on Soil Mechanics and Geotechnical Engineering*, Istanbul, Turkey, Vol. 1, pp. 633-638.
- Hardin, B. O., (1970), "Suggested Methods of Test for Shear Modulus and Damping of Soils by the Resonant Column," *ASTM STP 479*, Philadelphia, PA, pp. 516-529.
- Hardin, B. O. (1978), "The Nature of Stress-Strain Behavior of Soils," *Proceedings of the Geotechnical Engineering Division Specialty Conference on Earthquake Engineering and Soil Dynamics*, ASCE, Pasadena, CA, Vol. 1, pp. 1-90.
- Hardin, B. O., and Richart, F. E., Jr. (1963), "Elastic Wave Velocities in Granular Soils," *Journal of the Soil Mechanics and Foundations Division*, ASCE, Vol. 89, No. SM1, pp. 33-65.

- Hardin, B. O., and Black, W. L. (1966), "Sand Stiffness under Various Triaxial Stress," *Journal of the Soil Mechanics and Foundations Division*, ASCE, Vol. 92, No. SM2, pp. 27-42.
- Hardin, B. O., and Black, W. L. (1968), "Vibration Modulus of Normally Consolidated Clay," *Journal of the Soil Mechanics and Foundations Division*, ASCE, Vol. 94, No. SM2, pp. 353-369.
- Hardin, B. O., and Black, W. L. (1969), Closure to "Vibration Modulus of Normally Consolidated Clay," *Journal of the Soil Mechanics and Foundations Division*, ASCE, Vol. 95, No. SM6, pp. 1531-1537.
- Hardin, B. O., and Drnevich, V. P. (1972), "Shear Modulus and Damping in Soils: Design Equations and Curves," *Journal of the Soil Mechanics and Foundations Division*, ASCE, Vol. 98, No. SM7, pp. 667-692.
- Hardin, B. O., and Music, J. (1965), "Apparatus for Vibration during the Triaxial Test," *Symposium on Instrumentation and Apparatus for Soils and Rocks*, ASTM STP 392, pp. 55-74.
- Hardin, B. O., and Richart, F. E., Jr. (1963), "Elastic Wave Velocities in Granular Soils," *Journal of the Soil Mechanics and Foundations Division*, ASCE, Vol. 89, No. SM1, pp. 33-65.
- Hertz, H. (1881), "Über die Berührung fester elastischer Körper," *Journal Für die Reine und Angewandte Mathematik*, Vol. 92, pp. 156-171.
- Hill, J. J., Kurdziel, J. M., Nelson, C. R., Nystrom, J. A., and Sondag, M. (1999), "MnDOT Overload Field Tests of Standard and SIDD RCP Installations," *Transportation Research Board 78<sup>th</sup> Annual Meeting*, Washington, D.C. (CD-ROM)
- Hillel, D. (1980), *Fundamentals of Soil Physics*, Academic Press, Inc., San Diego, CA.
- Hoar, R. J., and Stokoe, K. H., II (1978), "Generation and Measurement of Shear Waves In Situ," *Dynamic Geotechnical Testing*, ASTM STP 654, Philadelphia, PA, pp. 3-29.
- Hryciw, R. D., and Thomann, T. G. (1993), "Stress-History-Based Model for  $G^{\circ}$  of Cohesionless Soils," *Journal of Geotechnical Engineering*, ASCE, Vol. 119, No. 7, pp. 1073-1093.
- Humboldt Mfg. Co. (1999), *Humboldt Soil Stiffness Gauge (GeoGauge) User Guide: Version 3.3*, Norridge, IL.
- Humboldt Mfg. Co. (2000a), *Test Results: Evaluation of the Humboldt GeoGauge on Soil-Fly Ash-Cement Mixtures*, Norridge, IL.

- Humboldt Mfg. Co. (2000b), *Test Results: Evaluation of the Humboldt GeoGauge on New Mexico Route 44*, Norridge, IL.
- Inci, G., Yesiller, N., and Kagawa, T. (2003), "Experimental Investigation of Dynamic Response of Compacted Clayey Soils," *Geotechnical Testing Journal*, ASTM, Vol. 26, No. 2, pp. 125-141.
- Isenhower, W. M. (1980), "Torsional Simple Shear/Resonant Column Properties of San Francisco Bay Mud," *M.S. Thesis*, The University of Texas at Austin, Austin, TX.
- Isenhower, W. M., and Stokoe, K. H., II (1981), "Strain-Rate Dependent Shear Modulus of San Francisco Bay Mud," *Proceedings of the International Conference on Recent Advances in Geotechnical Earthquake Engineering and Soil Dynamic*, St. Louis, MO, Vol. 2, pp. 597-602.
- Ishihara, K. (1996), *Soil Behavior in Earthquake Geotechnics*, Oxford University Press, Inc., New York, NY.
- Iwasaki, T. and Tatsuoka, F. (1977), "Effects of Grain Size and Grading on Dynamic Shear Moduli of Sands," *Soils and Foundations*, Vol. 17, No. 3, pp. 19-35.
- Iwasaki, T., Tatsuoka, F., and Takagi, Y. (1978), "Shear Moduli of Sands under Cyclic Torsional Shear Loading," *Soils and Foundations*, Vol. 18, No. 1, pp. 39-50.
- Jamiolkowski, M., Lancellotta, R., Lo Presti, D. C. F., and Pallera, O. (1994), "Stiffness of Toyoura Sand at Small and Intermediate Strain," *Proceedings of the 13<sup>th</sup> International Conference on Soil Mechanics and Foundation Engineering*, New Delhi, India, pp. 169-172.
- Janssen, D. J., and Dempsey, B. J. (1981), "Soil-Moisture Properties of Subgrade Soils," *Transportation Research Record*, No. 790, Washington, D.C., pp. 61-66.
- Jardine, R. J. (1992), "Some Observations on the Kinetic Nature of Soil Stiffness," *Soils and Foundations*, Vol. 32, No. 2, pp. 111-124.
- Jardine, R. J., and Potts, D. M. (1988), "Hutton Tension Platform Foundation: An Approach to the Prediction of Pile Behavior," *Geotechnique*, Vol. 38, No. 2, pp. 231-252.
- Jardine, R. J., Potts, D. M., Fourie, A. B., and Burland, J. B. (1986), "Studies of the Influence of Non-Linear Stress-Strain Characteristics in Soil-Structure Interaction," *Geotechnique*, Vol. 36, No. 3, pp. 377-396.

- Jong, D.-T., Bosscher, P. J., and Benson, C. H. (1998), "Field Assessment of Changes in Pavement Moduli Caused by Freezing and Thawing," *Transportation Research Record*, No. 1615, Washington, D.C., pp. 41-48.
- Jovičić, V., and Coop, M. R. (1998), "The Measurement of Stiffness Anisotropy in Clays with Bender Element Tests in the Triaxial Apparatus," *Geotechnical Testing Journal*, ASTM, Vol. 21, No. 1, pp. 3-10.
- Khoury, N. N., Zaman, M. M., Nevels, J. B., and Mann, J. (2003), "Effect of Soil Suction on Resilient Modulus of Subgrade Soil Using the Filter Paper Technique," *Transportation Research Board 82<sup>nd</sup> Annual Meeting*, Washington, D.C. (CD-ROM)
- Khoury, N. N., and Zaman, M. M., (2004), "Correlation between Resilient Modulus, Moisture Variation, Soil Suction for Subgrade Soils," *Transportation Research Record*, No. 1874, Washington, D.C., pp. 99-107.
- Kokusho, T. (1980), "Cyclic Triaxial Test of Dynamic Soil Properties for Wide Strain Range," *Soils and Foundations*, Vol. 20, pp. 45-60.
- Kokusho, T. (1987), "In Situ Dynamic Soil Properties and their Evaluation," *Proceedings of the 8<sup>th</sup> Asian Regional Conference on Soil Mechanics and Foundation Engineering*, Kyoto, Japan, Vol. 2, pp. 215-435.
- Kokusho, T., Yoshida, Y., and Esashi, Y. (1982), "Dynamic Properties of Soft Clays for Wide Strain Range," *Soils and Foundations*, Vol. 22, No. 4, pp. 1-18.
- Kramer, S. L. (1996), *Geotechnical Earthquake Engineering*, Prentice-Hall, Inc., Upper Saddle River, NJ.
- Kuribayashi, E., Iwasaki, T., Tatsuoka, F., and Horiuchi, S. (1975), "Effects of Particle Characteristics on Dynamic Deformational Properties of Soils," *Proceedings of the 5<sup>th</sup> Asian Regional Conference on Soil Mechanics and Foundation Engineering*, Bangalore, India, pp. 361-367.
- Lade, P. V., and Overton, D. D. (1989), "Cementation Effects in Frictional Materials," *Journal of Geotechnical Engineering*, ASCE, Vol. 115, pp. 1373-1387.
- Lambe, T. W., and Whitman, R. V. (1969), *Soil Mechanics*, John Wiley & Sons, Inc., New York, NY.
- Lane, K. S., and Washburn, D. E. (1946), "Capillary Tests by Capillarimeter and by Soil Filled Tubes," *Highway Research Record*, No. 26, Washington, D.C., pp. 245-473.
- Lawrence, F. V., Jr. (1963), "Propagation Velocity of Ultrasonic Wave Through Sand," *MIT Research Report R63-8*, Massachusetts Institute of Technology, Cambridge, MA.

- Lenke, L. R., McKeen, R. G., and Grush, M. (2001), "Evaluation of a Mechanical Stiffness Gauge for Compaction Control of Granular Media," *Report NM99MSC-07.2*, New Mexico State Highway and Transportation Department, Albuquerque, NM.
- Lenke, L. R., McKeen, R. G., and Grush, M. (2003), "Laboratory Evaluation of the GeoGauge for Compaction Control," *Transportation Research Record*, No. 1849, Washington, D.C., pp. 20-30.
- Levenson, S. M., and Lohnes, R. A. (1995), "Moisture Tension Relations in Sand," *Proceedings of the 1<sup>st</sup> International Conference on Unsaturated Soils*, Balkema, Paris, France, pp. 387-392.
- Lewis, M. D. (1990), "A Laboratory Study of the Effect of Stress State on the Elastic Moduli of Sand," *Ph.D. Thesis*, The University of Texas at Austin, Austin, TX.
- Li, D., and Selig, E. T. (1994), "Resilient Modulus for Fine-Grained Subgrade Soils," *Journal of Geotechnical Engineering*, ASCE, Vol. 120, No. 6, pp. 939-957.
- Li, J., and Qubain, B. S. (2003), "Resilient Modulus Variations with Water Content," *Resilient Modulus Testing for Pavement Components*, ASTM 1437, West Conshohocken, PA, pp. 59-69.
- Lo Presti, D. C. F., Pallara, O., Lancellota, R., Armandi, M., and Maniscalco, R. (1993), "Monotonic and Cyclic Loading Behavior of Two Sands at Small Strains," *Geotechnical Testing Journal*, ASTM, Vol. 16, No. 4, pp. 409-424.
- Lo Presti, D. C. F., Jamiolkowski, M., Pallara, O., Cavallaro, A., and Pedroni, S. (1997), "Shear Modulus and Damping of Soils," *Geotechnique*, Vol. 47, No. 3, pp. 603-617.
- Lytton, R. L. (1997), "Engineering Structures in Expansive Soils," Keynote Address, *Proceedings of the 3<sup>rd</sup> International Symposium on Unsaturated Soils*, Rio de Janeiro, Brazil, Vol. 2, pp. 333-354.
- Mair, R. J. (1993), "Developments in Geotechnical Engineering Research: Application to Tunnels and Deep Excavations," Unwin Memorial Lecture 1992, *Proceedings of the Institution of Civil Engineers-Civil Engineering*, Vol. 97, No. 1, pp. 27-41.
- Mancuso, C., Vassallo, R., and d'Onofrio, A. (2002), "Small Strain Behavior of a Silty Sand in Controlled-Suction Resonant Column-Torsional Shear Tests," *Canadian Geotechnical Journal*, Vol. 39, No. 1, pp. 22-31.
- Marcuson, W. F., III and Wahls, H. E. (1972), "Time Effects on Dynamic Shear Modulus of Clays," *Journal of the Soil Mechanics and Foundations Division*, ASCE, Vol. 98, No. SM12, pp. 1359-1373.

- Marinho, F. A. M., Chandler, R. J., and Crilly, M. S. (1996), "Stiffness Measurements on an Unsaturated High Plasticity Clay Using Bender Elements," *Proceedings of the 1<sup>st</sup> International Conference on Unsaturated Soils*, Paris, France, Vol. 1, pp. 1179-1200.
- Marinho, F. A. M., and Stuermer, M. M. (2000), "The Influence of the Compaction Energy on the SWCC of a Residual Soil," *Proceedings of Sessions of Geo-Denver 2000, Advances in Unsaturated Geotechnics*, ASCE, Geotechnical Special Publication, No. 99, Denver, CO, pp. 125-131.
- Mayne, P. W. (2001), "Stress-Strain-Strength-Flow Parameters from Enhanced In Situ Tests," *Proceedings of the International Conference on In Situ Measurement of Soil Properties and Case Histories*, Bali, Indonesia, pp. 27-48.
- Mayne, P. W., Christopher, B. R., and DeJong, J. (2001), *Manual on Subsurface Investigations*, National Highway Institute Publication No. FHWA NHI-01-031, FHWA, Washington, D.C.
- McKeen, R. G., and Johnson, L. D. (1990), "Climate-Controlled Soil Design Parameters for Mat Foundations," *Journal of Geotechnical Engineering*, ASCE, Vol. 116, No. 7, pp. 1073-1094.
- Miller, C. J., Yesiller, N., Yaldo, K., and Merayyan, S. (2002), "Impact of Soil Type and Compaction Conditions on Soil Water Characteristic," *Journal of Geotechnical and Geoenvironmental Engineering*, ASCE, Vol. 128, No. 9, pp. 733-742.
- Mitchell, J. K., and Soga, K. (2005), *Fundamentals of Soil Behavior*, John Wiley and Sons, Inc., NJ.
- Mitchell, P. W. (1979), "The Structural Analysis of Footings on Expansive Soil," *Research Report No. 1*, Kenneth W. G. Smith and Assoc., Adelaide, South Australia.
- Morris, D. V. (1990), "Automatic Feedback System for Resonant Column Testing," *Geotechnical Testing Journal*, ASTM, Vol. 13, No. 1, pp. 16-23.
- Motan, S. E., and Edil, T. B. (1982), "Repetitive-Load Behavior of Unsaturated Soils," *Transportation Research Record*, No. 872, Washington, D.C., pp. 41-48.
- Mualem, Y. (1986), "Hydraulic Conductivity of Unsaturated Soils: Prediction and Formulas," *Methods of Soils Analysis, Part 1, Physical and Mineralogical Methods*, American Society of Agronomy, Madison, WI, pp. 799-823.
- Muhanna, A. S., Rahman, M. S., and Lambe, P. C. (1999), "Resilient Modulus Measurement of Fine-Grained Subgrade Soils," *Transportation Research Record*, No. 1687, Washington, D.C., pp. 3-12.

- Nacci, V. A. and Taylor, K. J. (1967), "Influence of Clay Structure on Elastic Wave Velocities," *Proceedings of the International Symposium on Wave Propagation and Dynamic Properties of Earth Materials*, Albuquerque, NM, pp. 491-502.
- Nakagawa, K., Soga, K., and Mitchell, J. K. (1996), "Pulse Transmission System for Measuring Wave Propagation in Soils," *Journal of Geotechnical Engineering*, ASCE, Vol. 122, No. 4, pp. 302-308.
- Nazarian, S. and Stokoe, K. H., II (1987), "In Situ Determination of Elastic Moduli of Pavements Systems by Special-Analysis-of-Surface-Waves Method (Theoretical Aspects)," *Research Report 437-2*, Center for Transportation Research, The University of Texas at Austin, Austin, TX.
- Nazarian, S., Yuan, D., and Arellano, M. (2002), "Quality Management of Base and Subgrade Materials with Seismic Methods," *Transportation Research Record*, No. 1786, Washington, D.C., pp. 3-10.
- Nazarian, S., Yuan, D., and Baker, M. R. (1994), "Automation of SASW Method," *Dynamic Geotechnical Testing II, ASTM STP 1213*, Philadelphia, PA, pp. 88-100.
- Nazarian, S., Yuan, D., and Tandon, V. (1999), "Structural Field Testing of Flexible Pavement Layers with Seismic Methods for Quality Control," *Transportation Research Record*, No. 1654, Washington, D.C., pp. 50-60.
- Nelson, C. R., and Sondag, M. (1999), "Comparison of the Humboldt GeoGauge with In-Place Quasi-Static Plate Load Tests," *CNA Consulting Engineers Report*, Minneapolis, MN.
- Newitt, D. M., and Conway-Jones, J. M. (1958), "A Contribution to the Theory and Practice of Granulation," *Transaction of the Institution of Chemical Engineers*, Vol. 36, pp. 422-442.
- Ng, C. W. W., and Pang, Y. W. (2000), "Influence of Stress State on Soil-Water Characteristics and Slope Stability," *Journal of Geotechnical and Geoenvironmental Engineering*, ASCE, Vol. 126, No. 2, pp. 157-166.
- Ni, S. H. (1987), "Dynamic Properties of Sand under True Triaxial Stress States from Resonant Column and Torsion Shear Tests," *Ph.D. Thesis*, The University of Texas, Austin, TX.
- Ohara, S., and Matsuda, H. (1988), "Study on the Settlement of Saturated Clay Layer Induced by Cyclic Shear," *Soils and Foundations*, Vol. 28, pp. 103-113.
- Olson, R. E., and Langfelder, L. J. (1965), "Pore-Water Pressures in Unsaturated Soils," *Journal of the Soil Mechanics and Foundations Division*, ASCE, Vol. 91, No. SM4, pp. 127-160.

- Ooi, P. S. K., and Pu, J. (2003), "Use of Stiffness for Evaluating Compactness of Cohesive Pavement Geomaterials," *Transportation Research Record*, No. 1849, Washington, D.C., pp. 11-19.
- Perera, Y. Y., Zapata, C. E., Houston, W. N., Houston, S. L. (2004), "Moisture Equilibria beneath Highway Pavements," *Transportation Research Board 83<sup>rd</sup> Annual Meeting*, Washington, D.C. (CD-ROM)
- Petersen, L., Peterson, R., and Nelson, C. R. (2002), "Comparison of Quasi-Static Plate Load Tests with the Humboldt GeoGauge," *CNA Consulting Engineers Report*, Minneapolis, MN.
- Petrakis, E., and Dobry, R. (1987), "Micromechanical Modeling of Granular Soil at Small Strain by Arrays of Elastic Spheres," *Report CE-87-02*, Department of Civil Engineering, Rensselaer Polytechnic Institute, Troy, NY.
- Pietsch, W. (1991), *Size Enlargement by Agglomeration*, John Wiley & Sons, Inc., New York, NY.
- Post Tensioning Institute (PTI) (1996), *Design and Construction of Post-Tensioned Slabs-On-Ground*, 2<sup>nd</sup> Edition, Post Tensioning Institute, Phoenix, AZ.
- Puzrin, A. M., and Burland, J. B. (1996), "A Logarithmic Stress-Strain Function for Rocks and Soils," *Geotechnique*, Vol. 46, No. 1, pp. 157-164.
- Qian, X., Gray, D. H., and Woods, R. D. (1993), "Voids and Granulometry: Effects on Shear Modulus of Unsaturated Sands," *Journal of Geotechnical Engineering*, ASCE, Vol. 119, No. 2, pp. 295-314.
- Ray, R. P., and Woods, R. D. (1988), "Modulus and Damping Due to Uniform and Variable Cyclic Loading," *Journal of Geotechnical and Geoenvironmental Engineering*, ASCE, Vol. 114, No. 8, pp. 861-876.
- Reed, R. F., and Kelly, M. (2000), "Impact of Climatic Variation on Design Parameters for Slab on Ground Foundations in Expansive Soils," *Proceedings of Sessions of Geo-Denver 2000, Advances in Unsaturated Geotechnics*, ASCE, Geotechnical Special Publication, No. 99, Denver, CO, pp. 435-455.
- Richards, B. G. (1965), "Measurement of the Free Energy of Soil Moisture by the Psychrometric Technique Using Thermistors," *Moisture Equilibria and Moisture Changes in Soils beneath Covered Areas*, Butterworths, pp. 39-46.
- Richart, F.E., Jr. (1977), "Dynamic Stress-Strain Relations for Soils," *Proceedings of the 9<sup>th</sup> International Conference on Soil Mechanics and Foundation Engineering*, Tokyo, Vol. 2, pp. 605-612.

- Richart, F. E., Jr., Hall, J. R., and Woods, R. D. (1970), *Vibration of Soils and Foundations*, Prentice-Hall, Inc., NJ.
- Rinaldi, V. A., Santamarina, J. C., and Redolfi, E. R. (1998), "Characterization of Collapsible Soils with Combined Geophysical and Penetration Testing," *Proceedings of the 1<sup>st</sup> International Conference on Site Characterization*, Balkema, Brookfield, pp. 581-588.
- Rix, G. J., and Stokoe, K. H., II (1989), "Stiffness Profiling of Pavement Subgrades," *Transportation Research Record*, No. 1235, Washington, D.C., pp. 1-9.
- Robertson, P. K., Campanella, R. G., Gillespie, D., and Rice, A. (1986), "Seismic CPT to Measure In Situ Shear Wave Velocity," *Journal of Geotechnical Engineering*, ASCE, Vol. 112, No. 8, pp. 71-803.
- Roesler, S. K. (1979), "Anisotropic Shear Modulus due to Stress Anisotropy," *Journal of the Geotechnical Engineering Division*, ASCE, Vol. 105, No. GT7, pp. 871-880.
- Russam, K. (1958), "An Investigation into the Soil Moisture Conditions under Roads in Trinidad, B. W. I.," *Geotechnique*, Vol. 8, No. 1, pp. 57-71.
- Russam, K. (1965), "The Prediction of Subgrade Moisture Conditions for Design Purposes," *Moisture Equilibria and Moisture Changes in Soils Beneath Covered Areas*, Butterworth, Sydney, Australia.
- Russam, K., and Coleman, J. D. (1961), "The Effect of Climatic Factors on Subgrade Moisture Conditions," *Geotechnique*, Vol. 11, No. 1, pp. 22-28.
- Saada, A. S. (1988), "Hollow Cylinder Torsional Devices: Their Advantages and Limitation," *Advanced Triaxial Testing of Soil and Rock*, ASTM STP 977, Philadelphia, PA. pp. 766-779.
- Sanchez-Salinero, I., Roesset, J. M., Shao, K., Stokoe, K. H., II, and Rix, G. J. (1987), "Analytical Evaluation of Variables Affecting Surface Wave Testing of Pavements," *Transportation Research Record 1136*, Washington, D.C., pp. 132-144.
- Santamarina, J. C., Klein, K. A., and Fam, M. A. (2001), *Soils and Waves*, John Wiley & Sons, Chichester, UK.
- Sargand, S. M. (2001), "Direct Measurement of Backfill Stiffness for Installation and Design of Buried Pipes," *Ohio Research Institute for Transportation and the Environment*, Ohio University, Athens, OH.

- Sargand, S. M., Edwards, W. F., and Salimath, S. (2000a), "Evaluation of Soil Stiffness via Non-Destructive Testing," *Ohio Research Institute for Transportation and the Environment*, Ohio University, Athens, OH.
- Sauer, E. K., and Monismith, C. L. (1968), "Influence of Soil Suction on Behavior of a Glacial Till Subjected to Repeated Loading," *Highway Research Record*, No. 215, Washington, D.C., pp. 18-23.
- Sawanguriya, A., Bosscher, P. J., and Edil, T. B. (2002), "Laboratory Evaluation of the Soil Stiffness Gauge," *Transportation Research Record*, No. 1808, Washington, D.C., pp. 30-37.
- Sawanguriya, A., Edil, T. B., and Bosscher, P. J. (2003), "Relationship between Soil Stiffness Gauge Modulus and Other Test Moduli for Granular Soils," *Transportation Research Record*, No. 1849, Washington, D.C., pp. 3-10.
- Sawanguriya, A., Edil, T. B., and Bosscher, P. J. (2004), "Assessing Small-Strain Stiffness of Soils Using the SSG," *Proceedings of the 15<sup>th</sup> Southeast Asia Geotechnical Conference*, Bangkok, Thailand, pp. 101-106.
- Sawanguriya, A., Edil, T. B., and Bosscher, P. J. (2005), "Stiffness Behavior of an Unsaturated Pavement Subgrade Soil," *Proceedings of International Conference on Problematic Soils*, Famagusta, N. Cyprus, pp. 209-217.
- Saxena, S. K., Avramidis, A. S., and Reddy, K. R. (1988), "Dynamic Moduli and Damping Ratios for Cemented Sands at Low Strains," *Canadian Geotechnical Journal*, Vol. 25, No. 2, pp. 353-368.
- Seed, H. B., and Idriss, I. M. (1970), "Soil Moduli and Damping Factors for Dynamic Response Analyses," *Report EERC 70-10*, Earthquake Engineering Research Center, University of California, Berkeley, CA.
- Shackel, B. (1973), "Changes in Soil Suction in a Sand-Clay Subjected to Repeated Triaxial Loading," *Transportation Research Record*, No. 429, Washington, D.C., pp. 29-39.
- Sharma, P. V. (1997), *Environmental and Engineering Geophysics*, Cambridge University Press, Cambridge, UK.
- Sheeran, D. E., Baker, W. H., and Krizek, R. J. (1967), "Experimental Study of Pulse Velocities in Compacted Soils," *Highway Research Record*, No. 177, Washington, D.C., pp. 226-238.
- Shibata, T., and Soelarno, D. S. (1975), "Stress-Strain Characteristics of Sands under Cyclic Loading," *Proceedings of the Japan Society of Civil Engineering*, No. 239, pp. 57-65. (in Japanese)

- Shibuya, S., Hwang, S. C., and Mitachi, T. (1997), "Elastic Shear Modulus of Soft Clays from Shear Wave Velocity Measurement," *Geotechnique*, Vol. 47, No. 3, pp. 593-601.
- Shibuya, S., Mitachi, T., Fukuda, F., and Degoshi, T. (1995), "Strain Rate Effect on Modulus and Damping of Normally Consolidated Clay," *Geotechnical Testing Journal*, ASTM, Vol. 18, No. 3, pp. 365-375.
- Shibuya, S., and Tanaka, H. (1996), "Estimate of Elastic Shear Modulus in Holocene Soil Deposits," *Soils and Foundations*, Vol. 36, No. 4, pp. 45-55.
- Shibuya, S., Tatsuoka, S., Teachavorasinskun, S., Kong, X. J., Abe, F., Kim, Y. S., and Park, C. S. (1992), "Elastic Deformation Properties of Geomaterials," *Soils and Foundations*, Vol. 32, No. 3, pp. 26-46.
- Siekmeier, J. A., Young, D., and Beberg, D. (1999), "Comparison of the Dynamic Cone Penetrometer with Other Tests during Subgrade and Granular Base Characterization in Minnesota," *Nondestructive Testing of Pavements and Backcalculation of Moduli*, ASTM STP 1375, West Conshohocken, PA, pp. 175-188.
- Silver, M. L., and Park, T. K. (1975), "Testing Procedure Effects on Dynamic Soil Behavior," *Journal of the Geotechnical Engineering Division*, ASCE, Vol. 101, No. GT10, pp. 1061-1083.
- Silver, M. L., and Seed, H. B. (1971), "Deformation Characteristics of Sands under Cyclic Loading," *Journal of the Soil Mechanics and Foundations Division*, ASCE, Vol. 97, No. SM8, pp. 1081-1098.
- Silvestri, F. (1991), "Stress-Strain Behaviour of Natural Soils by Means of Cyclic/Dynamic Torsional Shear Tests," *Experimental Characterization and Modelling of Soils and Soft Rocks*, The University of Napoli Federico, pp. 7-73.
- Souto, A., Hartikainen, J., and Özüdoğru, K. (1994), "Measurement of Dynamic Parameters of Road Pavement Materials by the Bender Element and Resonant Column Tests," *Geotechnique*, Vol. 44, No. 3, pp. 519-526.
- Stanculescu, I., and Fodor, G. (1975), "Influence of Climatic Factors on the Elastic Pavements Deformability," *Symposium on Recent Developments in the Analysis of Soil Behavior and their Application to Geotechnical Structures*, pp. 471-485.
- Stokoe, K. H., II, Hwang, S. K., Lee, J. N.-K., and Andrus, R. D. (1995), "Effects of Various Parameters on the Stiffness and Damping of Soils at Small to Medium Strains," *Pre-failure Deformation of Geomaterials*, Balkema, Rotterdam, Vol. 2, pp. 785-816.

- Stokoe, K. H., II, Lee, S. H. H., and Knox, D. P. (1985), "Shear Moduli Measurement under True Triaxial Stresses," *Proceedings of the Geotechnical Engineering Division: Advances in the Art of Testing Soil Under Cyclic Conditions*, ASCE, Detroit, MI, pp. 166-185.
- Stokoe, K. H., II and Richart, F. E., Jr. (1973), "In Situ and Laboratory Shear Wave Velocities," *Proceedings of the 8<sup>th</sup> International Conference on Soil Mechanics and Foundation Engineering*, Vol. 1, Part 2, Moscow, U.S.S.R., pp. 403-409.
- Stokoe, K. H., II and Woods, R. D. (1972), "In Situ Shear Wave Velocity by Cross-Hole Method," *Journal of the Soil Mechanics and Foundations Division*, ASCE, Vol. 98, No. SM5, pp. 443-460.
- Swenson, J., Guzina, B., Labuz, J., and Drescher, A. (2006), *Moisture Effects on PVD and DCP Measurements*, Final Report 2006-26, Minnesota Department of Transportation, St. Paul, MN
- Tatsuoka, F., Jardine, R. J., Lo Presti, D. C. F., Di Benedetto, H., and Kodako, T. (1997), "Characterizing the Pre-Failure Deformation Properties of Geomaterials," *Proceedings of the 14<sup>th</sup> International Conference of Soil Mechanics and Foundation Engineering*, Hamburg, Germany, Vol. 4, pp. 2129-2164.
- Tatsuoka, F., Siddiquee, M. S., Park, C. S., Sakamoto, M., and Abe, F. (1993), "Modeling Stress-Strain Relations of Sand," *Soils and Foundations*, Vol. 33, No. 2, pp. 60-81.
- Tatsuoka, F., and Shibuya, S. (1991), "Deformation Characteristics of Soils and Rocks from Field and Laboratory Tests," *Proceedings of the 9<sup>th</sup> Asian Regional Conference on Soil Mechanics and Foundation Engineering*, Bangkok, Thailand, Vol. 2, pp. 101-170.
- Thomann, T. G., and Hryciw, R. D. (1990), "Laboratory Measurement of Small Strain Shear Modulus under  $K_0$  Conditions," *Geotechnical Testing Journal*, ASTM, Vol. 13, No. 2, pp. 97-105.
- Thorntwaite, C. W. (1948), "An Approach toward a Rational Classification of Climate," *Geographical Review*, Vol. 38, No. 1, pp. 55-94.
- Tian, P., Zaman, M. M., and Laguros, J. G. (1998), "Gradation and Moisture Effects on Resilient Moduli of Aggregate Bases," *Transportation Research Record*, No. 1619, Washington, D.C., pp. 75-83.
- Timoshenko, S. P., and Goodier, J. N. (1951), *Theory of Elasticity*, McGraw-Hill, NY.

- Tinjum, J. M., Benson, C. H., and Blotz, L. R. (1997), "Soil-Water Characteristic Curves for Compacted Clays," *Journal of Geotechnical and Geoenvironmental Engineering*, ASCE, Vol. 123, No. 11, pp. 1060-1069.
- Trudeau, P. J., Whitman, R. V., and Christian, J. T. (1974), "Shear Wave Velocity and Modulus of a Marine Clay," *Journal of the Boston Society of Civil Engineers*, Vol. 61, No. 1, pp. 12-25.
- van Genuchten, M. (1980), "A Closed-Form Equation for Predicting the Hydraulic Conductivity of Unsaturated Soils," *Soil Science Society of America Journal*, Vol. 44, pp. 892-898.
- van Genuchten, M., Leij, F., and Yates, S. (1991), "The RETC Code Quantifying the Hydraulic Functions of Unsaturated Soils," *Report No. EPA/600/2-91/065*, U.S., EPA, Office of Research and Development, Washington, D.C.
- Vanapalli, S. K. (1994), "Simple Test Procedures and their Interpretation in Evaluating the Shear Strength of an Unsaturated Soil," *Ph.D. Thesis*, The University of Saskatchewan, Canada.
- Vanapalli, S. K., Fredlund, D. G., and Pufahl, D. E. (1999), "The Influence of Soil Structure and Stress History on the Soil-Water Characteristics of a Compacted Till," *Geotechnique*, Vol. 49, No. 2, pp. 143-159.
- Vanapalli, S. K., Fredlund, D. G., Pufahl, D. E., and Clifton, A. W. (1996), "Model for the Prediction of Shear Strength with Respect to Soil Suction," *Canadian Geotechnical Journal*, Vol. 33, No. 3, pp. 379-392.
- Viggiani, G., and Atkinson, J. H. (1995a), "Stiffness of Fine-Grained Soil at Very Small Strains," *Geotechnique*, Vol. 45, No. 2, pp. 249-265.
- Viggiani, G., and Atkinson, J. H. (1995b), "Interpretation of Bender Element Tests," *Geotechnique*, Vol. 45, No. 1, pp. 149-154.
- Viggiani, G., and Atkinson, J. H. (1997), Discussion: "Interpretation of Bender Element Tests," *Geotechnique*, Vol. 47, No. 4, pp. 873-877.
- Vucetic, M., and Dobry, R. (1991), "Effect of Soil Plasticity on Cyclic Response," *Journal of Geotechnical Engineering*, ASCE, Vol. 117, No. 1, pp. 89-107.
- Wan, A. W.-L., Gray, M. N., and Graham, J. (1995), "On the Relations of Suction Moisture Content and Soil Structure in Compacted Clays," *Proceedings of the 1<sup>st</sup> International Conference on Unsaturated Soils*, Paris, France, pp. 215-222.
- Weaver, E., Ormsby, W. C., and Zhao, X. (2001), *Pavement Variability Study: Phase I Interim Report*, National Pooled Fund Study 2(212), Non-Nuclear Testing of Soils

and Granular Bases Using the GeoGauge (Soil Stiffness Gauge) and Other Similar Devices, U.S. Department of Transportation, Federal Highway Administration.

Wilson, S. D., and Dietrich, R. J. (1960), "Effect of Consolidation Pressure on Elastic and Strength Properties of Clay," *Proceedings of the Soil Mechanics and Foundations Division, Research Conference on Shear Strength of Cohesive Soils*, ASCE, Boulder, CO, pp. 419-435.

Woods, R. D. (1978), "Measurement of Dynamic Soil Properties," *Proceedings of the Earthquake Engineering and Soil Dynamics Specialty Conference*, ASCE, Pasadena, CA, Vol. 1, pp. 91-178.

Wright, S. G., Stokoe, K. E., II, and Roesset, J. M. (1994), "SASW Measurements at Geotechnical Sites Overlaid by Water," *Dynamic Geotechnical Testing II, ASTM STP 1213*, Philadelphia, PA, pp. 39-57.

Wu, W., Arellano, M., Chen, D.-H., Bilyeu, J., and He., R. (1998), "Using a Stiffness Gauge as an Alternative Quality Control Device in Pavement Construction," *Texas Department of Transportation Report*, Austin, TX.

Wu, S., Gray, D. H., and Richart, F. E., Jr. (1984), "Capillary Effects on Dynamic Modulus of Sands and Silts," *Journal of the Geotechnical Engineering Division*, ASCE, Vol. 110, No. GT9, pp. 1188-1203.

Yesiller, N., Inci, G., and Miller, C. J. (2000), "Ultrasonic Testing for Compacted Clayey Soils," *Proceedings of Sessions of Geo-Denver 2000, Advances in Unsaturated Geotechnics*, ASCE, Geotechnical Special Publication, No. 99, Denver, CO, pp. 54-68.

Yu, P., and Richart, F. E., Jr. (1984), "Stress Ratio Effects on Shear Modulus of Dry Sands," *Journal of the Geotechnical Engineering Division*, ASCE, Vol. 110, No. GT3, pp. 331-345.

Yuan, D., and Nazarian, S. (2003), "Variation in Moduli of Base and Subgrade with Moisture," *Transportation Research Board 82<sup>nd</sup> Annual Meeting*, Washington, D.C. (CD-ROM)

Yun, T. S., and Santamarina, J. C. (2005), "Decementation, Softening, and Collapse: Changes in Small-Strain Shear Stiffness in  $K_0$  Loading," *Journal of Geotechnical and Geoenvironmental Engineering Division*, ASCE, Vol. 131, No. 3, pp. 350-358.

Zen, K., Umehara, Y., and Hamada, K. (1978), "Laboratory Tests and In Situ Seismic Survey on Vibratory Shear Modulus of Clayey Soils with Various Plasticities," *Proceedings of the 5<sup>th</sup> Japanese Earthquake Engineering Symposium*, pp. 721-728.

Zeng, X., and Ni, B. (1998), "Application of Bender Elements in Measuring  $G_{\max}$  of Sand under  $K_0$  Condition," *Geotechnical Testing Journal*, ASTM, Vol. 21, No. 3, pp. 251-263.

**APPENDIX B: SPECIMEN PREPARATION  
AND MR TESTING PROTOCO**

## **B1. Specimen Preparation**

According to NCHRP 1-28A, the definition of a certain type of material is related to both the process of preparing the material for compaction and the method of compaction. Fig. B-1 illustrates the classification of the test soils for MR test in accordance with NCHRP 1-28A. For laboratory compacted specimens, all of the test soils in this study are classified as Type 3, which includes all untreated subgrade soils with a maximum particle size less than 9.5 mm (0.375 in) and more than 10% passing the 75  $\mu$ m (No. 200) sieve (see Fig. B-1). In addition, since the maximum particle size of test soils is less than 19 mm (0.75 in), a 102 mm (4 in) diameter by 204 mm (8 in) high specimen will be used in the study.

The methods of compaction in the NCHRP protocol are a function of the material type, mechanical behavior of the material, and field conditions (NCHRP 1-28A, 2003). NCHRP 1-28A recommends that for the Type 3 soils, either impact or kneading compaction shall be used. Since no significant difference in soil structure for fine-grained materials (i.e., Type 3) compacted using either impact or kneading compaction (NCHRP 1-28A, 2003), the impact compaction procedure is selected for preparing the soil specimens for the MR testing. The specimen were compacted in a 102 mm (4 in) diameter mold with a 5.5 lbf (24.4 N) rammer dropped from a height of 305 mm (12 in) producing a standard compactive effort of 600 kN-m/m<sup>3</sup> (12,400 ft-lbf/ft<sup>3</sup>). Since the maximum particle size less than 19 mm (0.75 in), Procedure A of impact compaction procedure was selected. The specimen were compacted in eight layers in accordance with Procedure A of impact compaction procedure. For a 102-mm by 204-mm specimen compacted with standard compactive effort, the number of blows per layer is calculated to be about 17 based on the equation suggested in the impact compaction procedure, however, the number of blows per layer needs to be adjusted to achieve the target density.

B-2. Summary of NCHRP 1-28A Test Protocol

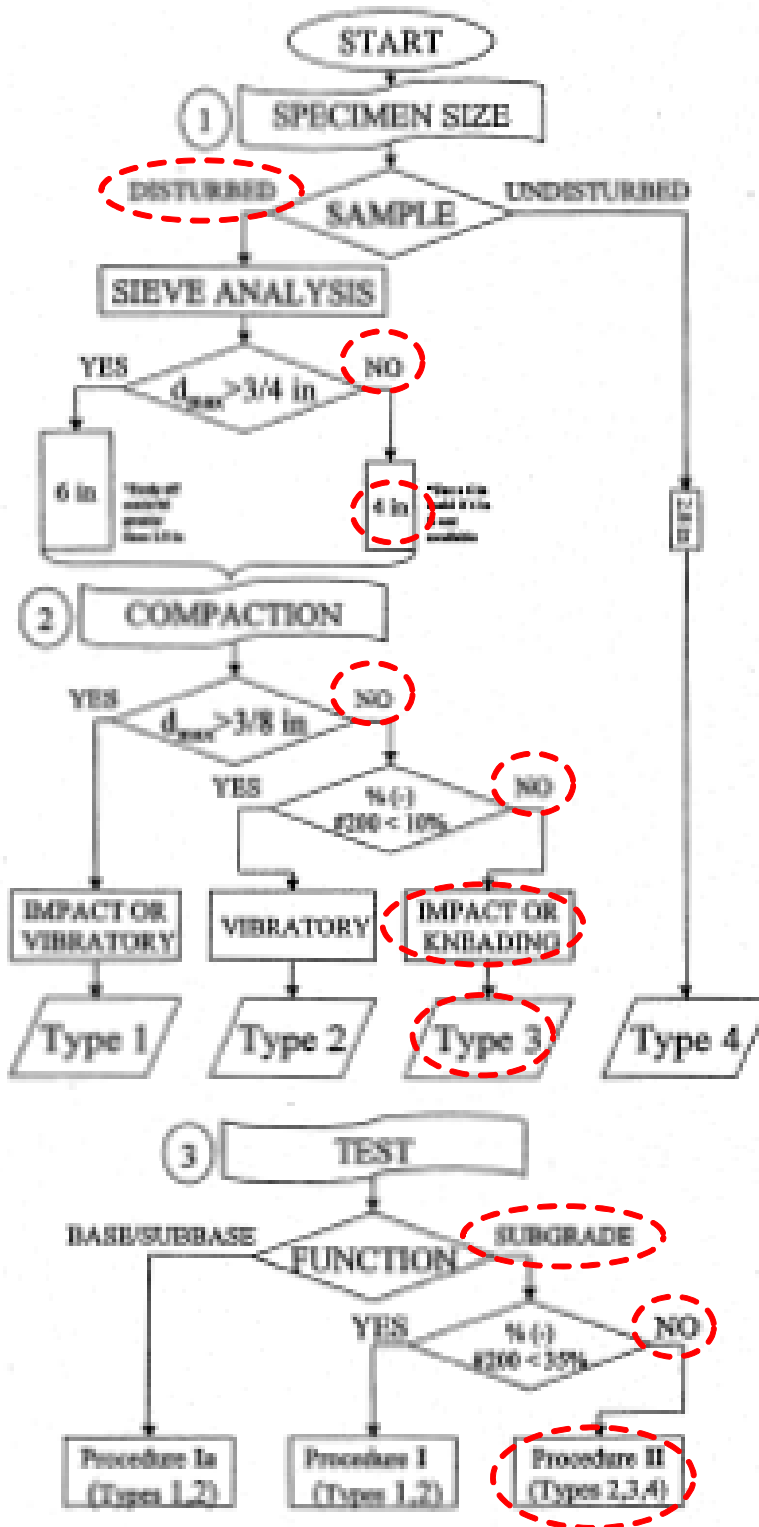


Fig. B-1. Classification of test soils for MR test in accordance with NCHRP 1-28A.

Table B-1. Test sequence for fine-grained subgrades (NCHRP 1-28A: Procedure II)

Sequence	Confining Pressure		Contact Stress		Cyclic Stress		Principal Stresses Ratio	Maximum Stress		$\sigma_1$		Number of Repetition
	(psi)	(kPa)	(psi)	(kPa)	(psi)	(kPa)		(psi)	(kPa)	(psi)	(kPa)	
Conditioning	4.0	27.6	0.8	5.5	7.0	48.3	2.8	7.8	53.8	11.8	81.4	1000
1	8.0	55.2	1.6	11.0	4.0	27.6	1.5	5.6	38.6	13.6	93.8	100
2	6.0	41.4	1.2	8.3	4.0	27.6	1.7	5.2	35.9	11.2	77.3	100
3	4.0	27.6	0.8	5.5	4.0	27.6	2.0	4.8	33.1	8.8	60.7	100
4	2.0	13.8	0.4	2.8	4.0	27.6	3.0	4.4	30.4	6.4	44.2	100
5	8.0	55.2	1.6	11.0	7.0	48.3	1.9	8.6	59.3	16.6	114.5	100
6	6.0	41.4	1.2	8.3	7.0	48.3	2.2	8.2	56.6	14.2	98.0	100
7	4.0	27.6	0.8	5.5	7.0	48.3	2.8	7.8	53.8	11.8	81.4	100
8	2.0	13.8	0.4	2.8	7.0	48.3	4.5	7.4	51.1	9.4	64.9	100
9	8.0	55.2	1.6	11.0	10.0	69.0	2.3	11.6	80.0	19.6	135.2	100
10	6.0	41.4	1.2	8.3	10.0	69.0	2.7	11.2	77.3	17.2	118.7	100
11	4.0	27.6	0.8	5.5	10.0	69.0	3.5	10.8	74.5	14.8	102.1	100
12	2.0	13.8	0.4	2.8	10.0	69.0	6.0	10.4	71.8	12.4	85.6	100
13	8.0	55.2	1.6	11.0	14.0	96.6	2.8	15.6	107.6	23.6	162.8	100
14	6.0	41.4	1.2	8.3	14.0	96.6	3.3	15.2	104.9	21.2	146.3	100
15	4.0	27.6	0.8	5.5	14.0	96.6	4.5	14.8	102.1	18.8	129.7	100
16	2.0	13.8	0.4	2.8	14.0	96.6	8.0	14.4	99.4	16.4	113.2	100

**APPENDIX C: MACHINE DRAWING OF SUCTION CELL,  
SPECIMEN MOUNTING IN THE SUCTION CELL, THERMAL  
DISSIPATION SENSOR AND SUCTION MEASUREMENT**

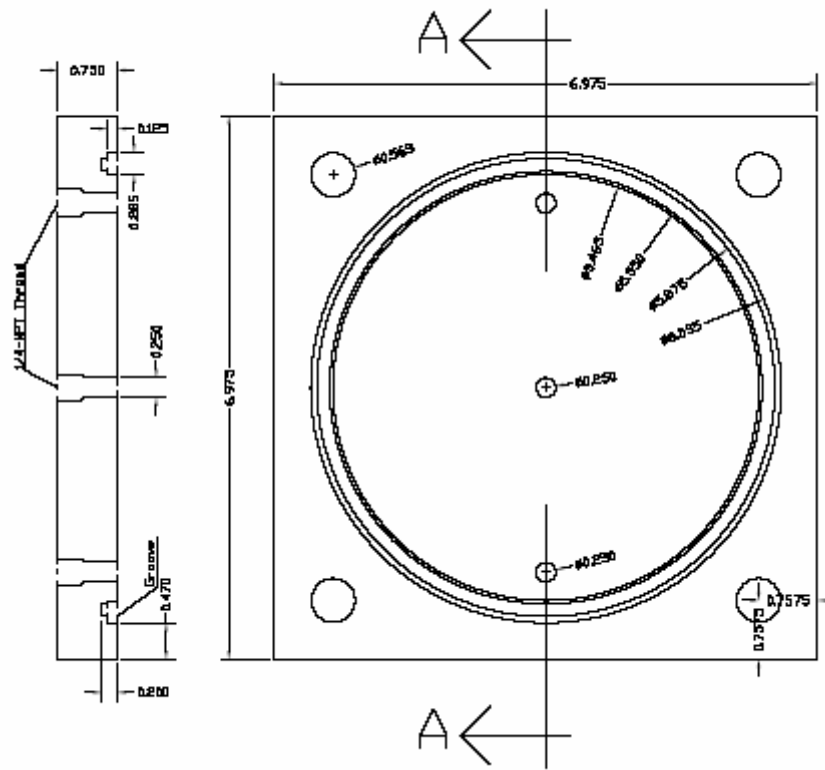


Fig. C-1. Aluminum top plate.

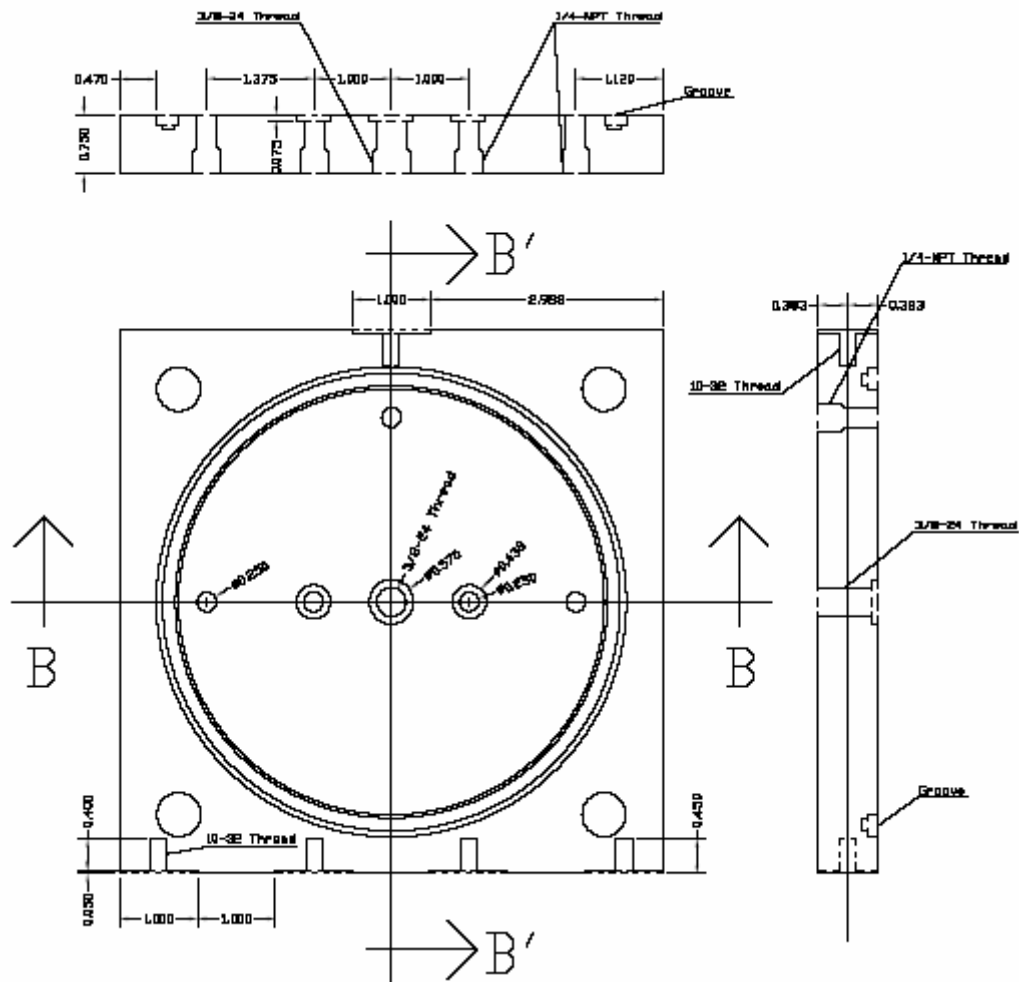


Fig. C-2. Aluminum base plate.

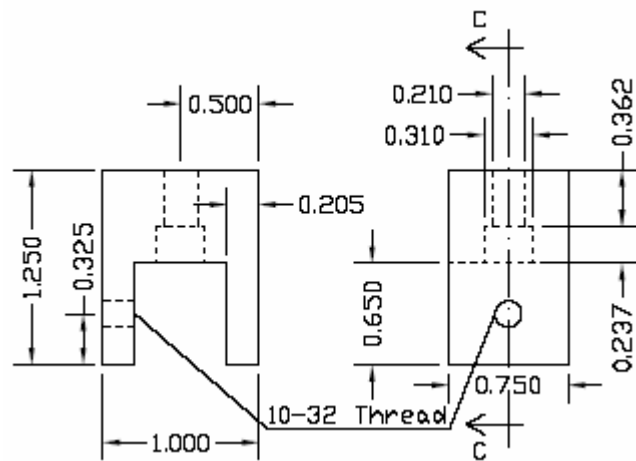


Fig. C-3. Aluminum socket.

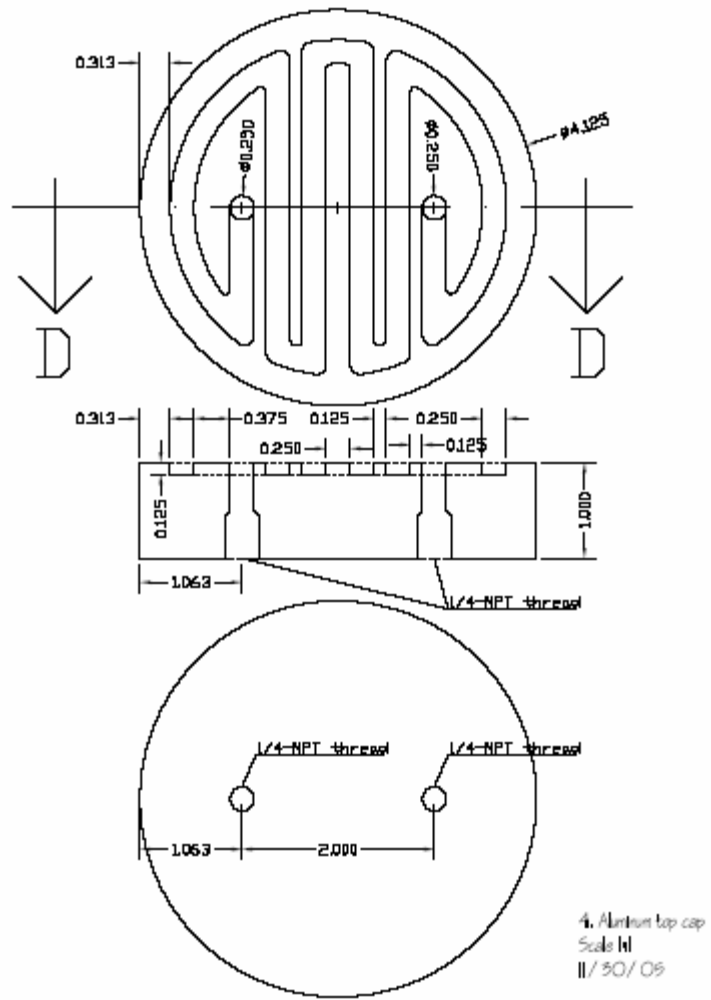


Fig. C-4. Aluminum top cap.

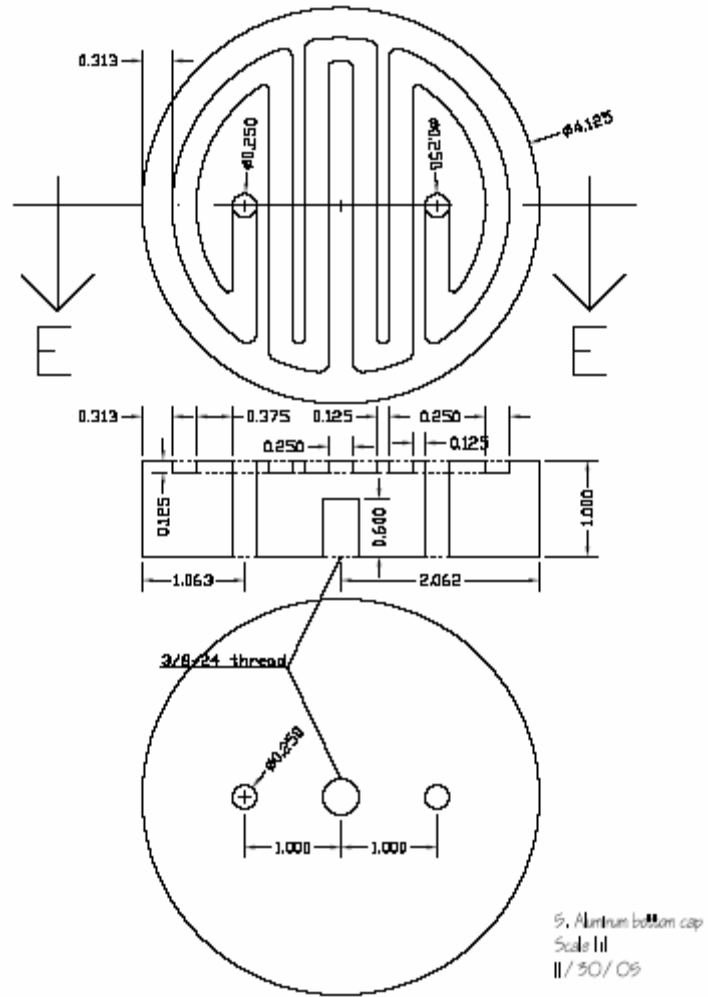
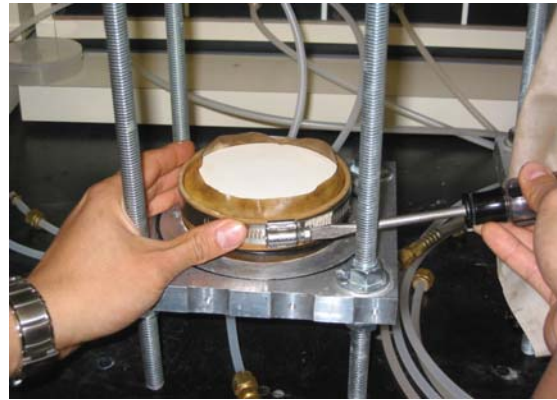


Fig. C-5. Aluminum pedestal.

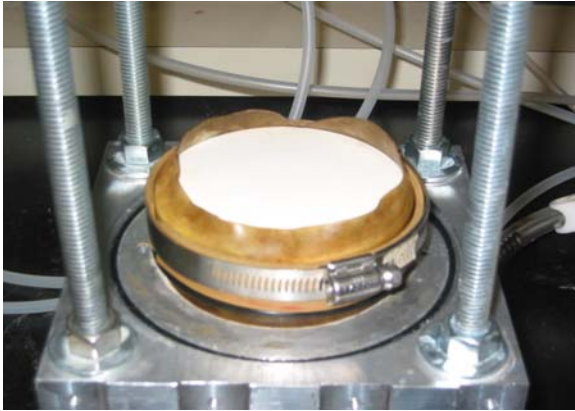
## MOUNTING OF SPECIMEN IN SUCTION CELL



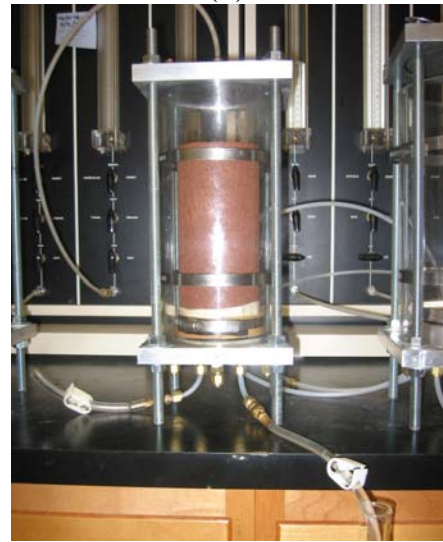
(a)



(b)

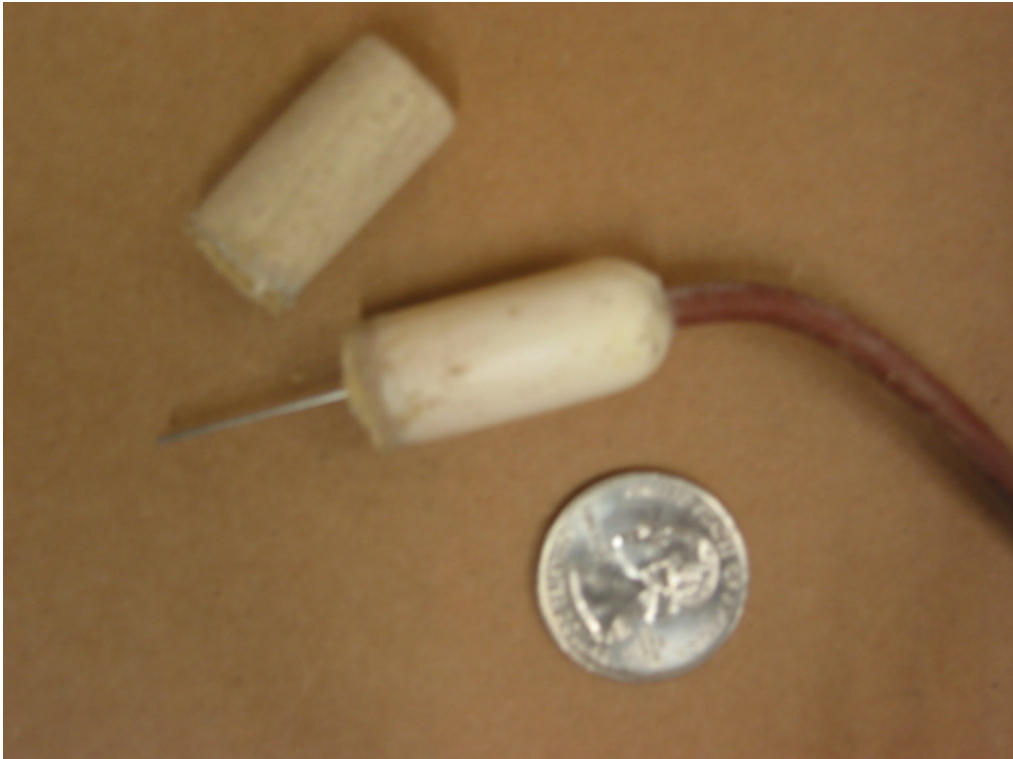


(c)

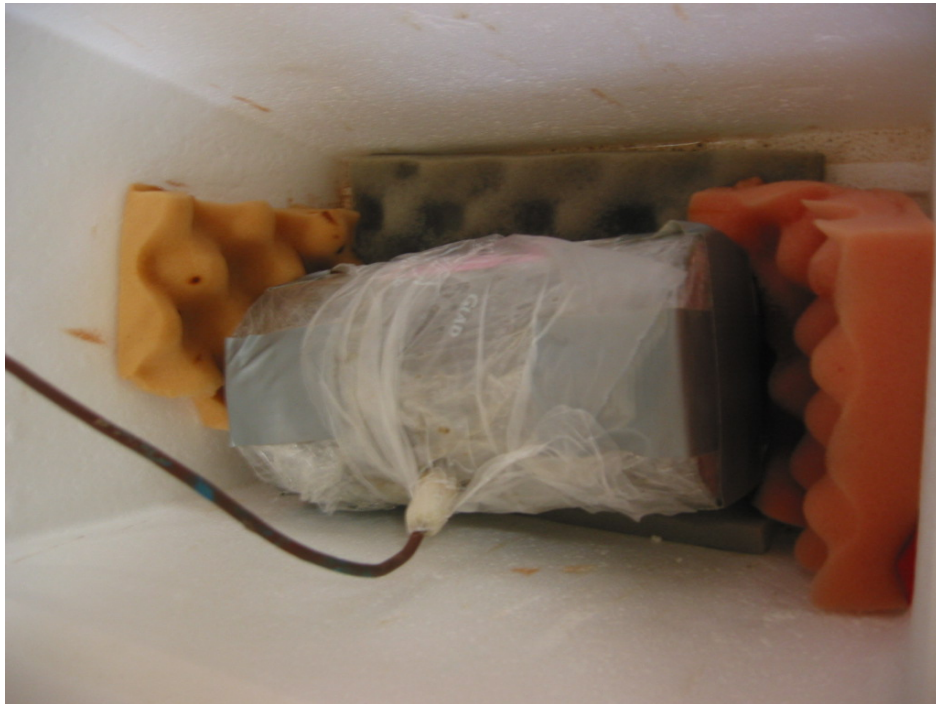


(d)

**THERMAL DISSIPATION SENSOR**



**SUCTION MEASUREMENT**



**APPENDIX D: POWER FUNCTION RELATIONSHIPS OF  
DEVIATOR STRESS TO TEXTURAL PROPERTIES  
AND PLASTIC LIMIT**

This appendix was put together by Satish Gupta and A. Ranivoson of the University of  
Minnesota

FOLLOWING DIAGRAMS ARE FOR 103% OF STANDRD PROCTOR DENSITY  
AND DEVIATOR STRESS AT 1% STRAIN

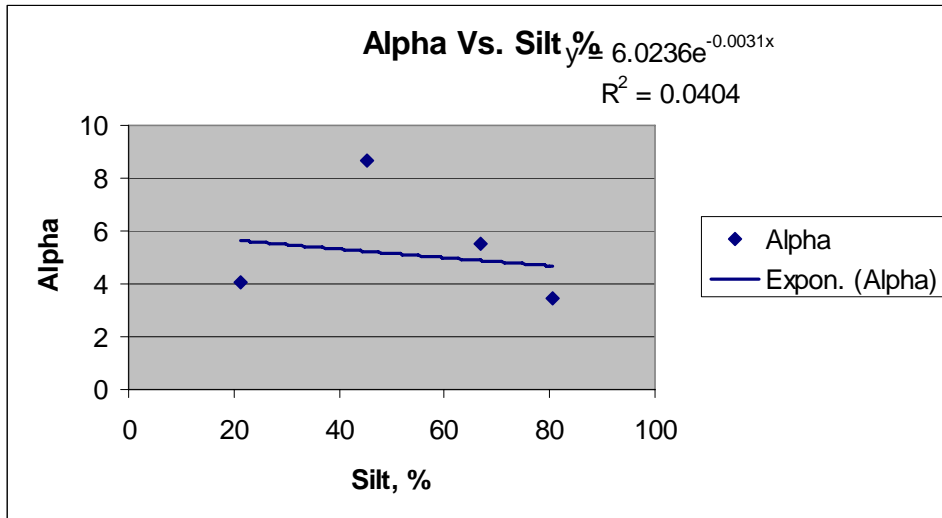


Figure 1D: Variation in the power function coefficient  $\alpha$  as a function of soil silt content.

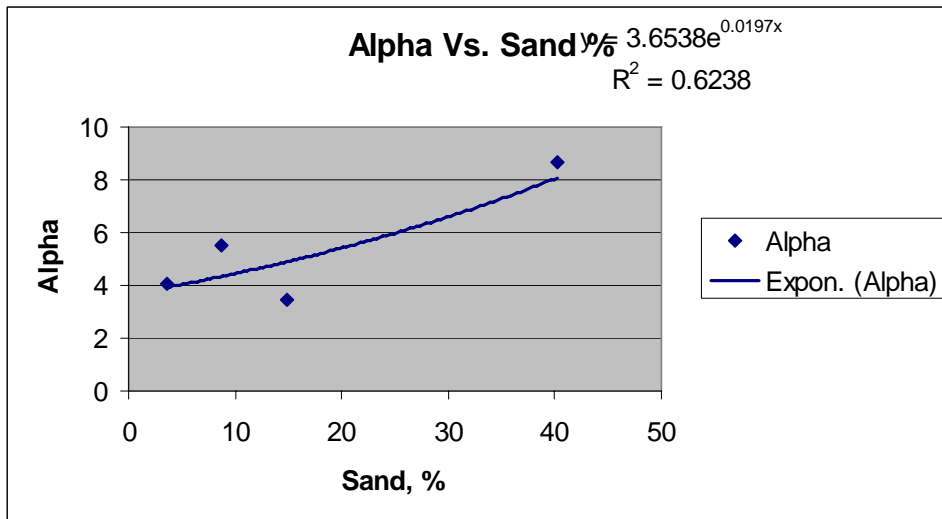


Figure 2D: Variation in the power function coefficient  $\alpha$  as a function of soil sand content.

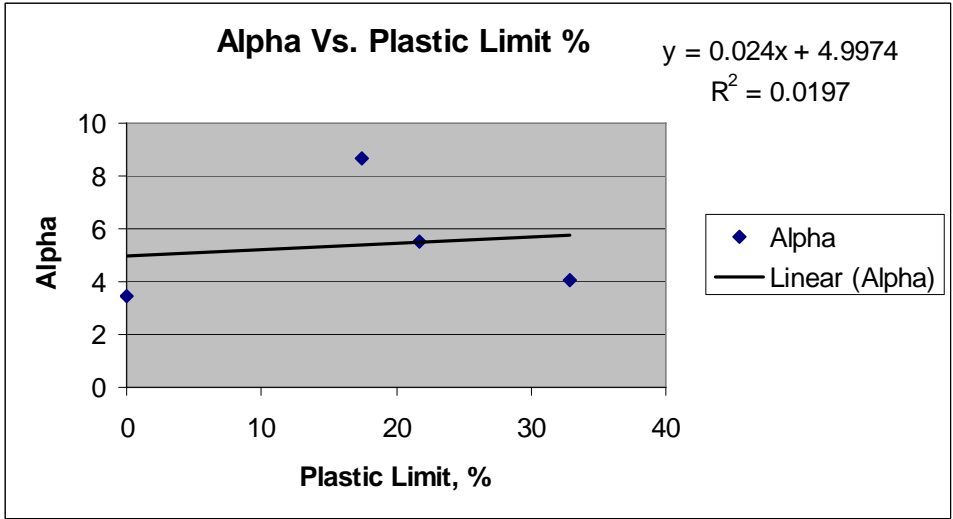


Figure 3D: Variation in the power function coefficient  $\alpha$  as a function of soil plastic limit.

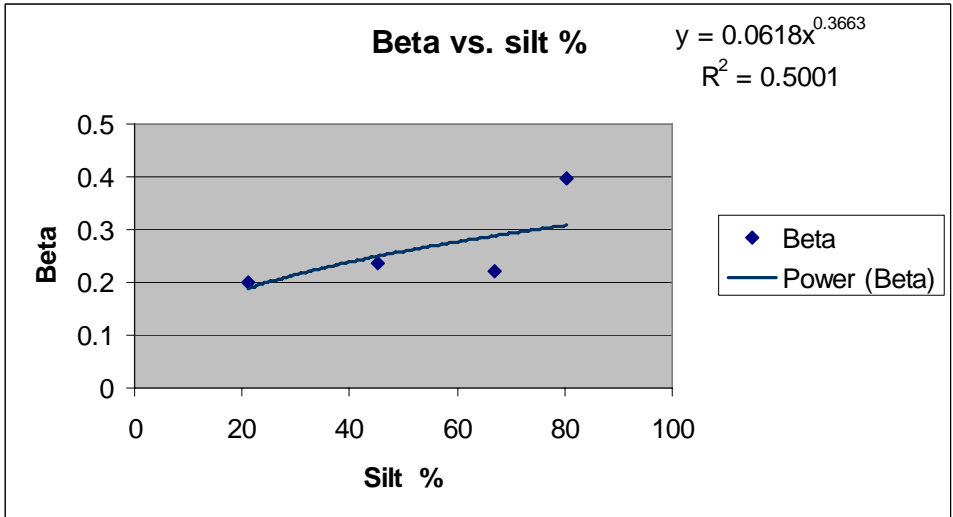


Figure 4D: Variation in the power function coefficient  $\beta$  as a function of soil silt content.

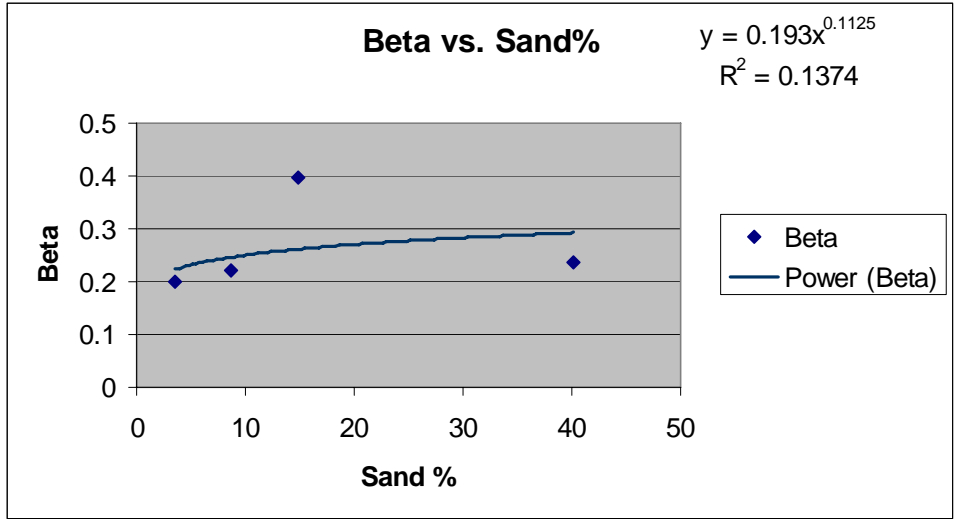


Figure 5D: Variation in the power function coefficient  $\beta$  as a function of soil sand content.

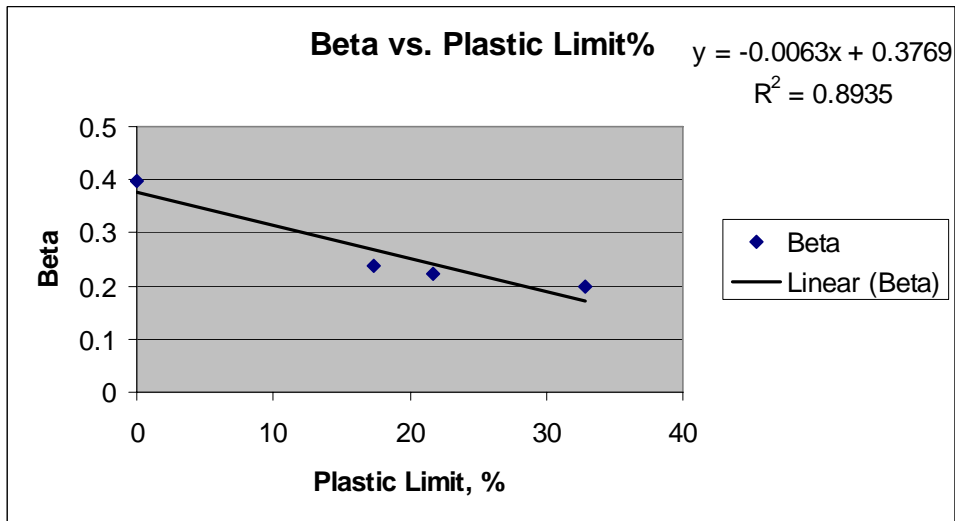


Figure 6D: Variation in the power function coefficient  $\beta$  as a function of soil plastic limit.

FOLLOWING DIAGRAMS ARE FOR 98% OF PROCTOR DENSITY AND  
DEVIATOR STRESS AT 1% STRAIN

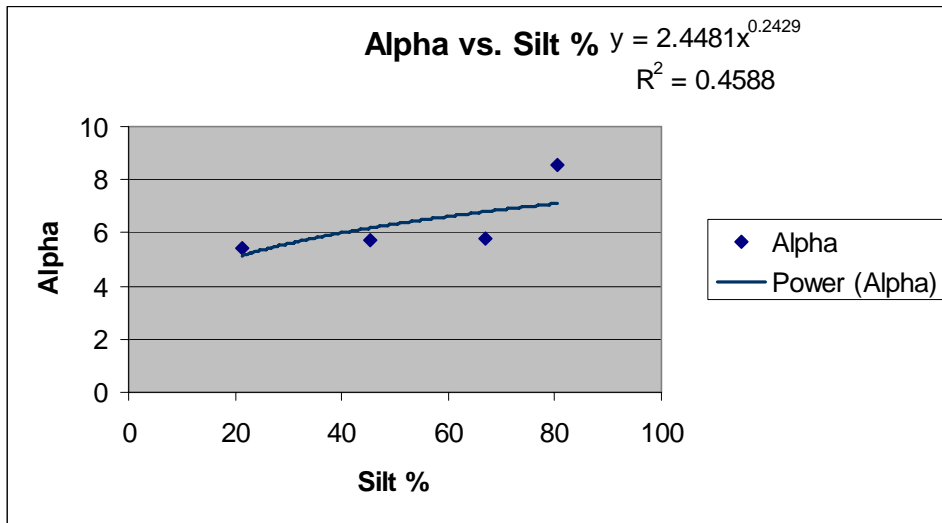


Figure 7D: Variation in the power function coefficient  $\alpha$  as a function of soil silt content.

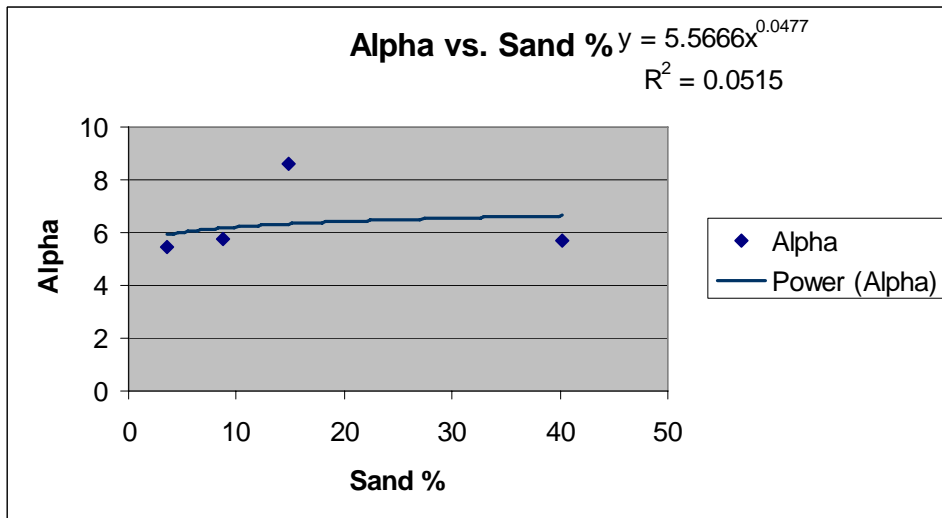


Figure 8D: Variation in the power function coefficient  $\alpha$  as a function of soil sand content.

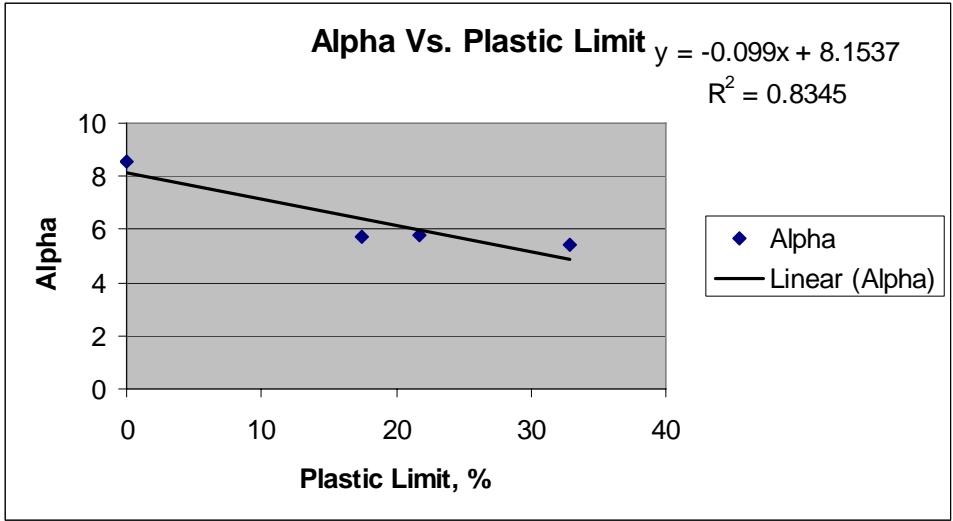


Figure 9D: Variation in the power function coefficient  $\alpha$  as a function of soil plastic limit.

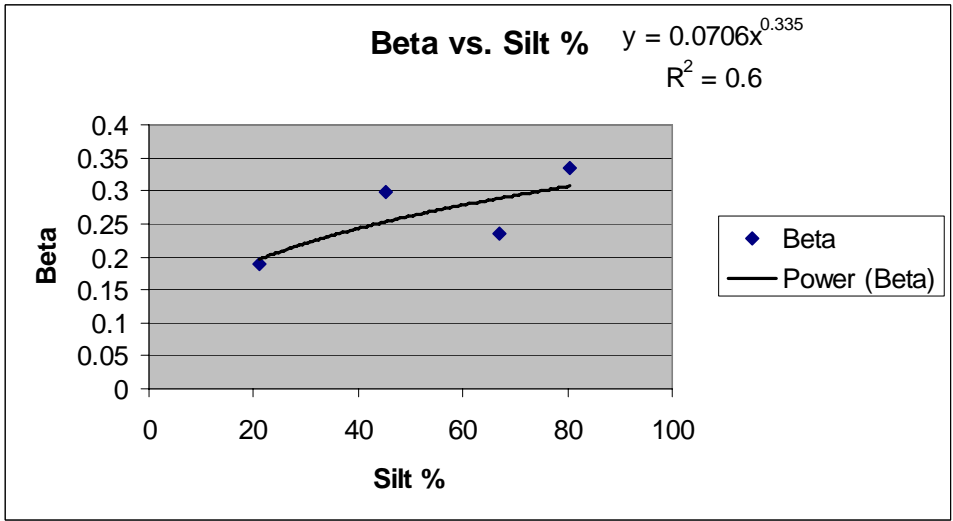


Figure 10D: Variation in the power function coefficient  $\beta$  as a function of soil silt content.

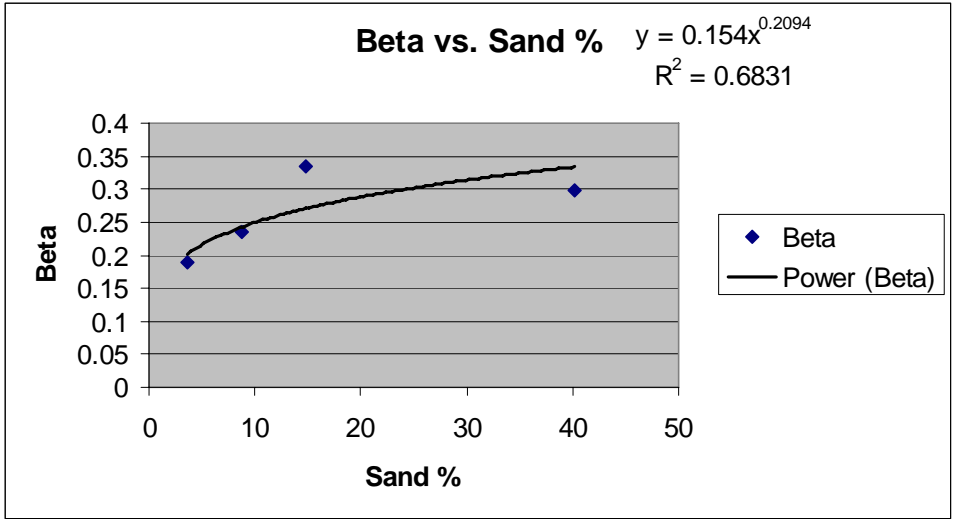


Figure 11D: Variation in the power function coefficient  $\beta$  as a function of soil sand content.

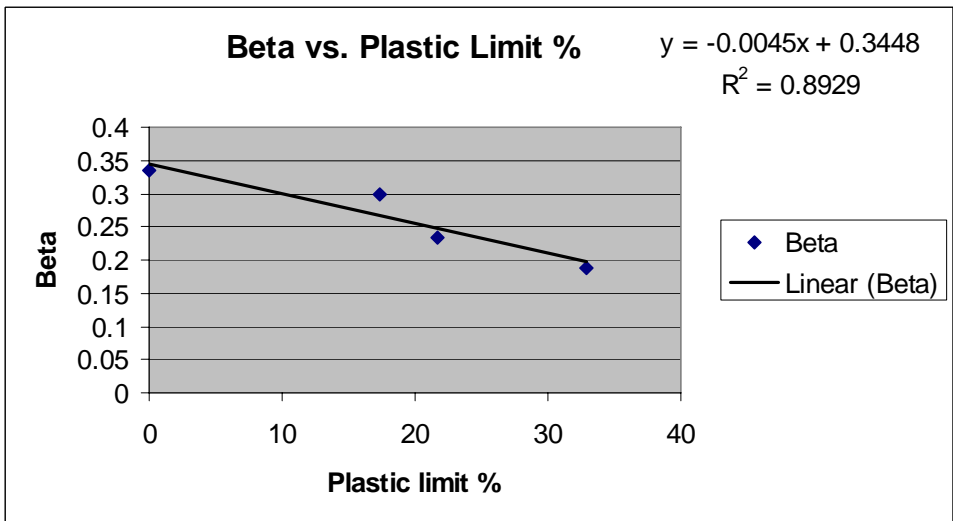


Figure 12D: Variation in the power function coefficient  $\beta$  as a function of soil plastic limit.

**APPENDIX E: RESILIENT MODULUS TEST DATA SHEETS**

**Specimen ID** MnRd-98%S0-R1 **Test Date** 7/19/2006

**Specimen Property**

*As-compacted state*

Dry unit weight 17.55 kN/m3  
 Moisture content 15.47%

*Post-compact state*

Matric suction 27.03 kPa  
 Moisture content 17.60%

**Specimen Geometry**

*As-compacted state*

Diameter 101.6 mm  
 Height 203.2 mm

*Post-compact state*

Diameter 101.6 mm  
 Height 204.8 mm

**MR Test Protocol NCHRP 1-28A**

Initial specimen height 204.8 mm  
 Final specimen height 199.0 mm  
 Final specimen diameter 103.0 mm  
 Initial gauge length 101.9 mm  
 Final gauge length 101.1 mm

**Bender Element Test**

Tip-to-tip distance 189 mm  
 Total unit weight 20.66 kN/m3  
 S-wave travel time 0.001257 second  
 Shear modulus 47608.90 kPa

Load Step	Deviator Stress (kPa)	Bulk Stress (kPa)	Confining Pressure (kPa)	Octahedral Shear Stress (kPa)	External LVDT 1 Deformation (mm)	External LVDT 2 Deformation (mm)	Internal LVDT 1 Deformation (mm)	Internal LVDT 2 Deformation (mm)	Measured MR-Ext (kPa)	Predicted MR-Ext (kPa)	Measured MR-Int (kPa)	Predicted MR-Int (kPa)
1	39.90	210.68	56.93	18.81	0.211	0.199	0.093	0.102	30317.51	27217.65	32012.47	28669.82
2	34.30	162.68	42.79	16.17	0.254	0.237	0.106	0.117	23868.76	23487.92	26371.87	24580.75
3	29.35	116.91	29.18	13.84	0.322	0.300	0.131	0.154	17755.31	19362.89	19460.37	20272.27
4	25.47	68.73	14.42	12.01	0.384	0.358	0.155	0.178	14818.48	14242.59	16558.78	15213.07
5	57.92	229.64	57.24	27.30	0.399	0.388	0.182	0.204	24448.45	25161.00	25043.02	26742.23
6	53.79	185.38	43.86	25.36	0.465	0.450	0.205	0.228	20980.36	22061.92	22262.79	23288.86
7	48.90	137.02	29.37	23.05	0.591	0.564	0.252	0.291	16438.20	18377.47	17564.17	19339.98
8	43.75	88.20	14.82	20.62	0.642	0.597	0.292	0.320	14629.05	14217.18	14894.33	15102.76
9	76.85	248.02	57.06	36.23	0.637	0.642	0.323	0.341	20902.00	23170.44	20251.14	24840.31
10	72.75	201.55	42.93	34.30	0.648	0.658	0.321	0.331	20390.39	20335.39	20521.19	21632.14
11	67.39	154.29	28.97	31.77	0.704	0.703	0.328	0.397	18413.04	17337.74	17963.89	18350.46
12	62.91	106.11	14.40	29.66	0.964	0.927	0.476	0.538	13401.97	13791.95	12561.09	14650.44
13	104.43	275.84	57.14	49.23	0.898	0.919	0.372	0.416	20763.10	20796.42	24055.13	22560.95
14	99.89	234.39	44.83	47.09	0.945	0.940	0.370	0.441	19836.97	18860.87	23171.83	20301.19
15	95.98	182.53	28.85	45.24	1.123	1.124	0.471	0.539	16587.35	15995.52	18540.62	17090.36
16	90.66	134.45	14.60	42.74	1.266	1.265	0.554	0.626	14526.74	13269.19	15651.85	14144.37

**Five-parameter log-log model**

External LVDTs		Internal LVDTs	
k1	<u>183.6838</u>	k1	<u>167.636</u>
k2	<u>0.896054</u>	k2	<u>1.041914</u>
k3	<u>-2.143079</u>	k3	<u>-2.150767</u>
k6	<u>-11.74816</u>	k6	<u>-21.83804</u>
k7	<u>1.024488</u>	k7	<u>1.086526</u>

**Specimen ID** MnRd-98%S22-R1 **Test Date** 7/6/2006

**Specimen Property**

*As-compacted state*

Dry unit weight 17.50 kN/m<sup>3</sup>  
 Moisture content 15.47%

*Post-compact state*

Matric suction 37.17 kPa  
 Moisture content 14.82%

**Specimen Geometry**

*As-compacted state*

Diameter 101.6 mm  
 Height 203.2 mm

*Post-compact state*

Diameter 101.6 mm  
 Height 203.8 mm

**MR Test Protocol NCHRP 1-28A**

Initial specimen height 203.8 mm  
 Final specimen height 203.3 mm  
 Final specimen diameter 101.6 mm  
 Initial gauge length 103.6 mm  
 Final gauge length 103.6 mm

**Bender Element Test**

Tip-to-tip distance 193.3 mm  
 Total unit weight 20.23 kN/m<sup>3</sup>  
 S-wave travel time 0.000908 second  
 Shear modulus 93404.98 kPa

Load Step	Deviator Stress (kPa)	Bulk Stress (kPa)	Confining Pressure (kPa)	Octahedral Shear Stress (kPa)	External LVDT 1 Deformation (mm)	External LVDT 2 Deformation (mm)	Internal LVDT 1 Deformation (mm)	Internal LVDT 2 Deformation (mm)	Measured MR-Ext (kPa)	Predicted MR-Ext (kPa)	Measured MR-Int (kPa)	Predicted MR-Int (kPa)
1	39.82	208.37	56.18	18.77	0.080	0.074	0.020	0.022	73042.24	72632.56	136770.91	128520.74
2	36.22	167.25	43.68	17.07	0.096	0.090	0.027	0.027	60650.70	60148.23	107643.28	107579.88
3	31.16	121.45	30.10	14.69	0.124	0.119	0.034	0.034	46350.06	45669.26	84932.73	85099.82
4	25.66	70.00	14.78	12.10	0.187	0.182	0.046	0.039	27058.07	27604.39	60191.18	58778.82
5	61.60	230.43	56.28	29.04	0.159	0.149	0.052	0.053	64795.35	66354.58	97327.57	105202.18
6	56.81	187.45	43.55	26.78	0.181	0.169	0.061	0.058	56910.33	56120.77	85310.85	89878.41
7	51.49	137.89	28.80	24.27	0.229	0.215	0.073	0.069	43442.02	43110.18	69235.76	71034.04
8	48.31	92.84	14.84	22.78	0.326	0.315	0.099	0.090	29450.73	29737.98	50792.70	52123.30
9	80.66	248.01	55.78	38.02	0.236	0.227	0.082	0.082	59675.90	61144.42	85738.10	88689.49
10	76.97	208.23	43.75	36.29	0.264	0.256	0.095	0.093	52990.72	52777.82	74526.79	76649.45
11	72.22	160.96	29.58	34.04	0.322	0.318	0.115	0.111	42733.84	42290.16	61501.31	62281.48
12	67.69	111.57	14.63	31.91	0.481	0.441	0.155	0.144	29135.52	30317.06	45774.37	46647.71
13	105.93	273.88	55.98	49.93	0.365	0.330	0.138	0.125	55392.77	55779.93	74561.15	72684.53
14	103.72	231.09	42.46	48.89	0.404	0.368	0.151	0.141	50000.62	47754.12	67376.35	61562.77
15	99.21	186.61	29.13	46.77	0.494	0.449	0.182	0.168	40690.29	39788.57	55886.55	51558.42
16	95.06	140.40	15.11	44.81	0.673	0.610	0.234	0.217	29473.79	30798.15	42734.61	40664.49

**Five-parameter log-log model**

External LVDTs		Internal LVDTs	
k1	<u>528.02</u>	k1	<u>699.6097</u>
k2	<u>1.009609</u>	k2	<u>1.440673</u>
k3	<u>-2.335943</u>	k3	<u>-3.921041</u>
k6	<u>0</u>	k6	<u>-22.80215</u>
k7	<u>1.010439</u>	k7	<u>1.057035</u>

**Specimen ID** MnRd-98%S50-R1 **Test Date** 7/1/2006

**Specimen Property**

*As-compacted state*

Dry unit weight 17.63 kN/m<sup>3</sup>  
 Moisture content 16.07%

*Post-compact state*

Matric suction 650.23 kPa  
 Moisture content 13.69%

**Specimen Geometry**

*As-compacted state*

Diameter 101.6 mm  
 Height 203.2 mm

*Post-compact state*

Diameter 101.6 mm  
 Height 200.0 mm

**MR Test Protocol NCHRP 1-28A**

Initial specimen height 200.0 mm  
 Final specimen height 200.0 mm  
 Final specimen diameter 101.6 mm  
 Initial gauge length 99.6 mm  
 Final gauge length 99.6 mm

**Bender Element Test**

Tip-to-tip distance 190.0 mm  
 Total unit weight 20.62 kN/m<sup>3</sup>  
 S-wave travel time 0.0006443 second  
 Shear modulus 182867.33 kPa

Load Step	Deviator Stress (kPa)	Bulk Stress (kPa)	Confining Pressure (kPa)	Octahedral Shear Stress (kPa)	External LVDT 1 Deformation (mm)	External LVDT 2 Deformation (mm)	Internal LVDT 1 Deformation (mm)	Internal LVDT 2 Deformation (mm)	Measured MR-Ext (kPa)	Predicted MR-Ext (kPa)	Measured MR-Int (kPa)	Predicted MR-Int (kPa)
1	41.35	216.10	58.25	19.49	0.051	0.045	0.007	0.013	119400.92	124041.65	282799.72	258010.93
2	38.73	165.48	42.25	18.26	0.056	0.049	0.010	0.017	108691.55	101960.86	204416.82	206433.14
3	34.48	119.83	28.45	16.25	0.067	0.062	0.012	0.021	87801.02	81099.53	166390.23	161279.73
4	31.15	74.79	14.55	14.68	0.106	0.102	0.020	0.030	54382.70	56883.54	113086.29	109926.71
5	62.14	235.91	57.92	29.29	0.092	0.086	0.023	0.029	109239.97	115540.19	185273.31	212258.02
6	58.60	188.86	43.42	27.62	0.098	0.094	0.025	0.035	101040.93	98894.72	162607.07	178758.67
7	54.51	141.35	28.95	25.70	0.124	0.120	0.029	0.043	80133.15	80507.48	133991.90	142715.44
8	51.32	94.76	14.48	24.19	0.181	0.176	0.043	0.059	55215.05	59640.18	96916.74	102432.52
9	83.13	253.28	56.72	39.19	0.127	0.121	0.036	0.044	111242.12	107158.78	171728.31	174937.47
10	79.09	208.76	43.22	37.29	0.148	0.145	0.041	0.052	93882.23	94025.93	148281.23	151887.93
11	75.43	162.70	29.09	35.56	0.174	0.172	0.047	0.062	79216.05	78712.31	125500.43	124694.17
12	71.18	114.86	14.56	33.55	0.239	0.237	0.062	0.083	57083.37	61102.13	93229.73	94433.48
13	109.87	285.07	58.40	51.79	0.196	0.188	0.059	0.069	99653.78	100864.59	149745.57	144301.52
14	106.17	234.94	42.92	50.05	0.214	0.210	0.064	0.075	90278.33	88140.66	137240.49	124141.21
15	103.37	189.19	28.61	48.73	0.248	0.246	0.073	0.090	78275.88	75234.48	117918.15	103606.63
16	99.53	142.43	14.30	46.92	0.319	0.318	0.094	0.120	59783.52	61210.31	88540.24	82306.49

**Five-parameter log-log model**

External LVDTs

k1 918.9493  
 k2 0.804258  
 k3 -1.795663  
 k6 0  
 k7 1

Internal LVDTs

k1 2133.08  
 k2 1.03998  
 k3 -3.600149  
 k6 -4.229015  
 k7 1.009776

**Specimen ID** MnRd-103%S0-R1 **Test Date** 7/16/2006

**Specimen Property**

*As-compacted state*

Dry unit weight 18.16398 kN/m<sup>3</sup>  
 Moisture content 15.54%

*Post-compact state*

Matric suction 24.92371 kPa  
 Moisture content 16.36%

**Specimen Geometry**

*As-compacted state*

Diameter 101.6 mm  
 Height 203.2 mm

*Post-compact state*

Diameter 101.6 mm  
 Height 205.0 mm

**MR Test Protocol NCHRP 1-28A**

Initial specimen height 205.0 mm  
 Final specimen height 203.0 mm  
 Final specimen diameter 101.6 mm  
 Initial gauge length 102.4 mm  
 Final gauge length 102.4 mm

**Bender Element Test**

Tip-to-tip distance 193.0 mm  
 Total unit weight 21.31 kN/m<sup>3</sup>  
 S-wave travel time 0.001281 second  
 Shear modulus 49298.54 kPa

Load Step	Deviator Stress (kPa)	Bulk Stress (kPa)	Confining Pressure (kPa)	Octahedral Shear Stress (kPa)	External LVDT 1 Deformation (mm)	External LVDT 2 Deformation (mm)	Internal LVDT 1 Deformation (mm)	Internal LVDT 2 Deformation (mm)	Measured MR-Ext (kPa)	Predicted MR-Ext (kPa)	Measured MR-Int (kPa)	Predicted MR-Int (kPa)
1	38.68	206.80	56.04	18.24	0.179	0.171	0.061	0.088	35978.62	36142.73	42393.36	43421.97
2	35.16	164.49	43.11	16.57	0.213	0.200	0.069	0.097	31047.84	32875.76	38737.76	39577.25
3	29.75	117.56	29.27	14.02	0.216	0.205	0.073	0.104	28456.98	28691.77	34072.02	34690.44
4	25.27	69.46	14.73	11.91	0.252	0.235	0.089	0.120	23666.19	22455.91	27705.37	26875.26
5	58.56	230.47	57.30	27.61	0.302	0.290	0.119	0.146	34738.59	32807.93	38817.53	36596.34
6	54.69	182.63	42.65	25.78	0.346	0.332	0.135	0.171	30047.66	29796.17	33370.75	33306.46
7	50.84	138.99	29.38	23.97	0.412	0.391	0.152	0.197	25409.92	26486.31	29269.25	29604.12
8	46.09	90.50	14.80	21.73	0.433	0.411	0.162	0.218	23604.67	21813.37	26375.12	24257.05
9	77.67	245.68	56.00	36.62	0.469	0.454	0.205	0.235	30363.07	29555.21	31932.77	30793.51
10	73.65	205.97	44.11	34.72	0.516	0.497	0.224	0.261	27655.77	27645.76	29010.04	28942.69
11	69.99	156.72	28.91	32.99	0.623	0.594	0.264	0.316	23046.45	24489.16	24219.70	25592.24
12	65.82	109.59	14.59	31.03	0.687	0.657	0.300	0.357	20621.47	20814.65	21180.07	21654.03
13	105.79	274.72	56.31	49.87	0.730	0.703	0.354	0.409	27364.11	25997.02	25783.62	24724.70
14	100.54	230.53	43.33	47.39	0.851	0.818	0.403	0.475	23198.15	24463.43	22118.47	23446.08
15	95.78	185.52	29.92	45.15	0.896	0.862	0.431	0.501	21885.26	22446.12	20678.12	21597.60
16	92.24	136.76	14.84	43.48	1.025	0.987	0.491	0.573	18861.83	19493.45	17892.60	18662.58

**Five-parameter log-log model**

External LVDTs

k1 343.3414  
 k2 0.541729  
 k3 -2.038932  
 k6 -0.205028  
 k7 1.001357

Internal LVDTs

k1 472.3652  
 k2 0.597537  
 k3 -3.091198  
 k6 -0.138244  
 k7 1.000669

**Specimen ID** MnRd-103%S22-R1 **Test Date** 7/15/2006

**Specimen Property**

*As-compacted state*

Dry unit weight 17.90 kN/m<sup>3</sup>  
 Moisture content 16.73%

*Post-compact state*

Matric suction 96.24 kPa  
 Moisture content 15.46%

**Specimen Geometry**

*As-compacted state*

Diameter 101.6 mm  
 Height 203.2 mm

*Post-compact state*

Diameter 101.6 mm  
 Height 202.0 mm

**MR Test Protocol NCHRP 1-28A**

Initial specimen height 202.0 mm  
 Final specimen height 202.0 mm  
 Final specimen diameter 101.6 mm  
 Initial gauge length 102.1 mm  
 Final gauge length 102.1 mm

**Bender Element Test**

Tip-to-tip distance 192.0 mm  
 Total unit weight 21.04 kN/m<sup>3</sup>  
 S-wave travel time 0.000914 second  
 Shear modulus 94748.65 kPa

Load Step	Deviator Stress (kPa)	Bulk Stress (kPa)	Confining Pressure (kPa)	Octahedral Shear Stress (kPa)	External LVDT 1 Deformation (mm)	External LVDT 2 Deformation (mm)	Internal LVDT 1 Deformation (mm)	Internal LVDT 2 Deformation (mm)	Measured MR-Ext (kPa)	Predicted MR-Ext (kPa)	Measured MR-Int (kPa)	Predicted MR-Int (kPa)
1	40.83	210.98	56.72	19.25	0.096	0.082	0.023	0.031	74720.65	71367.94	123750.67	112648.76
2	35.60	164.61	43.00	16.78	0.110	0.095	0.034	0.037	59726.61	61358.30	87090.90	98862.96
3	32.26	118.39	28.71	15.21	0.135	0.117	0.037	0.045	49979.56	49763.41	77512.25	78645.76
4	29.50	73.66	14.72	13.91	0.177	0.155	0.049	0.057	38057.85	38045.13	59992.68	54825.99
5	60.73	230.89	56.72	28.63	0.176	0.150	0.055	0.065	64377.00	64786.48	88165.87	90446.25
6	57.76	187.49	43.25	27.23	0.207	0.179	0.065	0.075	54450.09	55944.18	76069.04	79003.47
7	53.48	139.93	28.82	25.21	0.244	0.212	0.075	0.086	45518.40	46367.64	65487.20	65481.84
8	49.43	92.55	14.37	23.30	0.300	0.263	0.092	0.110	36767.70	36334.89	51728.63	48843.79
9	81.05	252.54	57.17	38.21	0.268	0.233	0.092	0.107	57423.52	59361.29	72870.30	73709.83
10	78.88	207.34	42.82	37.19	0.304	0.268	0.104	0.124	51963.34	51105.13	65760.56	64093.27
11	74.39	162.79	29.47	35.07	0.362	0.321	0.123	0.145	42450.36	43679.90	54458.30	55386.19
12	68.68	113.22	14.84	32.38	0.426	0.374	0.149	0.182	35113.01	35196.17	42798.93	43927.60
13	109.32	278.20	56.29	51.53	0.414	0.356	0.158	0.194	52227.53	52282.12	57739.24	55828.79
14	104.93	233.64	42.90	49.47	0.447	0.391	0.177	0.217	47613.79	46377.31	51168.89	50734.67
15	100.96	188.00	29.01	47.59	0.530	0.466	0.217	0.251	39763.51	39896.35	42798.11	44259.03
16	96.10	139.89	14.60	45.30	0.588	0.525	0.245	0.294	35304.35	32974.91	36763.62	36541.89

**Five-parameter log-log model**

External LVDTs		Internal LVDTs	
k1	<u>405.9838</u>	k1	<u>1187.101</u>
k2	<u>1.128712</u>	k2	<u>0.857583</u>
k3	<u>-2.456874</u>	k3	<u>-3.921536</u>
k6	<u>-25.5249</u>	k6	<u>-0.13054</u>
k7	<u>1.098823</u>	k7	<u>1.001216</u>

Specimen ID MnRd-103%S50-R1 Test Date 7/12/2006

**Specimen Property**

*As-compacted state*

Dry unit weight 18.14 kN/m<sup>3</sup>

Moisture content 16.07%

*Post-compact state*

Matric suction 24461.41 kPa

Moisture content 10.33%

**Specimen Geometry**

*As-compacted state*

Diameter 101.6 mm

Height 203.2 mm

*Post-compact state*

Diameter 101.6 mm

Height 200.0 mm

**MR Test Protocol NCHRP 1-28A**

Initial specimen height 200.0 mm

Final specimen height 200.0 mm

Final specimen diameter 101.6 mm

Initial gauge length 101.6 mm

Final gauge length 101.6 mm

**Bender Element Test**

Tip-to-tip distance 190.0 mm

Total unit weight 20.55 kN/m<sup>3</sup>

S-wave travel time 0.000339 second

Shear modulus 658067.57 kPa

Load Step	Deviator Stress (kPa)	Bulk Stress (kPa)	Confining Pressure (kPa)	Octahedral Shear Stress (kPa)	External LVDT 1 Deformation (mm)	External LVDT 2 Deformation (mm)	Internal LVDT 1 Deformation (mm)	Internal LVDT 2 Deformation (mm)	Measured MR-Ext (kPa)	Predicted MR-Ext (kPa)	Measured MR-Int (kPa)	Predicted MR-Int (kPa)
1	42.25	212.97	56.91	19.92	0.039	0.033	0.002	0.006	157480.60	156648.92	738186.15	696569.12
2	38.52	170.25	43.91	18.16	0.048	0.041	0.002	0.009	127729.13	124940.18	508330.56	523815.16
3	34.92	121.88	28.99	16.46	0.062	0.054	0.003	0.013	97379.62	88326.21	357522.20	332799.73
4	31.22	75.71	14.83	14.72	0.111	0.106	0.005	0.024	52050.62	53527.71	191850.09	170875.31
5	63.38	234.16	56.93	29.88	0.071	0.059	0.003	0.014	150985.55	157645.18	558786.34	597768.48
6	59.31	191.93	44.21	27.96	0.083	0.071	0.004	0.019	127431.38	129234.95	432518.55	467128.62
7	55.83	140.23	28.13	26.32	0.108	0.095	0.007	0.027	96652.14	93228.62	289553.81	304271.32
8	51.90	98.25	15.45	24.47	0.174	0.163	0.012	0.045	57640.19	64401.26	174168.95	187320.24
9	83.49	254.86	57.12	39.36	0.099	0.081	0.005	0.021	153900.31	158698.94	530200.97	523031.67
10	79.62	210.30	43.56	37.53	0.114	0.096	0.008	0.028	132002.03	130777.02	394434.71	410257.90
11	75.96	162.12	28.72	35.81	0.144	0.125	0.011	0.039	102865.44	99992.41	280873.44	289604.87
12	72.23	117.06	14.94	34.05	0.228	0.204	0.019	0.061	64033.85	71225.07	175293.37	185407.69
13	110.69	281.96	57.09	52.18	0.136	0.107	0.012	0.032	159199.22	159189.28	449086.71	439402.99
14	106.83	235.31	42.83	50.36	0.152	0.124	0.015	0.038	139635.40	132624.72	373717.43	349140.16
15	103.40	190.04	28.88	48.74	0.186	0.159	0.019	0.052	112271.95	106448.59	279152.36	262740.59
16	99.73	144.84	15.04	47.01	0.273	0.249	0.027	0.076	73760.58	80299.07	190445.19	181677.70

**Five-parameter log-log model**

External LVDTs

Internal LVDTs

k1 856.8257 k1 4338.912

k2 1.090474 k2 1.519737

k3 -1.216797 k3 -3.723034

k6 0 k6 -0.034812

k7 1 k7 1

**Specimen ID** RLF-98%S0-R1 **Test Date** 7/4/2006

**Specimen Property**

*As-compacted state*

Dry unit weight 15.91 kN/m3  
 Moisture content 21.81%

*Post-compact state*

Matric suction 58.75 kPa  
 Moisture content 24.47%

**Specimen Geometry**

*As-compacted state*

Diameter 101.6 mm  
 Height 203.2 mm

*Post-compact state*

Diameter 101.6 mm  
 Height 206.0 mm

**MR Test Protocol NCHRP 1-28A**

Initial specimen height 206.0 mm  
 Final specimen height 204.0 mm  
 Final specimen diameter 101.6 mm  
 Initial gauge length 102.4 mm  
 Final gauge length 102.4 mm

**Bender Element Test**

Tip-to-tip distance 194.0 mm  
 Total unit weight 19.94 kN/m3  
 S-wave travel time 0.00167 second  
 Shear modulus 27434.66 kPa

Load Step	Deviator Stress (kPa)	Bulk Stress (kPa)	Confining Pressure (kPa)	Octahedral Shear Stress (kPa)	External LVDT 1 Deformation (mm)	External LVDT 2 Deformation (mm)	Internal LVDT 1 Deformation (mm)	Internal LVDT 2 Deformation (mm)	Measured MR-Ext (kPa)	Predicted MR-Ext (kPa)	Measured MR-Int (kPa)	Predicted MR-Int (kPa)
1	40.75	211.00	56.75	19.21	0.167	0.165	0.059	0.069	33365.08	33923.83	43342.95	44217.21
2	36.92	165.24	42.77	17.41	0.181	0.179	0.066	0.074	30812.94	31184.81	39473.88	39901.26
3	32.92	119.23	28.77	15.52	0.192	0.189	0.071	0.079	28468.61	27470.07	35875.28	35026.43
4	28.40	72.78	14.79	13.39	0.253	0.253	0.092	0.093	21050.51	22217.12	28643.88	29645.64
5	58.76	231.55	57.60	27.70	0.334	0.330	0.128	0.138	28270.75	28126.40	35193.96	34880.57
6	55.40	184.41	43.00	26.12	0.359	0.354	0.144	0.150	26322.53	25849.50	31931.09	31275.45
7												
8	46.71	90.66	14.65	22.02	0.433	0.425	0.191	0.174	21402.71	19468.17	25066.78	23727.41
9	76.58	250.82	58.08	36.10	0.547	0.536	0.225	0.232	24361.60	23562.42	28826.58	27891.96
10	69.58	197.95	42.79	32.80	0.617	0.602	0.259	0.256	22081.75	22471.45	26056.83	26110.93
11	66.71	155.44	29.58	31.45	0.685	0.667	0.292	0.286	19413.98	20332.87	22705.39	23190.48
12	64.91	108.11	14.40	30.60	0.769	0.749	0.337	0.324	16844.89	16961.94	19297.61	19218.61
13	100.88	269.41	56.18	47.55	0.965	0.937	0.409	0.464	18875.25	18511.02	20542.51	20532.44
14	96.89	225.34	42.81	45.68	1.045	1.014	0.450	0.519	17374.79	17508.74	18449.87	18963.09
15	92.53	179.52	29.00	43.62	1.148	1.110	0.498	0.562	15695.28	16194.46	16700.96	17177.26
16	87.99	131.47	14.49	41.48	1.304	1.252	0.579	0.640	13686.95	14325.05	14329.06	15031.87

**Five-parameter log-log model**

External LVDTs		Internal LVDTs	
k1	<u>417.335</u>	k1	<u>368.0026</u>
k2	<u>0.561375</u>	k2	<u>1.121579</u>
k3	<u>-3.493874</u>	k3	<u>-4.733837</u>
k6	<u>0</u>	k6	<u>-37.95042</u>
k7	<u>1.004274</u>	k7	<u>1.079635</u>

**Specimen ID** RLF-98%S22-R1 **Test Date** 7/10/2006

**Specimen Property**

*As-compacted state*

Dry unit weight 15.58 kN/m3  
 Moisture content 23.19%

*Post-compact state*

Matric suction 42.74 kPa  
 Moisture content 27.03%

**Specimen Geometry**

*As-compacted state*

Diameter 101.6 mm  
 Height 203.2 mm

*Post-compact state*

Diameter 101.6 mm  
 Height 206.0 mm

**MR Test Protocol NCHRP 1-28A**

Initial specimen height 206.0 mm  
 Final specimen height 198.0 mm  
 Final specimen diameter 101.6 mm  
 Initial gauge length 103.6 mm  
 Final gauge length 101.3 mm

**Bender Element Test**

Tip-to-tip distance 188.0 mm  
 Total unit weight 20.57 kN/m3  
 S-wave travel time 0.001901 second  
 Shear modulus 20507.38 kPa

Load Step	Deviator Stress (kPa)	Bulk Stress (kPa)	Confining Pressure (kPa)	Octahedral Shear Stress (kPa)	External LVDT 1 Deformation (mm)	External LVDT 2 Deformation (mm)	Internal LVDT 1 Deformation (mm)	Internal LVDT 2 Deformation (mm)	Measured MR-Ext (kPa)	Predicted MR-Ext (kPa)	Measured MR-Int (kPa)	Predicted MR-Int (kPa)
1	40.00	208.76	56.25	18.86	0.333	0.302	0.138	0.141	15428.10	15998.37	17805.06	18262.12
2	36.38	169.86	44.49	17.15	0.304	0.278	0.136	0.132	16416.31	15196.53	18125.39	17585.86
3	31.87	119.19	29.11	15.03	0.367	0.336	0.156	0.149	13412.74	13695.30	15713.49	16120.75
4	28.20	72.23	14.68	13.29	0.412	0.381	0.173	0.163	11731.41	11521.63	14075.75	13746.17
5	58.10	226.96	56.29	27.39	0.627	0.573	0.279	0.282	14101.12	14020.51	15293.66	14942.93
6	53.72	186.80	44.36	25.32	0.673	0.618	0.290	0.286	12834.30	13443.09	14603.25	14552.88
7	49.44	139.70	30.09	23.31	0.725	0.667	0.315	0.302	11807.92	12379.38	13514.27	13606.09
8	44.59	89.69	15.03	21.02	0.793	0.730	0.361	0.324	10548.56	10760.44	11886.08	12031.73
9	74.01	246.55	57.51	34.89	0.952	0.882	0.480	0.458	13066.65	12646.82	12966.85	12737.22
10	69.71	201.90	44.07	32.86	1.019	0.937	0.503	0.483	11974.30	12065.47	12048.07	12327.96
11	66.18	154.51	29.45	31.20	1.077	0.994	0.535	0.507	11235.85	11121.21	11322.83	11496.33
12	61.69	105.42	14.58	29.08	1.172	1.089	0.584	0.538	10153.51	9856.36	10384.60	10341.70
13												
14												
15												
16												

**Five-parameter log-log model**

External LVDTs		Internal LVDTs	
k1	<u>178.2485</u>	k1	<u>242.5416</u>
k2	<u>0.418388</u>	k2	<u>0.421846</u>
k3	<u>-2.408004</u>	k3	<u>-3.407353</u>
k6	<u>-0.034715</u>	k6	<u>-0.055259</u>
k7	<u>1.000138</u>	k7	<u>1.002084</u>

Specimen ID RLF-98%S22-R2 Test Date 7/25/2006

**Specimen Property**

*As-compacted state*

Dry unit weight 15.88 kN/m<sup>3</sup>  
 Moisture content 21.81%

*Post-compact state*

Matric suction 82.36 kPa  
 Moisture content 22.75%

**Specimen Geometry**

*As-compacted state*

Diameter 101.6 mm  
 Height 203.2 mm

*Post-compact state*

Diameter 101.6 mm  
 Height 203.0 mm

**MR Test Protocol NCHRP 1-28A**

Initial specimen height 203.0 mm  
 Final specimen height 202.5 mm  
 Final specimen diameter 101.6 mm  
 Initial gauge length 101.9 mm  
 Final gauge length 101.9 mm

**Bender Element Test**

Tip-to-tip distance 192.5 mm  
 Total unit weight 19.63 kN/m<sup>3</sup>  
 S-wave travel time 0.001262 second  
 Shear modulus 46551.76 kPa

Load Step	Deviator Stress (kPa)	Bulk Stress (kPa)	Confining Pressure (kPa)	Octahedral Shear Stress (kPa)	External LVDT 1 Deformation (mm)	External LVDT 2 Deformation (mm)	Internal LVDT 1 Deformation (mm)	Internal LVDT 2 Deformation (mm)	Measured MR-Ext (kPa)	Predicted MR-Ext (kPa)	Measured MR-Int (kPa)	Predicted MR-Int (kPa)
1	38.07	209.20	57.05	17.94	0.092	0.085	0.025	0.034	72044.85	73720.31	108015.35	107774.38
2	37.20	165.97	42.92	17.54	0.100	0.092	0.030	0.036	65842.42	63693.63	95472.38	91173.28
3	32.84	120.59	29.25	15.48	0.120	0.113	0.039	0.041	52893.89	53787.32	77176.36	77756.67
4	29.69	73.53	14.62	13.99	0.157	0.151	0.052	0.049	40468.26	39918.77	61745.43	60545.71
5	62.18	232.41	56.75	29.31	0.176	0.163	0.065	0.069	61455.59	62644.69	78074.33	81741.65
6	56.43	186.18	43.25	26.60	0.183	0.169	0.070	0.072	57100.42	56983.40	71127.32	74332.84
7	54.73	140.91	28.73	25.80	0.211	0.198	0.086	0.081	50322.91	48056.53	61758.69	61869.68
8	49.94	94.21	14.76	23.54	0.274	0.261	0.108	0.095	37284.73	38429.00	49231.70	50885.38
9	82.84	254.97	57.37	39.05	0.260	0.239	0.107	0.106	57600.66	55443.37	67487.09	66289.63
10	77.60	209.24	43.88	36.58	0.283	0.261	0.120	0.114	51404.23	50830.88	59907.06	60425.44
11	73.18	159.37	28.73	34.50	0.333	0.312	0.142	0.133	42603.70	44047.81	50338.42	51978.36
12	69.97	113.50	14.51	32.98	0.399	0.380	0.176	0.157	35722.70	36119.62	42042.50	42824.84
13	106.63	278.41	57.26	50.26	0.426	0.390	0.190	0.175	46651.96	48310.17	52501.62	52551.40
14	104.89	238.58	44.56	49.45	0.447	0.410	0.202	0.183	45125.31	44174.26	50452.85	47102.68
15	100.24	186.96	28.91	47.25	0.504	0.466	0.236	0.205	39541.69	38957.20	43665.26	41012.62
16	96.76	140.32	14.52	45.61	0.621	0.579	0.300	0.264	31995.94	33076.15	34131.88	34588.93

**Five-parameter log-log model**

External LVDTs		Internal LVDTs	
k1	<u>684.9918</u>	k1	<u>813.801</u>
k2	<u>0.669268</u>	k2	<u>1.099162</u>
k3	<u>-2.536547</u>	k3	<u>-4.118489</u>
k6	<u>0</u>	k6	<u>-25.25998</u>
k7	<u>1.000892</u>	k7	<u>1.055828</u>

Specimen ID RLF-98%S50-R1 Test Date 7/11/2006

**Specimen Property**

*As-compacted state*

Dry unit weight 15.46 kN/m3

Moisture content 21.95%

*Post-compact state*

Matric suction 152.55 kPa

Moisture content 19.59%

**Specimen Geometry**

*As-compacted state*

Diameter 101.6 mm

Height 203.2 mm

*Post-compact state*

Diameter 101.6 mm

Height 202.0 mm

**MR Test Protocol NCHRP 1-28A**

Initial specimen height 202.0 mm

Final specimen height 202.0 mm

Final specimen diameter 101.6 mm

Initial gauge length 100.6 mm

Final gauge length 100.6 mm

**Bender Element Test**

Tip-to-tip distance 192.0 mm

Total unit weight 18.77 kN/m3

S-wave travel time 0.0008205 second

Shear modulus 104795.67 kPa

Load Step	Deviator Stress (kPa)	Bulk Stress (kPa)	Confining Pressure (kPa)	Octahedral Shear Stress (kPa)	External LVDT 1 Deformation (mm)	External LVDT 2 Deformation (mm)	Internal LVDT 1 Deformation (mm)	Internal LVDT 2 Deformation (mm)	Measured MR-Ext (kPa)	Predicted MR-Ext (kPa)	Measured MR-Int (kPa)	Predicted MR-Int (kPa)
1	39.55	210.84	57.10	18.64	0.062	0.052	0.009	0.006	99630.99	99813.60	395433.00	375643.65
2	36.04	167.86	43.94	16.99	0.072	0.060	0.010	0.006	87295.16	82479.03	355602.99	306487.52
3	31.72	117.81	28.70	14.95	0.093	0.081	0.012	0.013	65454.70	60868.77	222265.34	217578.41
4	27.77	71.37	14.53	13.09	0.157	0.141	0.023	0.024	36694.19	38981.61	117335.51	126904.70
5	56.60	227.08	56.83	26.68	0.132	0.092	0.024	0.023	87955.58	95070.72	209851.00	272503.85
6	55.89	185.22	43.11	26.35	0.146	0.108	0.030	0.027	79039.54	78744.65	175228.78	213379.44
7	52.04	138.62	28.86	24.53	0.171	0.138	0.038	0.030	63770.99	61415.57	145722.23	161282.85
8	46.42	90.72	14.77	21.88	0.250	0.216	0.055	0.045	39713.77	42722.03	92050.28	107333.62
9	80.87	250.64	56.59	38.12	0.190	0.130	0.049	0.036	87707.65	89220.95	165938.38	178657.39
10	76.56	205.63	43.02	36.09	0.209	0.148	0.056	0.039	78628.45	75971.18	147507.84	152270.57
11	70.80	157.76	28.99	33.37	0.254	0.199	0.066	0.048	61745.57	61293.33	122044.86	123175.49
12	50.37	95.02	14.88	23.75	0.275	0.233	0.074	0.035	39404.23	43424.83	91956.47	103430.94
13	108.11	278.99	56.96	50.96	0.279	0.186	0.077	0.056	83962.17	84019.25	146759.05	116583.80
14	103.18	232.14	42.99	48.64	0.299	0.210	0.085	0.061	76558.53	72601.82	132425.51	101633.96
15	97.09	184.73	29.22	45.77	0.367	0.273	0.103	0.071	60757.02	60571.14	111037.70	85804.72
16	92.71	136.39	14.56	43.70	0.450	0.375	0.131	0.046	45007.37	46620.75	104230.72	63654.10

**Five-parameter log-log model**

External LVDTs

Internal LVDTs

k1 686.5112 k1 4270.614

k2 0.94827 k2 1.282765

k3 -1.834579 k3 -6.347818

k6 0 k6 0

k7 1.012659 k7 1

**Specimen ID** RLF-103%S0-R1 **Test Date** 7/17/2006

**Specimen Property**

*As-compacted state*

Dry unit weight 16.10 kN/m3  
 Moisture content 0.22314

*Post-compact state*

Matric suction 27.44 kPa  
 Moisture content 0.25655

**Specimen Geometry**

*As-compacted state*

Diameter 101.6 mm  
 Height 203.2 mm

*Post-compact state*

Diameter 101.6 mm  
 Height 208.0 mm

**MR Test Protocol NCHRP 1-28A**

Initial specimen height 208.0 mm  
 Final specimen height 200.8 mm  
 Final specimen diameter 104.1 mm  
 Initial gauge length 105.4 mm  
 Final gauge length 103.4 mm

**Bender Element Test**

Tip-to-tip distance 190.8 mm  
 Total unit weight 19.81 kN/m3  
 S-wave travel time 0.001983 second  
 Shear modulus 18682.31 kPa

Load Step	Deviator Stress (kPa)	Bulk Stress (kPa)	Confining Pressure (kPa)	Octahedral Shear Stress (kPa)	External LVDT 1 Deformation (mm)	External LVDT 2 Deformation (mm)	Internal LVDT 1 Deformation (mm)	Internal LVDT 2 Deformation (mm)	Measured MR-Ext (kPa)	Predicted MR-Ext (kPa)	Measured MR-Int (kPa)	Predicted MR-Int (kPa)
1	37.41	208.20	56.93	17.63	0.283	0.277	0.137	0.154	20924.29	20685.85	20551.29	20659.27
2	33.92	163.52	43.20	15.99	0.306	0.301	0.141	0.163	19124.48	18953.87	19498.39	19566.02
3	28.97	116.14	29.06	13.66	0.347	0.342	0.143	0.162	16203.33	16761.87	18646.77	18138.30
4	24.40	68.70	14.77	11.50	0.413	0.408	0.172	0.192	13468.05	13488.87	15514.32	15540.06
5	56.53	229.00	57.49	26.65	0.544	0.533	0.284	0.311	18019.47	18196.31	16679.39	16975.23
6	51.35	181.35	43.33	24.21	0.538	0.527	0.274	0.298	17391.17	16958.58	16563.35	16411.44
7	48.28	133.79	28.50	22.76	0.653	0.640	0.318	0.348	14673.71	14975.70	14548.89	15035.82
8	41.31	85.22	14.63	19.47	0.679	0.664	0.316	0.344	12965.31	12745.55	13489.14	13621.03
9	74.67	245.53	56.95	35.20	0.825	0.812	0.445	0.476	15884.01	16127.07	14416.75	14182.74
10	70.64	201.74	43.70	33.30	0.874	0.862	0.457	0.506	14998.18	15117.67	13795.11	13687.31
11	66.34	153.25	28.97	31.27	0.942	0.930	0.479	0.530	13797.69	13663.35	13080.07	12837.64
12	60.53	104.58	14.68	28.53	1.036	1.024	0.525	0.573	12117.00	11865.54	11606.01	11736.19
13												
14												
15												
16												

**Five-parameter log-log model**

External LVDTs		Internal LVDTs	
k1	<u>210.9797</u>	k1	<u>256.5689</u>
k2	<u>0.500678</u>	k2	<u>0.410833</u>
k3	<u>-2.381907</u>	k3	<u>-3.189233</u>
k6	<u>0</u>	k6	<u>0</u>
k7	<u>1.000037</u>	k7	<u>1</u>

**Specimen ID** RLF-103%S22-R1 **Test Date** 7/21/2006

**Specimen Property**

*As-compacted state*

Dry unit weight 16.00 kN/m<sup>3</sup>  
 Moisture content 23.19%

*Post-compact state*

Matric suction 193.42 kPa  
 Moisture content 21.58%

**Specimen Geometry**

*As-compacted state*

Diameter 101.6 mm  
 Height 203.2 mm

*Post-compact state*

Diameter 101.6 mm  
 Height 204.0 mm

**MR Test Protocol NCHRP 1-28A**

Initial specimen height 204.0 mm  
 Final specimen height 203.0 mm  
 Final specimen diameter 101.6 mm  
 Initial gauge length 101.9 mm  
 Final gauge length 101.9 mm

**Bender Element Test**

Tip-to-tip distance 193.0 mm  
 Total unit weight 19.78 kN/m<sup>3</sup>  
 S-wave travel time 0.000993 second  
 Shear modulus 76161.66 kPa

Load Step	Deviator Stress (kPa)	Bulk Stress (kPa)	Confining Pressure (kPa)	Octahedral Shear Stress (kPa)	External LVDT 1 Deformation (mm)	External LVDT 2 Deformation (mm)	Internal LVDT 1 Deformation (mm)	Internal LVDT 2 Deformation (mm)	Measured MR-Ext (kPa)	Predicted MR-Ext (kPa)	Measured MR-Int (kPa)	Predicted MR-Int (kPa)
1	39.58	211.27	57.23	18.66	0.071	0.064	0.014	0.018	93115.63	95822.54	194569.84	193648.42
2	35.77	166.14	43.45	16.86	0.080	0.073	0.016	0.021	83937.12	83588.49	172059.81	172770.42
3	34.46	121.02	28.85	16.25	0.095	0.086	0.019	0.024	74624.87	67671.42	156683.92	139642.74
4	27.52	71.44	14.64	12.98	0.144	0.135	0.031	0.030	44470.93	49644.62	101418.61	106529.30
5	61.33	232.70	57.12	28.91	0.135	0.122	0.038	0.039	83559.35	86102.29	139137.84	146542.83
6	57.85	187.90	43.35	27.27	0.146	0.131	0.043	0.044	78246.43	76133.23	124241.55	131988.30
7	55.62	144.91	29.76	26.22	0.174	0.158	0.048	0.048	67081.00	64559.73	116331.61	112706.88
8	47.63	91.18	14.52	22.45	0.228	0.213	0.065	0.059	46040.44	49719.83	82032.03	90835.09
9	83.74	254.29	56.85	39.47	0.202	0.182	0.070	0.062	79692.88	77603.00	115160.25	112188.87
10	78.63	210.04	43.80	37.07	0.216	0.196	0.075	0.070	72037.35	70400.25	102603.84	104781.01
11	73.08	159.85	28.92	34.45	0.249	0.226	0.085	0.080	61020.14	60535.81	88498.31	92819.16
12	69.66	114.71	15.02	32.84	0.305	0.286	0.102	0.090	49046.33	49193.57	75332.37	76339.25
13	108.40	279.51	57.04	51.10	0.319	0.287	0.125	0.104	66233.89	70031.33	88011.92	85795.62
14	105.49	235.99	43.50	49.73	0.338	0.306	0.133	0.112	62807.73	63393.08	82409.28	78628.38
15	101.40	189.87	29.49	47.80	0.368	0.333	0.146	0.127	57534.53	55932.30	73836.42	70676.93
16	97.00	140.06	14.36	45.73	0.436	0.405	0.162	0.148	47429.00	46547.43	64367.33	59860.31

**Five-parameter log-log model**

External LVDTs		Internal LVDTs	
k1	<u>835.8574</u>	k1	<u>2290.407</u>
k2	<u>0.701865</u>	k2	<u>0.742521</u>
k3	<u>-2.131146</u>	k3	<u>-4.228001</u>
k6	<u>0</u>	k6	<u>0</u>
k7	<u>1.013322</u>	k7	<u>1</u>

**Specimen ID** RLF-103%S50-R1 **Test Date** 7/23/2006

**Specimen Property**

*As-compacted state*

Dry unit weight 16.18 kN/m<sup>3</sup>

Moisture content 21.12%

*Post-compact state*

Matric suction 2079.31 kPa

Moisture content 18.65%

**Specimen Geometry**

*As-compacted state*

Diameter 101.6 mm

Height 203.2 mm

*Post-compact state*

Diameter 101.6 mm

Height 203.0 mm

**MR Test Protocol NCHRP 1-28A**

Initial specimen height 203.0 mm

Final specimen height 203.0 mm

Final specimen diameter 101.6 mm

Initial gauge length 101.9 mm

Final gauge length 101.9 mm

**Bender Element Test**

Tip-to-tip distance 193.0 mm

Total unit weight 19.47 kN/m<sup>3</sup>

S-wave travel time 0.0007621 second

Shear modulus 127307.27 kPa

Load Step	Deviator Stress (kPa)	Bulk Stress (kPa)	Confining Pressure (kPa)	Octahedral Shear Stress (kPa)	External LVDT 1 Deformation (mm)	External LVDT 2 Deformation (mm)	Internal LVDT 1 Deformation (mm)	Internal LVDT 2 Deformation (mm)	Measured MR-Ext (kPa)	Predicted MR-Ext (kPa)	Measured MR-Int (kPa)	Predicted MR-Int (kPa)
1	41.00	212.16	57.05	19.33	0.046	0.046	0.007	0.012	146849.37	141227.21	350367.19	313360.96
2	37.11	169.60	44.16	17.50	0.055	0.055	0.011	0.014	120312.58	117103.62	265576.79	268229.92
3	31.60	118.35	28.92	14.90	0.072	0.072	0.015	0.017	87736.62	86276.69	193217.58	206912.23
4	27.93	71.48	14.51	13.17	0.128	0.123	0.023	0.024	50334.29	54628.86	135147.24	135177.28
5	61.85	232.96	57.04	29.16	0.089	0.082	0.022	0.027	126577.46	134188.48	222864.93	253221.79
6												
7	54.43	143.05	29.54	25.66	0.124	0.116	0.032	0.032	91129.98	88240.07	171130.47	176178.81
8	49.55	94.45	14.97	23.36	0.195	0.188	0.044	0.042	55058.55	61224.77	123180.47	126977.51
9	82.15	251.70	56.52	38.72	0.129	0.119	0.039	0.041	119451.16	127267.67	185419.28	207494.74
10	78.27	209.15	43.63	36.90	0.141	0.130	0.043	0.044	110028.80	109087.06	172401.51	182755.21
11	74.67	162.07	29.13	35.20	0.172	0.162	0.049	0.048	89760.87	87321.37	154727.72	150097.62
12	69.16	113.69	14.84	32.60	0.243	0.234	0.063	0.058	60866.69	64317.13	119419.07	115055.42
13	108.96	278.88	56.64	51.37	0.177	0.163	0.061	0.058	120127.55	120236.21	171678.48	163990.28
14	105.03	237.68	44.22	49.51	0.195	0.181	0.067	0.065	107927.26	105424.25	154038.19	147475.37
15	101.61	189.78	29.39	47.90	0.226	0.212	0.074	0.070	92719.58	86596.21	141035.91	123862.09
16	97.21	140.17	14.32	45.82	0.294	0.284	0.089	0.083	69443.09	66391.34	117522.65	97766.66

**Five-parameter log-log model**

External LVDTs

k1 939.7836

k2 0.95977

k3 -1.780263

k6 0

k7 1

Internal LVDTs

k1 2994.573

k2 0.959236

k3 -3.826002

k6 0

k7 1

**Specimen ID** RW-98%S0-R1 **Test Date** 7/3/2006

**Specimen Property**

*As-compacted state*

Dry unit weight 17.43 kN/m3  
 Moisture content 13.49%

*Post-compact state*

Matric suction 9.85 kPa  
 Moisture content 19.64%

**Specimen Geometry**

*As-compacted state*

Diameter 101.6 mm  
 Height 203.2 mm

*Post-compact state*

Diameter 101.6 mm  
 Height 206.4 mm

**MR Test Protocol NCHRP 1-28A**

Initial specimen height 206.4 mm  
 Final specimen height 202.8 mm  
 Final specimen diameter 101.6 mm  
 Initial gauge length 101.9 mm  
 Final gauge length 101.9 mm

**Bender Element Test**

Tip-to-tip distance 192.8 mm  
 Total unit weight 21.01 kN/m3  
 S-wave travel time 0.002011 second  
 Shear modulus 19678.52 kPa

Load Step	Deviator Stress (kPa)	Bulk Stress (kPa)	Confining Pressure (kPa)	Octahedral Shear Stress (kPa)	External LVDT 1 Deformation (mm)	External LVDT 2 Deformation (mm)	Internal LVDT 1 Deformation (mm)	Internal LVDT 2 Deformation (mm)	Measured MR-Ext (kPa)	Predicted MR-Ext (kPa)	Measured MR-Int (kPa)	Predicted MR-Int (kPa)
1	41.37	210.39	56.34	19.50	0.112	0.093	0.034	0.040	55035.98	53831.13	75862.80	72166.54
2	34.43	166.15	43.91	16.23	0.143	0.121	0.045	0.052	43164.80	46050.04	59202.91	61429.43
3	33.28	120.12	28.95	15.69	0.159	0.139	0.053	0.063	37460.46	36327.59	47845.28	47169.59
4	28.93	74.11	15.06	13.64	0.233	0.213	0.077	0.093	24484.43	25710.03	32044.51	32282.23
5	61.06	231.89	56.95	28.78	0.198	0.167	0.068	0.077	54531.76	54994.40	68494.67	71111.19
6	57.31	188.66	43.78	27.02	0.224	0.193	0.076	0.088	46738.11	47642.53	59077.57	60950.32
7	54.72	141.25	28.84	25.80	0.265	0.234	0.094	0.108	39545.27	38700.26	48648.11	48491.02
8	53.50	97.34	14.62	25.22	0.326	0.296	0.117	0.139	31347.26	29463.73	37836.89	35775.25
9	84.96	255.68	56.91	40.05	0.258	0.223	0.092	0.104	58538.16	55843.05	71224.60	69279.72
10	80.94	213.20	44.09	38.16	0.291	0.254	0.104	0.118	51356.52	49264.63	62615.63	60598.28
11	69.57	156.25	28.89	32.80	0.369	0.331	0.139	0.159	39303.42	40199.48	46074.58	49209.28
12	73.19	117.85	14.88	34.50	0.444	0.413	0.169	0.195	32590.41	32336.58	38119.00	38276.13
13	107.98	278.45	56.82	50.90	0.377	0.339	0.140	0.156	54201.15	56535.78	65166.56	67599.97
14	106.54	238.19	43.89	50.22	0.402	0.365	0.148	0.167	50642.48	50515.53	61502.93	59701.27
15	104.75	192.56	29.27	49.38	0.476	0.426	0.177	0.202	43015.44	43316.79	50910.97	50370.34
16	101.53	144.90	14.45	47.86	0.585	0.545	0.229	0.257	34694.57	35332.64	40202.80	40270.95

**Five-parameter log-log model**

External LVDTs		Internal LVDTs	
k1	<u>360.4581</u>	k1	<u>487.9896</u>
k2	<u>0.740904</u>	k2	<u>0.833078</u>
k3	<u>-0.701859</u>	k3	<u>-1.280997</u>
k6	<u>0</u>	k6	<u>-0.013349</u>
k7	<u>1.043272</u>	k7	<u>1.00028</u>

Specimen ID RW-98%S22-R1 Test Date 6/21/2006

**Specimen Property**

*As-compacted state*

Dry unit weight 17.51 kN/m<sup>3</sup>

Moisture content 13.68%

*Post-compact state*

Matric suction 667.83 kPa

Moisture content 10.84%

**Specimen Geometry**

*As-compacted state*

Diameter 101.6 mm

Height 203.2 mm

*Post-compact state*

Diameter 101.6 mm

Height 203.2 mm

**MR Test Protocol NCHRP 1-28A**

Initial specimen height 203.2 mm

Final specimen height 203.2 mm

Final specimen diameter 203.2 mm

Initial gauge length 107.2 mm

Final gauge length 107.2 mm

**Bender Element Test**

Tip-to-tip distance 193.2 mm

Total unit weight 19.41 kN/m<sup>3</sup>

S-wave travel time 0.000886 second

Shear modulus 94074.41 kPa

Load Step	Deviator Stress (kPa)	Bulk Stress (kPa)	Confining Pressure (kPa)	Octahedral Shear Stress (kPa)	External LVDT 1 Deformation (mm)	External LVDT 2 Deformation (mm)	Internal LVDT 1 Deformation (mm)	Internal LVDT 2 Deformation (mm)	Measured MR-Ext (kPa)	Predicted MR-Ext (kPa)	Measured MR-Int (kPa)	Predicted MR-Int (kPa)
1	42.97	214.55	57.19	20.26	0.058	0.052	0.008	0.013	105806.32	106151.76	294015.77	268597.22
2	39.23	168.26	43.01	18.49	0.067	0.062	0.012	0.015	90090.79	85561.95	221404.88	217817.84
3												
4	31.46	74.43	14.32	14.83	0.136	0.132	0.026	0.024	42643.69	40273.14	119401.82	109548.08
5	62.56	235.02	57.49	29.49	0.102	0.098	0.022	0.031	98160.12	102914.06	194801.93	220692.71
6	59.86	187.83	42.66	28.22	0.121	0.113	0.028	0.035	85592.27	83839.88	167760.98	178509.62
7	55.56	144.03	29.49	26.19	0.155	0.146	0.036	0.042	65899.61	66215.59	134199.45	142818.42
8	51.31	95.70	14.79	24.19	0.231	0.222	0.059	0.053	43326.36	45406.36	92819.64	100741.86
9	83.01	254.50	57.16	39.13	0.149	0.140	0.037	0.048	96810.21	99000.30	172994.06	180746.00
10	79.74	209.29	43.18	37.59	0.175	0.163	0.047	0.056	83444.18	83123.45	144687.12	151300.46
11	75.70	162.33	28.88	35.68	0.218	0.207	0.061	0.064	65948.34	66182.96	118633.00	120957.16
12	71.58	115.50	14.64	33.74	0.314	0.302	0.089	0.081	45199.82	48431.37	86430.01	89811.45
13	110.21	282.34	57.38	51.95	0.208	0.197	0.061	0.071	96648.33	94960.67	155749.23	142593.11
14	107.04	236.05	43.00	50.46	0.242	0.227	0.073	0.080	83909.00	80874.91	135281.28	120670.74
15	102.97	187.39	28.14	48.54	0.300	0.282	0.091	0.094	67452.18	65765.90	111673.49	98032.04
16	99.05	142.18	14.38	46.69	0.412	0.395	0.125	0.117	48319.32	51115.86	84790.44	76508.84

**Five-parameter log-log model**

External LVDTs		Internal LVDTs	
k1	<u>675.6789</u>	k1	<u>1742.083</u>
k2	<u>0.986759</u>	k2	<u>1.310016</u>
k3	<u>-1.634476</u>	k3	<u>-4.066002</u>
k6	<u>0</u>	k6	<u>-11.46078</u>
k7	<u>1</u>	k7	<u>1.003472</u>

Specimen ID RW-98%S50-R1 Test Date 7/2/2006

**Specimen Property**

*As-compacted state*

Dry unit weight 17.35 kN/m<sup>3</sup>

Moisture content 13.49%

*Post-compact state*

Matric suction 83.12 kPa

Moisture content 10.75%

**Specimen Geometry**

*As-compacted state*

Diameter 101.6 mm

Height 203.2 mm

*Post-compact state*

Diameter 101.6 mm

Height 203.2 mm

**MR Test Protocol NCHRP 1-28A**

Initial specimen height 203.2 mm

Final specimen height 203.2 mm

Final specimen diameter 101.6 mm

Initial gauge length 101.3 mm

Final gauge length 101.3 mm

**Bender Element Test**

Tip-to-tip distance 193.2 mm

Total unit weight 19.39 kN/m<sup>3</sup>

S-wave travel time 0.001034 second

Shear modulus 69001.19 kPa

Load Step	Deviator Stress (kPa)	Bulk Stress (kPa)	Confining Pressure (kPa)	Octahedral Shear Stress (kPa)	External LVDT 1 Deformation (mm)	External LVDT 2 Deformation (mm)	Internal LVDT 1 Deformation (mm)	Internal LVDT 2 Deformation (mm)	Measured MR-Ext (kPa)	Predicted MR-Ext (kPa)	Measured MR-Int (kPa)	Predicted MR-Int (kPa)
1	43.69	213.83	56.71	20.60	0.055	0.055	0.011	0.014	105423.39	105251.42	229195.43	211423.47
2	37.22	166.03	42.94	17.55	0.066	0.069	0.016	0.018	84777.61	84836.08	167028.97	165457.93
3	34.04	119.26	28.41	16.05	0.090	0.092	0.027	0.026	63218.07	61922.23	108152.20	111519.76
4	29.52	73.30	14.59	13.92	0.144	0.145	0.044	0.046	39176.36	38942.44	63239.24	63114.66
5	60.99	231.16	56.72	28.75	0.102	0.101	0.029	0.031	97037.15	102638.19	164223.65	183365.27
6	61.53	192.32	43.60	29.01	0.111	0.116	0.035	0.037	87172.70	84913.72	137588.98	141779.54
7	56.37	142.89	28.84	26.57	0.145	0.151	0.051	0.047	67085.99	64773.98	99934.44	102125.58
8	50.05	94.37	14.77	23.60	0.235	0.239	0.079	0.076	41115.95	44181.10	62746.07	64404.26
9	84.04	256.09	57.35	39.62	0.138	0.142	0.047	0.046	99926.64	100094.91	149160.32	155033.02
10	77.67	207.73	43.35	36.61	0.160	0.166	0.061	0.057	86365.50	83814.88	119123.21	126649.24
11	78.32	163.86	28.51	36.92	0.201	0.205	0.077	0.071	69261.17	65667.79	95150.70	91107.80
12	72.79	116.30	14.50	34.32	0.281	0.290	0.108	0.104	48470.75	47834.75	65274.22	61927.46
13	108.62	279.12	56.83	51.21	0.200	0.204	0.073	0.070	96675.75	96202.70	136227.72	128832.92
14	103.90	231.54	42.55	48.98	0.233	0.241	0.089	0.082	82215.95	81506.18	112970.82	105636.50
15	100.38	186.00	28.54	47.32	0.284	0.292	0.116	0.102	67654.65	66458.47	89215.71	81892.21
16	96.75	142.20	15.15	45.61	0.435	0.443	0.171	0.163	44208.62	51575.66	58005.51	59624.49

**Five-parameter log-log model**

External LVDTs		Internal LVDTs	
k1	<u>656.389</u>	k1	<u>1439.136</u>
k2	<u>1.013402</u>	k2	<u>1.393585</u>
k3	<u>-1.591246</u>	k3	<u>-3.794614</u>
k6	<u>0</u>	k6	<u>-1.87427</u>
k7	<u>1</u>	k7	<u>1</u>

Specimen ID RW-98%S50-R2 Test Date 7/9/2006

**Specimen Property**

*As-compacted state*

Dry unit weight 17.47 kN/m<sup>3</sup>  
 Moisture content 13.37%

*Post-compact state*

Matric suction 34.26 kPa  
 Moisture content 15.31%

**Specimen Geometry**

*As-compacted state*

Diameter 101.6 mm  
 Height 203.2 mm

*Post-compact state*

Diameter 101.6 mm  
 Height 204.5 mm

**MR Test Protocol NCHRP 1-28A**

Initial specimen height 204.5 mm  
 Final specimen height 204.3 mm  
 Final specimen diameter 101.6 mm  
 Initial gauge length 103.4 mm  
 Final gauge length 103.4 mm

**Bender Element Test**

Tip-to-tip distance 194.3 mm  
 Total unit weight 20.16 kN/m<sup>3</sup>  
 S-wave travel time 0.001292 second  
 Shear modulus 46446.80 kPa

Load Step	Deviator Stress (kPa)	Bulk Stress (kPa)	Confining Pressure (kPa)	Octahedral Shear Stress (kPa)	External LVDT 1 Deformation (mm)	External LVDT 2 Deformation (mm)	Internal LVDT 1 Deformation (mm)	Internal LVDT 2 Deformation (mm)	Measured MR-Ext (kPa)	Predicted MR-Ext (kPa)	Measured MR-Int (kPa)	Predicted MR-Int (kPa)
1	41.78	213.25	57.16	19.70	0.072	0.061	0.017	0.008	87611.43	88994.06	229069.73	207935.16
2	38.30	170.29	44.00	18.05	0.087	0.075	0.023	0.017	71608.64	69591.33	146262.79	152265.43
3	34.30	120.54	28.75	16.17	0.121	0.109	0.034	0.028	50286.47	47536.68	93143.74	96024.16
4	30.29	74.25	14.65	14.28	0.199	0.181	0.054	0.044	29254.04	28009.39	57115.65	53802.21
5	62.40	232.73	56.78	29.42	0.137	0.111	0.039	0.029	82040.57	85358.41	152296.16	170280.29
6	57.68	185.88	42.73	27.19	0.158	0.133	0.046	0.039	68186.63	67146.25	117209.90	125815.93
7	54.26	141.33	29.02	25.58	0.209	0.186	0.063	0.057	50131.49	49515.15	83023.00	86038.76
8	49.18	93.45	14.76	23.19	0.330	0.305	0.098	0.087	30193.66	31597.37	52442.14	51647.26
9	83.18	252.96	56.59	39.21	0.191	0.154	0.059	0.048	82661.57	82279.18	135313.48	141951.42
10	78.04	208.50	43.49	36.79	0.235	0.180	0.072	0.061	67049.83	67214.29	106535.17	110007.88
11	72.24	158.57	28.78	34.05	0.325	0.257	0.103	0.088	47952.86	50192.30	74146.35	76846.00
12	69.82	113.30	14.49	32.91	0.459	0.403	0.143	0.132	31860.53	34232.00	50534.15	48004.58
13	110.10	280.35	56.75	51.90	0.270	0.208	0.088	0.071	82177.97	79065.80	124635.62	115107.76
14												
15	101.86	188.73	28.95	48.02	0.402	0.336	0.134	0.125	53044.51	51271.35	76751.91	65295.13
16	98.17	142.57	14.80	46.28	0.583	0.510	0.190	0.187	35613.27	37443.28	52229.32	43954.39

**Five-parameter log-log model**

External LVDTs		Internal LVDTs	
k1	<u>471.8215</u>	k1	<u>633.4334</u>
k2	<u>1.267178</u>	k2	<u>2.152771</u>
k3	<u>-1.926996</u>	k3	<u>-4.595895</u>
k6	<u>-3.017157</u>	k6	<u>-18.83191</u>
k7	<u>1.019608</u>	k7	<u>1.032006</u>

Specimen ID RW-103%SO-R1 Test Date 7/18/2006

**Specimen Property**

*As-compacted state*

Dry unit weight 17.97 kN/m3  
 Moisture content 13.09%

*Post-compact state*

Matric suction 22.72 kPa  
 Moisture content 17.59%

**Specimen Geometry**

*As-compacted state*

Diameter 101.6 mm  
 Height 203.2 mm

*Post-compact state*

Diameter 101.6 mm  
 Height 205.0 mm

**MR Test Protocol NCHRP 1-28A**

Initial specimen height 205.0 mm  
 Final specimen height 204.0 mm  
 Final specimen diameter 101.6 mm  
 Initial gauge length 104.1 mm  
 Final gauge length 104.1 mm

**Bender Element Test**

Tip-to-tip distance 194.0 mm  
 Total unit weight 21.22 kN/m3  
 S-wave travel time 0.001653 second  
 Shear modulus 29798.24 kPa

Load Step	Deviator Stress (kPa)	Bulk Stress (kPa)	Confining Pressure (kPa)	Octahedral Shear Stress (kPa)	External LVDT 1 Deformation (mm)	External LVDT 2 Deformation (mm)	Internal LVDT 1 Deformation (mm)	Internal LVDT 2 Deformation (mm)	Measured MR-Ext (kPa)	Predicted MR-Ext (kPa)	Measured MR-Int (kPa)	Predicted MR-Int (kPa)
1	42.03	210.02	56.00	19.81	0.102	0.100	0.028	0.036	63796.39	66809.82	102387.99	105427.20
2	38.08	167.78	43.23	17.95	0.106	0.104	0.031	0.038	60146.58	57630.56	92812.36	89751.24
3	34.36	122.82	29.49	16.20	0.130	0.130	0.038	0.047	49478.77	46673.63	77501.67	70907.27
4	29.65	74.07	14.81	13.98	0.195	0.196	0.065	0.070	31888.49	33026.41	47066.44	47967.35
5	64.23	232.12	55.96	30.28	0.167	0.163	0.053	0.063	66746.65	67011.69	96545.27	98822.60
6	58.99	188.42	43.14	27.81	0.181	0.177	0.058	0.068	59956.01	58636.02	87194.06	85796.39
7	54.74	142.62	29.30	25.80	0.222	0.218	0.073	0.083	48056.85	48673.76	68916.11	69824.10
8	51.51	95.71	14.73	24.28	0.303	0.301	0.107	0.114	35018.82	36958.57	48606.38	51020.71
9	83.60	251.74	56.04	39.41	0.237	0.231	0.078	0.095	63288.24	67188.03	87205.80	93806.51
10	80.55	210.39	43.28	37.97	0.244	0.239	0.083	0.099	62347.12	59599.43	84582.41	82170.95
11	76.71	165.12	29.47	36.16	0.286	0.281	0.101	0.116	52439.13	50661.98	69598.43	68619.46
12	72.42	117.17	14.92	34.14	0.376	0.373	0.139	0.159	39213.67	40127.01	50212.38	52811.44
13	112.53	283.98	57.15	53.05	0.306	0.296	0.102	0.126	68500.13	67853.48	92477.62	87951.38
14	108.36	238.32	43.32	51.08	0.332	0.324	0.116	0.140	62481.84	60495.15	81399.25	77663.80
15	104.49	191.20	28.90	49.26	0.402	0.397	0.144	0.173	50996.66	52192.35	65474.26	65939.52
16	100.53	145.40	14.95	47.39	0.487	0.484	0.187	0.227	42159.47	43352.10	50383.16	53562.39

**Five-parameter log-log model**

External LVDTs		Internal LVDTs	
k1	<u>455.5711</u>	k1	<u>778.8196</u>
k2	<u>0.71522</u>	k2	<u>0.840735</u>
k3	<u>-0.817967</u>	k3	<u>-1.776182</u>
k6	<u>0</u>	k6	<u>0</u>
k7	<u>1</u>	k7	<u>1</u>

Specimen ID RW-103%S22-R1 Test Date 7/20/2006

**Specimen Property**

*As-compacted state*

Dry unit weight 18.12 kN/m3

Moisture content 13.41%

*Post-compact state*

Matric suction 196.19 kPa

Moisture content 11.26%

**Specimen Geometry**

*As-compacted state*

Diameter 101.6 mm

Height 203.2 mm

*Post-compact state*

Diameter 101.6 mm

Height 205.0 mm

**MR Test Protocol NCHRP 1-28A**

Initial specimen height 205.0 mm

Final specimen height 205.0 mm

Final specimen diameter 101.6 mm

Initial gauge length 101.6 mm

Final gauge length 101.6 mm

**Bender Element Test**

Tip-to-tip distance 195.0 mm

Total unit weight 20.06 kN/m3

S-wave travel time 0.000906 second

Shear modulus 94822.21 kPa

Load Step	Deviator Stress (kPa)	Bulk Stress (kPa)	Confining Pressure (kPa)	Octahedral Shear Stress (kPa)	External LVDT 1 Deformation (mm)	External LVDT 2 Deformation (mm)	Internal LVDT 1 Deformation (mm)	Internal LVDT 2 Deformation (mm)	Measured MR-Ext (kPa)	Predicted MR-Ext (kPa)	Measured MR-Int (kPa)	Predicted MR-Int (kPa)
1	38.23	208.87	56.88	18.02	0.043	0.040	0.006	0.007	154581.10	155783.32	492336.01	460225.18
2	35.90	167.84	43.98	16.92	0.051	0.049	0.008	0.009	137012.96	129430.68	401384.01	367540.38
3	34.08	123.22	29.71	16.07	0.066	0.063	0.013	0.012	102855.94	98656.84	265532.20	263382.79
4	30.40	74.40	14.67	14.33	0.118	0.104	0.025	0.019	60055.16	63652.52	149757.26	160592.91
5	62.39	233.55	57.05	29.41	0.080	0.072	0.021	0.016	142904.86	148391.29	284754.41	349885.24
6	58.68	188.90	43.41	27.66	0.093	0.084	0.024	0.018	122366.28	124897.33	249302.92	286260.58
7	55.43	141.94	28.84	26.13	0.115	0.103	0.032	0.023	99498.52	98010.62	198104.52	214262.84
8	52.93	96.49	14.52	24.95	0.175	0.160	0.046	0.032	65818.64	69848.15	139847.40	143260.09
9	85.37	256.53	57.05	40.25	0.116	0.104	0.031	0.025	137159.92	141752.83	267086.08	274456.89
10	80.12	208.45	42.78	37.77	0.129	0.117	0.037	0.029	121502.18	120648.59	224104.51	229649.43
11	77.47	164.06	28.86	36.52	0.157	0.143	0.049	0.035	100644.11	98305.55	178709.97	178664.31
12	73.83	117.66	14.61	34.81	0.224	0.206	0.068	0.047	70624.57	73982.73	130706.67	127752.20
13	112.80	284.07	57.09	53.17	0.159	0.144	0.047	0.040	136402.46	134696.65	235259.68	210237.87
14	107.18	236.20	43.01	50.53	0.178	0.161	0.055	0.043	120168.44	117016.37	205650.92	180350.81
15	104.19	192.41	29.41	49.11	0.208	0.190	0.070	0.048	102700.31	98460.70	171848.87	146054.26
16	100.67	144.34	14.56	47.46	0.285	0.265	0.095	0.067	74916.78	77032.18	126160.46	108589.81

**Five-parameter log-log model**

External LVDTs		Internal LVDTs	
k1	<u>1040.041</u>	k1	<u>3147.191</u>
k2	<u>0.917515</u>	k2	<u>1.35262</u>
k3	<u>-1.640052</u>	k3	<u>-4.477273</u>
k6	<u>0</u>	k6	<u>-6.778063</u>
k7	<u>1</u>	k7	<u>1</u>

**Specimen ID** RW-103%S50-R1 **Test Date** 6/22/2006

**Specimen Property**

*As-compacted state*

Dry unit weight 18.40 kN/m<sup>3</sup>  
 Moisture content 13.55%

*Post-compact state*

Matric suction 43.92 kPa  
 Moisture content 11.71%

**Specimen Geometry**

*As-compacted state*

Diameter 101.6 mm  
 Height 203.2 mm

*Post-compact state*

Diameter 101.6 mm  
 Height 209.6 mm

**MR Test Protocol NCHRP 1-28A**

Initial specimen height 209.6 mm  
 Final specimen height 206.4 mm  
 Final specimen diameter 101.6 mm  
 Initial gauge length 100.3 mm  
 Final gauge length 100.3 mm

**Bender Element Test**

Tip-to-tip distance 196.4 mm  
 Total unit weight 20.28 kN/m<sup>3</sup>  
 S-wave travel time 0.001023 second  
 Shear modulus 76166.14 kPa

Load Step	Deviator Stress (kPa)	Bulk Stress (kPa)	Confining Pressure (kPa)	Octahedral Shear Stress (kPa)	External LVDT 1 Deformation (mm)	External LVDT 2 Deformation (mm)	Internal LVDT 1 Deformation (mm)	Internal LVDT 2 Deformation (mm)	Measured MR-Ext (kPa)	Predicted MR-Ext (kPa)	Measured MR-Int (kPa)	Predicted MR-Int (kPa)
1	43.20	214.73	57.18	20.37	0.057	0.051	0.013	0.015	109514.48	111349.32	200023.25	191322.98
2	39.15	168.15	43.00	18.45	0.069	0.062	0.019	0.018	89908.52	88259.81	155149.12	154380.34
3	34.92	120.94	28.67	16.46	0.092	0.083	0.024	0.025	65617.67	64326.26	112555.30	114275.60
4	31.94	75.89	14.65	15.05	0.142	0.133	0.030	0.040	42873.11	40822.03	81509.11	72478.57
5	64.12	233.52	56.47	30.23	0.103	0.092	0.029	0.032	105476.09	106705.38	161863.31	170755.02
6	59.09	189.01	43.31	27.86	0.121	0.110	0.034	0.036	87168.36	87868.28	138067.23	143481.80
7	55.54	142.17	28.88	26.18	0.157	0.144	0.044	0.046	67265.57	66555.11	107856.92	110221.87
8	51.42	95.95	14.84	24.24	0.236	0.222	0.059	0.071	43636.70	45490.49	73982.14	76065.76
9	83.64	254.16	56.84	39.43	0.149	0.134	0.044	0.048	102361.51	104165.80	152409.10	156656.87
10	79.73	207.91	42.73	37.59	0.174	0.156	0.052	0.054	87143.53	85964.34	130102.75	131393.36
11	76.46	162.53	28.69	36.04	0.219	0.201	0.066	0.069	68971.66	67502.09	103732.22	104558.58
12	71.95	114.97	14.34	33.92	0.321	0.298	0.088	0.100	46215.45	48293.47	73441.69	75827.90
13	110.99	284.37	57.79	52.32	0.207	0.184	0.064	0.068	103062.55	101269.79	146735.60	140493.20
14	106.60	236.59	43.33	50.25	0.241	0.216	0.076	0.077	87735.83	85088.37	126257.33	120052.07
15	101.60	188.81	29.07	47.90	0.306	0.279	0.095	0.098	68706.94	68727.29	100126.61	98753.09
16	99.25	143.50	14.75	46.79	0.423	0.391	0.126	0.138	49105.29	52128.24	72871.59	75582.13

**Five-parameter log-log model**

External LVDTs		Internal LVDTs	
k1	<u>647.2245</u>	k1	<u>1383.362</u>
k2	<u>1.104014</u>	k2	<u>1.045679</u>
k3	<u>-1.701764</u>	k3	<u>-2.559231</u>
k6	<u>-2.622684</u>	k6	<u>-0.055204</u>
k7	<u>1.018121</u>	k7	<u>1.000594</u>

**Specimen ID** TH23-98%S0-R1 **Test Date** 7/5/2006

**Specimen Property**

*As-compacted state*

Dry unit weight 14.44 kN/m3  
 Moisture content 27.64%

*Post-compact state*

Matric suction 40.67 kPa  
 Moisture content 32.90%

**Specimen Geometry**

*As-compacted state*

Diameter 101.6 mm  
 Height 203.2 mm

*Post-compact state*

Diameter 101.6 mm  
 Height 211.0 mm

**MR Test Protocol NCHRP 1-28A**

Initial specimen height 211.0 mm  
 Final specimen height 184.3 mm  
 Final specimen diameter 111.1 mm  
 Initial gauge length 110.0 mm  
 Final gauge length 110.0 mm

**Bender Element Test**

Tip-to-tip distance 174.3 mm  
 Total unit weight 18.14 kN/m3  
 S-wave travel time 0.002088 second  
 Shear modulus 12879.01 kPa

Load Step	Deviator Stress (kPa)	Bulk Stress (kPa)	Confining Pressure (kPa)	Octahedral Shear Stress (kPa)	External LVDT 1 Deformation (mm)	External LVDT 2 Deformation (mm)	Internal LVDT 1 Deformation (mm)	Internal LVDT 2 Deformation (mm)	Measured MR-Ext (kPa)	Predicted MR-Ext (kPa)	Measured MR-Int (kPa)	Predicted MR-Int (kPa)
1	37.73	206.73	56.33	17.79	0.308	0.308	0.084	0.095	16407.98	16561.45	29759.74	29551.24
2	34.49	165.48	43.66	16.26	0.332	0.332	0.095	0.099	14954.56	15958.85	26931.03	28571.40
3	30.19	118.90	29.57	14.23	0.302	0.302	0.090	0.095	16322.79	15006.53	27925.51	27043.63
4	26.31	71.15	14.95	12.40	0.384	0.383	0.111	0.109	13077.47	13092.42	23980.33	23717.46
5	56.05	228.30	57.42	26.42	0.631	0.629	0.184	0.230	13610.43	13286.24	21801.87	21155.75
6	50.66	181.45	43.60	23.88	0.608	0.606	0.176	0.221	13712.24	13111.52	22086.35	21181.64
7	47.46	136.03	29.52	22.37	0.720	0.719	0.217	0.256	11558.05	12286.63	18488.84	19820.44
8	36.13	80.06	14.64	17.03	0.639	0.638	0.197	0.212	11461.42	11818.43	19469.51	20026.92
9												
10												
11												
12												
13												
14												
15												
16												

**Five-parameter log-log model**

External LVDTs		Internal LVDTs	
k1	<u>228.2575</u>	k1	<u>487.5781</u>
k2	<u>0.380321</u>	k2	<u>0.517923</u>
k3	<u>-3.647096</u>	k3	<u>-5.423365</u>
k6	<u>0</u>	k6	<u>-6.676658</u>
k7	<u>1</u>	k7	<u>1.008061</u>

Specimen ID TH23-98%S22-R1 Test Date 6/21/2006

**Specimen Property**

*As-compacted state*

Dry unit weight 14.31 kN/m3  
 Moisture content 28.37%

*Post-compact state*

Matric suction 249.65 kPa  
 Moisture content 28.70%

**Specimen Geometry**

*As-compacted state*

Diameter 101.6 mm  
 Height 203.2 mm

*Post-compact state*

Diameter 101.6 mm  
 Height 205.0 mm

**MR Test Protocol NCHRP 1-28A**

Initial specimen height 205.0 mm  
 Final specimen height 205.0 mm  
 Final specimen diameter 101.6 mm  
 Initial gauge length 106.2 mm  
 Final gauge length 106.2 mm

**Bender Element Test**

Tip-to-tip distance 195.0 mm  
 Total unit weight 18.72 kN/m3  
 S-wave travel time 0.00135 second  
 Shear modulus 39821.48 kPa

Load Step	Deviator Stress (kPa)	Bulk Stress (kPa)	Confining Pressure (kPa)	Octahedral Shear Stress (kPa)	External LVDT 1 Deformation (mm)	External LVDT 2 Deformation (mm)	Internal LVDT 1 Deformation (mm)	Internal LVDT 2 Deformation (mm)	Measured MR-Ext (kPa)	Predicted MR-Ext (kPa)	Measured MR-Int (kPa)	Predicted MR-Int (kPa)
1	42.76	212.76	56.67	20.16	0.079	0.085	0.023	0.032	71166.04	71144.68	109656.28	105987.64
2	38.40	168.41	43.34	18.10	0.083	0.090	0.025	0.034	66659.13	63892.44	101794.57	100226.54
3	34.89	120.95	28.69	16.45	0.101	0.108	0.029	0.038	55683.53	53185.31	89459.32	88952.81
4	31.43	75.01	14.53	14.82	0.145	0.154	0.038	0.042	37767.49	40046.78	73751.35	73066.80
5	62.93	234.11	57.06	29.66	0.167	0.172	0.060	0.072	58433.52	60306.31	77992.44	82795.89
6	56.32	183.53	42.41	26.55	0.180	0.194	0.056	0.077	52582.06	54969.71	76792.31	80083.29
7	53.51	140.62	29.04	25.22	0.205	0.221	0.063	0.082	46132.34	47309.05	70409.54	72517.14
8	51.50	95.17	14.56	24.28	0.269	0.287	0.079	0.098	35689.20	37071.39	58194.03	60801.09
9	82.60	257.25	58.22	38.94	0.268	0.273	0.104	0.119	51426.46	52177.16	64526.32	66442.43
10	77.12	207.55	43.48	36.36	0.283	0.297	0.097	0.125	47481.98	47690.42	64393.01	63840.70
11	75.07	161.08	28.67	35.39	0.311	0.335	0.104	0.134	42963.98	40978.35	60394.57	57428.48
12	70.74	114.45	14.57	33.35	0.389	0.416	0.120	0.162	34095.99	33972.34	50367.58	50893.80
13	108.30	280.75	57.48	51.05	0.444	0.458	0.178	0.214	42428.02	42996.76	50572.56	50193.76
14	105.13	233.95	42.94	49.56	0.468	0.492	0.177	0.226	40135.51	39122.52	49482.00	47402.81
15	101.52	187.77	28.75	47.86	0.511	0.542	0.186	0.232	36517.73	34849.05	47613.05	44140.15
16	97.11	140.14	14.34	45.78	0.607	0.641	0.220	0.268	30503.26	29783.11	40445.32	39981.28

**Five-parameter log-log model**

External LVDTs		Internal LVDTs	
k1	<u>740.6502</u>	k1	<u>1458.259</u>
k2	<u>0.68335</u>	k2	<u>0.527112</u>
k3	<u>-3.028647</u>	k3	<u>-3.904879</u>
k6	<u>0</u>	k6	<u>0</u>
k7	<u>1</u>	k7	<u>1</u>

**Specimen ID** TH23-98%S50-R1\_2 **Test Date** 6/21/2006

**Specimen Property**

*As-compacted state*

Dry unit weight 14.17 kN/m3  
 Moisture content 26.94%

*Post-compact state*

Matric suction 37.81 kPa  
 Moisture content 32.78%

**Specimen Geometry**

*As-compacted state*

Diameter 101.6 mm  
 Height 203.2 mm

*Post-compact state*

Diameter 101.6 mm  
 Height 206.4 mm

**MR Test Protocol NCHRP 1-28A**

Initial specimen height 206.4 mm  
 Final specimen height 193.7 mm  
 Final specimen diameter 111.0 mm  
 Initial gauge length 103.8 mm  
 Final gauge length NA mm

**Bender Element Test**

Tip-to-tip distance 183.7 mm  
 Total unit weight 17.30 kN/m3  
 S-wave travel time 0.002 second  
 Shear modulus 14871.32 kPa

Load Step	Deviator Stress (kPa)	Bulk Stress (kPa)	Confining Pressure (kPa)	Octahedral Shear Stress (kPa)	External LVDT 1 Deformation (mm)	External LVDT 2 Deformation (mm)	Internal LVDT 1 Deformation (mm)	Internal LVDT 2 Deformation (mm)	Measured MR-Ext (kPa)	Predicted MR-Ext (kPa)	Measured MR-Int (kPa)	Predicted MR-Int (kPa)
1	38.05	210.43	57.46	17.94	0.332	0.319	0.134	0.167	14520.29	14328.15	16330.58	16482.03
2	34.28	162.36	42.69	16.16	0.358	0.344	0.143	0.165	13378.26	13195.04	15806.99	15955.72
3	30.33	116.74	28.80	14.30	0.379	0.365	0.146	0.164	12520.15	12060.30	15618.47	15445.74
4	26.13	70.09	14.65	12.32	0.416	0.400	0.149	0.159	11096.31	10794.69	15229.31	14830.06
5	55.14	228.04	57.63	25.99	0.670	0.650	0.271	0.359	12377.21	12739.25	13448.38	12619.97
6	50.48	178.20	42.57	23.80	0.728	0.706	0.296	0.372	11099.51	11812.28	12366.17	12352.46
7	45.98	132.31	28.78	21.68	0.774	0.750	0.312	0.376	10198.00	10883.87	11726.10	12059.57
8	41.36	84.40	14.35	19.50	0.832	0.807	0.330	0.382	9219.48	9794.57	11004.42	11628.54
9	71.17	242.94	57.25	33.55	0.962	0.963			11751.16	11440.73		
10	68.75	197.32	42.86	32.41	1.049	1.047			11026.21	10535.08		
11	63.34	150.25	28.97	29.86	1.128	1.124			9957.54	9792.73		
12	59.32	103.06	14.58	27.96	1.202	1.201			9242.21	8838.02		
13												
14												
15												
16												

**Five-parameter log-log model**

External LVDTs		Internal LVDTs	
k1	<u>92.53519</u>	k1	<u>117.6959</u>
k2	<u>0.937734</u>	k2	<u>1.108006</u>
k3	<u>-2.761049</u>	k3	<u>-5.200016</u>
k6	<u>-64.97559</u>	k6	<u>-112.8714</u>
k7	<u>1.193624</u>	k7	<u>1.16795</u>

**Specimen ID** TH23-98%S50-R2 **Test Date** 7/28/2006

**Specimen Property**

*As-compacted state*

Dry unit weight 14.48 kN/m3  
 Moisture content 27.64%

*Post-compact state*

Matric suction 121.63 kPa  
 Moisture content 30.09%

**Specimen Geometry**

*As-compacted state*

Diameter 101.6 mm  
 Height 203.2 mm

*Post-compact state*

Diameter 101.6 mm  
 Height 206.0 mm

**MR Test Protocol NCHRP 1-28A**

Initial specimen height 206.0 mm  
 Final specimen height 205.0 mm  
 Final specimen diameter 101.6 mm  
 Initial gauge length 102.1 mm  
 Final gauge length 102.1 mm

**Bender Element Test**

Tip-to-tip distance 195.0 mm  
 Total unit weight 18.74 kN/m3  
 S-wave travel time 0.00135 second  
 Shear modulus 39864.16 kPa

Load Step	Deviator Stress (kPa)	Bulk Stress (kPa)	Confining Pressure (kPa)	Octahedral Shear Stress (kPa)	External LVDT 1 Deformation (mm)	External LVDT 2 Deformation (mm)	Internal LVDT 1 Deformation (mm)	Internal LVDT 2 Deformation (mm)	Measured MR-Ext (kPa)	Predicted MR-Ext (kPa)	Measured MR-Int (kPa)	Predicted MR-Int (kPa)
1	39.63	207.35	55.91	18.68	0.109	0.110	0.043	0.046	55772.69	56878.32	68707.85	68209.21
2	36.58	167.09	43.50	17.24	0.114	0.116	0.045	0.048	53467.57	53215.94	65649.23	64860.85
3	33.99	121.33	29.11	16.02	0.131	0.132	0.056	0.051	47461.34	47120.16	57872.58	59696.07
4	30.78	75.57	14.93	14.51	0.162	0.164	0.056	0.053	38307.08	39080.46	56870.63	54698.07
5	60.96	228.92	55.99	28.74	0.217	0.216	0.098	0.102	46809.74	46656.63	50428.59	51204.66
6	56.88	187.77	43.63	26.81	0.222	0.223	0.103	0.103	45345.49	44406.28	48554.30	49406.50
7	52.37	139.17	28.93	24.69	0.240	0.242	0.118	0.107	40726.95	40486.66	43228.31	46628.10
8	49.87	93.21	14.45	23.51	0.288	0.290	0.118	0.109	34414.38	34392.14	43589.97	42355.69
9	79.77	249.42	56.55	37.60	0.353	0.351	0.166	0.166	39657.44	39752.86	41764.60	40583.69
10	76.64	208.62	43.99	36.13	0.377	0.375	0.175	0.178	38116.58	37704.08	40285.31	38669.58
11	72.80	159.69	28.96	34.32	0.389	0.389	0.203	0.182	35819.25	34544.66	35960.33	36160.95
12	69.40	112.56	14.39	32.71	0.451	0.453	0.212	0.196	30932.39	30297.82	33994.18	33308.05
13	105.78	274.70	56.31	49.86	0.599	0.589	0.304	0.305	31979.04	32169.35	30963.66	29908.85
14												
15	97.01	186.01	29.67	45.73	0.675	0.668	0.349	0.342	27850.79	29044.54	26917.60	27466.85
16	93.08	135.68	14.20	43.88	0.741	0.737	0.381	0.365	25149.16	25958.49	24746.56	25370.30

**Five-parameter log-log model**

External LVDTs		Internal LVDTs	
k1	<u>694.434</u>	k1	<u>436.6083</u>
k2	<u>0.478755</u>	k2	<u>1.16295</u>
k3	<u>-3.044422</u>	k3	<u>-4.681866</u>
k6	<u>0</u>	k6	<u>-92.77248</u>
k7	<u>1.010697</u>	k7	<u>1.159363</u>

**Specimen ID** TH23-103%S0-R1 **Test Date** 7/17/2006

**Specimen Property**

*As-compacted state*

Dry unit weight 14.95 kN/m3  
 Moisture content 26.52%

*Post-compact state*

Matric suction 31.85 kPa  
 Moisture content 33.50%

**Specimen Geometry**

*As-compacted state*

Diameter 101.6 mm  
 Height 203.2 mm

*Post-compact state*

Diameter 101.6 mm  
 Height 213.5 mm

**MR Test Protocol NCHRP 1-28A**

Initial specimen height 213.5 mm  
 Final specimen height 205.5 mm  
 Final specimen diameter 106.0 mm  
 Initial gauge length 101.6 mm  
 Final gauge length 96.8 mm

**Bender Element Test**

Tip-to-tip distance 195.5 mm  
 Total unit weight 18.37 kN/m3  
 S-wave travel time 0.00212 second  
 Shear modulus 15927.68 kPa

Load Step	Deviator Stress (kPa)	Bulk Stress (kPa)	Confining Pressure (kPa)	Octahedral Shear Stress (kPa)	External LVDT 1 Deformation (mm)	External LVDT 2 Deformation (mm)	Internal LVDT 1 Deformation (mm)	Internal LVDT 2 Deformation (mm)	Measured MR-Ext (kPa)	Predicted MR-Ext (kPa)	Measured MR-Int (kPa)	Predicted MR-Int (kPa)
1	38.13	208.40	56.76	17.97	0.280	0.276	0.128	0.121	21006.29	20700.80	22171.01	21927.50
2	34.68	164.41	43.24	16.35	0.301	0.299	0.136	0.129	19509.92	19794.37	20870.52	21000.86
3	30.80	117.87	29.02	14.52	0.339	0.338	0.156	0.146	17467.44	18327.55	18507.15	19426.74
4	26.82	70.31	14.50	12.64	0.348	0.348	0.161	0.150	16785.85	15754.81	17770.67	16557.78
5	55.97	226.06	56.70	26.38	0.557	0.552	0.283	0.236	17184.99	16280.59	17393.82	16285.40
6	51.95	182.17	43.41	24.49	0.633	0.628	0.323	0.268	15030.91	15786.39	15161.78	15849.03
7	47.04	133.33	28.76	22.18	0.619	0.619	0.314	0.275	14803.98	14914.91	14748.74	15012.63
8	42.00	86.39	14.80	19.80	0.681	0.682	0.337	0.309	12923.50	13438.29	12907.31	13498.14
9												
10												
11												
12												
13												
14												
15												
16												

**Five-parameter log-log model**

External LVDTs		Internal LVDTs	
k1	<u>292.8019</u>	k1	<u>348.1322</u>
k2	<u>0.423159</u>	k2	<u>0.468246</u>
k3	<u>-3.985556</u>	k3	<u>-4.872308</u>
k6	<u>-0.211453</u>	k6	<u>-0.209325</u>
k7	<u>1</u>	k7	<u>1.000528</u>

**Specimen ID** TH23-103%S22-R1 **Test Date** 6/22/2006

**Specimen Property**

*As-compacted state*

Dry unit weight 14.97 kN/m3  
 Moisture content 26.14%

*Post-compact state*

Matric suction 124.79 kPa  
 Moisture content 28.74%

**Specimen Geometry**

*As-compacted state*

Diameter 101.6 mm  
 Height 203.2 mm

*Post-compact state*

Diameter 101.6 mm  
 Height 209.6 mm

**MR Test Protocol NCHRP 1-28A**

Initial specimen height 209.6 mm  
 Final specimen height 208.0 mm  
 Final specimen diameter 101.6 mm  
 Initial gauge length 104.1 mm  
 Final gauge length 104.1 mm

**Bender Element Test**

Tip-to-tip distance 198.0 mm  
 Total unit weight 19.20 kN/m3  
 S-wave travel time 0.001528 second  
 Shear modulus 32843.72 kPa

Load Step	Deviator Stress (kPa)	Bulk Stress (kPa)	Confining Pressure (kPa)	Octahedral Shear Stress (kPa)	External LVDT 1 Deformation (mm)	External LVDT 2 Deformation (mm)	Internal LVDT 1 Deformation (mm)	Internal LVDT 2 Deformation (mm)	Measured MR-Ext (kPa)	Predicted MR-Ext (kPa)	Measured MR-Int (kPa)	Predicted MR-Int (kPa)
1	41.50	211.33	56.61	19.56	0.126	0.124	0.061	0.055	46848.74	47199.41	50098.97	50724.87
2	37.70	167.40	43.23	17.77	0.137	0.135	0.067	0.062	42878.83	43129.22	44866.36	46189.58
3	33.74	119.84	28.70	15.90	0.156	0.154	0.071	0.070	37189.89	37220.02	40660.20	40711.20
4	28.96	73.64	14.89	13.65	0.192	0.189	0.077	0.079	29180.46	29674.17	35782.50	35444.54
5	60.52	231.95	57.14	28.53	0.250	0.246	0.124	0.113	39821.98	39602.27	41565.17	41025.87
6	56.05	186.03	43.32	26.42	0.268	0.266	0.134	0.123	36287.24	36624.02	37591.33	37624.25
7	52.32	139.62	29.10	24.66	0.298	0.297	0.145	0.138	32534.06	32302.81	34108.05	33420.02
8	48.93	92.75	14.61	23.06	0.353	0.352	0.160	0.152	27521.73	26404.49	30916.79	28695.82
9	80.51	250.98	56.83	37.95	0.409	0.407	0.203	0.201	34381.41	33110.17	34571.23	33063.73
10	76.32	205.87	43.19	35.98	0.442	0.440	0.229	0.224	31517.41	30823.89	30554.67	30381.55
11	71.91	159.07	29.06	33.90	0.488	0.488	0.254	0.251	28101.20	27782.92	27102.50	27359.66
12	67.35	110.53	14.39	31.75	0.559	0.560	0.277	0.287	24110.28	23570.16	23857.91	23925.40
13	105.07	275.87	56.93	49.53	0.704	0.701	0.342	0.371	27203.81	27066.80	26736.16	25954.62
14	100.54	232.11	43.86	47.39	0.769	0.767	0.389	0.416	24622.17	25580.45	23417.82	24151.91
15	96.22	182.16	28.65	45.36	0.850	0.849	0.442	0.474	22102.64	23161.06	20460.30	21636.66
16	91.76	135.36	14.53	43.25	0.946	0.948	0.493	0.543	19602.61	20344.41	17872.12	19203.89

**Five-parameter log-log model**

External LVDTs		Internal LVDTs	
k1	<u>560.1601</u>	k1	<u>301.7372</u>
k2	<u>0.593558</u>	k2	<u>1.261871</u>
k3	<u>-3.227889</u>	k3	<u>-4.23787</u>
k6	<u>0</u>	k6	<u>-59.13495</u>
k7	<u>1.014394</u>	k7	<u>1.12975</u>

Specimen ID TH23-103%S50-R1 Test Date 7/19/2006

**Specimen Property**

*As-compacted state*

Dry unit weight 14.96 kN/m<sup>3</sup>

Moisture content 27.77%

*Post-compact state*

Matric suction 8542.10 kPa

Moisture content 21.53%

**Specimen Geometry**

*As-compacted state*

Diameter 101.6 mm

Height 203.2 mm

*Post-compact state*

Diameter 101.6 mm

Height 199.0 mm

**MR Test Protocol NCHRP 1-28A**

Initial specimen height 199.0 mm

Final specimen height 199.0 mm

Final specimen diameter 101.6 mm

Initial gauge length 99.3 mm

Final gauge length 99.3 mm

**Bender Element Test**

Tip-to-tip distance 189.0 mm

Total unit weight 18.92 kN/m<sup>3</sup>

S-wave travel time 0.0005761 second

Shear modulus 207544.61 kPa

Load Step	Deviator Stress (kPa)	Bulk Stress (kPa)	Confining Pressure (kPa)	Octahedral Shear Stress (kPa)	External LVDT 1 Deformation (mm)	External LVDT 2 Deformation (mm)	Internal LVDT 1 Deformation (mm)	Internal LVDT 2 Deformation (mm)	Measured MR-Ext (kPa)	Predicted MR-Ext (kPa)	Measured MR-Int (kPa)	Predicted MR-Int (kPa)
1	40.16	211.77	57.20	18.93	0.042	0.039	0.008	0.003	153354.42	158334.84	534740.77	552738.81
2	36.58	165.31	42.91	17.25	0.049	0.048	0.010	0.004	133875.41	126286.16	480067.51	450211.63
3	33.33	119.15	28.61	15.71	0.063	0.062	0.013	0.004	104692.21	92965.49	369397.39	336324.74
4	28.78	72.49	14.57	13.57	0.119	0.120	0.023	0.011	52940.77	58303.40	183686.37	215036.21
5	62.05	232.56	56.84	29.25	0.073	0.068	0.018	0.006	150615.68	156234.18	441193.72	452965.26
6	58.45	186.95	42.83	27.55	0.082	0.082	0.020	0.007	130037.15	128098.90	400413.11	378882.14
7	53.96	139.99	28.68	25.44	0.102	0.106	0.024	0.012	102178.28	98367.17	297151.89	298193.81
8	51.28	95.63	14.79	24.17	0.175	0.179	0.036	0.022	60411.26	68414.40	184913.31	208471.66
9	81.74	251.36	56.54	38.53	0.100	0.097	0.028	0.012	147039.03	154456.59	354572.38	383589.55
10	78.06	207.85	43.26	36.80	0.109	0.112	0.030	0.015	131769.19	130111.41	319302.69	329598.70
11	74.67	160.44	28.59	35.20	0.136	0.143	0.034	0.021	105494.46	102303.03	266091.45	262991.49
12	71.32	115.07	14.59	33.62	0.216	0.226	0.049	0.036	65839.50	74809.89	170379.28	194477.75
13	109.60	279.31	56.57	51.66	0.132	0.130	0.043	0.022	152776.10	152748.64	308476.37	309959.70
14	106.76	236.04	43.09	50.33	0.143	0.147	0.044	0.026	138690.89	130841.10	289754.93	268782.34
15	102.57	189.39	28.94	48.35	0.175	0.183	0.049	0.031	112756.39	107079.78	252070.57	224389.90
16	98.86	143.29	14.81	46.61	0.257	0.270	0.063	0.046	76378.17	82552.45	184134.15	175416.50

**Five-parameter log-log model**

External LVDTs

k1 941.4759

k2 0.986596

k3 -1.271189

k6 0

k7 1

Internal LVDTs

k1 4715.184

k2 1.033711

k3 -3.556544

k6 0

k7 1

**APPENDIX F: RELATIONSHIP OF  $\alpha_1$  and  $\beta_1$  TO SOIL TEXTURAL PROPERTIES**

This appendix was put together by Drs. Satish Gupta and A. Ranaivoson of the University of Minnesota

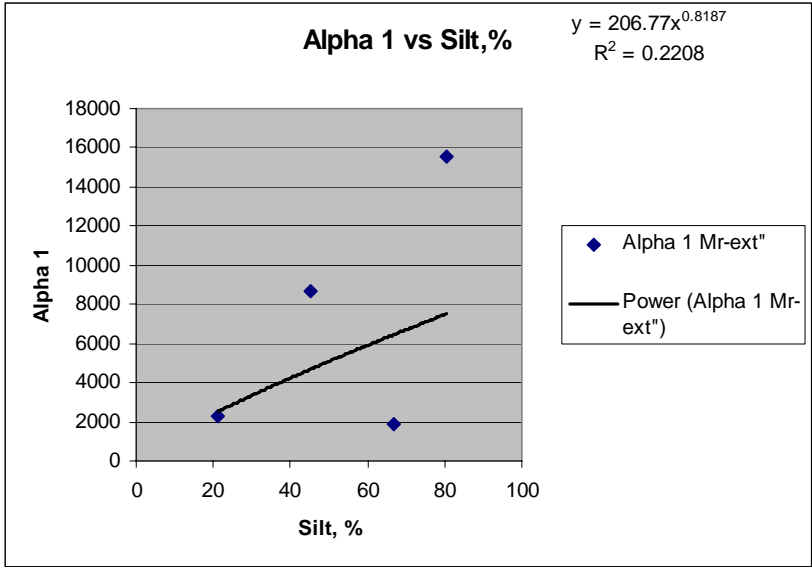


Fig. 1F: Relationship between  $\alpha_1$  vs. silt content.  $\alpha_1$  values are for  $M_r$  data measured with external LVDT.

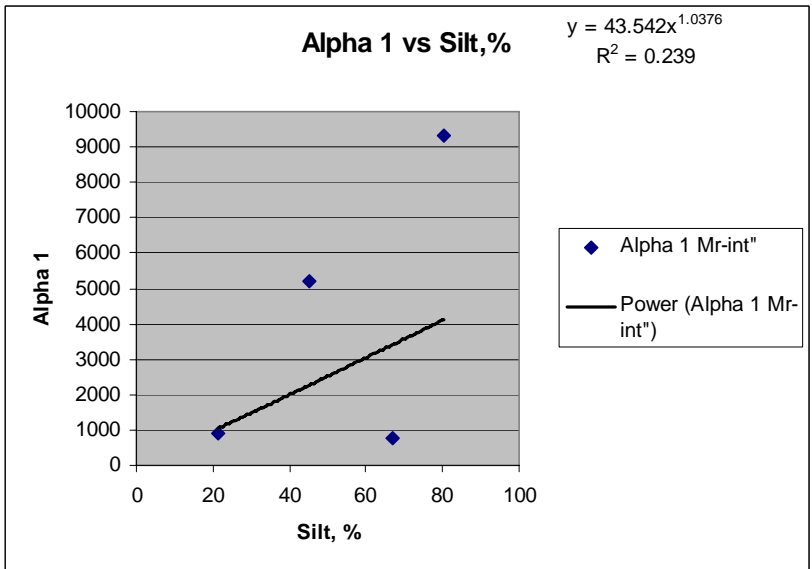


Fig. 2F: Relationship between  $\alpha_1$  vs. silt content.  $\alpha_1$  values are for  $M_r$  data measured with internal LVDT.

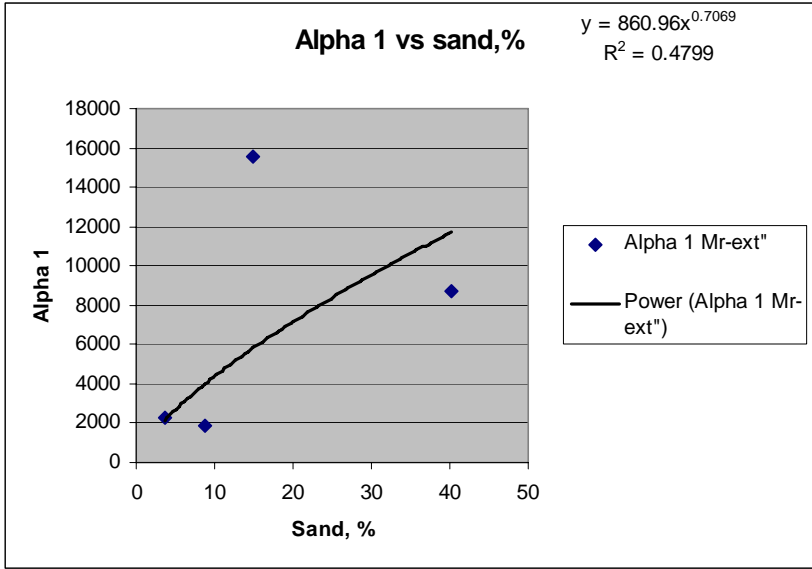


Fig. 3F: Relationship between  $\alpha_1$  vs. sand content.  $\alpha_1$  values are for  $M_r$  data measured with external LVDT.

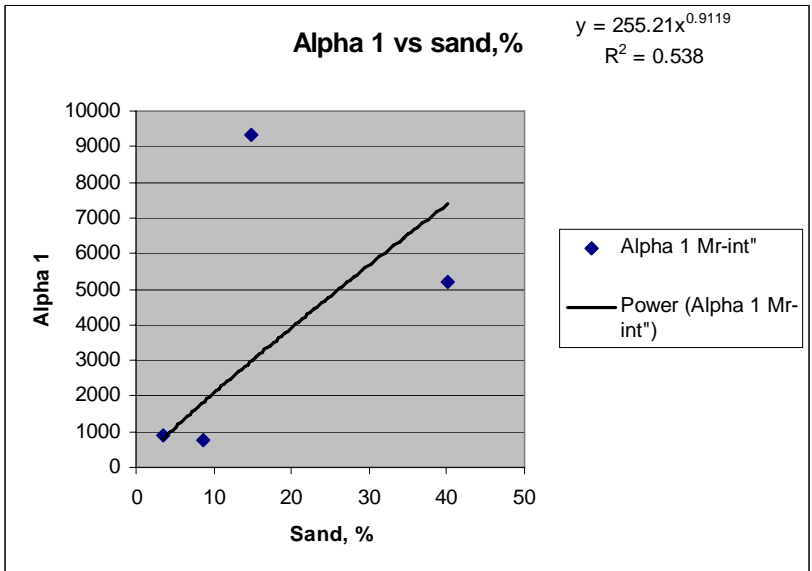


Fig. 4F: Relationship between  $\alpha_1$  vs. sand content.  $\alpha_1$  values are for  $M_r$  data measured with internal LVDT.

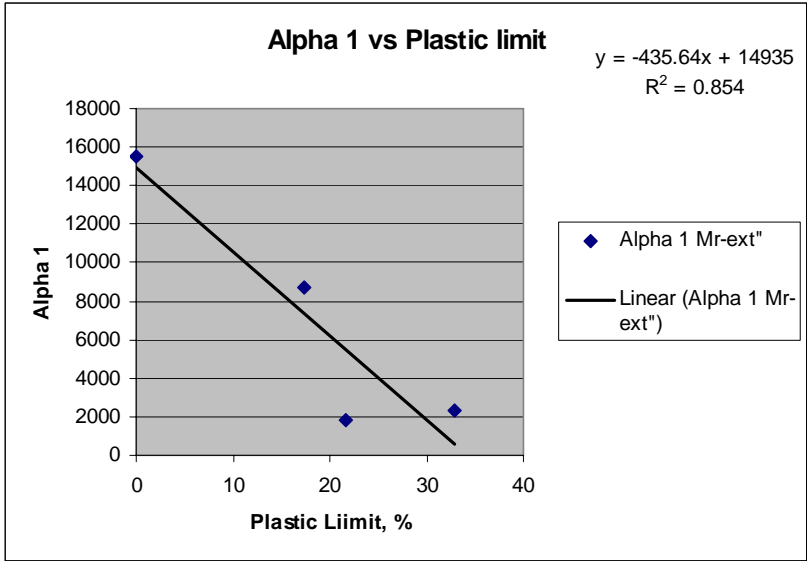


Fig. 5F: Relationship between  $\alpha_1$  vs. plastic limit.  $\alpha_1$  values are for  $M_r$  data measured with external LVDT.

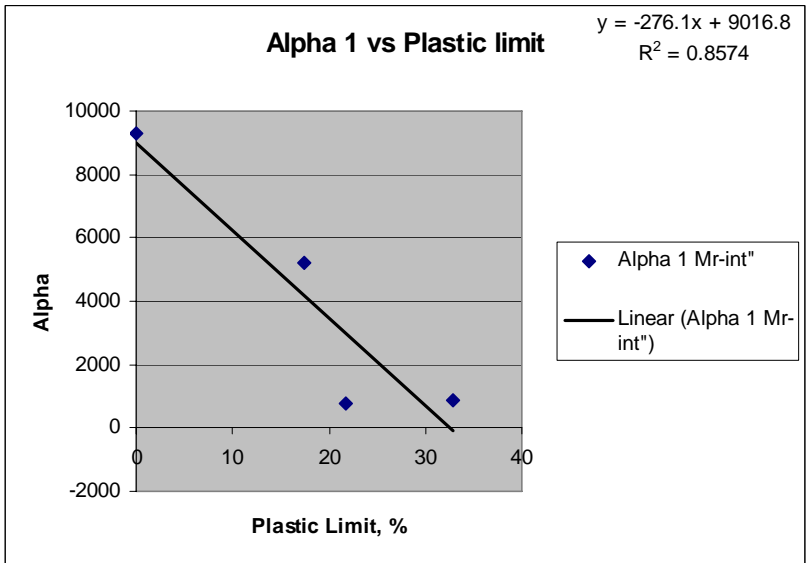


Fig. 6F: Relationship between  $\alpha_1$  vs. plastic limit.  $\alpha_1$  values are for  $M_r$  data measured with internal LVDT.

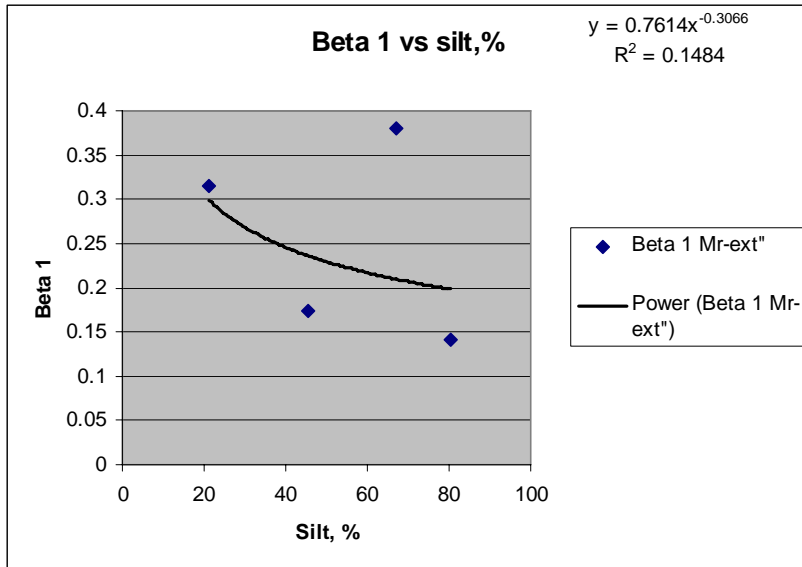


Fig. 7F: Relationship between  $\beta_1$  vs. silt content.  $\beta_1$  values are for  $M_r$  data measured with external LVDT.

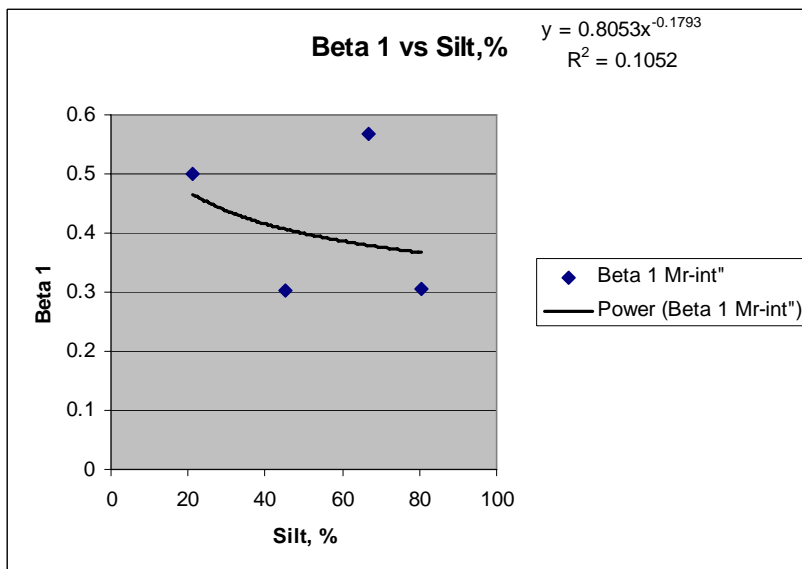


Fig. 8F: Relationship between  $\beta_1$  vs. silt content.  $\beta_1$  values are for  $M_r$  data measured with internal LVDT.

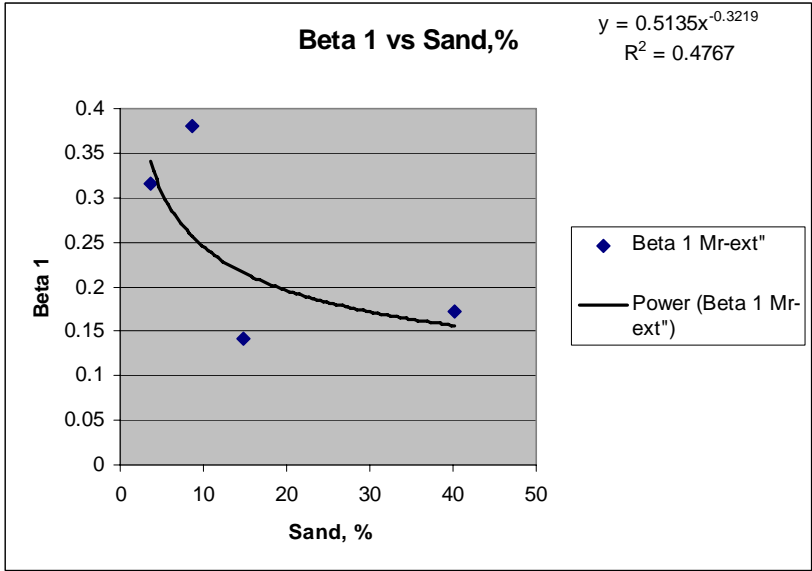


Fig. 9F: Relationship between  $\beta_1$  vs. sand content.  $\beta_1$  values are for  $M_r$  data measured with external LVDT.

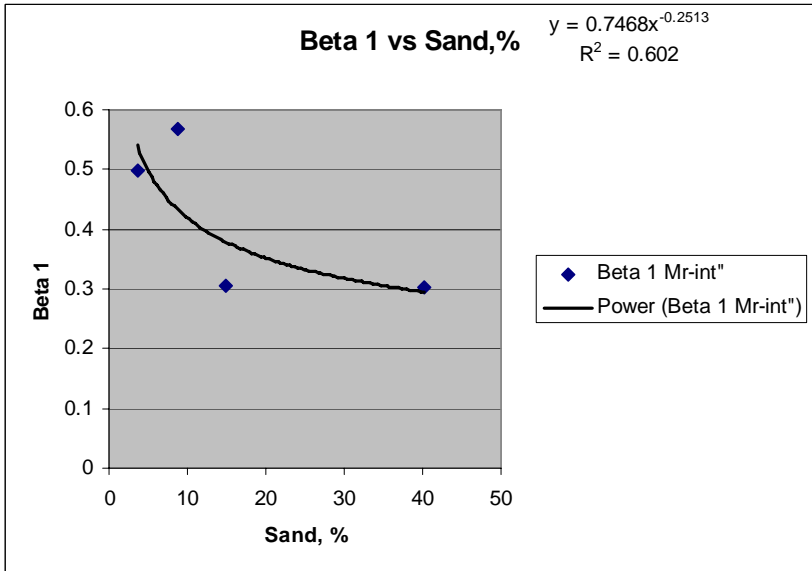


Fig. 10F: Relationship between  $\beta_1$  vs. sand content.  $\beta_1$  values are for  $M_r$  data measured with internal LVDT.

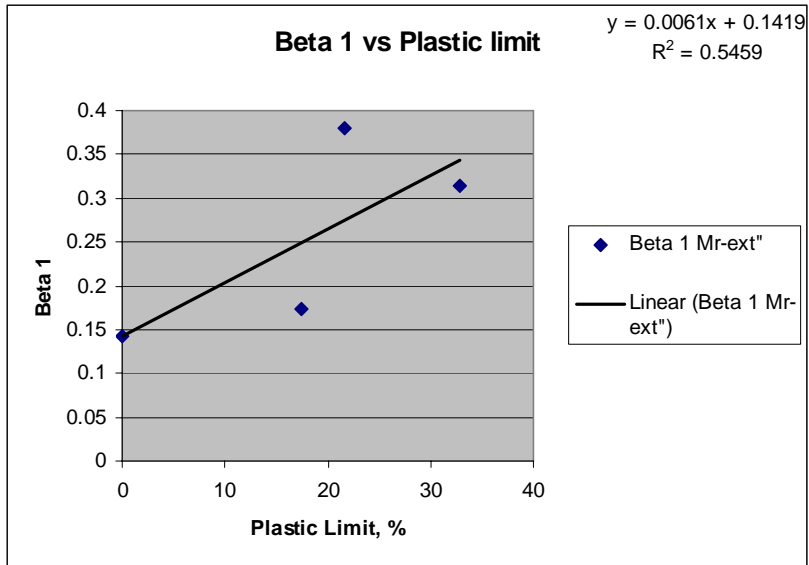


Fig. 11F: Relationship between  $\beta_1$  vs. plastic limit.  $\beta_1$  values are for  $M_r$  data measured with external LVDT.

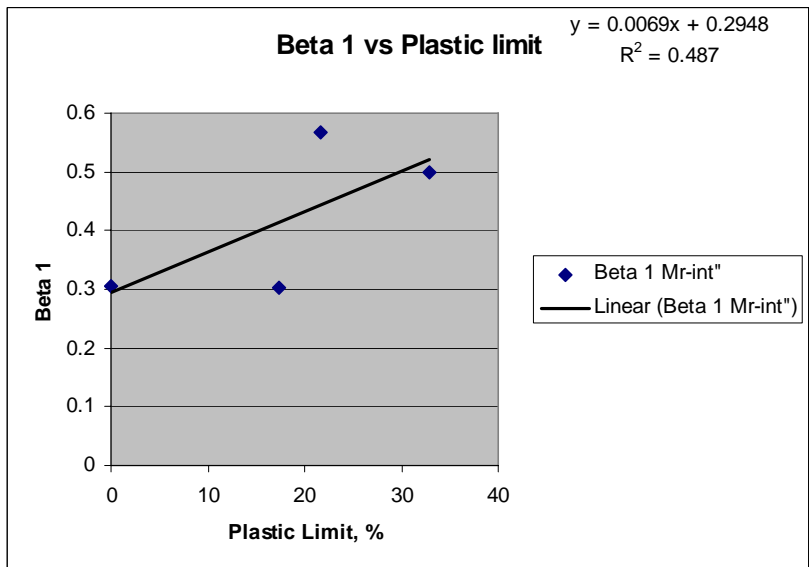


Fig. 12F: Relationship between  $\beta_1$  vs. plastic limit.  $\beta_1$  values are for  $M_r$  data measured with internal LVDT.